BETTER UNDERSTANDING OF PRODUCTION DECLINE IN SHALE GAS WELLS

By

Kananek Harongjit

RECOMMENDED:

Dr. Shirish Patil

Dr. Abhijit Dandekar

Dr. Mohabbat Ahmadi
Advisory Committee Chair

Dr. Abhijit Dandekar
Chair, Department of Petroleum Engineering

APPROVED:

Dr. Doug Goering
Dean, College of Engineering and Mines

Dr. John Eichelberger
Dean of the Graduate School

8/25/14

Date

BETTER UNDERSTANDING OF PRODUCTION DECLINE IN SHALE GAS WELLS

A

THESIS

Presented to the Faculty

of the University of Alaska Fairbanks

in Partial Fulfillment of the Requirements

for the Degree of

MASTER OF SCIENCE

By

Kananek Harongjit, B.Eng.

Fairbanks, Alaska

August 2014

ABSTRACT

Production data from the Eagle Ford shale (an analog to the Alaska Shublik shale) was collected from two neighboring counties and analyzed to correlate well performance with completion parameters including length of horizontal wellbore and number of hydraulic fracturing stages. Thirty-eight dry gas wells with production history range of 18-43 months were analyzed using 6 different decline curve analysis (DCA) models including Arps' exponential, harmonic and hyperbolic, power law exponential (PLE), logistic growth analysis (LGA) and Duong's models. In the matching process, 2/3 of history was used to tune the DCA models and their forecasts were compared to the remaining 1/3 of real history. The matching results were analyzed based on production history length and flow regime to have better understanding of limitations and capabilities of each DCA model. Reservoir simulation models, constructed using range of realistic data and actual completion practices of 4 select wells, were employed to assess reasonable values of remaining reserve and remaining well life that were used as benchmarks for comparison with DCA results.

The results showed that there was no strong correlation between well performance (average first year production rate) and the horizontal leg or the number of fracturing stages. This was an indication of extremely heterogeneous medium. In most cases, the accuracy of the DCA models increased when longer production history was used to tune the model parameters. LGA seems to be the most accurate DCA model since it gave the highest matching accuracy 71% of the total wells when using longest history length of 31 months. As the flow regime is concerned, LGA model also performed very well matched in 57% of the wells exhibiting only transient flow and 63% for the wells showing transient flow during early production time followed by boundary-dominated flow during late production. Moreover, the remaining reserve and well life of the select wells predicted by LGA fell into reasonably close range of the estimates from the reservoir simulations.

To the Lord Buddha for life direction and divine inspiration

TABLE OF CONTENTS

LIST OF FIGURES

LIST OF TABLES

LIST OF APPENDICES

ACKNOWLEDGEMENTS

I would like to express my very great appreciation to Dr. Ahmadi, my thesis committee chairman and advisor, for his patient guidance, enthusiastic encouragement and useful critiques of this thesis work.

I would like to extend my gratitude to Dr. Patil and Dr. Dandekar, my thesis committees, for giving me the precious opportunity to be a part of UAF petroleum engineering department, for advice and assistance that helped me through the difficult times.

My special thanks are extended to Mr. Delaihdem and Mr. Srichand, my friends and colleagues, for their great assistance in providing useful information and guidance on this thesis. I would also like to thank Mr. Brown, for his help in setup my office computer and simulation software. Thanks also go to the UAF petroleum department faculty, staff, and my friends for making my time at UAF an exceptional experience.

I would like to acknowledge Ms. Holz, International Program Associate Director, Ms. Wolfe, International Student (F-1) Program Coordinator and Ms. Bender, Graduate School Director, for their great help, advice and support through difficult circumstances.

My deepest thanks go to my family and my wife for their support, patience and love.

CHAPTER 1

INTRODUCTION

1.1 Overview

Natural gas is a safe, abundant and economical source of energy for the earth. North America has relied on natural gas for heating homes and buildings, as a fuel source for cooking and as a reliable supply for electricity generation for many years. In the past, oil and gas industry has explored and developed what are referred to as conventional natural gas deposits throughout the country. More recently as these supplies have relatively declined, the industry has concentrated their efforts more in developing unconventional gas resource, especially in shale formation. The shale reservoirs tend to be more expensive to develop and require special technologies to enable the gas to be produced due to its extremely low matrix permeability and porosity. One of the primary technologies is multi-stage hydraulic fracturing that creates high permeability paths along several thousand feet of horizontal leg, typical well completion for shale.

The hydraulic fracturing employed in shale reservoirs is the process of transmitting pressure, beyond fracturing gradient, by fracturing fluid to create fractures and/or to connect existing natural fractures in the reservoirs to the wellbore. The type of hydraulic fracturing used depends on a number of variables (Gidley et al., 1989) including type of well that has been drilled (vertical or horizontal), length of horizontal lateral, rock properties, depth, thickness, temperature and pressure of the reservoirs, well construction (type of wellbore cement and casing), number of fracturing stages to be completed in the wellbore, choice of fracturing fluids and materials, cost of fracturing and materials.

The oil and gas industry is interested in predicting the future production of each asset especially at depletion stage. This can be done using either complex, costly and time-consuming simulation that

needs large volume of data or can be done using simpler, less data demanding approach, decline curve analysis (DCA). Traditionally, Arps' equations are utilized to fit production rate-time plots during boundary-dominated flow (BDF) then use the fitted model to forecast to abandonment or economic rate. However, shale gas wells usually show long period of transient flow and do not reach BDF during most of their production life. The production rate also starts to decline shortly after production commencement. This has led to the development of many new DCA models to be more suitable for predicting estimated ultimate recovery (EUR) in the shale gas wells. The new DCA models include power law exponential (PLE)(Ilk et al., 2008), logistic growth analysis (LGA)(Clark et al., 2011) and Duong's model (Duong, 2011). They were formulated differently and will result in unique estimation of EUR and future production trend. Moreover, shale has very distinct characteristics even it lays next to each other in the same area (King, 2010). This also dictates the behavior of an outcome from each DCA model. Better understanding of gas production decline in a shale gas well in particular region with certain conditions of the reservoir characteristics will give a better insight of what is the most appropriate DCA model should be used. Recent advances in reservoir modeling software also provide more in-depth knowledge regarding the effects of factors controlling the behavior of the production decline. A reservoir simulation model constructed based on actual data can produce very reliable forecast which can be served as a benchmark for comparing with one calculated from DCA models.

Day gas wells located in the Eagle Ford shale play were selected to analyze in this study because the Eagle Ford shale is considered as an analog to the Shublik shale (Sondhi, 2011), which has been identified as a potential source rock to the vast hydrocarbon reserves at the Prudhoe Bay (Liu et al., 2009). The result that will be obtained from Eagle Ford production decline analysis and simulation can help to set expectation from Shublik shale and its development and leasing. As provided in recommendation more weight should be given to a similar study based solely on Shublik data when such a data is available in future.

1.2 Objective

This thesis looks at the relation between well hydraulic fracturing and completion that affect the behavior of the gas production trend. It also presents studies of production decline analysis and reservoir simulation using actual data from dry gas wells located in the Eagle Ford shale play. The objectives of the thesis are to:

- Identify possible correlations between (a) length of horizontal wellbore and (b) number of hydraulic fracturing stages and well performance
- Understand how different DCA models including Arps' exponential, Arps' harmonic, Arps' hyperbolic, PLE, LGA and Duong handle the production decline history based on (a) length of the production history and (b) type of flow regime
- Study how reliable is the prediction of (a) remaining reserves and (b) remaining well life by the DCA models compared with the results estimated by the reservoir simulation models applied on selected wells

CHAPTER 2

LITERATURE REVIEW

2.1 Shale Gas and Shale Gas Reservoirs

Shales are typically fine-grained, organic rich, sedimentary rocks (EIA, 2013) with grain-size ranged from extremely fine-grained smaller than 4 microns in diameter to silt-sized up to 62.5 microns (Passey et al., 2010). Over decades, shale formations have been considered as potential source rocks supplying hydrocarbon to conventional reservoirs and also being as conventional-reservoir seals. However, as the conventional resources have been depleted and more difficult to produce over time, shale formations themselves are being researched and developed as a hydrocarbon reservoir (Sondhi, 2011). Shale reservoir is one of so-called unconventional resources due to its unique characteristics do not meet the criteria for conventional resources. For instance, shale reservoirs do not have trap and do not contain a gas/water contact, they have low range of porosity from 6-12% and extremely low permeability, often in nano Darcy range. In this low permeability environment, hydrocarbon flow through the matrix is limited and insufficient for economic production (Kennedy et al., 2012).

Type of hydrocarbon generated by shale formations depends upon certain degree of thermal maturity of the formations. Consequently, shale gas is natural gas that is generated and trapped within shale formations that have been exposed to high heat in gas-generation window (212-570 °F) (Hanks, 2012). Shale gas is stored in shale reservoirs in three ways. 1) Free gas stored in the rock matrix porosity and/or in natural fractures. 2) Sorbed gas, either the gas is adsorbed (chemically bound) to the organic matter (kerogen) and 3) mineral surfaces within natural fractures or is absorbed (physically bound) to the organic matter (kerogen) and mineral surfaces within the rock matrix (Kennedy et al., 2012).

Based upon resource triangle by Masters (1979), hydrocarbon resources could be classified into a triangular distribution using criteria of their abundance, their reservoir quality and technology required to produce them economically, (see **Figure 2.1**). The deeper in the resource triangle indicates the more difficult to produce but however, the larger amount of technically recoverable unconventional resources. According to the estimation of the amount of the resources in seven major North America basins conducted by Old et al. (2008), only 10% of the total recoverable resources exist in the conventional reservoirs, whereas the remaining 90% is in the unconventional reservoirs. Assessed amount of original gas in place (OGIP) of shale gas in the US is 5905 Tcf, which is approximately 12% of the OGIP of shale gas worldwide (Dong et al., 2012). Statistical report by EIA (2011) shows that U.S. shale gas production comprises about 40% of total U.S. dry gas production since 2000, (see **Figure 2.2**). EIA (2013) also released the report in the same direction that the projection of US natural gas production is expected to increase 30% by 2040. According to **Figure 2.3**, shale gas would play a big role in natural gas industry in upcoming decades.

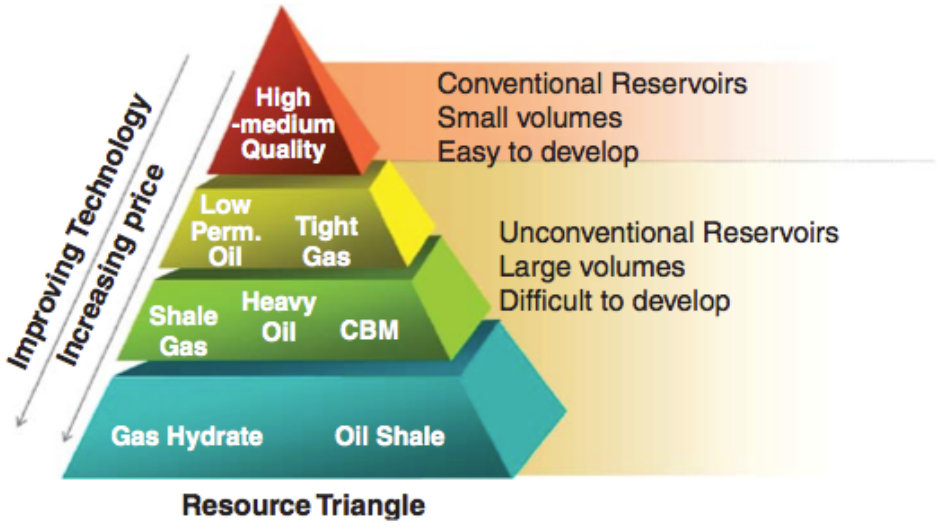

Figure 2.1: Resource triangle (Master, 1979)

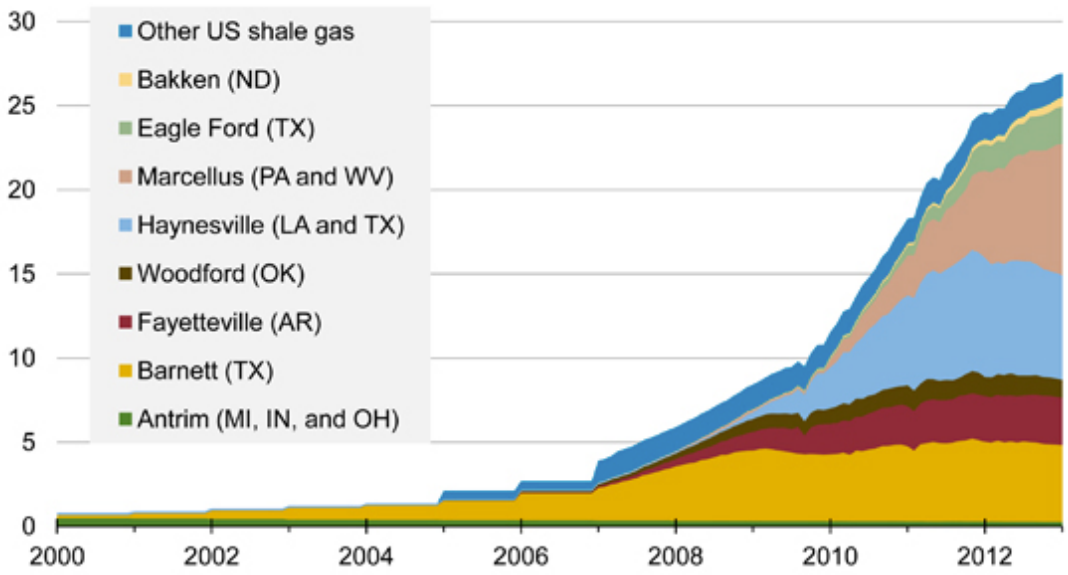

Figure 2.2: Historical shale gas production (dry) billion cubic feet per day (EIA, 2011)

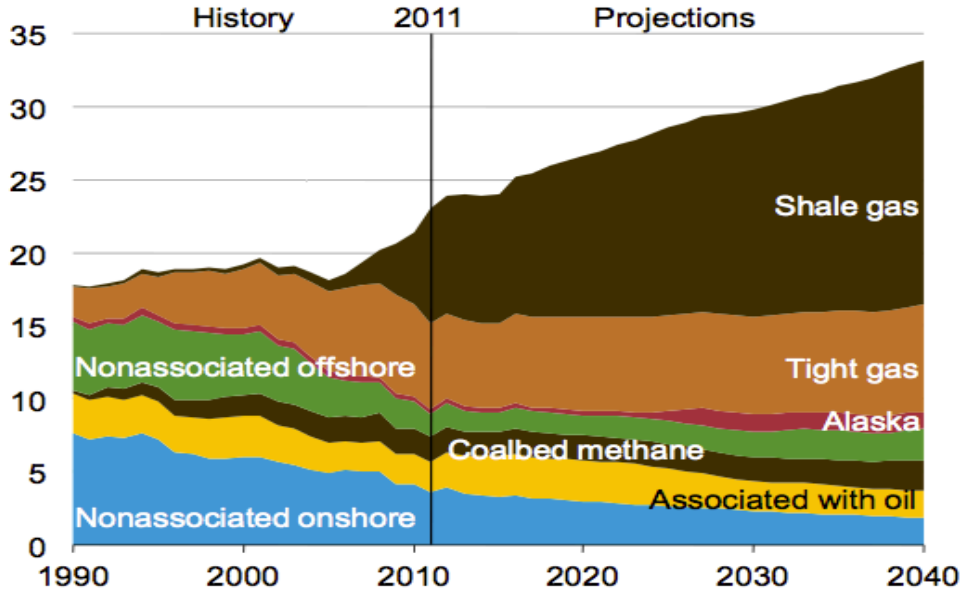

Figure 2.3: U.S. dry natural gas production by source, 1990-2040 (Tcf), (EIA, 2013)

2.2 Drilling, Completion and Stimulation in Shale Gas Reservoirs

Not only low range of matrix porosity and extremely low permeability of shales that creates difficulties in shale gas production but the characteristics of shales themselves are different from basin to basin and even in the same field (Economides and Martin, 2007). No two shales are alike; they vary areally and vertically within a trend and also along horizontal lateral wellbores (King, 2010). As the result, goals of drilling and completion operations in shale gas reservoirs are to be able to reach the best area in the shale reservoirs where the hydrocarbon (gas) was not migrated into conventional formations and complete the well at sweet spots (Jenkins and Boyer, 2008). Advancements in drilling, completion and stimulation technologies are the keys for shale play development and combination of horizontal well drilling and completion along with hydraulic fracturing techniques is well known as a current viable approach that has been used and intensely developed in the past several years.

Horizontal drilling is very important breakthrough in drilling technology. By drilling horizontally, the wellbore is more exposed to the reservoir providing higher possibility for hydraulic fractures created by stimulation techniques intersect a greater number of natural fractures in the reservoir, hence enhances gas production rates and recoverable gas reserves (Daniels et al., 2007). Drilling challenges in shale plays are usually associated with extreme conditions of each particular shale formation. Typical wells drilled in the shale plays are 10,000 ft to 14,000 ft TVD with horizontal section that can be extended up to 6,000 ft and beyond. The wells can have very high bottom hole temperature in some cases reaching 375°F. Moreover, some shale formations are very abrasive which causes friction-associated issues for instance; downhole friction generated heating failure and downhole stick-slip (Jellison et al., 2013).

Appropriate type of completion is a very challenging decision to be made in order to commence economic gas production in shale gas reservoirs. Agrawal et al. (2010) have developed very useful

decision flowcharts for selecting completion techniques, based upon key geological parameters obtained from comprehensive literature reviews of the completion trends in five major shale plays in the United States. The significant geologic parameters including 1) depositional environment; it is for determining what type of hydrocarbon may exist in the formation, 2) Total organic content (TOC); TOC is indicative of the quantity of organic materials available for hydrocarbons to be generated, which can be translated to the yield of gas, 3) Average gas content; it is used to forecast what in the formation can be recovered, shales with high gas content generally have higher gas permeability indicated that this formation would give high flow rate of gas when production commences and, 4) Thickness of the shale formation; if shale is less than 50 ft thick, it will be difficult to produce due to less reservoir contact area and possibly less amount of gas in place. However, if shale is too thick, difficulty in determining sweet spots in the formation will increase as the horizontal drilling capability is reduced in thick formations. Middle or relatively closed to the middle of the formation is where most completion operators place the lateral since in most cases have been confirmed by microseismic technology that height growth during the fracturing treatment is enough to connect entire shale formation to the horizontal wellbore (Agrawal et al., 2010).

Hydraulic fracturing is one of most successful stimulation techniques used by petroleum industry along with horizontal drilling to enable production from shale gas reservoirs. The key of the technique is to stimulate the natural fractures that may exist within shale formations or to stimulate the shale formation themselves by hydraulic-fracture treatments (Zhang et al., 2009). Typical fracturing process showed in **Figure 2.4** consists of 1) a high viscous fluid, called a pad is pumped to initiate fractures and to establish propagation. This is followed by 2) a slurry of mixed fluid with proppant. This slurry continues to extend fractures and carries the proppant deeply into the fractures. 3) Finally, chemical breakers are injected to lower the viscosity of previously injected fluids. The well is shut-in for a few hours before putting in on production. The fracturing fluid flows

back out of the well leaving highly conductive propped fractures held by the proppant for hydrocarbon (gas) easier to flow from the formations to the well (Gidley et al., 1989). As found by Zanganeh (2014) a fraction of fracturing fluid remains in the matrix around the fracture and reduces its productivity. The complete design of the hydraulic fracturing process is beyond the scope of this study. However, relevant fracturing designed parameters are briefly listed below as a general data set that may be used to assess reservoir-producing potential and to specify an appropriate design for fracturing treatment (Gidley et al., 1989); 1) Well drainage area, 2) vertical distribution of formation net pay, 3) formation permeability, porosity and hydrocarbon saturation, 4) formation fluid properties, 5) reservoir pressure, 6) formation temperature, 7) thermal conductivities of formations penetrated by the fracture, as well as in the vicinity of the fracture, 8) fracture height that will occur during the treatment, 9) fracture closure stress profiles, 10) critical net fracturing pressure, 11) formation effective modulus, Poisson's ratio and density profiles, 12) fracturing-fluid apparent viscosity, 13) fracturing-fluid friction data, 14) fracturing-fluid spurt loss, 15) fracturing fluid combined leakoff coefficient, 16) vertical extent of net leakoff height, 17) fluid thermal properties, 18) proppant size distribution, 19) proppant density, 20) propped fracture conductivity, 21) formation embedment pressure, 22) perforation configuration, and 23) wellhead configuration.

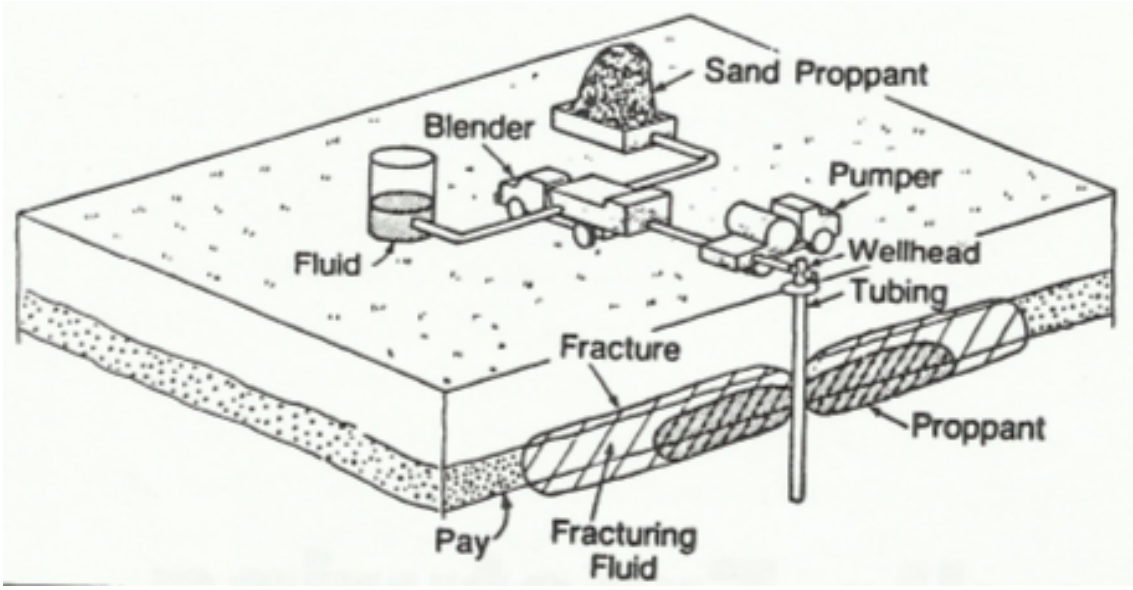

Figure 2.4: Conceptual version of typical fracturing process, (Gidley et al., 1989)

2.3 Hydraulic Fracturing

In designing a successful fracturing treatment, the more complete and consistent of relevant information lead to the more reliable design. Gidley et al. (1989) classified fracturing design parameters into two groups, controllable and uncontrollable parameters. Uncontrollable parameters are generally reservoir characteristics that cannot be modified for instance permeability, porosity, stress level, temperature, pressure etc. Controllable parameters are completion characteristics that can be optimized to increase the treatment effectiveness such as wellbore and wellhead configurations, perforation location and density, fracturing fluid and proppant properties, etc. Three optimizable parameter, fracture length, fracture conductivity and fracture height are important factors directly affecting recovery and production rate that can be at least partially controlled in the fracture treatment.

McGuire and Sikora (1960) studied the effect of vertical fractures on well productivity and released useful result to service companies to be used as a fracturing guidance. The experiment was conducted by creating an electric analogue of drainage system of a well on a computer; various lengths of shunts and resistances were used to represent vertical fractures extending from the well into the reservoir perpendicular to the drainage boundary. Several assumptions were made to reduce the complexity of the system. For instance, all fractures have the same size and they are vertical symmetrically from the well, the reservoir is homogeneous and isotropic. The result was summarized as a chart of productivity index versus dimensionless relative conductivity, which also shows the results experimented by using various fracture lengths. It indicates that in reservoirs with permeability ranged from 1 to 10 md, the productivity index can be increased twofold and sixfold when the relative conductivity is increased from 10^2 to 10^3 and 10^4 respectively. In such range of the permeability, contribution to the productivity of a well from the fracture length is considered relatively minute. This study clearly indicates that the relative conductivity plays a significant role in improving productivity in low-permeability reservoirs, which can be controlled by fracture width with proper concentration of proppant.

Sahai et al. (2013) analyzed the impact of fracture length heterogeneity and non-uniform fracture spacing on well performance and optimal numbers of wells determination. The experiment involved simulating recovery from synthetic wells and actual field cases from Marcellus shale gas wells. The first two synthetic hydraulic fracturing cases are simulated in nano-Darcy range (5-500 nD) reservoir with different type of completions, symmetric (uniform half length) and pyramid (longest half length at the heel). The recovery results show that the longest half-length in each case has strong influence on optimal number of wells required to maximize the recovery regardless the type of completion used. However, the ultimate recovery from the pyramid case is relatively lower than the other despite the same total fracture area because of less contribution from external reservoir volume. This can be concluded that non-uniform fracture half-lengths reduce the

recovery. The second part of the simulation is performed by using uniform spacing (80 ft) and non-uniform spacing (40 ft - 100 ft). The result indicates that the non-uniform fracture spacing reduces the recovery compared to the uniform spacing case; however, it does not affect the optimal number of wells needed per section. The results simulated from actual data collected from Marcellus shale gas wells also confirm the finding of synthetic cases.

Fracture conductivity generally is the product of fracture permeability and fracture width left after the fracture has undergone the closure stress from the formation. Fracture conductivity is one of the most important keys in hydraulic fracturing design. In some circumstances, it can be expressed as dimensionless fracture conductivity to compare the capacity of the fracture to transmit fluids down the fracture and into the wellbore with the ability of the formation to deliver fluids into the fracture (Pearson, 2001)

Lolon et al. (2003) conducted reservoir simulation to determine the effect of fracture conductivity on effective fracture length. The relationship between fracture fluid production, effective length and gas productivity was also studied. One-fourth of a 640-acre rectangle with reservoir permeability in milli-Darcy range (0.05-5 md) is used as drainage area in the simulation model. Frederick and Graves's correlation (1994) is employed in multiphase model (gas/water) to determine non-Darcy flow effects in the fracture. Frederick and Graves's correlation is preferred because in two-phase flow, particularly for high water saturation, this correlation gives more realistic pressure drops in the fracture than Geertsma's correlation (1974). This study also presents the effects of fracturing fluid cleanup and non-Darcy flow on reservoir and fracture properties obtained from pressure transient analysis (PTA). The simulation results show that the effective fracture length is strongly influenced by fracture conductivity. Higher fracture conductivity results in longer effective fracture lengths and greater cumulative gas production because efficient fracturing fluid cleanup increases fracture conductivity. Fracturing fluid remained in the fracture and formation after hydraulic

fracturing treatment can reduce the relative permeability of the gas and block the gas flow into the fracture, thus reduce the effective fracture length. Moreover, effective fracture lengths and fracture conductivity calculated from PTA are relatively lower than actual values in the design due to the cleanup influence at early times and multiphase and non-Darcy flow effects at late times.

A series of laboratory experiments were conducted by Zhang et al. (2013) to measure the hydraulic fracture conductivities in the Barnett shale and determine the effects of proppant size, proppant concentration and closure stress. Modified API conductivity cell was employed in the experiments at room temperature. Fractures are induced along the natural bedding planes to preserve fracture surface asperities. Various sizes of proppants are placed between rough-fracture surfaces at different concentrations. The conductivities are measured by flowing nitrogen through the fractures. The results show that propped fracture conductivity increases with larger proppant size and higher proppant concentration. The results from long-term fracture conductivity measurements also indicate that propped fracture conductivity in this particular shale will reduce approximately 20% in the first 20 hours after hydraulic fracturing treatment and will be somewhat stable for the following 30 hours. We should be aware that these times are very short compared to well producing life.

Since no two shales are alike as mentioned earlier, the fracture treatment type performed in Barnett shale is not applicable in all other shale plays. Consolidated guidelines on how to select the proper fracture treatment type are represented in the comprehensive research done by Ramurthy et al. (2011). The guidelines are made based upon the results from several tests including fluid sensitivity test, Brinell hardness test (BHN), unpropped fracture conductivity test and Diagnostic Fracture Injection test (DFIT). Data sources in this research are collected from major shale plays in the USA, the Gothic, Haynesville, Eagle Ford and Barnett shale plays. Surface area type fracture treatment is the current treatment type being used in Barnett shale. The treatment involved

pumping a large volume of water with small quantities of sand to contact as much surface area as possible and create dendritic type fractures. The applicable shale reservoir has to be conductive for creating dendritic networks, exhibits high brittleness (high BHN), embedment potential is low, and the unpropped fracture conductivity is high. Inversely, shale that exhibits the opposite side of these parameters is applicable for conductivity type fracture treatment, Eagle Ford shale for instance. This method is sometime called hybrid-type fracture treatment where more sand is pumped in conjunction with fluid (water with friction reducer and breaker followed by cross-linked gel) to obtain higher residual dynamic conductivity.

Fracture height has at least two effects on hydraulic fracturing response. When the fracture height increases, the recovery will increase in case it reaches other hydrocarbon-rich zone or intersects natural fracture area in the reservoir adding more communication with the wellbore. However, the stimulation operation may experience difficulties when excessive fracture height takes place. This is because it may reach undesirable zone in the reservoir, gas cap, water-bearing layers or aquifer for instance. That will not only cause less recovery and more remedy expense but also cause the environmental impact such as aquifer contamination. In late 90s, early age of hydraulic fracturing era, most operators controlled the fracture height growth by carefully designed and predicted it (Gidley et al., 1989) and adjusted pump rate, treatment size and rheology of fracturing fluid (Liu et al., 1998). Over decades, many studies show that the in-situ stress contrasts are the largest factor controlling the fracture height, but other factors such as layering and high permeability layers are also controlling the fracture height growth mechanisms (Warpinski, 2011). Based on microseismic fracture-mapping data and proof from mineback collected from major shale plays in the USA by Fisher and Warpinski (2011), it is clear that fractures are much more complex than envisioned by early researchers. In **Figure 2.5**, instead of simple planar fracture presented in the upper left, fractures created by hydraulic fracturing nowadays are becoming more complex network toward the lower right. By this complexity, fracture heights tend to limit themselves and grow shorter. To

summarize, the operation of multi-stage stimulations of shale reservoirs in horizontal wells nowadays is not a threat to aquifer or gas cap via excessive fracture heights.

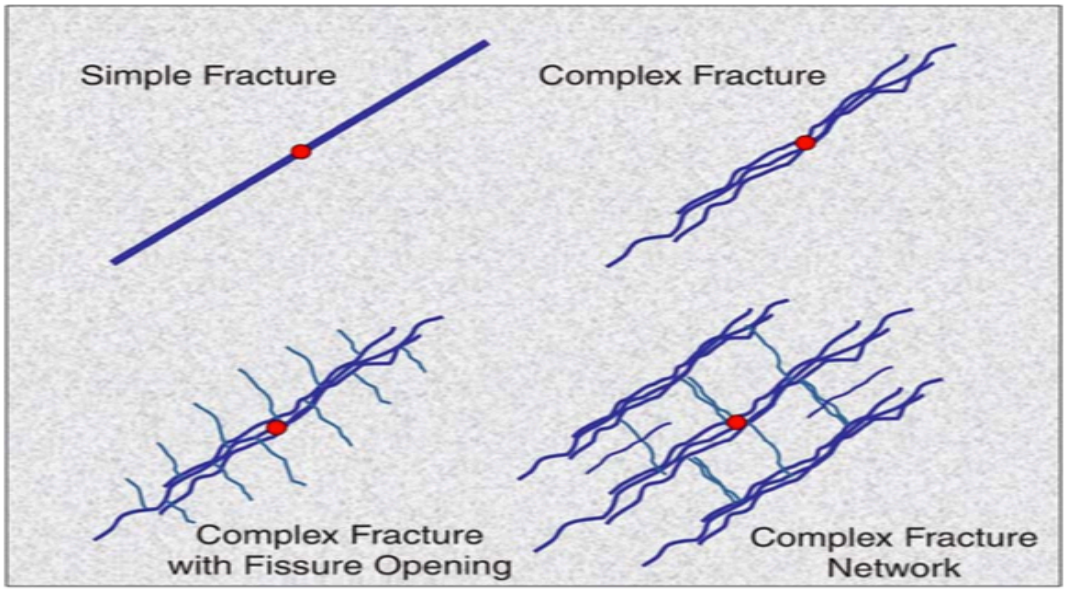

Figure 2.5: Schematics of levels of complexity observed in hydraulic fractures, (Fisher and Warpinski, 2011)

2.4 Production Decline Curve Analysis (DCA)

Hydraulically fractured shale gas wells typically show a unique production decline character. Usual initial gas production rates are relatively low (2-10 MMscf range) and these rates decline steeply during the first year of production by 65-80%. The second-year decline is approximately 35-45%, and the third-year decline is around 20-30%. After the first three years, the production keeps declining at fairly steady rate about 5% per year to abandonment rate that could last for 25 to 30 years (Kennedy et al., 2012). Due to the unique decline rate of shale gas production, many DCA models have been developed to match actual production data for engineers to be able to accurately predict the future production performance.

Arps (1944) introduced the DCA based on graphically extrapolating production semi-log plots (*log* q vs. t) to abandonment rate. Arps classified the declines of production rates into three different types by utilizing the well-known concept of loss ratio and its derivatives: exponential decline, harmonic decline, and hyperbolic decline.

The loss ratio is defined as,

$$\frac{1}{D} = -\frac{q}{dq/dt} \tag{1}$$

Derivative of loss ratio,

$$b = \frac{d}{dt}\left[-\frac{q}{dq/dt}\right] \tag{2}$$

Important assumptions associated with usage of Arps' model are a well exhibits a constant productivity index, drainage radius is constant and production remains at a constant bottomhole pressure.

The three types of declines have b values (Arps' decline exponent) in 0 to 1 range. b = 0 represents the exponential decline, 0 < b < 1 the hyperbolic decline, and b = 1 indicates the harmonic decline. The exponential rate decline relation can be derived for the case of pseudo-steady state flow (boundary-dominated flow, BDF) in a closed reservoir containing slightly compressible fluids with constant bottom-hole pressure (Fetkovich, 1971, Fetkovich, 1980). This model is usually used for single-phase liquid production or high-pressure gas wells (McNeil et al, 2009). Arps' exponential rate decline equation is given as,

$$q = q_i\, e^{-D_i t} \tag{3}$$

Where q is the flow rate at time t, q_i is the initial flow rate and D_i is the initial nominal decline rate.

For the hyperbolic and harmonic rate decline relations, not only they can be derived using the same approach as for the exponential rate relation but they also can be observed in multilayered reservoir during the BDF (Fetkovich et al., 1990). Arps' hyperbolic rate decline equation is typically applied for gas wells (McNeil et al., 2009). The equation is given as,

$$q = q_i (1 + bD_i t)^{-1/b} \quad (4)$$

For Arps' harmonic rate decline equation will be reduced to equation (5) where b = 1,

$$q = q_i (1 + D_i t)^{-1} \quad (5)$$

Arps' models have an important drawback because they are only applicable to the BDF. In typical gas well in shale reservoirs, the transient period is usually longer and the production data that we have may be still in transition zone between transient linear flow and the BDF. Thus using Arps' models (forcing b-values to be greater than 1 to obtain better-looking matches of production history) while b > 1 will give inaccurate estimated reserve and future production trend (McNeil et al., 2009), infinite remaining reserve at infinite time.

Power law exponential model (PLE) is a new approach introduced by Ilk et al. (2008), which is modified from Arps' exponential relation to be able to match production data in both transient linear and BDF flows. The PLE loss ratio is defined as,

$$D = D_\infty + D_1 t^{-(1-n)} \quad (6)$$

Where D_∞ is the decline constant at infinite time, D_1 is the decline constant intercept at one time unit and n is the time exponent.

The first term of the equation (6) represents the loss ratio at the infinite time, which is negligible in early times making model a power law function to match linear or bilinear flow. The second term is

a power law function, which is dominated by the first term in late times making the model to be constant to match the loss ratio of exponential decline (Kanfar and Wattenbarger, 2012).

The PLE rate equation is given as,

$$q = \hat{q}_i \, e^{(-D_\infty t - \frac{D_1}{n} t^n)} \tag{7}$$

Where $\hat{q}_i$ is the rate intercept.

Equation (7) can be reduced to the power law–loss ratio rate decline relation as defined by Ilk et al. (2008),

$$q = \hat{q}_i \, e^{(-D_\infty t - \hat{D}_i t^n)} \tag{8}$$

Where $\widehat{D}_i$ is the decline constant.

Logistic Growth Analysis model (LGA) is one of useful statistical tools widely used to model the population growth. In early development of the LGA, Hubbert (1956) adapted it to model the production in oil and gas industry. Later, Clark et al. (2011) developed the LGA to model growths in cumulative oil and gas production in single wells. The rate and cumulative equations are defined respectively as,

$$q = \frac{Knat^{n-1}}{(a+t^n)^2} \tag{9}$$

$$Q = \frac{Kt^n}{a+t^n} \tag{10}$$

Where *K* is the carrying capacity, *a* is a constant and *n* is a hyperbolic exponent.

Clark et al. (2011) observe that *K* can be considered as EUR without an economic limit and can be estimated by curve fitting. The *n* value is determined using dimensionless rate and cumulative

production terms, which controls the curvature of the decline trend. The constant a is the time to the power n at which half of K is reached that equates to the initial decline D_i in the Arps' DCA models.

Duong's model (2011) is an alternative approach to estimate gas reserve and remaining life of a gas well. The model was developed on the basis that production rate and production time either have a power law relation or display a straight line when plotted on a log-log scale. This model is specifically applicable to wells in which fracture flow is dominant and contribution from the matrix is negligible. Model equations are derived based upon a long-term linear flow in many tight and shale gas reservoirs (Duong, 2011). For field application, the relationship of gas production rate, accumulative production and production time is derived as,

$$\frac{q}{G_p} = at^{-m} \tag{11}$$

The result calculated by equation (11) and plotted on a log-log plot will give a straight line with a negative slope, *-m* and an intercept of *a*. Note that the slope is negative but *m* is always a positive value. Based on the results of Duong's research, the value of *m* is always greater than unity in case of shale reservoirs, and the value of *m* less than unity indicates conventional tight reservoirs. Moreover, while the model is typically accurate for transient linear flow, the beginning of the BDF can also be identified when the production trends curve down from the log-log straight line (Kanfar and Wattenbarger, 2012). Duong's equations for production rate and cumulative are finally derived as,

$$q = q_1 t(a, m) \tag{12}$$

$$G_p = \frac{q_1 t(a,m)}{at^{-m}} \tag{13}$$

Where,

$$t(a,m) = t^{-m} e^{\frac{a}{1-m}(t^{1-m}-1)} \quad (14)$$

Kanfar and Wattenbarger (2012) also summarized the constraints of matching parameters used in each production decline analysis model mentioned earlier to avoid obtaining unreasonable results. The constraints are provided in **Table 2.1**.

Table 2.1: Parameter constraints for each production decline analysis model

Arps			**LGA**		
Parameters	**Min.**	**Max.**	**Parameters**	**Min.**	**Max.**
D	0	10,000	a	10^{-9}	10,000
b	0	5	n	10^{-9}	1
q_i(Mscf/D)	10^{-9}	10^{10}	K (Mscf)	10^{-9}	10^{10}
PLE			**Duong**		
Parameters	**Min.**	**Max.**	**Parameters**	**Min.**	**Max.**
n	0.02	1	a	10^{-9}	10
D_1	0.0001	1	m	10^{-9}	10
D_∞	10^{-9}	1	q_i(Mscf/D)	10^{-9}	10^{10}
q_i(Mscf/D)	10	10^{15}	q_∞(Mscf/D)	-1,000	10,000

Shale gas production declines in five major shale plays including Barnett, Fayetteville, Woodford, Haynesville and Eagle Ford and the capability of Arps' decline analysis models were comprehensively studied by Baihly et al. (2010). The goal of his research is being able to assess the decline trends and estimated ultimate recoveries (EUR) of these shale plays more accurately. The reliability of future production trends and predicted EURs resulted from DCA is strongly influenced by length of production history. The *b* exponent in Arps' DCA generally increases when more

production history is available, which leads to higher forecasted EUR values. However, it is not always true. The DCA results show that the *b* exponent calculated from Barnett shale play decreases with length of production history. Consequently, applying the DCA too early in shale play that exhibiting high initial decline rate will result in an underestimation of EUR. On the other hand, an overestimation of reserves is likely if performs the DCA too early in shale play with gradual decline rate. These observations highlight the uncertainties in accurately predicting EUR where a short period of production data exists.

Vanorsdale (2013) looked into the long-term applicability of PLE and Duong's techniques to estimate reserves in contemporary, high profile shale gas plays. Reserves calculated from Duong and PLE in classic shale gas wells are toward conservative numbers during the first ten years, which indicates there is a single and uniform flow regime. However, multi-stage hydraulically fractured horizontal wells usually undergo many flow regime changes during their producing lives (Thompson et al., 2012). As the results, Duong and PLE techniques may overestimate reserves during the first ten years at this condition.

Meyet et al. (2013) comprehensively studied the uncertainty associated with EUR forecast when using various DCA models including Arps, PLE, LGA and Duong DCA models in comparison to reservoir simulation. The analysis was performed on different unconventional plays having variety of reservoir types, well geometry and fluid types including Barnett Shale in Texas, the Bakken Shale in North Dakota and the Pinedale tight gas sands in Wyoming. The EUR forecast results indicate that the LGA model does not seem to be reliable when data history is very limited because it overestimates the EUR. The authors also suggest that using curve fitting to obtain the carrying capacity (*K)* will produce a more reliable solution. Moreover, the EUR forecasted by PLE and Duong models show slight differences regardless of the production history length across all plays, well

types and fluid types. It is observed that in general, the DCA models seem to converge toward the PLE and Duong's models.

To understand more about the behaviors of different DCA approaches including Arps, LGA, PLE and Duong models, Kanfar and Wattenbarger (2012) applied these DCA simulation results of four different flow regimes and compared them. Two simulation models were created, horizontal well with infinite-conductivity hydraulic fractures and horizontal well with infinite-conductivity hydraulic fractures in naturally fractured formation as showed in **Figure 2.6**. The simulation results show that different DCAs provide different forecasts. Arps' hyperbolic can be fit either bilinear or linear flow with b values of 2 and 4 respectively. However, it cannot model multiple flow regimes. Moreover, all DCA approaches give reasonable forecasts when the flow regime is strictly transient. As we can see from this study, reservoir simulation is a powerful tool to replicate in-situ conditions of the reservoir. However, the accuracy of the model depends on validity of our input data, and proper modeling for fluid flow.

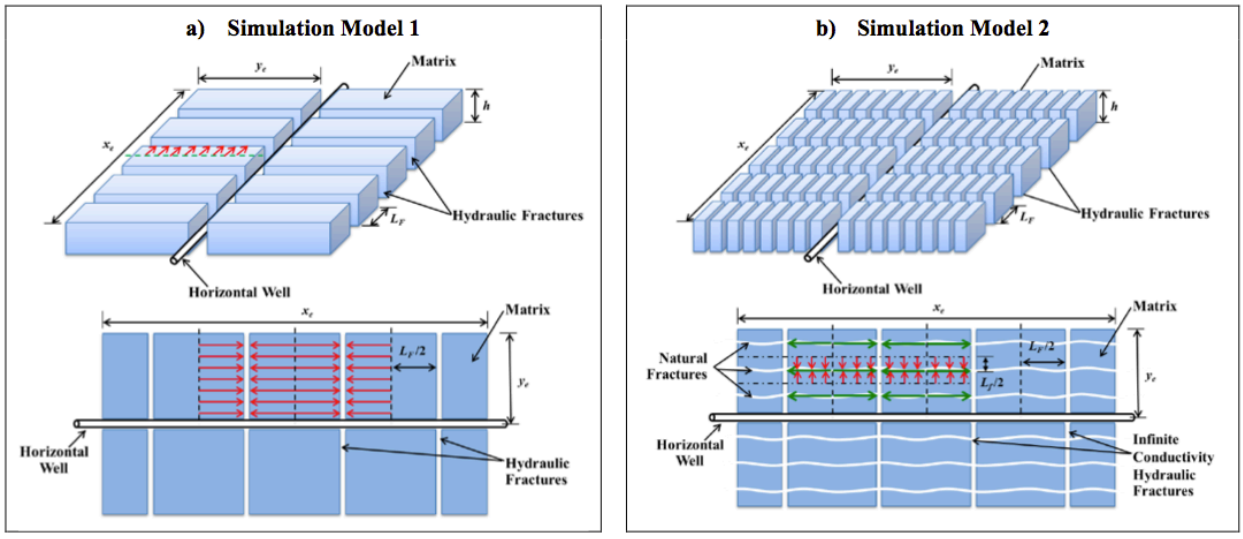

Figure 2.6: a) Horizontal well with infinite-conductivity hydraulic fractures b) Horizontal well with infinite-conductivity hydraulic fractures in naturally fractured formation, (Kanfar and Wattenbarger, 2012)

2.5 Shale Gas Reservoir Simulation and Parameters Affecting Production Trend

The advancement of computing technology has increased the capability of shale gas reservoir simulators to better simulate the impact of variation in reservoir properties and completion characteristics on well performance. Obtaining good history match of a well performance from reservoir simulation is challenging when required valid data is unavailable.

Boulis et al. (2013) described the factors influencing well performance in shale gas reservoirs into three categories: geological and petrophysical parameters impacting amount of the original gas in place (OGIP); rock mechanical properties affecting hydraulic fracturing; and completion and reservoir parameters impacting gas flow in the shale and the wellbore. The synthetic reservoir volume in the simulation employed in this study consists of stimulated reservoir volume (SRV) created by multiple transverse fractures in horizontal well and a volume of undisturbed external reservoir volume (XRV) for a specified drainage area. Basic flow regimes typically found in horizontal well exist in this synthetic case observed from a typical log-log diagnostic plot as showed in **Figure 2.7**.

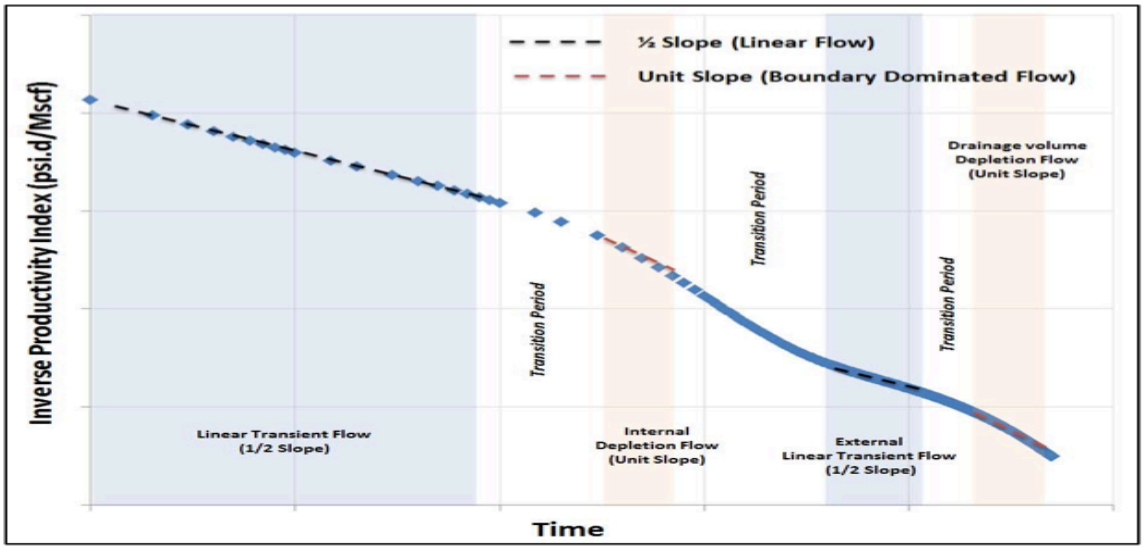

Figure 2.7: A typical log-log diagnostic plot, (Boulis et al., 2013)

Yu and Sepehrnoori (2013) conducted reservoir simulations and production history matching to evaluate the impacts of gas desorption and geomechanics (i.e. stress dependent propped fracture conductivity) on gas production for different shale reservoirs. The simulations were performed on CMG-IMEX simulator using real reservoir data and current configurations of well completions from Barnett, Marcellus, Eagle Ford, Haynesville and New Albany shale plays. Langmuir isotherm in a black oil model and specific compaction data table were integrated within the simulations to model the effects of gas desorption and geomechanics in hydraulic fractures respectively. Their simulation results clearly show that gas desorption increases in EUR of all shale plays approximately 10% to 20% in 30 years of production.

The history matching results also specifically indicate that for low Young's modulus shales, the geomechanical effect is dominant during early period of gas production, while the gas desorption affects more during the late period of the production. Marcellus shale for instance, smaller reduction in fracture conductivity occurred in early time due to the lower closure stress. In case of high Young's modulus shale, Barnett shale for instance, the results note that the gas desorption takes effect only during late period of gas production and geomechanics plays negligible role in gas production.

Hassanpoor et al. (2013) studied in-depth relationship between shale and water (fracturing fluid) that affects the closure stress in shale formation. Hayatdavoudi Hydration Index (HHI) and shale fractal dimension were employed in a model he proposed to describe the relationship between capillary effect, shale-clay type potential, the morphology of the shale aggregate and production decline behavior. Based on the modeling results, placing hydraulic fractures in shale-clays with high HHI and high pseudo-capillary effect will increase hydration stress. The stress adds to the original fracture closure that can cause greater decrease in fracture conductivity; consequently less gas will be produced over time.

Li et al. (2013) presented comprehensive modeling studies using multiple-continuum model to simulate gas production from 5-staged hydraulic fractured horizontal well with single-phase gas flow. The simulation model included adsorption, geomechanics, Klinkenberg and non-Darcy effects in flow modeling. The sensitivity analysis results indicate that adsorption (gas desorption in reality) is the most important effect in increasing cumulative production of shale gas reservoirs. On the other hand, geomechanics (pressure-sensitive rock deformation) provides the negative effect on reducing cumulative production. However, the Klinkenberg effect has little influence on cumulative production at higher pressure.

2.6 Eagle Ford Shale

Ford Shale is a calcareous shale play located in South Texas, US, which lied beneath the Austin Chalk and extends laterally all the way across Texas from the southwest to the northeast part of the state (Inamdar et al., 2010; Stegent et al., 2010; Mullen, 2010). The Eagle Ford Shale, which has been well known as source rock for overlying Austin Chalk, is being developed as a hydrocarbon reservoir (Sondhi, 2011). Its depth ranges from 2,500 ft to 14,000 ft, the thickness ranges from 50 ft to more than 300 ft, the pressure gradients are between 0.4 and 0.8 psi/ft and TOC ranges from 2% to 9% (Stegent et al., 2010). Results from core analysis show that the gas saturation is between 83% and 85%, permeability varies from 1 nd to 800 nd (Inamdar et al., 2010). The hydrocarbon types of Eagle Ford Shale were identified by average GOR from the first three months of production. Fluid types vary from black oil, volatile oil, gas condensate and dry gas. They are correlating with increasing formation depth and thermal maturity (Tian et al., 2013) as showed in **Figure 2.8**.

In late 2008, the first few exploration wells in Eagle Ford were drilled in LaSalle County in the gas window of the play (Stegent et al., 2010). Hydraulic fracturing technique was employed in these wells and initially yielded 7.6 MMscf/day (Sondhi, 2011). Since then, horizontal drilling and

hydraulic fracturing activities have increased tremendously over time. According to the information regarding shale gas play reported by EIA (2011), the average active area in Eagle Ford is 1,100 square mile, depth ranges from 10,500 ft to 13,500 ft, thickness is between 180 ft and 375 ft, average horizontal length ranges from 3,800 ft to 5,500 ft, gas production rate is approximately 6.0 MMscf/day, average EUR is 5.0 Bscf per well and 4 wells per square mile.

The Eagle Ford Shale is a booming young shale play; results indicate there will be development activity for a long time to come. Since no two shales are alike, the more understanding in production decline behaviors will lead to more accurate forecasts.

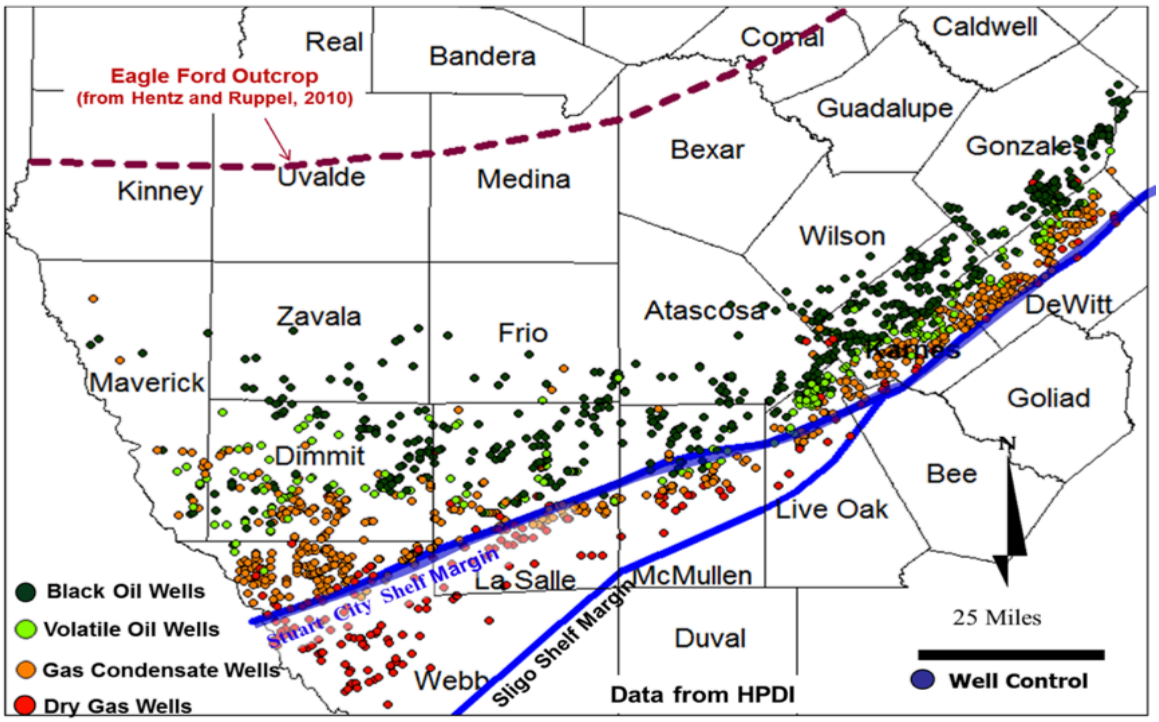

Figure 2.8: Fluid types of Eagle Ford Shale identified by the average GOR from first three months of production, (Tian et al., 2013)

CHAPTER 3

METHODOLOGY AND DATA

3.1 Methodology

The workflow of this study consists of 2 important parts as showed in **Figure 3.1** including data mining (green) and production decline analysis (blue). Gas production history and completion data were collected from 38 wells located in LaSalle County and Webb County in the Eagle Ford shale play. Each selected well is producing only dry gas through a single horizontal wellbore with the employment of multi-stage hydraulic fracturing technique. The production decline analysis part comprises of 4 aspects including determination of possible correlations between completion geometry and well performance, identification of possible flow regime, and application of 6 different DCA models. In the last part the performances of four wells are matched in reservoir simulation and results are used as benchmark to evaluate the performance of the decline curve models.

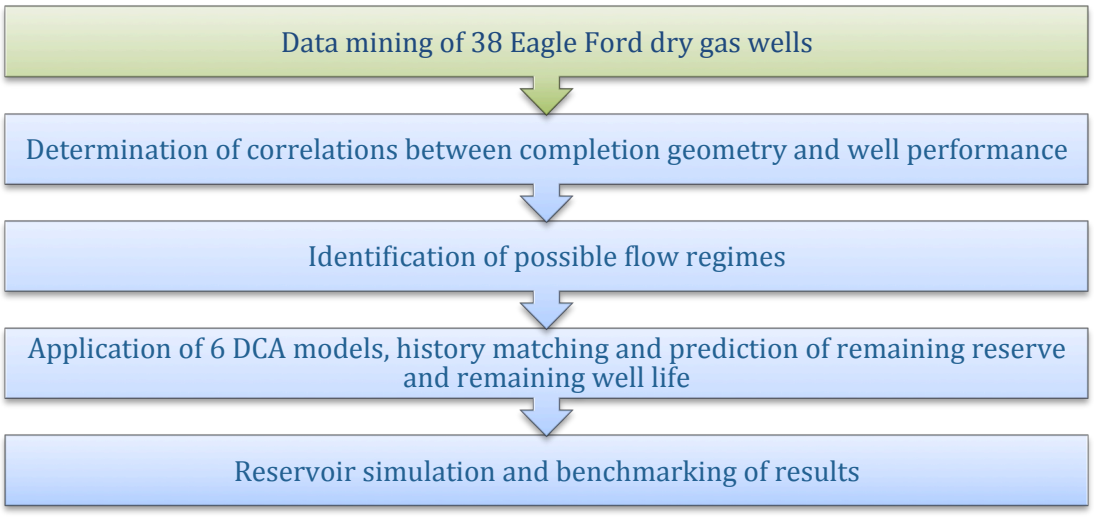

Figure 3.1: Thesis workflow

3.1.1 Possible Correlations between Well Performance and Completion Geometry

In the first part of the analysis, average production rates for the first 12 months of 38 Eagle Ford dry gas wells in both LaSalle and Webb counties have been plotted against horizontal length and number of fracturing stages in order to obtain correlations (if any) between well performance and completion geometry.

3.1.2 Identification of Flow Regimes

Generally, flow regime can be determined from a diagnostic log-log plot of normalized rate with pressure versus time ($[m(p_i) - m(p_{wf})]/q_g$ vs. $t^{0.5}$ plot and ($[m(p_i) - m(p_{wf})]/q_g$ vs. $t^{0.25}$ plot.) However when the pressure data is missing or limited, a simple log-log plot of rate versus time diagnostic plot also can be used. A slope on the diagnostic plot identifies various types of flow regimes. Moreover, a change in the slope indicates a change in flow regime (Okouma et al, 2012):

- Bilinear flow: 1/4 slope – very low conductivity vertical fractures;
- Multi-fracture flow: 1/3 slope – observed occasionally in practice and from simulations with multiple sets of vertical and horizontal fractures;
- Linear flow: 1/2 slope – very high conductivity vertical fractures;
- Boundary-dominated flow (BDF): unit slope – when boundary is reached

Since the pressure data was not available, the simple log-log diagnosis plot of production rate (Mscf/day) versus producing time (days) was employed in this study to identify flow regime of the wells. The flow regime will be used as a criterion in categorizing the wells in conjunction with decline curve analysis results.

3.1.3 Decline Curve Analysis (DCA)

Six different decline curve analysis (DCA) models were employed to evaluate actual production data from Eagle Ford shale gas wells. DCA models consist of Arps' Exponential, Arps' Harmonic, Arps' Hyperbolic, Power Law Exponential (PLE), Logistic Growth Analysis (LGA) and Duong's model. Model parameters of Arps' Hyperbolic, PLE and LGA were estimated via nonlinear regression using Excel-SOLVER.

Forecasting capability of the DCA models was studied by comparing forecasted outcomes (production rates) generated from each model and actual production rate, the part was not used in tuning the DCA models. The first two-third of production data (ended in 2012) was selected to use in the DCA models to forecast future production rate that later was compared to the remaining one-third of the production history and recently updated data (ended in 2013). Likewise, the whole production data history (ended in 2012) was also used in the DCA models for forecasting future production rate and compared with recently updated data (ended in 2013).

The obtained matching results were statistically categorized based on regions, lengths of the available production history and flow regimes to enable observations of the capability of each DCA model.

3.1.4 Reservoir Simulation

This part of this study utilized reservoir simulation models to obtain estimates of remaining reserve and remaining life of 4 select wells (2 wells from LaSalle County and the other 2 wells from Webb County). Actual and researched reservoir characteristics and completion geometry parameters were used to create the simulation models. The remaining reserve and remaining life resulted from the simulation stand as a benchmark in the comparison of them predicted by each DCA model from the select wells. Contrasting the simulation results with the results from decline curve analysis will give better understanding of how gas production is declining and what factors may play a big role in affecting the predictive performance of each DCA model.

3.1.4.1 Description of Simulators

Black-oil reservoir simulator, CMG-IMEX, developed by Computer Modeling Group (CMG) was used in this study to match the history first then forecast future production trend of the select wells. Additional modules of the CMG simulator were also employed to process the data and result. WinProp module is used to build a desirable fluid model that will be used as an input in the simulator. Builder module is a useful tool to create a reservoir model with many options of completion configurations. Simulation result is processed and consolidated by Results Graph module.

FracPro simulator developed by CARBO was used to obtain an optimal hydraulic fracture half-length, amount of hydraulic fracturing fluid injected and hydraulic fracture conductivity distribution along the fracture face.

3.1.4.2 Hydraulic Fracture Design

The first step of the simulation workflow is to model one-fourth of a hydraulic fracture (red dashed rectangular in **Figure 3.2**) to obtain an optimal hydraulic fracture half-length, amount of hydraulic fracturing fluid injected and hydraulic fracture conductivity distribution using the fracturing design software, FracPro. Typical mechanical properties of the Eagle Ford shale play were used in the models as listed in **Table 3.1**.

The creation of the models was broken down into 8-10 sequential propagation stages based on the type and rate of injected fluid and the proppant concentration. The pumping schedules of 4 selected wells (well#1, 16, 26 and 31) are listed in **Tables 3.2 – 3.5**. Moreover, **Figure 3.3 (a-d)** shows the hydraulic fracture conductivity distributions of the final propagation stage of each selected well. Since FracPro assumes both wings of the fracture are equivalent and generates a profile for only one wing, the amount of fluid injected will have to be divided by 2 to be used properly later in the one-fourth model in CMG simulator.

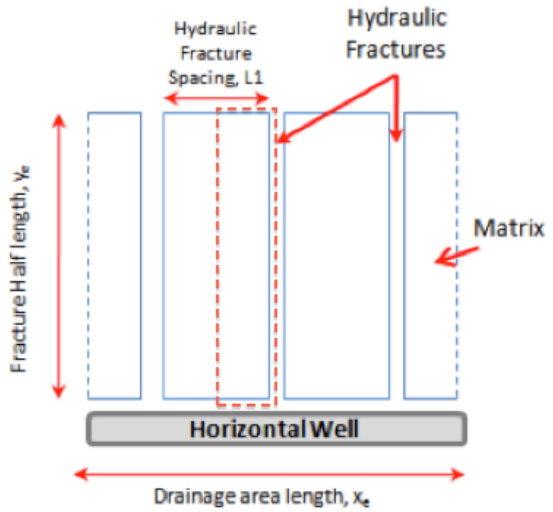

Figure 3.2: 2-D schematic of one wing of a hydraulic fracture. The zone inside red dashed rectangular is chosen for reservoir simulation.

Table 3.1: Summary of mechanical properties used for fracturing design simulation (Manchanda et al., 2012)

Property	Value
Closure Stress Gradient, psi/ft	0.7
Young's Modulus, psi	1,500,000
Poisson's Ratio	0.26
Fracture Toughness, psi.in$^{1/2}$	800
Rock Embedment Strength, psi	40,000

Table 3.2: Hydraulic fracturing fluid pumping schedule of well#1 (8 stages)

Stage Type	Flow Rate (bpm)	Concentration (ppg)	Volume (gal)	Stage Length (min:sec)	Fluid Type	Proppant Type
Main frac pad	65	0	3,000	1:06	Slickwater	
Main frac slurry	65	0.25	2,000	0:44	Slickwater	CarboProp 20/40
Main frac slurry	65	0.5	2,000	0:45	Slickwater	CarboProp 20/40
Main frac slurry	65	0.75	2,000	0:45	Slickwater	CarboProp 20/40
Main frac slurry	65	1	2,000	0:46	Slickwater	CarboProp 20/40
Main frac slurry	65	1.25	20,000	7:39	Slickwater	CarboProp 20/40
Main frac slurry	65	1.5	19,000	7:20	Slickwater	CarboProp 20/40
Main frac flush	65	0	12,012	4:24	Slickwater	

Table 3.3: Hydraulic fracturing fluid pumping schedule of well#16 (10 stages)

Stage Type	Flow Rate (bpm)	Concentration (ppg)	Volume (gal)	Stage Length (min:sec)	Fluid Type	Proppant Type
Main frac pad	65	0	3,000	1:06	Slickwater	
Main frac slurry	65	0.25	2,000	0:44	Slickwater	CarboProp 20/40
Main frac slurry	65	0.5	2,000	0:45	Slickwater	CarboProp 20/40
Main frac slurry	65	0.75	2,000	0:45	Slickwater	CarboProp 20/40
Main frac slurry	65	1	2,000	0:46	Slickwater	CarboProp 20/40
Main frac slurry	65	1.25	2,000	0:46	Slickwater	CarboProp 20/40
Main frac slurry	65	1.5	2,000	0:46	Slickwater	CarboProp 20/40
Main frac slurry	65	1.75	22,000	8:34	Slickwater	CarboProp 20/40
Main frac slurry	65	2	21,000	8:14	Slickwater	CarboProp 20/40
Main frac flush	65	0	14,237	5:13	Slickwater	

Table 3.4: Hydraulic fracturing fluid pumping schedule of well#26 (10 stages)

Stage Type	Flow Rate (bpm)	Concentration (ppg)	Volume (gal)	Stage Length (min:sec)	Fluid Type	Proppant Type
Main frac pad	65	0	2,000	0:44	Slickwater	
Main frac slurry	65	0.25	2,000	0:44	Slickwater	CarboProp 20/40
Main frac slurry	65	0.5	2,000	0:45	Slickwater	CarboProp 20/40
Main frac slurry	65	0.75	2,000	0:45	Slickwater	CarboProp 20/40
Main frac slurry	65	1	2,000	0:46	Slickwater	CarboProp 20/40
Main frac slurry	65	1.25	2,000	0:46	Slickwater	CarboProp 20/40
Main frac slurry	65	1.5	2,000	0:46	Slickwater	CarboProp 20/40
Main frac slurry	65	1.75	17,000	6:37	Slickwater	CarboProp 20/40
Main frac slurry	65	2	16,000	6:17	Slickwater	CarboProp 20/40
Main frac flush	65	0	14,237	5:13	Slickwater	

Table 3.5: Hydraulic fracturing fluid pumping schedule of well#31 (10 stages)

Stage Type	Flow Rate (bpm)	Concentration (ppg)	Volume (gal)	Stage Length (min:sec)	Fluid Type	Proppant Type
Main frac pad	65	0	4,000	1:28	Slickwater	
Main frac slurry	65	0.25	2,000	0:44	Slickwater	CarboProp 20/40
Main frac slurry	65	0.5	2,000	0:45	Slickwater	CarboProp 20/40
Main frac slurry	65	0.75	2,000	0:45	Slickwater	CarboProp 20/40
Main frac slurry	65	1	2,000	0:46	Slickwater	CarboProp 20/40
Main frac slurry	65	1.25	2,000	0:46	Slickwater	CarboProp 20/40
Main frac slurry	65	1.5	2,000	0:46	Slickwater	CarboProp 20/40
Main frac slurry	65	1.75	28,000	10:54	Slickwater	CarboProp 20/40
Main frac slurry	65	2	26,000	10:12	Slickwater	CarboProp 20/40
Main frac flush	65	0	14,237	5:13	Slickwater	

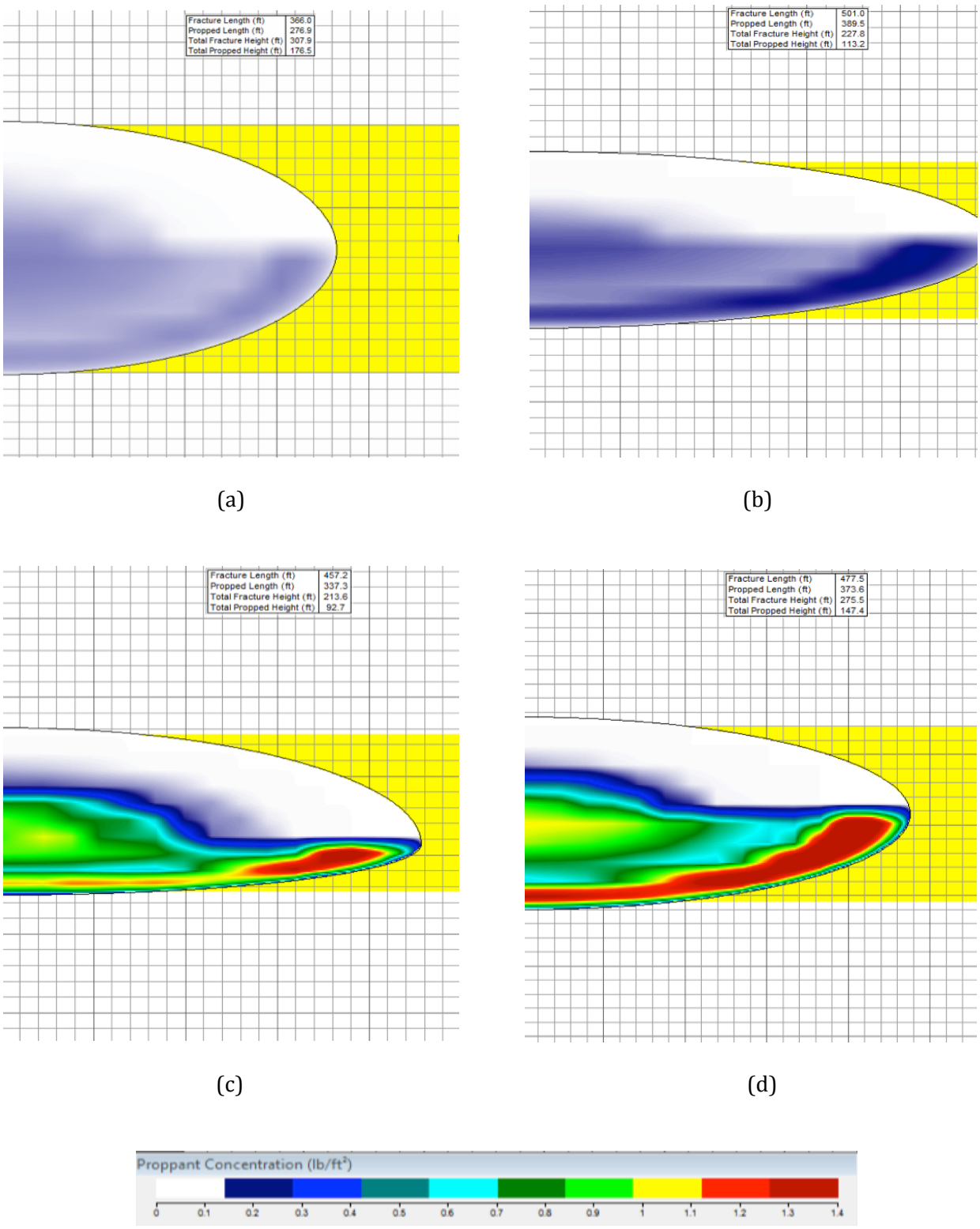

Figure 3.3 (a-d): Final stages of hydraulic fracture propagation of (a) well#1, (b) well#16, (c) well#26 and (d) well#31

3.1.4.3 Simulation Model Description

The completion geometry and configuration of the simulation models were constructed based on a typical completion practice of horizontal well with multiple transverse hydraulic fractures. The vertical wellbore is firstly drilled down to a desirable depth of the Eagle Ford shale formation and then drilled horizontally into layers of the formation for later execution of hydraulic fracturing along the lateral. The model assumptions include

- The reservoir matrix is homogeneous
- The drainage volume equal to the stimulated reservoir volume (SRV)
- Constant fracture spacing
- All hydraulic fractures are the same
- No natural fractures existed since there is no record reported in the database for the select wells used in the simulation

From the model assumptions, fluid in the matrix strictly flows to hydraulic fractures and hydraulic fractures to the wellbore.

Figure 3.4 (a-d) shows 3-D views of one-fourth of a hydraulic fracture model of each selected well built in the CMG-Builder simulator based on the hydraulic fracture half-length estimated by FracPro and actual completion data from TRRC database. The simulation model is divided into 25*16*10 (i*j*k) grid blocks, for the total of 4,000 grid blocks. The grid blocks are logarithmically spaced refined from the proximity of the hydraulic fracture plane (i-j plane) toward the edge of the half fracture spacing (width of the model) to increase accuracy of the simulation. Model thickness (k-axis) is equal to the formation thickness of each particular well (**Tables 3.6 – 3.7**). The hydraulic fracture is modeled with 0.5 ft wide blocks and the fracture permeability profile defined in the model (color ranges in **Figure 3.4 (a-d)**) is back calculated from the fracture conductivity

distribution generated by FracPro since the hydraulic fracture conductivity is equal to fracture permeability (k_f) multiplied by fracture width (W_f). Moreover, the model also accounts the presence of fracturing fluid in the hydraulic fracture prior production commencement.

Since the simulation model represents only a quarter of a hydraulic fracture, the resulted production rates for instance, have to be multiplied by 4 to represent one fracture and then multiplied by number of fracturing stages of each well (**Tables 3.6 - 3.7**) to cover the whole lateral. The assumption of identical hydraulic fracture is not correct based on actual practice but it helps to simplify the study and reduce simulation time.

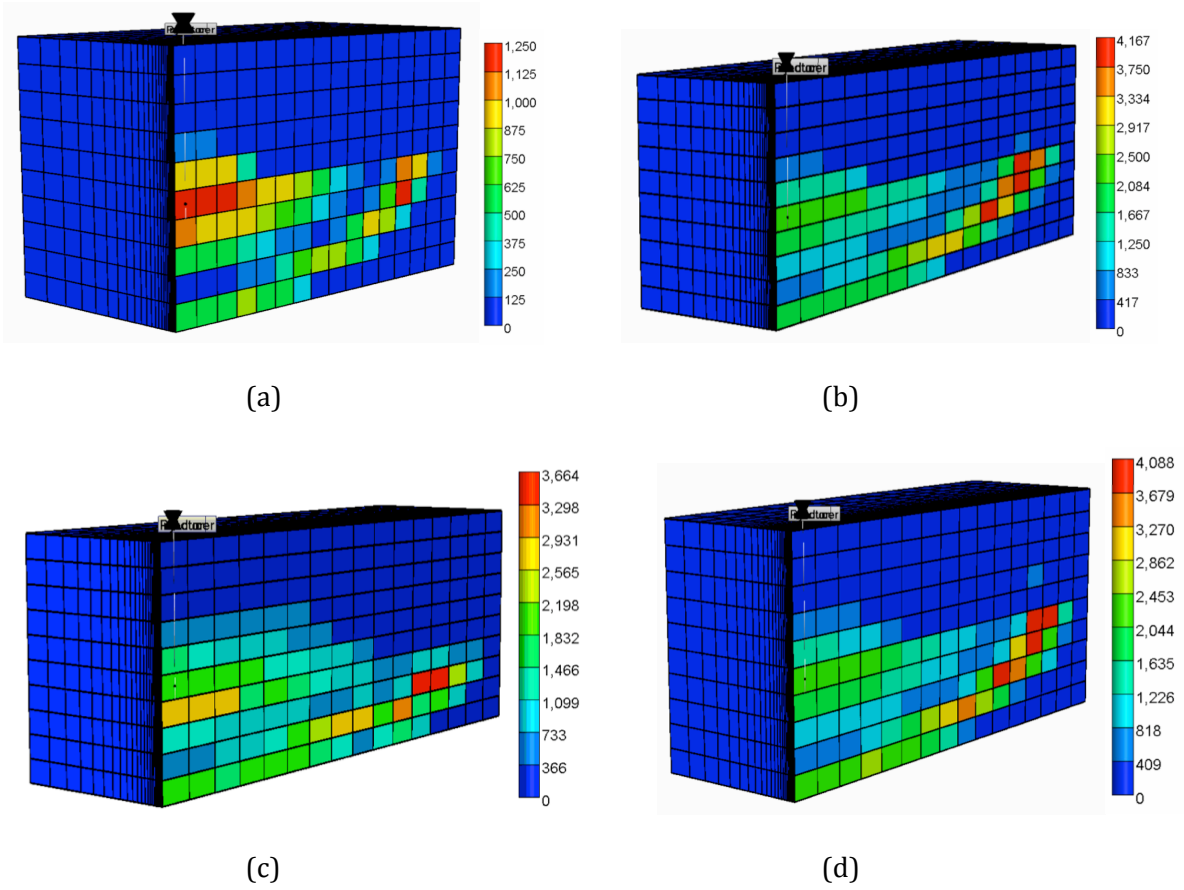

(a) (b)

(c) (d)

Figure 3.4 (a-d): 3-D views of one-fourth of a hydraulic fracture model of (a) well#1, (b) well#16, (c) well#26 and (d) well#31, color ranges represent hydraulic fracture permeability distribution.

Figure 3.5 (a-b) shows an example of the simulation model in details. The simulation model of well#1 is divided into 25*16*10 (i*j*k) grid blocks, for the total of 4,000 grid blocks covering 24 million cubic feet of the matrix volume. Please note that this volume is for a model representing one quarter of fracture as in **Figure 3.2** not the whole well. The grid blocks are logarithmically spaced refined from the proximity of the hydraulic fracture plane (i-j plane) toward the edge of the half fracture spacing (200 ft) in the total of 25 blocks. Model thickness (k-axis) is equal to the formation thickness of this well (10*30 ft = 300 ft thickness). 366 ft is the hydraulic fracture half-length estimated by Fracpro, however in j direction 400 ft was used and divided into 16 equally spaced blocks. The hydraulic fracture is modeled with 0.5 ft wide blocks and the fracture permeability profile defined in the model (color ranges in **Figure 3.5 (a)**) is back calculated from the fracture conductivity distribution generated by FracPro.

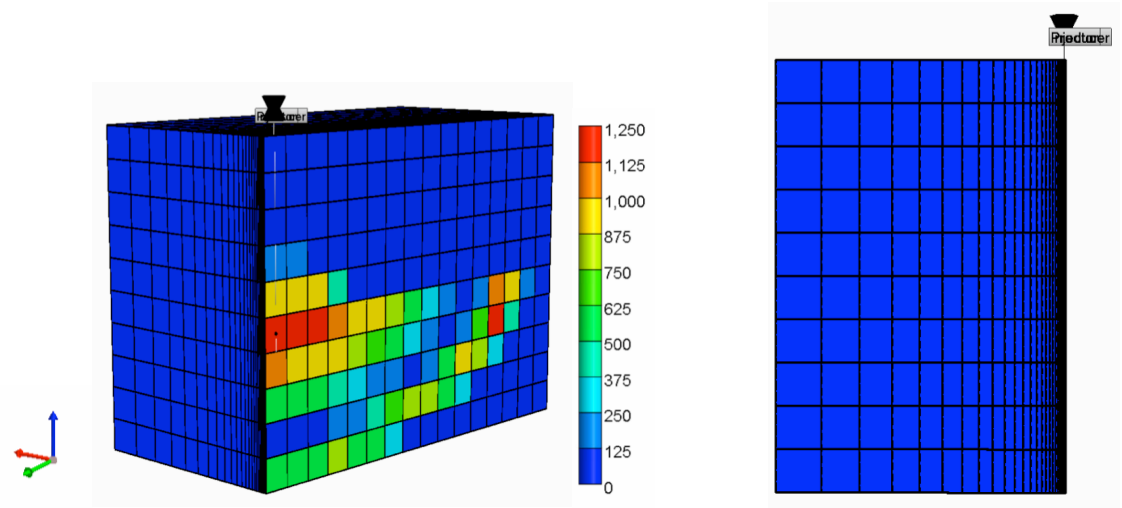

Figure 3.5 (a-b): (a) 2-D (i-k plane) and (b) 3-D views of one-fourth of a hydraulic fracture of well#1 model, color range represents hydraulic fracture permeability distribution.

3.2 Data

3.2.1 Production History

Collecting data was a very critical part of this study. Most of the data used was obtained from two main sources: The Railroad Commission of Texas database (2013) and dissertations on the Eagle Ford Shale play (Ikewun, 2012, Zanganeh, 2014). The importance of data obtained was that the use of realistic data would make results from this study more applicable to be used in real situations.

The wells in this study were specifically selected on the basis of classified as dry gas well, had single well in its unit area and located in LaSalle County and Webb County in the Eagle Ford shale play. The data required for the DCA included production data (production rates, production time and cumulative production) and completion data (horizontal length and number of hydraulic fracturing stages). The summary of the production and completion data can be found in **Appendix I** and **Tables 3.6 – 3.7** respectively.

Table 3.6: Summary of completion data (LaSalle County)

Well Number	Unit/Well	Hydraulic Fracturing Stages	Horizontal Length
1	HENDERSON-CENIZO, Lease No. 251105	10	2,766
2	STS-A, Lease No. 252769	12	3,319
3	MARTIN, DORA 1716, Lease No. 251816	12	4,154
4	NUECES MINERALS COMPANY, Lease No. 251773		4,147
5	HENDERSON-CENIZO, Lease No. 251817	18	4,291
6	HENDERSON-CENIZO, Lease No. 255994	15	4,365
7	NUECES MINERALS COMPANY, Lease No. 255435	17	4,597
8	GOLLA 7, Lease No. 255730	13	3,682
9	CAROLINE PIELOP, Lease No. 254447	16	5,588
10	MARTIN FAMILY, Lease No. 263658		4,343
11	BROWN DISTRIBUTING, Lease No. 25810		5,662
12	BROWN DISTRIBUTING, Lease No. 258900		5,971
13	MARTIN, DORA, Lease No. 257263		4,536
14	MARTIN, DORA, Lease No. 257862		4,971
15	MARTIN, DORA, Lease No. 254843	15	4,817
16	APPLING 695, Lease No. 258036	14	4,257
17	MARTIN UNIT 1, Lease No. 257955		5,406
18	BURKS RANCH EAST, Lease No. 259883		4,750
19	HENDERSON-CENIZO, Lease No. 259429		6,409
20	GUTIERREZ-LEYENDECKER, Lease No. 258903		5,659
21	HEIM, Lease No. 260129		5,020
22	ROBERT GUTIERREZ, Lease No. 260720		4,951
23	APPLING 698 GU, Lease No. 261439		4,899
24	CHALOS MINERALS, Lease No. 260211		5,354

Table 3.7: Summary of completion data (Webb County)

Well Number	Unit/Well	Hydraulic Fracturing Stages	Horizontal Length
25	BENAVIDES, ROSA VELA, Lease No. 258131		3,696
26	GALVAN RANCH, Lease No. 257683	14	3,881
27	STATE OF TEXAS HILL RANCH, Lease No. 257687	10	2,872
28	FASKEN "A" EF, Lease No. 257628	12	3,371
29	NEEL, Lease No. 257685		4,796
30	ROSA V. BENAVIDES, Lease No. 260046		
31	ROSA VELA BENAVIDES, Lease No. 260047	13	4,200
32	FASKEN "A" EF, Lease No. 260071		4,141
33	FASKEN "A" EF, Lease No. 260182		4,125
34	HACHAR, Lease No. 261381		3,762
35	FASKEN A5, Lease No. 260379		4,922
36	ST OF TX-LA CRUZ TRES LAND, LTD., Lease No. 261320		4,702
37	LA CRUZ LAND GAS UNIT, Lease No. 261632		4,672
38	STATE OF TEXAS - A.E. PUIG, Lease No. 261443		3,622

3.2.2 Simulation Parameters

Reliable results from simulation models depend on how valid the input variables are, which make the data very important in creating simulation model. The data required for simulation included model size (formation thickness and lateral length), formation depth, matrix permeability and porosity, relative permeability and capillary pressure data, bottomhole pressure and temperature, desorption parameters (Langmuir pressure and volume), stress sensitive rock mechanics parameter (fracture closure parameter), hydraulic fracturing parameters (fracture half-length, conductivity, spacing, and width) and gas gravity to generate PVT data. The data used for simulation models were obtained from previous work done on the Eagle Ford presented in

technical papers. Other simulation data were obtained from the Texas Railroad Commission website. The summary of the simulation of the selected wells is tabulated in **Table 3.8.**

Table 3.8: Simulation parameters of 4 selected wells

Parameter	Well#1	Well#16	Well#26	Well#31
Formation thickness, ft	300	200	200	250
Formation depth, ft	11,000	12,693	10,847	13,160
Depth of water-gas contact, ft	15,000	15,000	15,000	15,000
Horizontal leg, ft	4,000	4,200	3,920	4,160
Number of fracturing stages	10	14	14	13
Hydraulic fracture spacing, ft	400	300	280	320
Hydraulic fracture half-length, ft	366	501	457	478
Fracture width, ft	0.5	0.5	0.5	0.5
Bottomhole temperature, °F	301	328	291	337
Initial bottomhole pressure, psi	8,300	8,500	8,000	9,000
Gas gravity	0.660	0.643	0.595	0.591
Medium permeability, nD	10	30	20	10
Un-propped zone permeability, nD	100	300	200	100
Langmuir volume, scf/ton	175	175	175	175
Langmuir pressure, psi	1500	1500	1500	1500
Matrix porosity, %	6	6	6	5
Initial water saturation, %	30	30	30	30
Reservoir rock compressibility, psi^{-1}	10^{-6}	10^{-6}	10^{-6}	10^{-6}
Maximum surface gas rate, MMscf/day	10	10	10	10
Minimum bottom hole pressure, psi	1,500	1,500	1,500	1,500
Amount of water injection, bbl	29,530	48,158	40,825	52,147

Desorption parameters integrated with simulation models used in both reservoir matrix and hydraulic fractures were obtained from previously studied literatures on the Eagle Ford (Freeman et al., 2009; Yu and Sepehrnoori, 2013). The desorption parameters includes ranges of Langmuir volumes and pressures. Langmuir volume measured in scf/ton is referred to as the gas volume at the infinite pressure representing the maximum storage capacity for gas; Langmuir pressure measured in psi is defined as the pressure corresponding to one-half Langmuir volume. It is noted that higher Langmuir pressure releases more adsorbed gas at the same reservoir pressure (Yu and Sepehrnoori, 2013). Langmuir isotherm is shown in **Figure 3.6.**

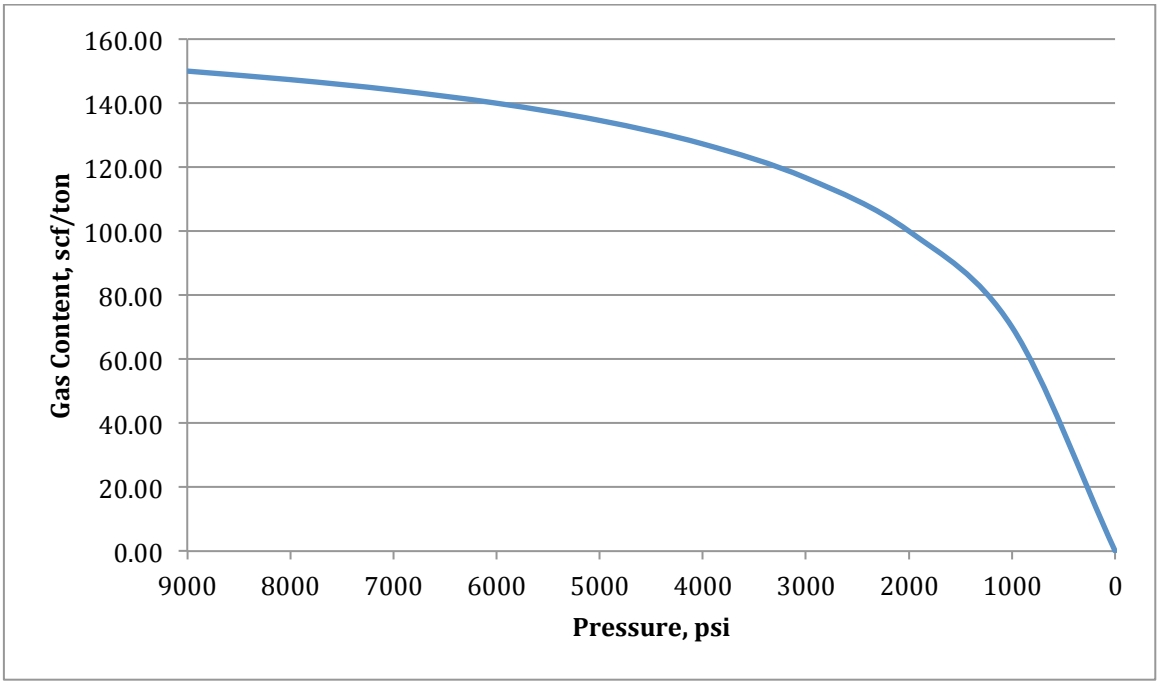

Figure 3.6: Langmuir isotherm

Fracture closure parameter was also obtained from previous studies summarized in public literature (Orangi et al., 2011). The literature provides fracture permeability multipliers with pressure based on laboratory tests performed on the rock samples from the Eagle Ford as showed in **Figure 3.7**.

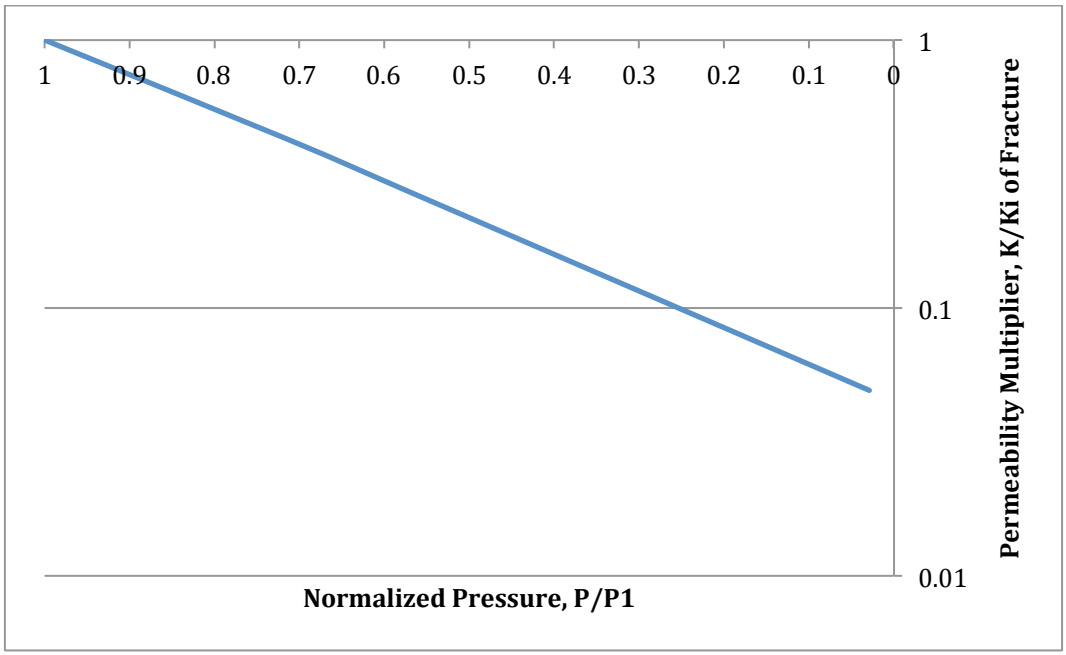

Figure 3.7: Pressure-dependent permeability multipliers for hydraulic fractures

Effect of non-Darcy flow was also included in the simulation models to account the fluid flow that deviates from Darcy's law, which assumes laminar flow in the formation. The non-Darcy flow is typically observed in high-rate gas wells when the flow converging to the wellbore reaches flow velocities exceeding the Reynolds number for Darcy flow and results in turbulent flow. It is recommended by CMG to use General Correlation from non-Darcy flow options for simulation models with gas and water phases (no oil or solvent). The correlation is defined only in the grid blocks representing the hydraulic fracture. Relevant coefficients of the General Correlation are listed in **Table 3.9**.

Table 3.9: Non-Darcy coefficients of General Correlation by CMG

Phase	Alpha	N1	N2	Forchheimer Maximum
Gas	1.48×10^9	1.021	0	10,000
Water	1.48×10^9	1.021	0	10,000

CHAPTER 4

RESULTS AND DISCUSSION

4.1 Correlations between Well Performance and Completion Geometry

Actual production data and completion information of 38 Eagle Ford wells in LaSalle and Webb counties have been specifically selected on the basis of having single wellbore and producing only dry gas. All the selected wells have been completed horizontally and producing solely dry gas in Eagle Ford shale that lies between Austin chalk and Edwards limestone (Sondhi, 2011). Minimum horizontal length is 2,766 ft and the maximum is 6,409 ft with number of hydraulic fracturing stages in range of 10-18. The wells used in this study are considered very young due to their relatively short production history (18-43 month range). Using the data collected from these two neighboring counties, LaSalle and Webb, would allow varieties of reservoir characteristics and completion techniques to be accounted as possible factors affecting well performance. Hence it would provide an opportunity to obtain more realistic correlations (if any) between well performance and completion practices. In this part of the study, average production rate of the first 12 months of each well have been calculated (**Table 4.1**) and plotted against completion geometry (horizontal length and hydraulic fracturing stages) (**Figures 4.1 – 4.6**).

Table 4.1: Summary of completion data and first year average production rate (LaSalle County)

Well Number	Hydraulic Fracturing Stages	Horizontal Length	Average Production Rate, Mscf/Day
1	10	2,766	2,957.5
2	12	3,319	2,085.6
3	12	4,154	2,656.3
4		4,147	1,853.5
5	18	4,291	3,212.5
6	15	4,365	3,128.5
7	17	4,597	2,646.2
8	13	3,682	2,779.0
9	16	5,588	4,245.2
10		4,343	1,341.8
11		5,662	2,621.0
12		5,971	2,460.0
13		4,536	1,895.9
14		4,971	1,592.7
15	15	4,817	1,369.6
16	14	4,257	3,045.3
17		5,406	1,922.0
18		4,750	3,042.4
19		6,409	4,584.7
20		5,659	4,003.0
21		5,020	5,969.8
22		4,951	5,012.6
23		4,899	2,643.0
24		5,354	2,485.1

Table 4.2: Summary of completion data and first year average production rate (Webb County)

Well Number	Hydraulic Fracturing Stages	Horizontal Length	Average Production Rate, Mscf/Day
25		3,696	1,182.4
26	14	3,881	2,079.6
27	10	2,872	1,410.2
28	12	3,371	3,463.2
29		4,796	1,548.0
30			1,547.4
31	13	4,200	1,547.5
32		4,141	4,394.3
33		4,125	4,586.9
34		3,762	1,875.1
35		4,922	4,767.3
36		4,702	973.7
37		4,672	1,997.4
38		3,622	1,595.0

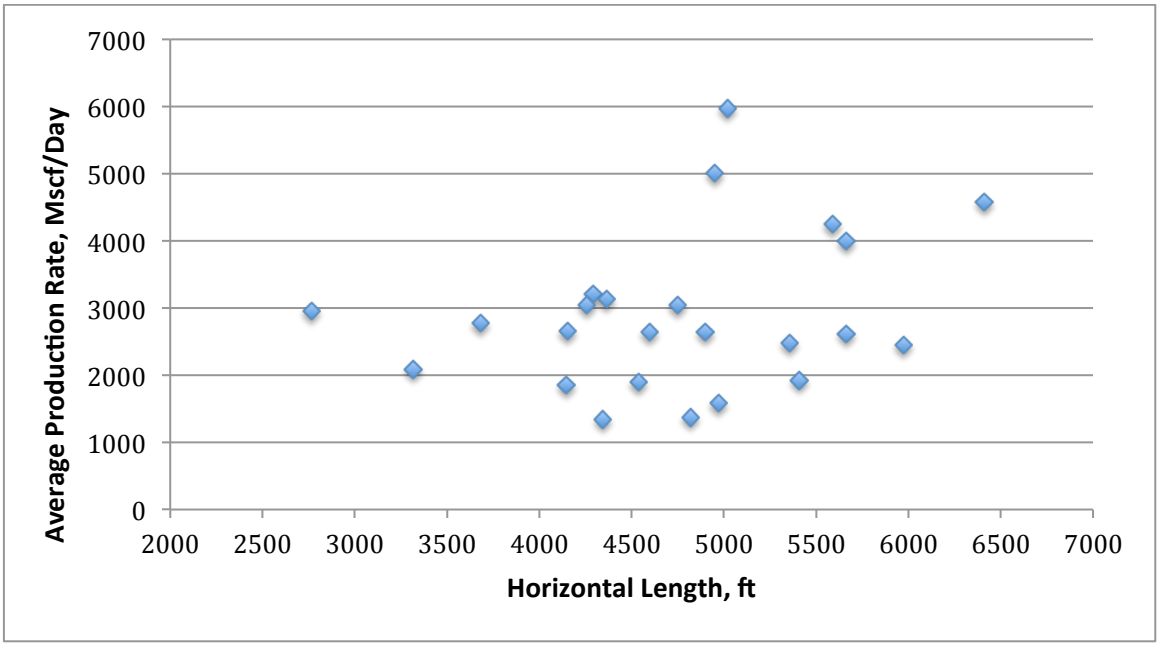

Figure 4.1: Average production rate (first 12 months) vs. horizontal length, LaSalle County

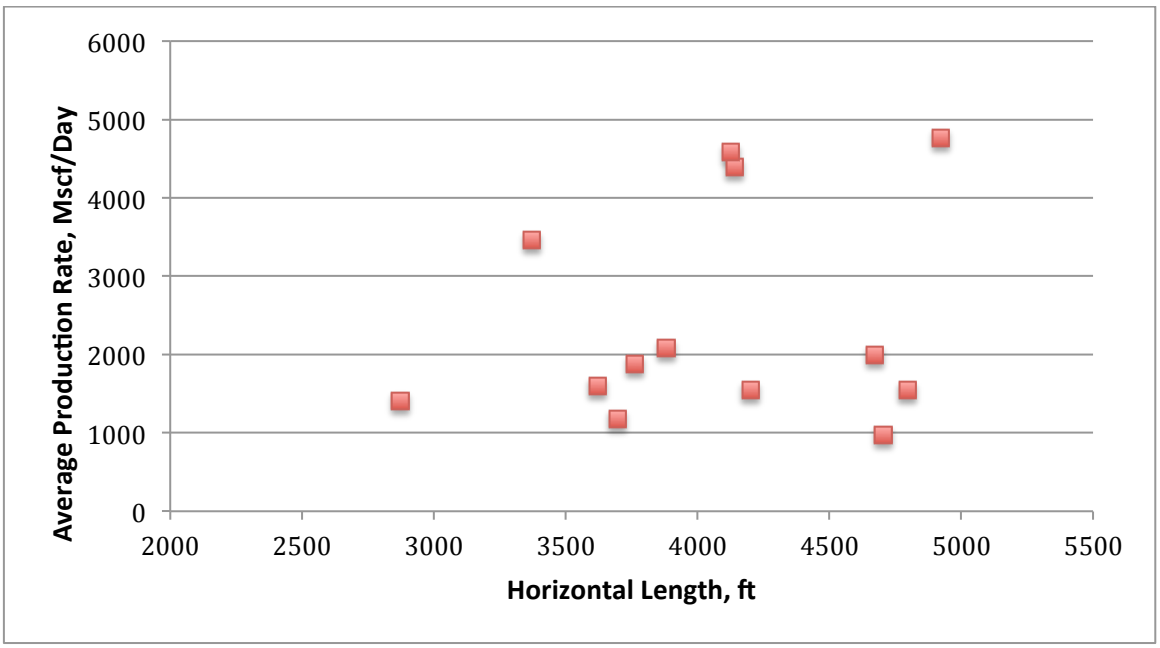

Figure 4.2: Average production rate (first 12 months) vs. horizontal length, Webb County

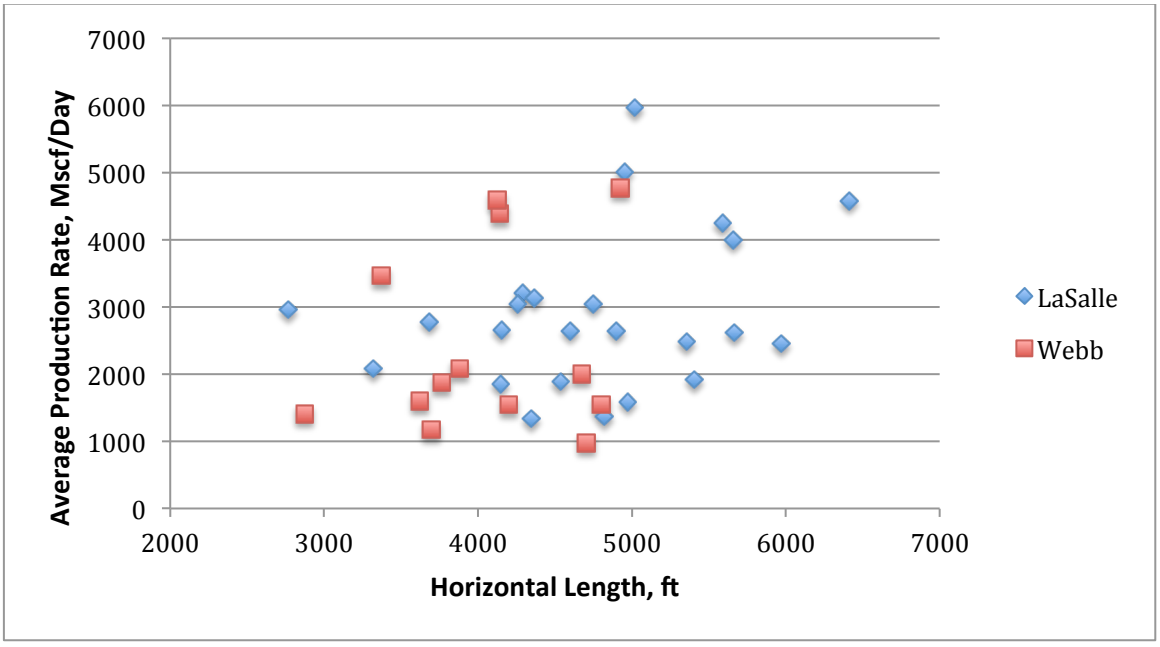

Figure 4.3: Average production rate (first 12 months) vs. horizontal length, LaSalle and Webb

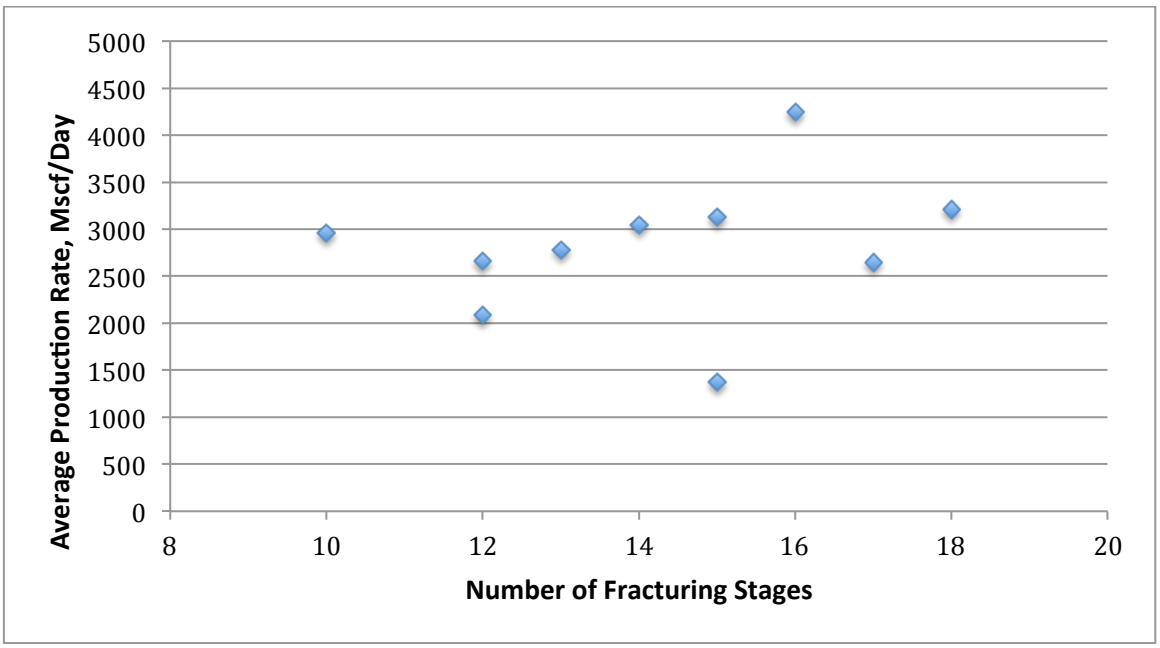

Figure 4.4: Average production rate (first 12 months) vs. fracturing stages, LaSalle County

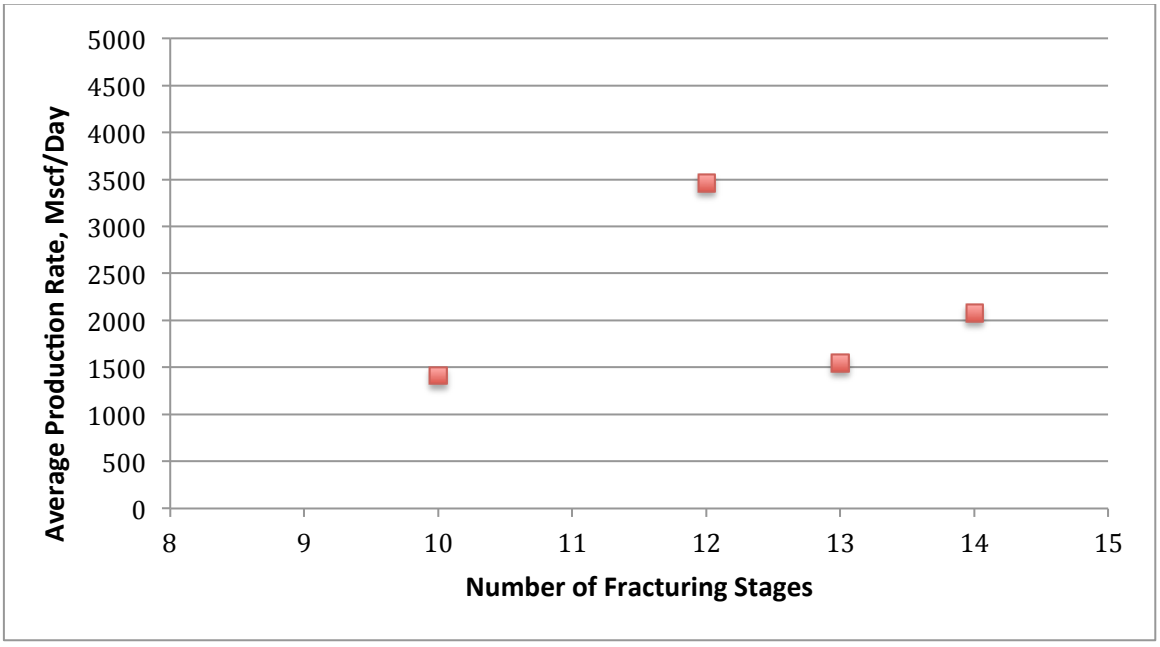

Figure 4.5: Average production rate (first 12 months) vs. fracturing stages, Webb County

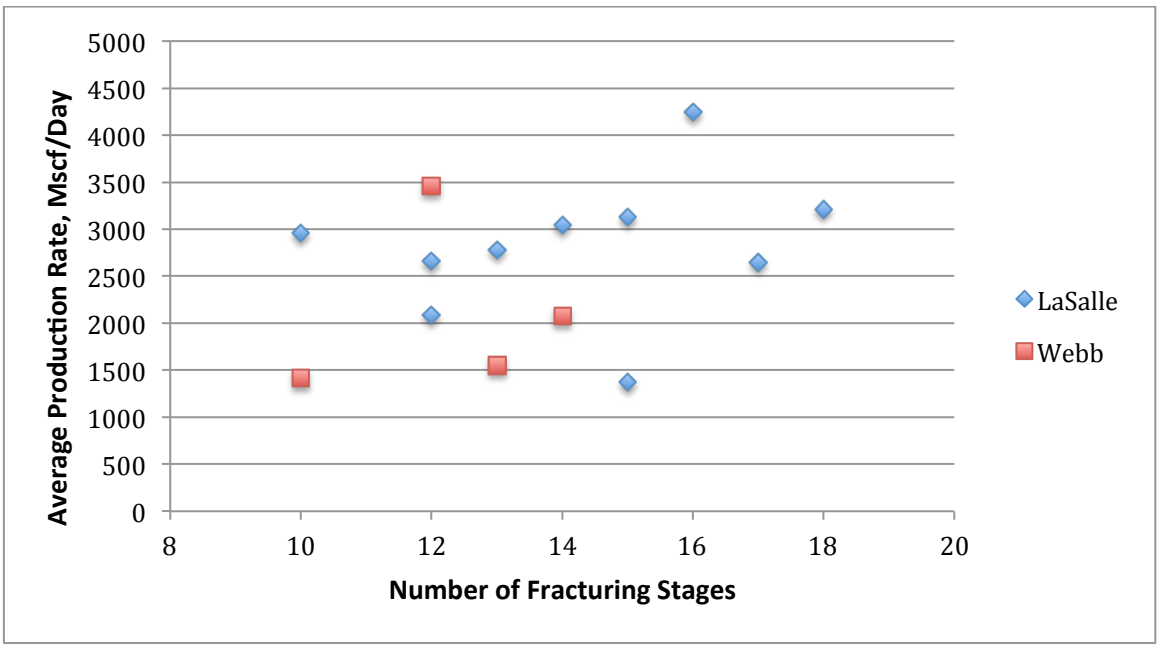

Figure 4.6: Average production rate (first 12 months) vs. fracturing stages, LaSalle and Webb

4.2 Observation and Discussion

As average production rate for the first 12 months has been used as a proxy of well performance in this part of the study, observations can be drawn from **Figures 4.1 – 4.6** that there is no strong correlations between well performance and completion practices both horizontal length of wellbore and number of hydraulic fracturing stages for the wells in these two counties. However, the combined result trends in **Figure 4.3** and **Figure 4.6** exhibited slightly upward trends. The results may be implied that when horizontal length of wellbore is extended further into layers of shale, more contact area would be in the reservoir, which increases an opportunity for hydraulic fracturing design to be able to reach more sweet spots along the lateral and result in higher production rate. Likewise, more hydraulic fracturing stages in the wellbore could also increase the production rate as more gas flows to the wellbore from increased number of potential sweet spots. Moreover, there are other possible factors that may affect well performance for instance variation

of reservoir characteristics. The results suggest that reservoir simulation is required for better understanding of other relevant factors that may contribute to well performance in shale gas reservoirs. The final remark is that shales are very heterogeneous and there is no guarantee as increasing horizontal length or number of fracturing stages would necessary increase the production rate proportionally.

4.3 Decline Curve Analysis – History Matching Results

In this aspect of the study, 6 different decline curve analysis (DCA) models including Arps' Exponential, Arps' Harmonic, Arps' Hyperbolic, Power Law Exponential (PLE), Logistic Growth Analysis (LGA) and Duong's Model were applied on 24 wells from LaSalle County and 14 wells from Webb County. Results from history matching between actual production data and DCA-model-generated data would provide more understanding of predictive capability of the DCA models. Two sets of production data from each well (first two-third data and whole data) were selected to use in each DCA model separately to be able to see how well each DCA model performs in matching past history when different length of production data is used as input.

Table 4.3: History matching summary (LaSalle County)

Well No.	Arps' Harmonic			Arps' Hyperbolic			PLE			LGA			Duong		
	2/3	2/3*	W	2/3	2/3*	W	2/3	2/3*	W	2/3	2/3*	W	2/3	2/3*	W
1	1	1	1	0	0	1	0	0	1	1	1	1	1	1	2
2	1	1	1	1*	1*	2	0	0	2	2	2	2	2	2	2
3	0	0	1	0	0	0	0	0	1	1	1	1	1	1	2
4	0	0	0	0	0	0	2	2	2	2	2	1	1	1	2
5	0	0	1	0	0	0	0	0	1	1	1	1	1	1	2
6	1	1	1	0	0	1*	1	1	1	1	1	1	2	2	2
7	0	0	0	0	0	0	0	0	0	1	1	1	1	1	1
8	1	1	1	1	1	1	1	1	1	2	2	2	2	2	1
9	0	0	1	0	0	0	0	0	1	0	0	0	2	2	2
10	0	0	0	0	0	0	0	0	0	0	0	0	1	1	1
11	0	0	2	0	0	1	0	0	1	2	2	2	2	2	2
12	0	0	0	0	0	1*	1	1	1	2	1	1	2	2	2
13	0	0	1	0	1*	0	1	1	1	1	1	1	2	2	2
14	0	0	0	0	0	0	0	0	2	1	1	1	1	1	2
15	1	1	1	1*	1*	1*	1	1	1	1	1	1	2	2	2
16	1	1	1	0	1	2	0	0	1	1	1	1	2	2	2
17	0	0	1	0	0	1*	0	0	2	0	0	0	1	1	2
18	2	2	2	1	1	1*	0	0	2	1	1	1	2	2	2
19	1	1	1	0	0	0	0	0	1	1	1	1	1	1	2
20	0	0	0	0	0	1*	1	1	1	0	0	0	2	2	2
21	0	1	1	0	0	1	0	0	1	1	1	1	0	1	2
22	0	0	1	0	0	1	1	1	1	1	1	1	2	2	2
23	2	2	2	0	0	1*	0	0	0	1	1	1	2	2	2
24	2	2	1	2	2	2	0	0	0	1	1	1	2	1	1

2/3 – Using the first two-third of production data in DCA models to match the rest one-third
2/3* – Using the first two-third of production data in DCA models to match the rest one-third and 12 months of recently updated data
W – Using whole production data in DCA models to match 12 months of recently updated data
0, 1, 2 – Under predicted, matched and over predicted respectively
1* – Matched (b>1 for Arps' Hyperbolic Model)
Arps' Exponential model is excluded from the table since its diagnostic plots indicate unsuitability

Table 4.4: History matching summary (Webb County)

Well No.	Arps' Harmonic			Arps' Hyperbolic			PLE			LGA			Duong		
	2/3	2/3*	W	2/3	2/3*	W	2/3	2/3*	W	2/3	2/3*	W	2/3	2/3*	W
25	1	1	1	0	0	0	1	1	1	1	1	1	2	2	2
26	2	2	2	0	0	2	1	1	1	1	1	1	2	2	2
27	0	0	0	0	0	0	0	0	0	0	0	0	1	1	1
28	0	0	0	0	0	0	0	0	0	0	0	0	1	0	0
29	0	0	0	0	0	0	1	1	0	0	0	0	2	2	2
30	0	0	0	1*	1*	0	0	0	0	0	0	0	2	2	2
31	1	1	1	0	0	0	0	0	0	1	1	1	2	2	2
32	1	1	1	0	0	0	0	0	0	1	0	0	2	1	1
33	2	2	2	0	0	0	0	0	0	0	0	0	1	1	1
34	1	1	1	0	0	0	0	0	0	0	0	0	1	1	1
35	1	0	0	0	0	0	0	0	0	0	0	0	2	0	0
36	1	1	1	2	2	1	1	1	1	1	1	1	2	2	1
37	2	0	0	0	0	0	1	0	0	1	0	0	2	2	1
38	2	0	0	0	0	0	0	0	1	1	1	1	2	2	2

2/3 – Using the first two-third of production data in DCA models to match the rest one-third
2/3* – Using the first two-third of production data in DCA models to match the rest one-third and 12 months of recently updated data
W – Using whole production data in DCA models to match 12 months of recently updated data
0, 1, 2 – Under predicted, matched and over predicted respectively
1* – Matched (b>1 for Arps' Hyperbolic Model)
Arps' Exponential model is excluded from the table since its diagnostic plots indicate unsuitability

Tables 4.5 and **4.6** show the summary of flow regimes of each individual well in LaSalle and Webb counties respectively. Detailed diagnosis plots of the wells can be found in Appendix III. The results show that 20 out of 24 wells or approximately 83% in LaSalle County are still in the transient flow until the end of 2012 and only remaining 4 wells or 17% exhibiting transient flow at early dates and BDF at late time. For Webb County, the production trends in 10 out of 14 wells or 71% show the transient flow regime and the remaining 4 wells or 29% show both transient flow and BDF. The flow regime of total of 38 wells in both counties in general is 79% exhibiting only transient flow and

21% showing transient flow at early time and BDF at late time. Moreover, when adding recently updated data in the diagnosis plots, 3 more wells in LaSalle County including well#1, #6 and #21 started to show BDF.

Table 4.5: Summary of flow regime of wells in LaSalle County

Well Number	Flow Regime
1	Linear flow and BDF (shows when added more updated data)
2	Linear flow and BDF (shows at 550 days)
3	Linear flow
4	Linear flow
5	Linear flow
6	Linear flow and BDF (shows when added more updated data)
7	Linear flow
8	Linear flow and BDF (shows at 300 days)
9	Linear flow
10	Linear flow
11	Linear flow
12	Linear flow
13	Linear flow
14	Linear flow
15	Linear flow
16	Linear flow and BDF (shows at 400 days)
17	Linear flow
18	Linear flow
19	Linear flow
20	Linear flow
21	Linear flow and BDF (shows when added more updated data)
22	Linear flow
23	Linear flow
24	Linear flow and BDF (shows at 100 days)

Table 4.6: Summary of flow regime of wells in Webb County

Well Number	Flow Regime
25	Linear flow and BDF (shows at 200 days)
26	Linear flow and BDF (shows at 400 days)
27	Linear flow
28	Linear flow
29	Linear flow
30	Linear flow
31	Linear flow and BDF (shows at 100 days)
32	Linear flow
33	Linear flow and BDF (shows at 250 days)
34	Linear flow
35	Linear flow
36	Linear flow
37	Linear flow
38	Linear flow

4.3.1 Arps' Exponential Decline Curve Analysis

Arps utilized the concept of loss ratio by using its derivative (b) equal to zero representing an exponential decline trend.

4.3.2 Observation and Discussion

Semi-log production rate vs. producing time and production rate vs. cumulative production plots generated by Arps' exponential model did not (simultaneously) exhibit straight lines for all 38 wells in LaSalle and Webb counties. **Figures 4.7** and **4.8** are selected examples of Arps' exponential diagnosis plots. **Figure 4.7 (a-d)** included the diagnosis plots of dry gas wells #1 and #10 in LaSalle County with the production history of maximum 43 months and minimum 18 months respectively. Likewise **Figure 4.8 (a-d)** showing the diagnosis plots of dry gas wells #29 and #35 in Webb County with the production history of maximum 30 months and minimum 18 months respectively. The plots did not give a straight line regardless of the length of the production history. This suggests that Arps' exponential model is not applicable with the production decline trend from dry gas wells in LaSalle and Webb counties.

One uncertainty that may affect Arps' exponential diagnosis plots is the fluctuation of the production data. Based upon the information collected from TRRC database, there is no record regarding additional operation activities, such as changing choke size that might be employed during the production period to justify/identify noises in production data. Moreover, when a well is shut-in for certain period of time, down hole pressure will build up causing the relatively high initial rate when the well is put back online.

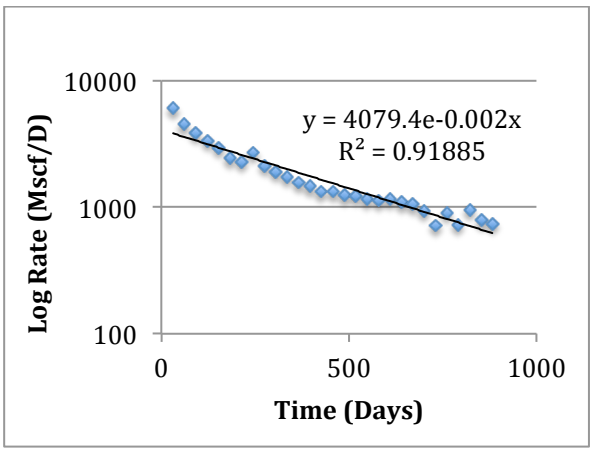

(a)

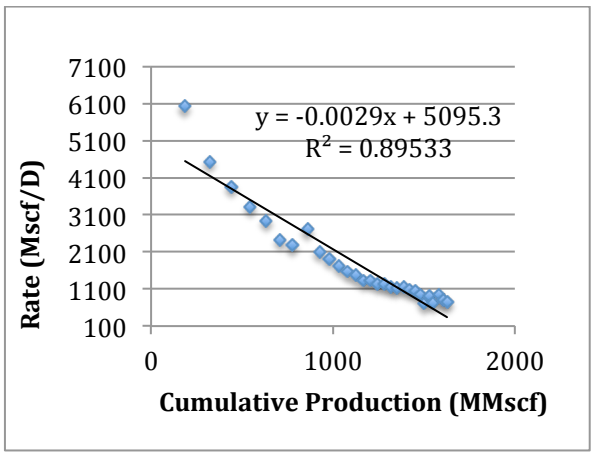

(b)

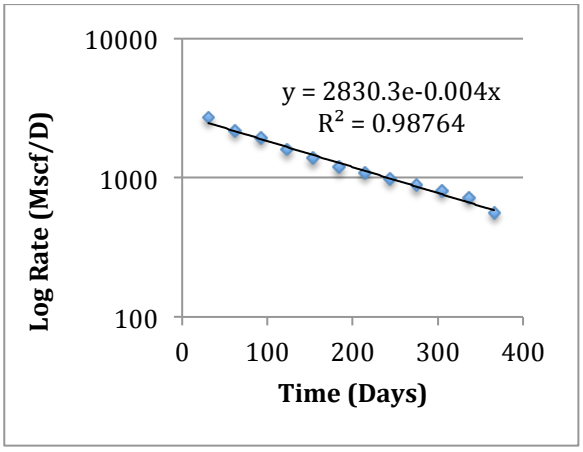

(c)

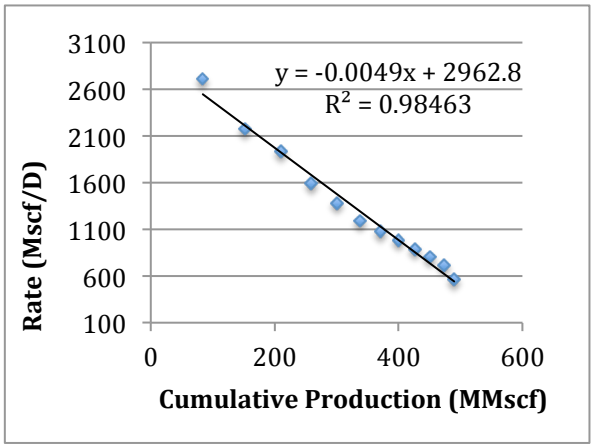

(d)

Figure 4.7 (a-d): Arps' Exponential decline diagnostic plots for (a-b) well#1 and (c-d) well#10

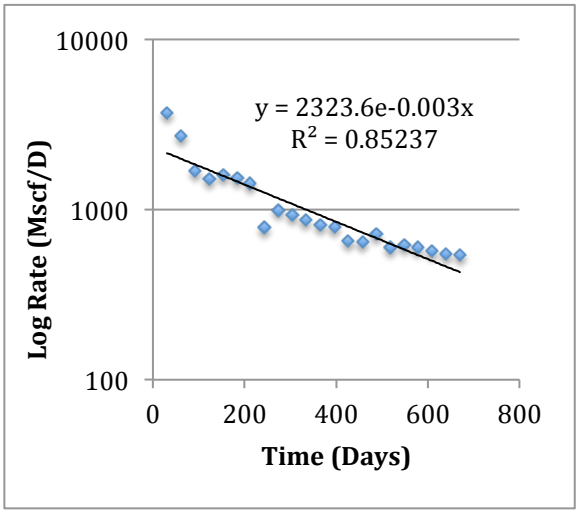

(a)

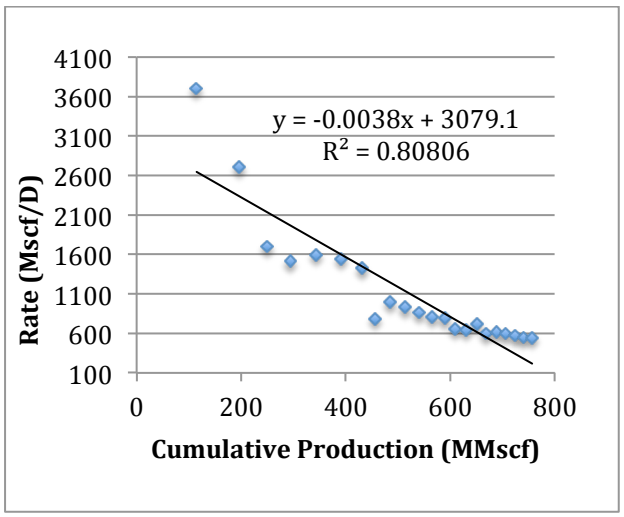

(b)

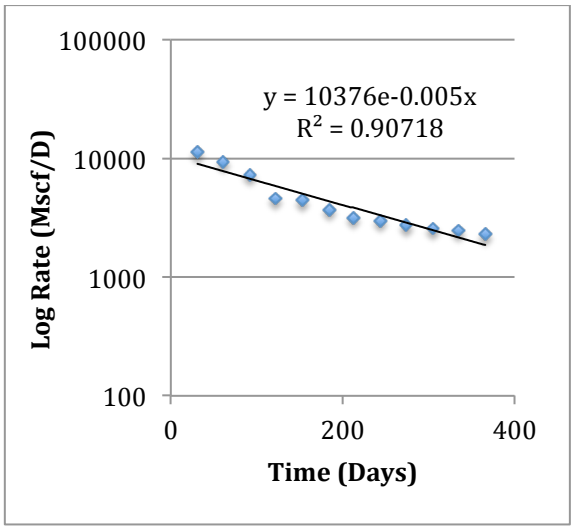

(c)

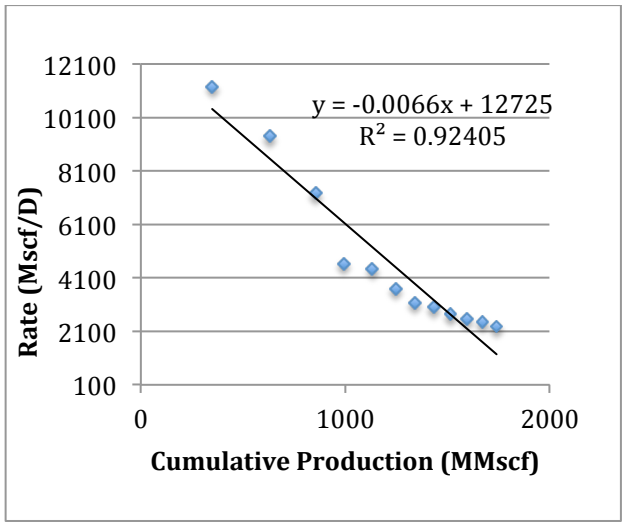

(d)

Figure 4.8 (a-d): Arps' Exponential decline diagnostic plots for (a-b) well#29 and (c-d) well#35

4.3.3 Arps' Harmonic Decline Curve Analysis

Similarly to Arps' exponential decline model, harmonic decline model can be derived by utilizing the concept of loss ratio but given its derivative (b) equal to unity. **Tables 4.7** and **4.8**, are representing the summary of the associated parameters in Arps' Harmonic model including initial rate (q_i) and initial decline constant (D_i) calculated from dry gas wells in LaSalle and Webb counties respectively. Matching results of the individual well can be found in **Appendix II**, which have been done by mean of visual observation between the forecasts from Arps' Harmonic model and their actual production history. The history matching is conducted in 3 different approaches based on different length of the production history used as input;

- Using the first 2/3 of the data ended in 2012 as input and compare with the remaining 1/3 of the data ended in 2012.
- Using the first 2/3 of the data ended in 2012 as input and compare with the remaining 1/3 of the data ended in 2012 plus 12 more months of recently updated data ended in 2013 which is named as extended forecast.
- Using the whole data ended in 2012 as input and compare with the 12 months of recently updated data ended in 2013.

Table 4.9 summarizes the numbers of the wells from the matching results, which are classified into 3 types, matched, under-predicted and over-predicted based on different length of the production history. For better clarification, **Table 4.9** is calculated as percentage and plotted in bar charts based on each county as showed in **Figures 4.9** through **4.11**. **Figure 4.12** also shows the matching results based on different types of flow regimes including the wells showing only transient flow and the wells showing both transient flow and BDF.

Table 4.7: Arps' Harmonic decline model parameters, LaSalle County wells

Well Number	Model Parameters	Value Calculated Using 2/3 Data	Value Calculated Using Whole Data
1	Initial Rate, q_i (Mscf/day)	7,230.1	5,800.0
	Initial Decline Constant, D_i (1/day)	0.00723	0.00661
2	Initial Rate, q_i (Mscf/day)	5,830.7	5,614.6
	Initial Decline Constant, D_i (1/day)	0.01166	0.01123
3	Initial Rate, q_i (Mscf/day)	8,287.4	5,064.6
	Initial Decline Constant, D_i (1/day)	0.01657	0.00506
4	Initial Rate, q_i (Mscf/day)	4,167.0	3,706.2
	Initial Decline Constant, D_i (1/day)	0.00833	0.00741
5	Initial Rate, q_i (Mscf/day)	10,062.0	7,585.9
	Initial Decline Constant, D_i (1/day)	0.02012	0.00759
6	Initial Rate, q_i (Mscf/day)	7,365.2	6,265.8
	Initial Decline Constant, D_i (1/day)	0.00737	0.00627
7	Initial Rate, q_i (Mscf/day)	8,164.2	7,852.0
	Initial Decline Constant, D_i (1/day)	0.01633	0.01570
8	Initial Rate, q_i (Mscf/day)	7,979.8	10,243.0
	Initial Decline Constant, D_i (1/day)	0.01596	0.02049
9	Initial Rate, q_i (Mscf/day)	9,746.1	8,728.4
	Initial Decline Constant, D_i (1/day)	0.00877	0.00698
10	Initial Rate, q_i (Mscf/day)	3,920.1	3,879.7
	Initial Decline Constant, D_i (1/day)	0.01568	0.01552
11	Initial Rate, q_i (Mscf/day)	6,640.7	6,208.6
	Initial Decline Constant, D_i (1/day)	0.01328	0.00621
12	Initial Rate, q_i (Mscf/day)	6,162.9	5,668.4
	Initial Decline Constant, D_i (1/day)	0.01233	0.01134
13	Initial Rate, q_i (Mscf/day)	3,754.7	3,134.7
	Initial Decline Constant, D_i (1/day)	0.00751	0.00313
14	Initial Rate, q_i (Mscf/day)	3,610.6	2,990.8
	Initial Decline Constant, D_i (1/day)	0.00722	0.00598
15	Initial Rate, q_i (Mscf/day)	2,682.4	2,409.3
	Initial Decline Constant, D_i (1/day)	0.00536	0.00482

Table 4.7: Continued

Well Number	Model Parameters	Value Calculated Using 2/3 Data	Value Calculated Using Whole Data
16	Initial Rate, q_i (Mscf/day)	5,946.4	5,721.5
	Initial Decline Constant, D_i (1/day)	0.00595	0.00572
17	Initial Rate, q_i (Mscf/day)	3,935.3	3,159.2
	Initial Decline Constant, D_i (1/day)	0.00787	0.00316
18	Initial Rate, q_i (Mscf/day)	6,563.1	6,599.2
	Initial Decline Constant, D_i (1/day)	0.00656	0.00660
19	Initial Rate, q_i (Mscf/day)	17,447.0	14,205.0
	Initial Decline Constant, D_i (1/day)	0.01745	0.01421
20	Initial Rate, q_i (Mscf/day)	8,960.0	8,036.4
	Initial Decline Constant, D_i (1/day)	0.00806	0.00643
21	Initial Rate, q_i (Mscf/day)	15,624.0	12,266.0
	Initial Decline Constant, D_i (1/day)	0.01094	0.00736
22	Initial Rate, q_i (Mscf/day)	14,266.0	11,643.0
	Initial Decline Constant, D_i (1/day)	0.01284	0.00815
23	Initial Rate, q_i (Mscf/day)	5,870.7	5,756.6
	Initial Decline Constant, D_i (1/day)	0.00587	0.00576
24	Initial Rate, q_i (Mscf/day)	17,653.0	20,947.0
	Initial Decline Constant, D_i (1/day)	0.05296	0.08379

Table 4.8: Arps' Harmonic decline model parameters, Webb County wells

Well Number	Model Parameters	Value Calculated Using 2/3 Data	Value Calculated Using Whole Data
25	Initial Rate, q_i (Mscf/day)	4,972.9	5,085.5
	Initial Decline Constant, D_i (1/day)	0.02486	0.02543
26	Initial Rate, q_i (Mscf/day)	3,696.1	3,765.8
	Initial Decline Constant, D_i (1/day)	0.00370	0.00377
27	Initial Rate, q_i (Mscf/day)	3,889.2	3,568.5
	Initial Decline Constant, D_i (1/day)	0.01167	0.01071
28	Initial Rate, q_i (Mscf/day)	12,922.0	11,951.0
	Initial Decline Constant, D_i (1/day)	0.02584	0.02390
29	Initial Rate, q_i (Mscf/day)	4,080.9	3,769.6
	Initial Decline Constant, D_i (1/day)	0.01224	0.01131
30	Initial Rate, q_i (Mscf/day)	6,748.2	6,074.0
	Initial Decline Constant, D_i (1/day)	0.02699	0.02430
31	Initial Rate, q_i (Mscf/day)	6,815.4	7,004.4
	Initial Decline Constant, D_i (1/day)	0.02726	0.02802
32	Initial Rate, q_i (Mscf/day)	12,775.0	12,562.0
	Initial Decline Constant, D_i (1/day)	0.01278	0.01256
33	Initial Rate, q_i (Mscf/day)	17,619.0	18,057.0
	Initial Decline Constant, D_i (1/day)	0.01762	0.01806
34	Initial Rate, q_i (Mscf/day)	7,395.8	8,052.4
	Initial Decline Constant, D_i (1/day)	0.02219	0.02416
35	Initial Rate, q_i (Mscf/day)	18,193.0	16,110.0
	Initial Decline Constant, D_i (1/day)	0.01819	0.01611
36	Initial Rate, q_i (Mscf/day)	3,771.0	3,937.7
	Initial Decline Constant, D_i (1/day)	0.02263	0.02363
37	Initial Rate, q_i (Mscf/day)	6,422.6	6,441.1
	Initial Decline Constant, D_i (1/day)	0.01927	0.01932
38	Initial Rate, q_i (Mscf/day)	4,619.0	4,046.8
	Initial Decline Constant, D_i (1/day)	0.01386	0.01214

Table 4.9: Result summary of Arps' Harmonic decline model predictive performance

County	Predictive Performance	Number of Wells		
		Using 2/3 Data	Using 2/3 Data (Compared with recently updated data)	Using Whole Data
LaSalle	Matched	7	8	15
	Under Predicted	14	13	6
	Over Predicted	3	3	3
Webb	Matched	6	5	5
	Under Predicted	6	7	7
	Over Predicted	2	2	2
Total	Matched	13	13	20
	Under Predicted	20	20	13
	Over Predicted	5	5	5

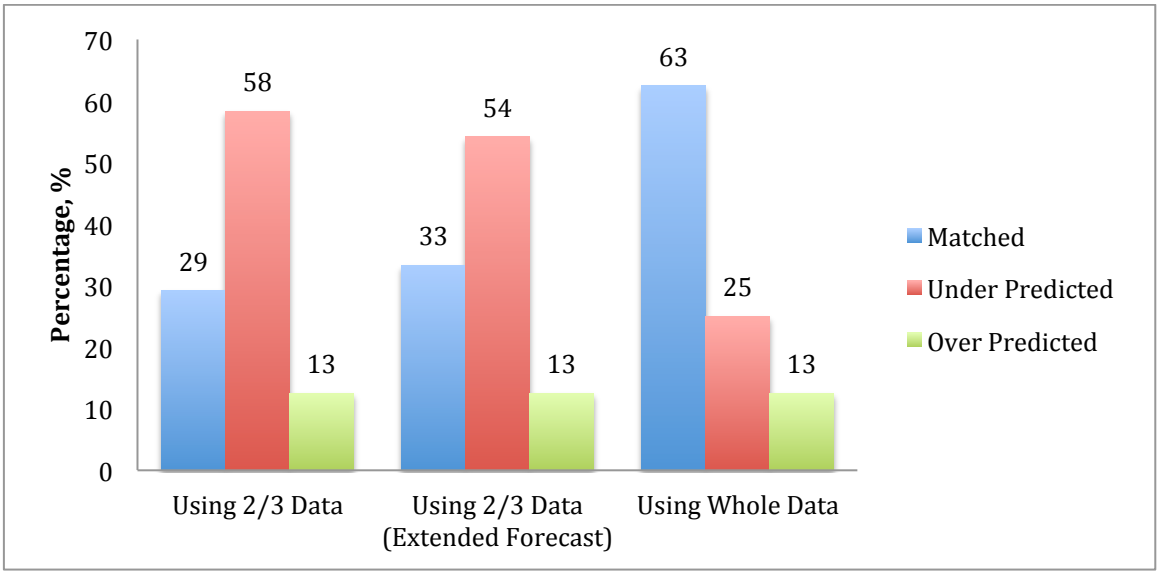

Figure 4.9: Arps' Harmonic decline model predictive performance (LaSalle County)

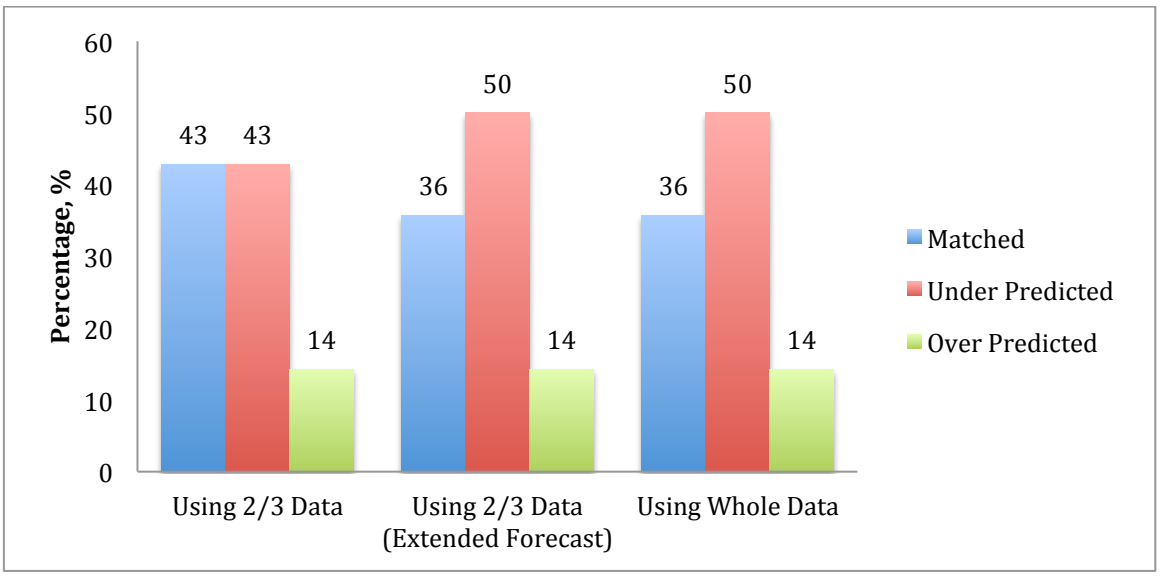

Figure 4.10: Arps' Harmonic decline model predictive performance (Webb County)

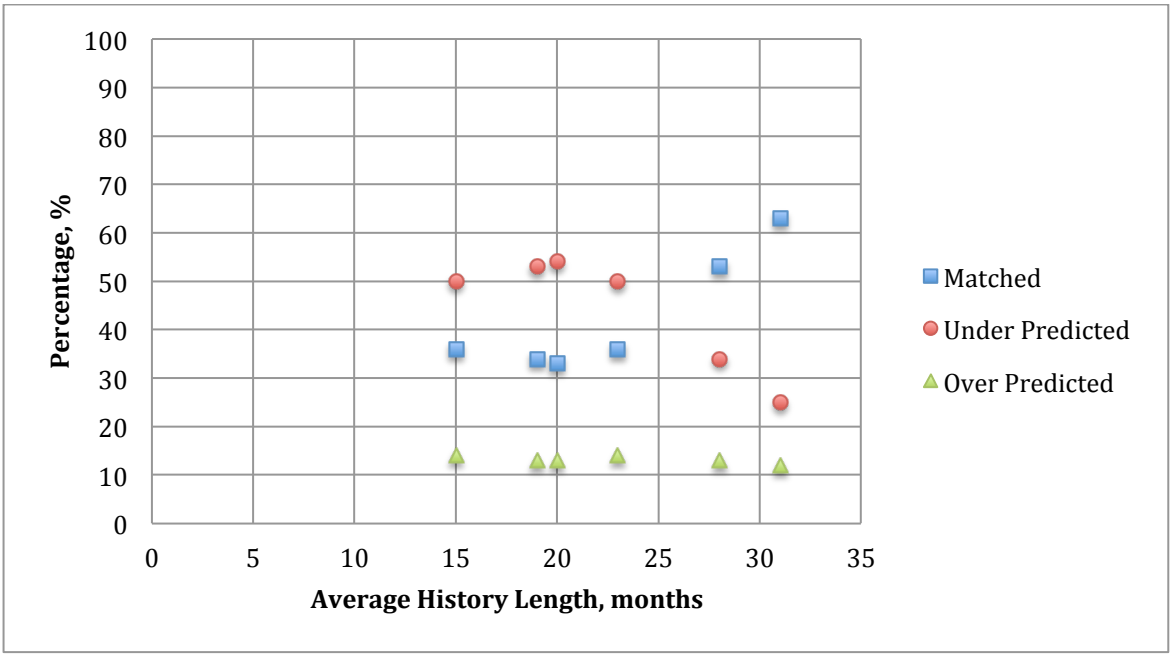

Figure 4.11: Summary of Arps' Harmonic decline model predictive performance based on different production history length

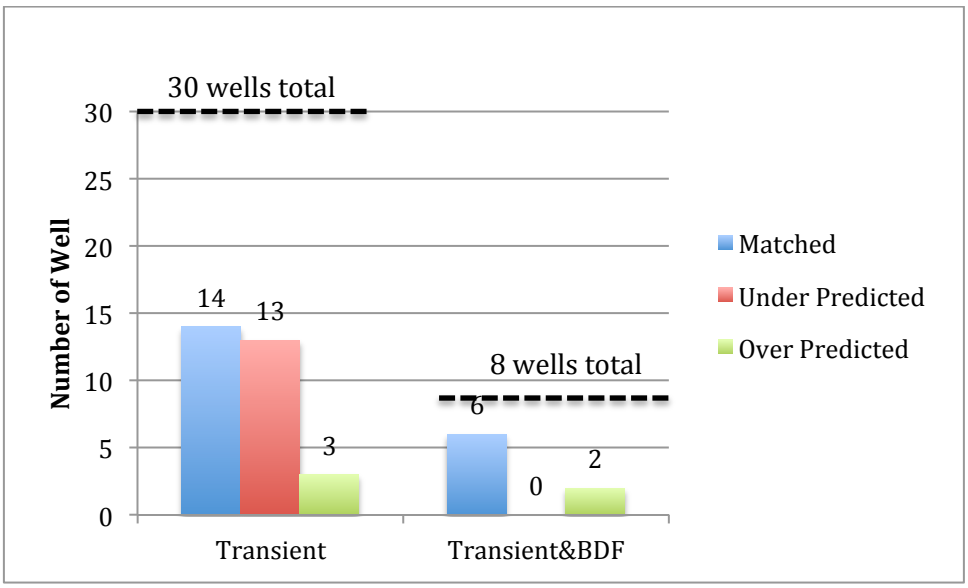

Figure 4.12: Summary of Arps' Harmonic decline model predictive performance based on different types of flow regimes

4.3.4 Observation and Discussion

24 dry gas wells in LaSalle County have an average production history length of 31 months ranged from 43 months to as short as 18 months. The results in **Figure 4.9** clearly shows that for wells in LaSalle, majority of the forecasts generated by Arps' Harmonic decline model are more than 50% under-predicted when used only two-third (21 month average) of the acquired production data. However, when applied Arps' Harmonic model to the whole data, number of matched wells increased significantly from 33% to 63%. In Webb County, there are 14 dry gas wells with average history length of 23 months ranged from the longest 30 months to 18 months. The results in **Figure 4.10** are not exactly exhibiting the same trend as the one for LaSalle County. With longer production history, number of matched wells did not increase but remained unchanged, 36%. However, when the results were combined as showed in **Figure 4.11**, it clearly indicates that the length of the production history affects the predictive performance of Arps' Harmonic model. The

maximum accuracy is 63% when using the longest length of the production history of 31 months. The accuracy percentage relatively decreases to 36% when the history length as short as of 23 months is used. The results also show that when using the history length shorter than 23 months, the majority of the forecasts are under-predicted.

As a flow regime is concerned as shown in **Figure 4.12**, out of the 30 wells that exhibiting solely transient flow, Arps' Harmonic model matched only in 14 wells (47%). Moreover, the model gave a good fit of the production history in 6 out of the 8 wells (75%) that showing transient flow at early time and BDF at later time. The 2 unmatched wells may be caused by their erratic production history. The results indicate that the Arps' Harmonic model seems to be suitable for modeling the decline trend of dry gas production that shows both transient flow and BDF since it can match up to 75%.

Obvious notice that can be drawn from **Table 4.7** is that the initial production rate (q_i) and initial decline constant (D_i) calculated by using two-third of the production data from LaSalle are greater than ones calculated using whole data in general. **Figure 4.13** clearly shows how production-rate trends calculated by using two-third and whole data are behaving compared with actual production data on rate-time plot of well#3 in LaSalle that has 43 months of production history. The trend using two-third of data seems to be highly influenced by very high decline rate at early age of the production as confirmed by high value of initial decline constant (D_i) in **Table 4.7** and that would result in under-predicted production-rate trend at late age of the production in this case. On the contrary, the trend using longer production history or whole data in this case would have less influence from early-age high decline rate and that would result in matched trend of production rate at late date of the production. There seems to be a change in production trend around 900 days with an increase in production rate. It is difficult to find the reason without knowing the well operating history.

Values of initial production rate (q_i) and initial decline constant (D_i) of wells in Webb County as shown in **Table 4.8** are very close even when they were calculated using different length of production history in Arps' Harmonic model. Certain length of production history may play a big role in Arps' Harmonic decline model. **Figure 4.14** exhibits how close the production rate trends are when they were calculated by Arps' Harmonic model using relatively short production history, 20 months for well#37 in Webb County in this case. Corresponding data for this particular well can be found in **Table 4.8**, the initial production rate (q_i) for the trends using two-third and whole data are 6,422.60 Mscf/Day and 6,441.10 Mscf/Day respectively and the initial decline constant (D_i) for the trends using two-third and whole data are 0.01927 1/day and 0.01932 1/day respectively.

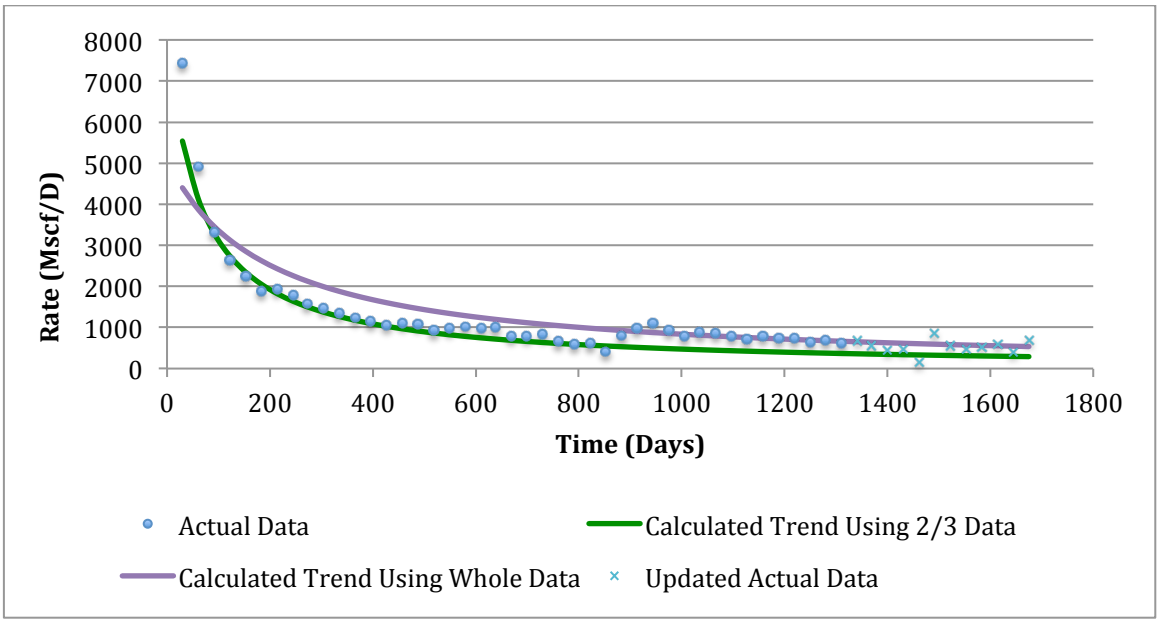

Figure 4.13: Comparison of production-rate trends calculated by Arps' Harmonic model using different history length, well#3 in Lasalle County

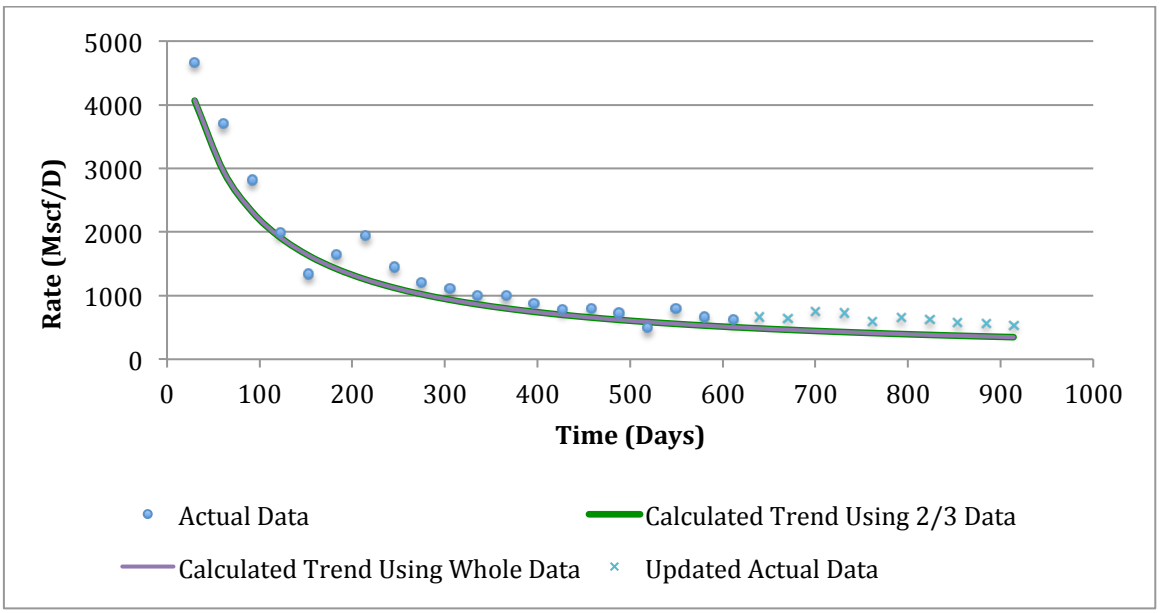

Figure 4.14: Comparison of production-rate trends calculated by Arps' Harmonic model using different history length, well#37 in Webb County

4.3.5 Arps' Hyperbolic Decline Curve Analysis

The third decline analysis model that Arps introduced in 1944 is hyperbolic model. The model can be derived similarly as the other two models developed by Arps. However instead of assuming loss ratio ($1/D$) to be constant for exponential decline and decline exponent (b) to be unity for harmonic decline, hyperbolic model can have the decline exponent (b) in the range of 0 to 1 due to utilization of arithmetic series of the loss ratio. **Tables 4.10** and **4.11**, are showing the summary of the related parameters of Arps' Hyperbolic model including initial rate (q_i), initial decline constant (D_i) and decline exponent (b) calculated from dry gas wells in LaSalle and Webb counties respectively. Matching results of the individual well can be also found in **Appendix II**, which has been done by the same way of visual observation between the forecasts and their actual production history as **Section 4.3.3** throughout this study. **Table 4.12** summarizes the numbers of the wells from the matching results, which are classified into 3 categories, matched, under-predicted and over-

predicted. For better clarification, the summary of the calculated percentage from **Table 4.12** is plotted into 3 bar charts based on county as showed in **Figures 4.15** through **4.17**. **Figure 4.18** also shows the matching results based on different types of flow regimes including the wells showing only transient flow and the wells showing both transient flow and BDF.

Table 4.10: Arps' Hyperbolic decline model parameters, LaSalle County wells

Well Number	Model Parameters	Value Calculated Using 2/3 Data	Value Calculated Using Whole Data
1	Decline Exponent, b	0.742	0.906
	Initial Decline Constant, D_i (1/day)	0.00591	0.00609
	Initial Rate, q_i (Mscf/day)	5,825.0	5,640.1
2	Decline Exponent, b	1.081	1.364
	Initial Decline Constant, D_i (1/day)	0.01238	0.01195
	Initial Rate, q_i (Mscf/day)	5,368.2	4,585.1
3	Decline Exponent, b	0.659	1.009
	Initial Decline Constant, D_i (1/day)	0.00725	0.00867
	Initial Rate, q_i (Mscf/day)	6,008.7	5,868.1
4	Decline Exponent, b	1.032	1.187
	Initial Decline Constant, D_i (1/day)	0.00780	0.00906
	Initial Rate, q_i (Mscf/day)	3,895.9	4,001.8
5	Decline Exponent, b	0.228	0.951
	Initial Decline Constant, D_i (1/day)	0.00439	0.00990
	Initial Rate, q_i (Mscf/day)	6,290.9	7,775.1
6	Decline Exponent, b	0.877	1.102
	Initial Decline Constant, D_i (1/day)	0.00745	0.00826
	Initial Rate, q_i (Mscf/day)	6,741.3	6,666.3
7	Decline Exponent, b	0.359	0.529
	Initial Decline Constant, D_i (1/day)	0.00505	0.00505
	Initial Rate, q_i (Mscf/day)	5,332.8	5,089.7
8	Decline Exponent, b	0.414	0.443
	Initial Decline Constant, D_i (1/day)	0.00501	0.00498
	Initial Rate, q_i (Mscf/day)	5,488.2	5,439.0

Table 4.10: Continued

Well Number	Model Parameters	Value Calculated Using 2/3 Data	Value Calculated Using Whole Data
9	Decline Exponent, b	0.604	0.786
	Initial Decline Constant, D_i (1/day)	0.00505	0.00508
	Initial Rate, q_i (Mscf/day)	8,049.6	7,785.3
10	Decline Exponent, b	0.356	0.504
	Initial Decline Constant, D_i (1/day)	0.00584	0.00629
	Initial Rate, q_i (Mscf/day)	2,873.3	2,889.7
11	Decline Exponent, b	0.605	0.962
	Initial Decline Constant, D_i (1/day)	0.00595	0.00787
	Initial Rate, q_i (Mscf/day)	5,405.0	5,672.2
12	Decline Exponent, b	0.598	1.102
	Initial Decline Constant, D_i (1/day)	0.00597	0.00967
	Initial Rate, q_i (Mscf/day)	5,100.7	5,664.0
13	Decline Exponent, b	1.911	1.438
	Initial Decline Constant, D_i (1/day)	0.03248	0.00862
	Initial Rate, q_i (Mscf/day)	5,831.2	3,857.9
14	Decline Exponent, b	1.487	1.227
	Initial Decline Constant, D_i (1/day)	0.01605	0.00834
	Initial Rate, q_i (Mscf/day)	4,098.9	3,309.9
15	Decline Exponent, b	1.439	1.416
	Initial Decline Constant, D_i (1/day)	0.00994	0.00848
	Initial Rate, q_i (Mscf/day)	2,929.1	2,764.1
16	Decline Exponent, b	0.820	1.313
	Initial Decline Constant, D_i (1/day)	0.00475	0.00822
	Initial Rate, q_i (Mscf/day)	5,369.9	6,109.0
17	Decline Exponent, b	1.059	1.435
	Initial Decline Constant, D_i (1/day)	0.00718	0.00845
	Initial Rate, q_i (Mscf/day)	3,863.3	3,827.2
18	Decline Exponent, b	0.892	1.119
	Initial Decline Constant, D_i (1/day)	0.00597	0.00790
	Initial Rate, q_i (Mscf/day)	5,838.9	6,271.2

Table 4.10: Continued

Well Number	Model Parameters	Value Calculated Using 2/3 Data	Value Calculated Using Whole Data
19	Decline Exponent, b	0.167	0.447
	Initial Decline Constant, D_i (1/day)	0.00593	0.00635
	Initial Rate, q_i (Mscf/day)	10,539.9	10,214.6
20	Decline Exponent, b	0.749	1.166
	Initial Decline Constant, D_i (1/day)	0.00596	0.00811
	Initial Rate, q_i (Mscf/day)	7,919.2	8,311.9
21	Decline Exponent, b	0.480	0.995
	Initial Decline Constant, D_i (1/day)	0.00590	0.00798
	Initial Rate, q_i (Mscf/day)	12,603.1	12,944.4
22	Decline Exponent, b	0.351	0.910
	Initial Decline Constant, D_i (1/day)	0.00593	0.00776
	Initial Rate, q_i (Mscf/day)	10,904.0	11,018.2
23	Decline Exponent, b	0.794	1.241
	Initial Decline Constant, D_i (1/day)	0.00596	0.00942
	Initial Rate, q_i (Mscf/day)	5,172.1	5,739.9
24	Decline Exponent, b	0.348	0.421
	Initial Decline Constant, D_i (1/day)	0.00590	0.00627
	Initial Rate, q_i (Mscf/day)	5,101.0	5,044.2

Table 4.11: Arps' Hyperbolic decline model parameters, Webb County wells

Well Number	Model Parameters	Value Calculated Using 2/3 Data	Value Calculated Using Whole Data
25	Decline Exponent, b	0.165	0.364
	Initial Decline Constant, D_i (1/day)	0.00594	0.00632
	Initial Rate, q_i (Mscf/day)	2,751.2	2,696.0
26	Decline Exponent, b	0.246	1.476
	Initial Decline Constant, D_i (1/day)	0.00272	0.00852
	Initial Rate, q_i (Mscf/day)	3,191.8	4,091.1
27	Decline Exponent, b	0.484	0.703
	Initial Decline Constant, D_i (1/day)	0.00592	0.00636
	Initial Rate, q_i (Mscf/day)	2,975.1	2,935.1
28	Decline Exponent, b	0.162	0.409
	Initial Decline Constant, D_i (1/day)	0.00586	0.00631
	Initial Rate, q_i (Mscf/day)	7,956.6	7,775.1
29	Decline Exponent, b	0.568	0.884
	Initial Decline Constant, D_i (1/day)	0.00596	0.00786
	Initial Rate, q_i (Mscf/day)	3,223.3	3,404.1
30	Decline Exponent, b	1.360	0.324
	Initial Decline Constant, D_i (1/day)	0.08527	0.00634
	Initial Rate, q_i (Mscf/day)	10,069.4	3,612.7
31	Decline Exponent, b	0.404	0.290
	Initial Decline Constant, D_i (1/day)	0.00589	0.00630
	Initial Rate, q_i (Mscf/day)	3,243.4	3,613.9
32	Decline Exponent, b	0.383	0.564
	Initial Decline Constant, D_i (1/day)	0.00588	0.00633
	Initial Rate, q_i (Mscf/day)	9,373.5	9,351.7
33	Decline Exponent, b	0.141	0.306
	Initial Decline Constant, D_i (1/day)	0.00497	0.00627
	Initial Rate, q_i (Mscf/day)	9,527.3	10,480.6
34	Decline Exponent, b	0.111	0.336
	Initial Decline Constant, D_i (1/day)	0.00585	0.00627
	Initial Rate, q_i (Mscf/day)	4,368.2	4,288.8

Table 4.11: Continued

Well Number	Model Parameters	Value Calculated Using 2/3 Data	Value Calculated Using Whole Data
35	Decline Exponent, b	0.005	0.347
	Initial Decline Constant, D_i (1/day)	0.00590	0.00633
	Initial Rate, q_i (Mscf/day)	11,307.5	10,917.0
36	Decline Exponent, b	1.713	1.158
	Initial Decline Constant, D_i (1/day)	0.09368	0.02607
	Initial Rate, q_i (Mscf/day)	5,330.1	3,591.1
37	Decline Exponent, b	0.219	0.440
	Initial Decline Constant, D_i (1/day)	0.00590	0.00631
	Initial Rate, q_i (Mscf/day)	4,448.1	4,397.3
38	Decline Exponent, b	0.365	0.647
	Initial Decline Constant, D_i (1/day)	0.00593	0.00636
	Initial Rate, q_i (Mscf/day)	3,444.1	3,363.3

Table 4.12: Result summary of Arps' Hyperbolic decline model predictive performance

County	Predictive Performance	Number of Wells		
		Using 2/3 Data	Using 2/3 Data (Compared with recently updated data)	Using Whole Data
LaSalle	Matched	2	3	5
	Under Predicted	19	17	9
	Over Predicted	1	1	3
	Matched (b>1)	2	3	7
Webb	Matched	0	0	0
	Under Predicted	12	12	12
	Over Predicted	1	1	1
	Matched (b>1)	1	1	1
Total	Matched	2	3	5
	Under Predicted	31	29	21
	Over Predicted	2	2	4
	Matched (b>1)	3	4	8

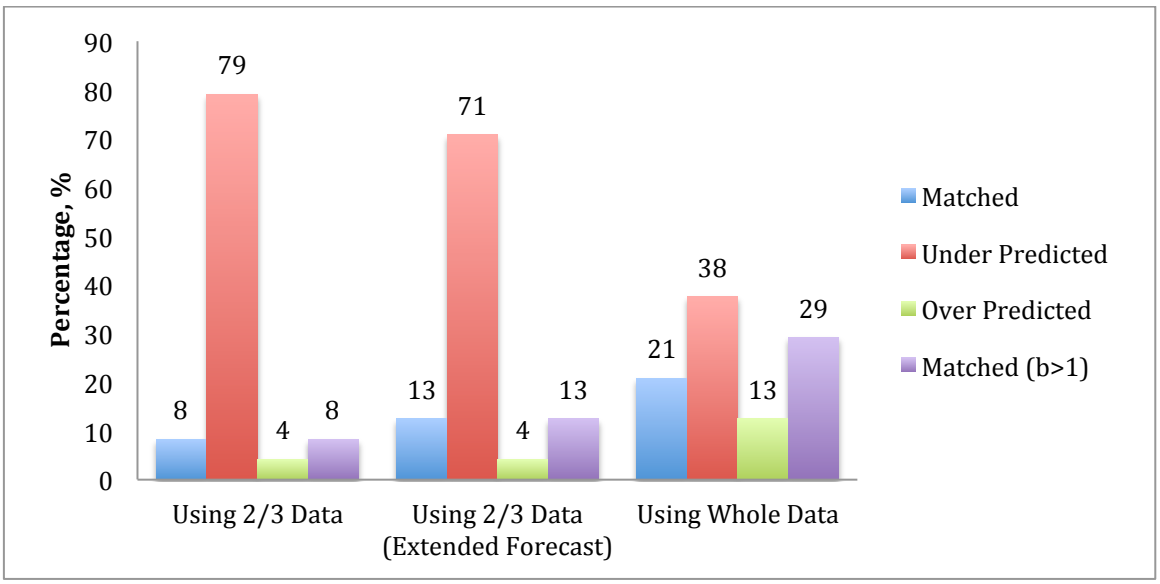

Figure 4.15: Arps' Hyperbolic decline model predictive performance (LaSalle County)

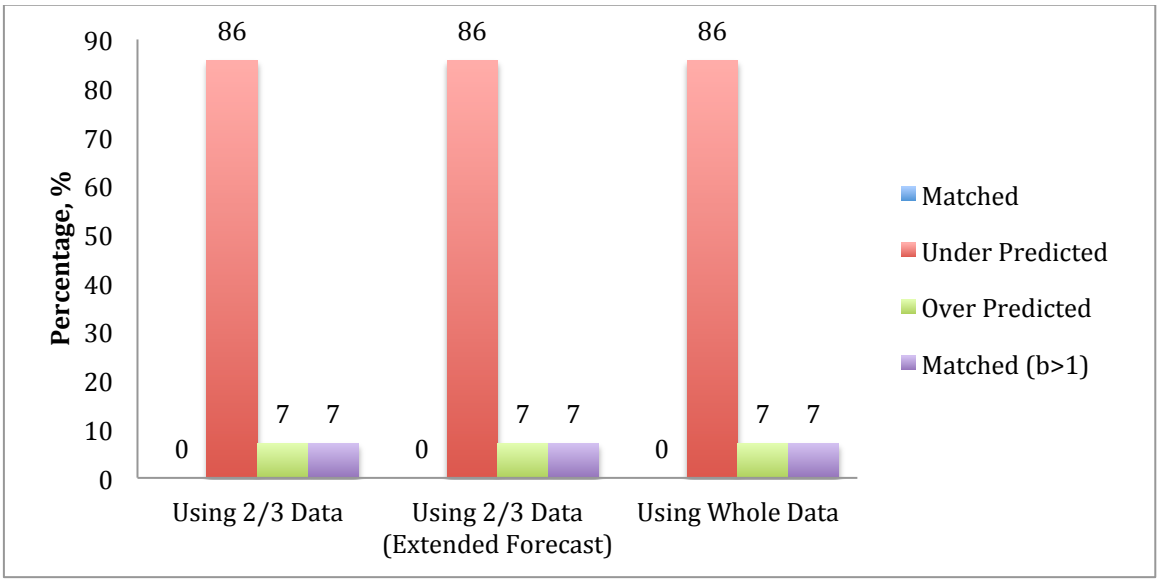

Figure 4.16: Arps' Hyperbolic decline model predictive performance (Webb County)

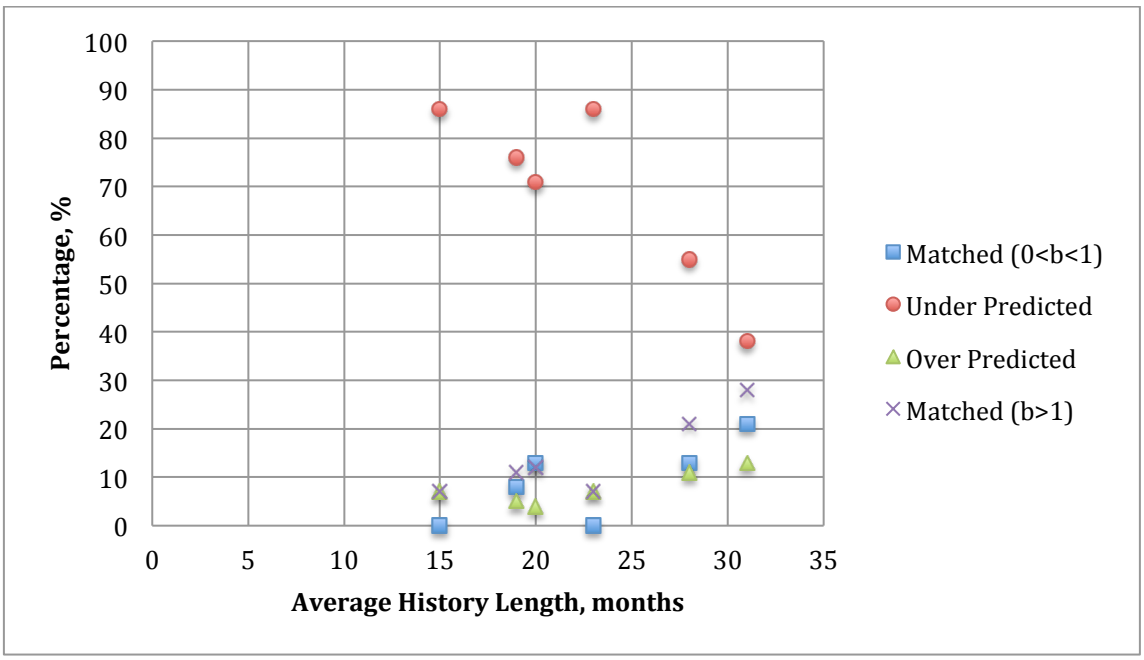

Figure 4.17: Summary of Arps' Hyperbolic decline model predictive performance based on different production history length

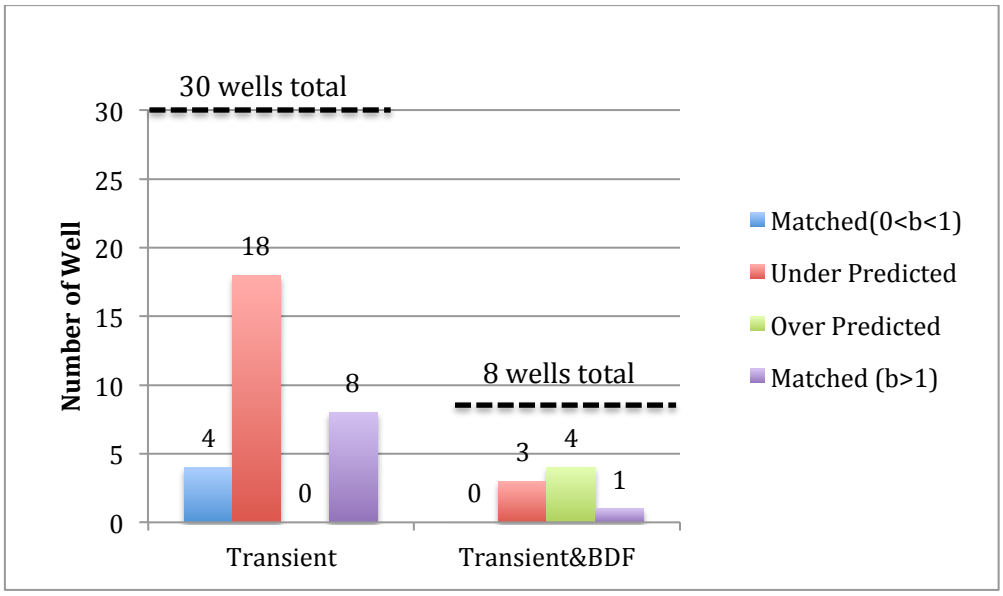

Figure 4.18: Summary of Arps' Hyperbolic decline model predictive performance based on different types of flow regimes

4.3.6 Observation and Discussion

Matching results of 24 LaSalle dry gas wells generated by Arps' Hyperbolic model is showed in **Figure 4.15**. The majority of the predictions are noticeably under-predicted. Number of under-predicted wells is accounted as more than 70% when used two-third of production data in the model and reduced to 38% when used the whole data. Only 21% of LaSalle wells matched the production history when decline exponent (b) of Arps' Hyperbolic model is in range of 0 to 1. When the decline exponent (b) has been adjusted to be higher than unity, 29% of the wells could be matched. However, the matching results of the wells in Webb County are not corresponded to LaSalle wells. As showed in **Figure 4.16**, there is none of matched wells when the decline exponent (b) is in range 0 to 1 and there is very high percentage of under-predicted wells, 86%, regardless of whether two-third or whole production data has been used in the model. The results indicate that the predictive capability of Arps' Hyperbolic model will be reduced when limited length of production history is available to use in the model. From the overall predictive performance of Arps' Hyperbolic model which is summarized in **Figure 4.17**, its accuracy reaches the maximum of 21% (matched with $0<b<1$) when using the longest history length of 31 months. However, the majority of the forecasts are under-predicted indicating that Arps' Hyperbolic model does not seem to be applicable to dry gas wells in these particular areas.

When considering flow regime as a criterion to have another angle of the decline analysis, the results in **Figure 4.18** shows that only 4 out of the 30 wells (13%) that exhibiting solely transient flow are matched and none of the wells showing both transient flow and BDF is matched with the production history when applying Arps' Harmonic model. The majority of the results for the first case and the latter are 60% under-predicted and 50% over-predicted respectively. The overall results indicate that Arps' Hyperbolic model does not seem to be a good decline model for

forecasting future production trend of the dry gas wells those are still in the transient flow and ones showing both transient flow followed by BDF.

4.3.7 Power Law Exponential Decline Analysis (PLE)

To better estimate future production trend of dry gas wells, Ilk et al. (2008) introduced the PLE model which was developed from Arps' Exponential decline model by integrated the effects of transient and boundary-dominated flows (BDF) into the model since Arps' DCA models are applicable to only BDF. **Tables 4.13** and **4.14**, are the summary of 4 important parameters in PLE model including rate intercept ($\hat{q}_i$), decline constant at time infinity (D_∞), decline constant, ($\widehat{D}_i$) and time exponent (n) that has been calculated from the wells in LaSalle and Webb counties respectively. To be able to study the natural capability of this model, the decline constant at time infinity (D_∞) is not restricted to zero. Matching results of the each well can be also found in **Appendix II**, which has been done by visual observation between the forecasts and their actual production history similarly as **Section 4.3.3**. **Table 4.15** summarizes the numbers of the wells from the matching results, which are divided into 3 categories, matched, under-predicted and over-predicted. For better comparison, the summary in **Table 4.15** is calculated in percentage and plotted separately into 3 bar charts based on county as showed in **Figures 4.19** through **4.21**. **Figure 4.22** also shows the matching results based on different types of flow regimes including the wells showing only transient flow and the wells showing both transient flow and BDF.

Table 4.13: Power Law Exponential model parameters, LaSalle County wells

Well Number	Model Parameters	Value Calculated Using 2/3 Data	Value Calculated Using Whole Data
1	Rate Intercept, $\hat{q}_i$ (Mscf/Day)	27,867.8	34,242.9
	Decline Constant at Infinity, D_∞ (1/day)	0.000425513	0
	Decline Constant, $\widehat{D}_i$ (1/day)	0.6970	0.7991
	Time Exponent, n	0.23	0.23
2	Rate Intercept, $\hat{q}_i$ (Mscf/Day)	17,477.5	16,648.9
	Decline Constant at Infinity, D_∞ (1/day)	0	0.00005
	Decline Constant, $\widehat{D}_i$ (1/day)	0.4731	0.5305
	Time Exponent, n	0.30	0.27
3	Rate Intercept, $\hat{q}_i$ (Mscf/Day)	18,551.2	17,722.7
	Decline Constant at Infinity, D_∞ (1/day)	0.00024518	0.000156648
	Decline Constant, $\widehat{D}_i$ (1/day)	0.4677	0.5294
	Time Exponent, n	0.29	0.26
4	Rate Intercept, $\hat{q}_i$ (Mscf/Day)	66,972.3	17,114.4
	Decline Constant at Infinity, D_∞ (1/day)	0.000563243	0.000002058
	Decline Constant, $\widehat{D}_i$ (1/day)	1.8581	0.6498
	Time Exponent, n	0.13	0.24
5	Rate Intercept, $\hat{q}_i$ (Mscf/Day)	35,546.7	18,188.2
	Decline Constant at Infinity, D_∞ (1/day)	0.000131501	0.000199615
	Decline Constant, $\widehat{D}_i$ (1/day)	0.5616	0.6426
	Time Exponent, n	0.29	0.22
6	Rate Intercept, $\hat{q}_i$ (Mscf/Day)	2,290,706.8	2,397,368.6
	Decline Constant at Infinity, D_∞ (1/day)	0	0
	Decline Constant, $\widehat{D}_i$ (1/day)	4.1722	4.2437
	Time Exponent, n	0.09	0.09
7	Rate Intercept, $\hat{q}_i$ (Mscf/Day)	2,241,132.8	2,232,128.2
	Decline Constant at Infinity, D_∞ (1/day)	0.000130529	0.00008302
	Decline Constant, $\widehat{D}_i$ (1/day)	4.1691	4.1420
	Time Exponent, n	0.13	0.22
8	Rate Intercept, $\hat{q}_i$ (Mscf/Day)	2,232,087.0	2,232,087.0
	Decline Constant at Infinity, D_∞ (1/day)	0.00119063	0.001344024
	Decline Constant, $\widehat{D}_i$ (1/day)	4.7192	4.7649
	Time Exponent, n	0.06	0.06

Table 4.13: Continued

Well Number	Model Parameters	Value Calculated Using 2/3 Data	Value Calculated Using Whole Data
9	Rate Intercept, $\hat{q}_i$ (Mscf/Day)	2,232,081.6	2,232,081.6
	Decline Constant at Infinity, D_∞ (1/day)	0.000745494	0.000377172
	Decline Constant, $\widehat{D}_i$ (1/day)	4.3647	4.2597
	Time Exponent, n	0.07	0.08
10	Rate Intercept, $\hat{q}_i$ (Mscf/Day)	2,232,113.0	2,232,113.0
	Decline Constant at Infinity, D_∞ (1/day)	0.003221023	0.002210293
	Decline Constant, $\widehat{D}_i$ (1/day)	6.0831	5.8173
	Time Exponent, n	0.02	0.04
11	Rate Intercept, $\hat{q}_i$ (Mscf/Day)	2,232,309.8	2,232,309.8
	Decline Constant at Infinity, D_∞ (1/day)	0.000879119	0.000567046
	Decline Constant, $\widehat{D}_i$ (1/day)	4.7451	4.6630
	Time Exponent, n	0.07	0.07
12	Rate Intercept, $\hat{q}_i$ (Mscf/Day)	2,232,178.0	2,232,178.0
	Decline Constant at Infinity, D_∞ (1/day)	0.000225776	0.000164942
	Decline Constant, $\widehat{D}_i$ (1/day)	4.5259	4.5120
	Time Exponent, n	0.08	0.08
13	Rate Intercept, $\hat{q}_i$ (Mscf/Day)	2,232,095.7	2,232,095.7
	Decline Constant at Infinity, D_∞ (1/day)	4.86254E-05	4.65984E-07
	Decline Constant, $\widehat{D}_i$ (1/day)	5.2076	5.2037
	Time Exponent, n	0.06	0.06
14	Rate Intercept, $\hat{q}_i$ (Mscf/Day)	2,233,168.1	2,233,167.0
	Decline Constant at Infinity, D_∞ (1/day)	0.000137467	0.000771742
	Decline Constant, $\widehat{D}_i$ (1/day)	5.0256	6.4832
	Time Exponent, n	0.07	0.02
15	Rate Intercept, $\hat{q}_i$ (Mscf/Day)	2,232,093.7	2,232,093.7
	Decline Constant at Infinity, D_∞ (1/day)	0.000142975	0.00010696
	Decline Constant, $\widehat{D}_i$ (1/day)	5.3839	5.3739
	Time Exponent, n	0.06	0.06
16	Rate Intercept, $\hat{q}_i$ (Mscf/Day)	2,232,100.9	2,232,100.9
	Decline Constant at Infinity, D_∞ (1/day)	0.001364921	0.000963705
	Decline Constant, $\widehat{D}_i$ (1/day)	5.3449	5.1955
	Time Exponent, n	0.03	0.04

Table 4.13: Continued

Well Number	Model Parameters	Value Calculated Using 2/3 Data	Value Calculated Using Whole Data
17	Rate Intercept, $\hat{q}_i$ (Mscf/Day)	2,233,182.4	2,233,173.5
	Decline Constant at Infinity, D_∞ (1/day)	0.00023529	0.000383067
	Decline Constant, $\widehat{D}_i$ (1/day)	5.0443	6.5693
	Time Exponent, n	0.07	0.02
18	Rate Intercept, $\hat{q}_i$ (Mscf/Day)	2,232,098.6	2,232,098.6
	Decline Constant at Infinity, D_∞ (1/day)	0.001826468	0.001438879
	Decline Constant, $\widehat{D}_i$ (1/day)	5.3542	5.2386
	Time Exponent, n	0.03	0.04
19	Rate Intercept, $\hat{q}_i$ (Mscf/Day)	2,232,130.2	2,232,130.4
	Decline Constant at Infinity, D_∞ (1/day)	0.001484394	0.000347431
	Decline Constant, $\widehat{D}_i$ (1/day)	3.9116	3.7156
	Time Exponent, n	0.09	0.10
20	Rate Intercept, $\hat{q}_i$ (Mscf/Day)	2,258,878.8	2,258,878.8
	Decline Constant at Infinity, D_∞ (1/day)	0.000200757	0.000104415
	Decline Constant, $\widehat{D}_i$ (1/day)	4.2481	4.2232
	Time Exponent, n	0.08	0.08
21	Rate Intercept, $\hat{q}_i$ (Mscf/Day)	2,232,068.1	2,232,072.6
	Decline Constant at Infinity, D_∞ (1/day)	0.003115234	0.000961504
	Decline Constant, $\widehat{D}_i$ (1/day)	4.8492	4.2219
	Time Exponent, n	0.02	0.06
22	Rate Intercept, $\hat{q}_i$ (Mscf/Day)	2,232,150.1	2,232,150.1
	Decline Constant at Infinity, D_∞ (1/day)	0	0.000008604
	Decline Constant, $\widehat{D}_i$ (1/day)	3.6565	3.7594
	Time Exponent, n	0.10	0.10
23	Rate Intercept, $\hat{q}_i$ (Mscf/Day)	2,232,262.2	2,232,262.2
	Decline Constant at Infinity, D_∞ (1/day)	0.001658807	0.001246824
	Decline Constant, $\widehat{D}_i$ (1/day)	5.3277	5.2101
	Time Exponent, n	0.04	0.04
24	Rate Intercept, $\hat{q}_i$ (Mscf/Day)	2,232,263.3	2,232,263.3
	Decline Constant at Infinity, D_∞ (1/day)	0.004741219	0.003586506
	Decline Constant, $\widehat{D}_i$ (1/day)	4.7713	4.5472
	Time Exponent, n	0.05	0.06

Table 4.14: Power Law Exponential model parameters, Webb County wells

Well Number	Model Parameters	Value Calculated Using 2/3 Data	Value Calculated Using Whole Data
25	Rate Intercept, $\hat{q}_i$ (Mscf/Day)	2,232,045.8	2,232,045.8
	Decline Constant at Infinity, D_∞ (1/day)	0.000772311	0.000656609
	Decline Constant, $\widehat{D}_i$ (1/day)	4.8454	4.8218
	Time Exponent, n	0.09	0.09
26	Rate Intercept, $\hat{q}_i$ (Mscf/Day)	2,232,170.0	2,233,119.2
	Decline Constant at Infinity, D_∞ (1/day)	0.000695467	0.00129982
	Decline Constant, $\widehat{D}_i$ (1/day)	5.5682	6.3309
	Time Exponent, n	0.04	0.01
27	Rate Intercept, $\hat{q}_i$ (Mscf/Day)	2,232,414.6	2,232,046.0
	Decline Constant at Infinity, D_∞ (1/day)	0.000859764	0.000498241
	Decline Constant, $\widehat{D}_i$ (1/day)	5.2229	5.1308
	Time Exponent, n	0.07	0.07
28	Rate Intercept, $\hat{q}_i$ (Mscf/Day)	2,286,989.8	2,232,083.7
	Decline Constant at Infinity, D_∞ (1/day)	0.003079804	0.001682365
	Decline Constant, $\widehat{D}_i$ (1/day)	4.7548	4.4000
	Time Exponent, n	0.05	0.07
29	Rate Intercept, $\hat{q}_i$ (Mscf/Day)	2,255,295.4	2,232,050.9
	Decline Constant at Infinity, D_∞ (1/day)	0.000004529	0.000279659
	Decline Constant, $\widehat{D}_i$ (1/day)	4.7667	4.8911
	Time Exponent, n	0.09	0.08
30	Rate Intercept, $\hat{q}_i$ (Mscf/Day)	194,493.1	2,267,663.1
	Decline Constant at Infinity, D_∞ (1/day)	0	0.000014306
	Decline Constant, $\widehat{D}_i$ (1/day)	2.1628	4.3683
	Time Exponent, n	0.16	0.10
31	Rate Intercept, $\hat{q}_i$ (Mscf/Day)	2,000,004.4	2,232,047.7
	Decline Constant at Infinity, D_∞ (1/day)	0.002171871	0.001513792
	Decline Constant, $\widehat{D}_i$ (1/day)	4.8858	4.8617
	Time Exponent, n	0.07	0.07
32	Rate Intercept, $\hat{q}_i$ (Mscf/Day)	2,232,081.3	2,232,081.4
	Decline Constant at Infinity, D_∞ (1/day)	0.002615014	0.00173151
	Decline Constant, $\widehat{D}_i$ (1/day)	4.7044	4.4800
	Time Exponent, n	0.04	0.06

Table 4.14: Continued

Well Number	Model Parameters	Value Calculated Using 2/3 Data	Value Calculated Using Whole Data
33	Rate Intercept, $\hat{q}_i$ (Mscf/Day)	338,710.6	2,232,061.2
	Decline Constant at Infinity, D_∞ (1/day)	0.004679768	0.003614662
	Decline Constant, $\widehat{D}_i$ (1/day)	3.1744	4.8242
	Time Exponent, n	0.02	0.03
34	Rate Intercept, $\hat{q}_i$ (Mscf/Day)	2,232,047.3	2,232,047.3
	Decline Constant at Infinity, D_∞ (1/day)	0.002668544	0.001923603
	Decline Constant, $\widehat{D}_i$ (1/day)	5.0944	4.9310
	Time Exponent, n	0.05	0.06
35	Rate Intercept, $\hat{q}_i$ (Mscf/Day)	2,232,081.6	2,232,082.1
	Decline Constant at Infinity, D_∞ (1/day)	0.002650444	0.001028067
	Decline Constant, $\widehat{D}_i$ (1/day)	4.1095	3.8181
	Time Exponent, n	0.07	0.09
36	Rate Intercept, $\hat{q}_i$ (Mscf/Day)	2,232,436.9	2,232,436.9
	Decline Constant at Infinity, D_∞ (1/day)	0	0.000019132
	Decline Constant, $\widehat{D}_i$ (1/day)	4.7596	4.7926
	Time Exponent, n	0.10	0.10
37	Rate Intercept, $\hat{q}_i$ (Mscf/Day)	2,232,078.8	2,232,078.8
	Decline Constant at Infinity, D_∞ (1/day)	0.001211824	0.001003061
	Decline Constant, $\widehat{D}_i$ (1/day)	4.7751	4.7309
	Time Exponent, n	0.07	0.08
38	Rate Intercept, $\hat{q}_i$ (Mscf/Day)	2,232,084.1	2,232,084.1
	Decline Constant at Infinity, D_∞ (1/day)	0.00061254	0.000139719
	Decline Constant, $\widehat{D}_i$ (1/day)	4.9287	4.8273
	Time Exponent, n	0.08	0.08

Table 4.15: Result summary of Power Law Exponential decline model predictive performance

Well Number	Predictive Performance	Number of Wells		
		Using 2/3 Data	Using 2/3 Data (Compared with recently updated data)	Using Whole Data
LaSalle	Matched	7	7	15
	Under Predicted	16	16	4
	Over Predicted	1	1	5
Webb	Matched	5	4	4
	Under Predicted	9	10	10
	Over Predicted	0	0	0
Total	Matched	12	11	19
	Under Predicted	25	26	14
	Over Predicted	1	1	5

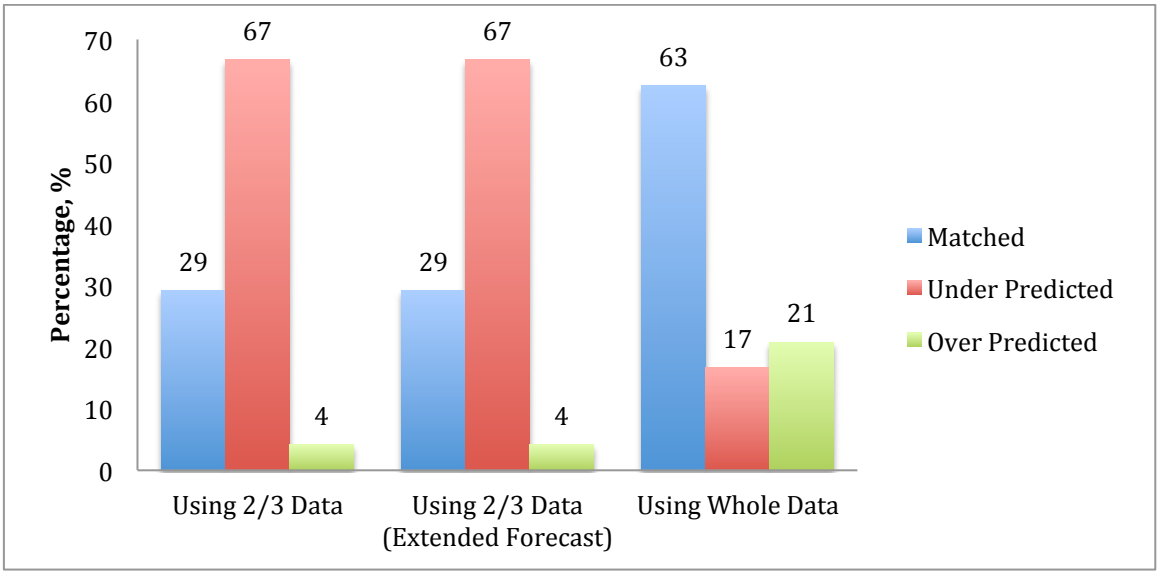

Figure 4.19: Power Law Exponential decline model predictive performance (LaSalle County)

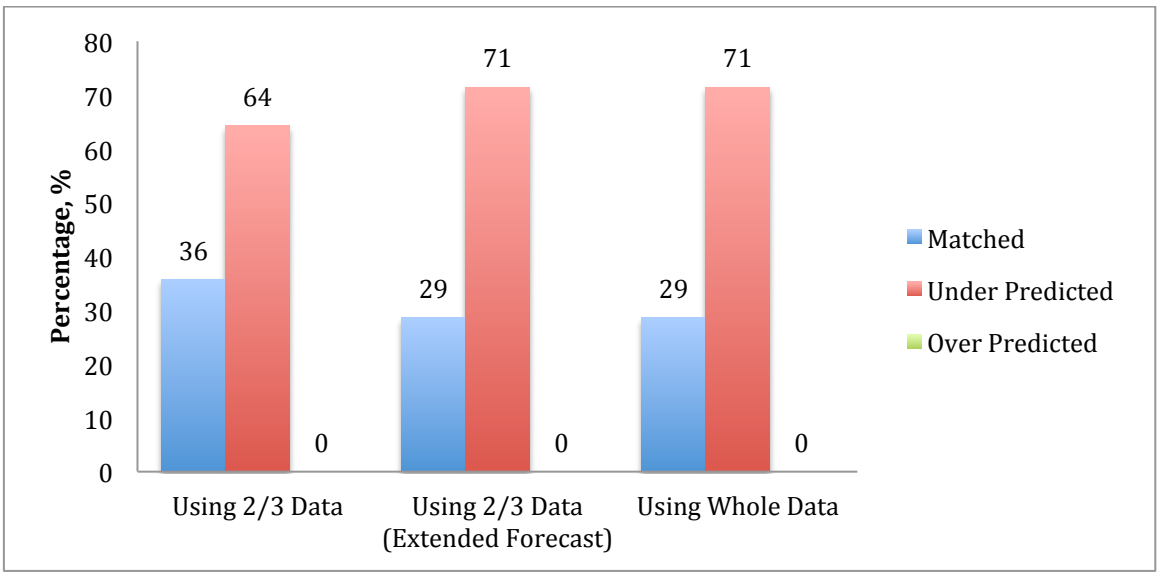

Figure 4.20: Power Law Exponential Decline Model Predictive Performance (Webb County)

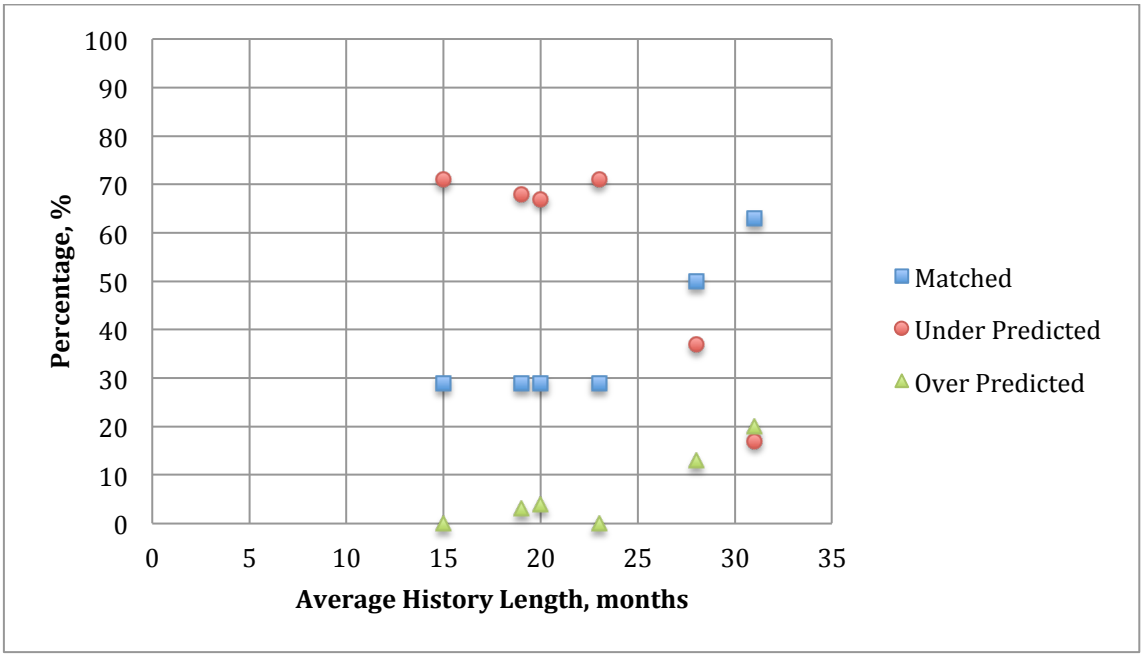

Figure 4.21: Summary of PLE decline model predictive performance based on different production history length

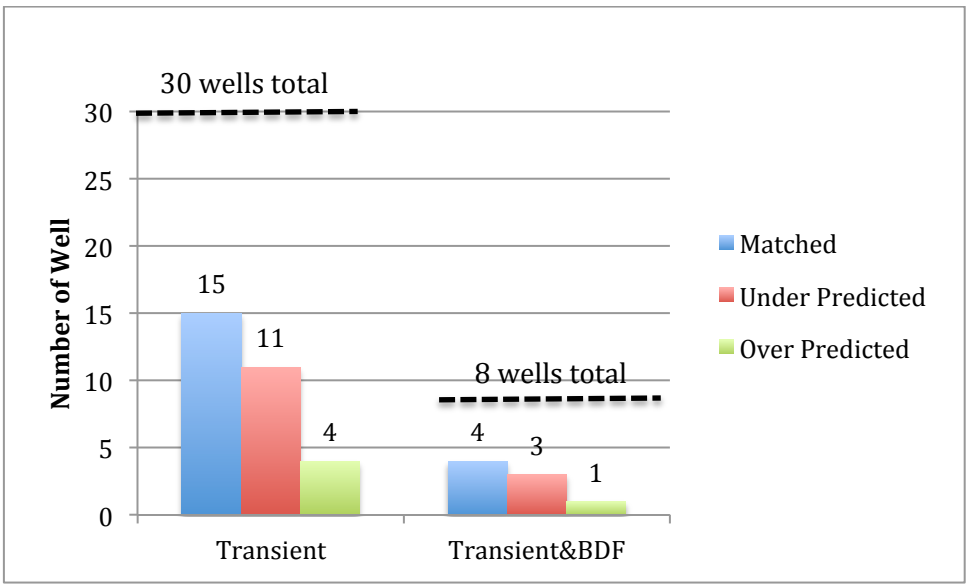

Figure 4.22: Summary of PLE decline model predictive performance based on different types of flow regimes

4.3.8 Observation and Discussion

Figure 4.19 clearly shows that when shorter length of production history (two-third of the data length) has been used, forecast outcomes generated by PLE model are mainly under-predicted (67%). However, number of matched wells significantly increased from 29% to 63% and number of under-predicted wells reduced from 67% down to 17% when the whole data has been used in PLE model. This observation can imply that longer production history if available would contribute to higher accuracy of the future forecast generated by PLE model. On the contrary for the 14 wells in Webb County, number of matched wells slightly decreased from 36% to 29% when used the whole data over the two-third of the data according to **Figure 4.20**. Since the average history length of the wells in Webb County is 23 months that is considered younger than the wells in LaSalle (31 month average), this phenomenon may indicate the limitation of PLE model that using too short production history would impair the predictive performance of the model. Overall result in **Figure**

4.21 shows that the model gives the highest accuracy of 63% when using the longest length of the production history of 31 months, which is comparable to the results of Arps' Harmonic model. However, when using the history length shorter than 23 months, the forecasts are mainly under-predicted approximately 70% of the total wells. The results suggest that, to obtain more accurate forecast from PLE model, the model requires sufficient amount of production history.

When looked into the possible effect of the flow regime against the predictive accuracy of PLE model, the results in **Figure 4.22** shows that 15 out of the 30 wells (50%) that exhibiting only transient flow and 4 out of the 8 wells (50%) that showing the transient flow followed by BDF are matched with the production history. The results in general cannot conclude that PLE is a reliable model for either only transient flow or transient flow with BDF unless again more data history is available and regression of the current data is applied.

4.3.9 Logistic Growth Analysis (LGA)

Logistic Growth Analysis or LGA is a mathematical method that has been widely used as a statistical tool to analyze and predict future growth in population. LGA has been developed into oil and gas industry by several researchers to model the future production trend and estimate total reserve. The LGA applied in this study was developed by Clark et al. in 2011. **Tables 4.16** and **4.17** show the calculation results of associated parameters in LGA model including carrying capacity (K), hyperbolic exponent (n) and LGA model constant (a). Matching results of individual well can be also found in **Appendix II**, which has been done by mean of visual observation between the forecasts and their actual production history similarly as **Section 4.3.3**. **Table 4.18** summarizes the numbers of the wells from the matching results, which are divided into 3 categories, matched, under-predicted and over-predicted. For better comparison, the summary in **Table 4.18** is calculated in percentage and plotted separately into 3 bar charts based on county as showed in **Figures 4.23**

through **4.25**. **Figure 4.26** also shows the matching results based on different types of flow regimes including the wells showing only transient flow and the wells showing both transient flow and BDF.

Table 4.16: Logistic Growth Analysis model parameters, LaSalle County wells

Well Number	Model Parameters	Value Calculated Using 2/3 Data	Value Calculated Using Whole Data
1	Carrying Capacity, *K* (Mscf)	3,393,516	4,181,670
	Hyperbolic Exponent, *n*	0.858112307	0.739569109
	Model Constant, *a*	274.5544523	231.3584012
2	Carrying Capacity, *K* (Mscf)	7,735,460	7,735,460
	Hyperbolic Exponent, *n*	0.615187253	0.607912889
	Model Constant, *a*	360.4089774	360.4089808
3	Carrying Capacity, *K* (Mscf)	4,428,648	7,735,460
	Hyperbolic Exponent, *n*	0.735418495	0.653830815
	Model Constant, *a*	130.1119731	360.4089615
4	Carrying Capacity, *K* (Mscf)	3,209,813	6,375,176
	Hyperbolic Exponent, *n*	0.856744313	0.607767913
	Model Constant, *a*	300.0372972	311.1126497
5	Carrying Capacity, *K* (Mscf)	5,529,708	6,375,176
	Hyperbolic Exponent, *n*	0.693099704	0.704810393
	Model Constant, *a*	199.9999212	311.1126013
6	Carrying Capacity, *K* (Mscf)	6,175,155	6,721,577
	Hyperbolic Exponent, *n*	0.667233919	0.635772531
	Model Constant, *a*	217.3903765	206.7684508
7	Carrying Capacity, *K* (Mscf)	3,493,675	6,123,116
	Hyperbolic Exponent, *n*	0.793808159	0.561645661
	Model Constant, *a*	166.9083135	149.9999371
8	Carrying Capacity, *K* (Mscf)	5,178,935	5,198,926
	Hyperbolic Exponent, *n*	0.617818599	0.612815475
	Model Constant, *a*	159.9999828	159.9999873
9	Carrying Capacity, *K* (Mscf)	5,916,505	5,969,648
	Hyperbolic Exponent, *n*	0.709142055	0.667677897
	Model Constant, *a*	184.9996677	141.615138

Table 4.16: Continued

Well Number	Model Parameters	Value Calculated Using 2/3 Data	Value Calculated Using Whole Data
10	Carrying Capacity, *K* (Mscf)	940,864	972,941
	Hyperbolic Exponent, *n*	0.985598881	0.955027582
	Model Constant, *a*	294.5993948	274.9792754
11	Carrying Capacity, *K* (Mscf)	3,507,753	5,337,804
	Hyperbolic Exponent, *n*	0.841028428	0.656763396
	Model Constant, *a*	238.7116613	222.9426844
12	Carrying Capacity, *K* (Mscf)	3,695,961	5,337,804
	Hyperbolic Exponent, *n*	0.772991918	0.645531136
	Model Constant, *a*	212.2439551	222.9426925
13	Carrying Capacity, *K* (Mscf)	7,892,589	7,870,660
	Hyperbolic Exponent, *n*	0.654041738	0.659687845
	Model Constant, *a*	492.8521754	509.1545487
14	Carrying Capacity, *K* (Mscf)	3,547,769	7,361,776
	Hyperbolic Exponent, *n*	0.785870411	0.62556702
	Model Constant, *a*	260.4401143	474.9523179
15	Carrying Capacity, *K* (Mscf)	2,344,845	2,764,132
	Hyperbolic Exponent, *n*	0.793662003	0.75189304
	Model Constant, *a*	353.6275661	383.7744131
16	Carrying Capacity, *K* (Mscf)	3,300,375	3,680,889
	Hyperbolic Exponent, *n*	0.951543734	0.885277455
	Model Constant, *a*	477.354305	433.4270165
17	Carrying Capacity, *K* (Mscf)	2,909,297	3,832,136
	Hyperbolic Exponent, *n*	0.826413536	0.752687298
	Model Constant, *a*	315.4310614	382.8293086
18	Carrying Capacity, *K* (Mscf)	2,915,963	3,010,377
	Hyperbolic Exponent, *n*	0.935427376	0.916137302
	Model Constant, *a*	390.4055597	380.7509693
19	Carrying Capacity, *K* (Mscf)	3,885,877	4,436,865
	Hyperbolic Exponent, *n*	0.826838451	0.748451149
	Model Constant, *a*	145.4958531	136.3830412

Table 4.16: Continued

Well Number	Model Parameters	Value Calculated Using 2/3 Data	Value Calculated Using Whole Data
20	Carrying Capacity, *K* (Mscf)	4,577,413	4,437,939
	Hyperbolic Exponent, *n*	0.815399161	0.755179867
	Model Constant, *a*	276.0600696	165.5898978
21	Carrying Capacity, *K* (Mscf)	7,924,637	7,923,126
	Hyperbolic Exponent, *n*	0.763719543	0.764329658
	Model Constant, *a*	237.2154557	237.2154554
22	Carrying Capacity, *K* (Mscf)	7,924,144	7,923,126
	Hyperbolic Exponent, *n*	0.724636864	0.72495007
	Model Constant, *a*	237.2154827	237.2154827
23	Carrying Capacity, *K* (Mscf)	2,539,559	2,757,280
	Hyperbolic Exponent, *n*	0.931051115	0.885027127
	Model Constant, *a*	358.3915548	342.827464
24	Carrying Capacity, *K* (Mscf)	1,276,684	1,307,883
	Hyperbolic Exponent, *n*	1.029571121	0.988054918
	Model Constant, *a*	167.7605509	149.1577062

Table 4.17: Logistic Growth Analysis model parameters, Webb County wells

Well Number	Model Parameters	Value Calculated Using 2/3 Data	Value Calculated Using Whole Data
25	Carrying Capacity, *K* (Mscf)	902,376	911,737
	Hyperbolic Exponent, *n*	0.808215986	0.800962011
	Model Constant, *a*	126.9561416	125.2574089
26	Carrying Capacity, *K* (Mscf)	2,033,034	2,162,123
	Hyperbolic Exponent, *n*	1.032030993	0.98883111
	Model Constant, *a*	687.6561625	633.5187553
27	Carrying Capacity, *K* (Mscf)	1,312,121	1,504,068
	Hyperbolic Exponent, *n*	0.870471669	0.798497604
	Model Constant, *a*	227.3818386	212.4479508
28	Carrying Capacity, *K* (Mscf)	2,382,413	2,685,325
	Hyperbolic Exponent, *n*	0.958443145	0.840215187
	Model Constant, *a*	205.3949801	158.5625191
29	Carrying Capacity, *K* (Mscf)	1,632,291	1,812,570
	Hyperbolic Exponent, *n*	0.796996017	0.753858009
	Model Constant, *a*	189.5979253	188.4732606
30	Carrying Capacity, *K* (Mscf)	1,351,146	1,504,743
	Hyperbolic Exponent, *n*	0.739913708	0.69239456
	Model Constant, *a*	99.02607676	98.04289223
31	Carrying Capacity, *K* (Mscf)	1,027,828	1,072,087
	Hyperbolic Exponent, *n*	0.895488091	0.8584692
	Model Constant, *a*	151.424866	140.6005379
32	Carrying Capacity, *K* (Mscf)	3,470,542	3,650,406
	Hyperbolic Exponent, *n*	0.912155923	0.874641974
	Model Constant, *a*	236.7728154	222.8848578
33	Carrying Capacity, *K* (Mscf)	2,715,165	2,855,180
	Hyperbolic Exponent, *n*	1.046469242	0.977123538
	Model Constant, *a*	270.7702349	224.8099817
34	Carrying Capacity, *K* (Mscf)	1,244,887	1,323,350
	Hyperbolic Exponent, *n*	0.92813018	0.873889702
	Model Constant, *a*	178.3950463	160.3161869

Table 4.17: Continued

Well Number	Model Parameters	Value Calculated Using 2/3 Data	Value Calculated Using Whole Data
35	Carrying Capacity, *K* (Mscf)	3,472,857	4,045,604
	Hyperbolic Exponent, *n*	0.901940271	0.795517783
	Model Constant, *a*	159.4510083	143.2223886
36	Carrying Capacity, *K* (Mscf)	913,930	782,242
	Hyperbolic Exponent, *n*	0.726269557	0.785179466
	Model Constant, *a*	125.2279614	124.508202
37	Carrying Capacity, *K* (Mscf)	1,730,093	1,677,598
	Hyperbolic Exponent, *n*	0.809581873	0.823894216
	Model Constant, *a*	168.5635247	169.1844138
38	Carrying Capacity, *K* (Mscf)	1,738,110	1,979,232
	Hyperbolic Exponent, *n*	0.78218606	0.736878113
	Model Constant, *a*	179.3460532	185.5427561

Table 4.18: Result Summary of Logistic Growth Analysis Model Predictive Performance

Well Number	Predictive Performance	Number of Wells		
		Using 2/3 Data	Using 2/3 Data (Compared with recently updated data)	Using Whole Data
LaSalle	Matched	15	16	17
	Under Predicted	4	4	4
	Over Predicted	5	4	3
Webb	Matched	7	5	5
	Under Predicted	7	9	9
	Over Predicted	0	0	0
Total	Matched	22	21	22
	Under Predicted	11	13	13
	Over Predicted	5	4	3

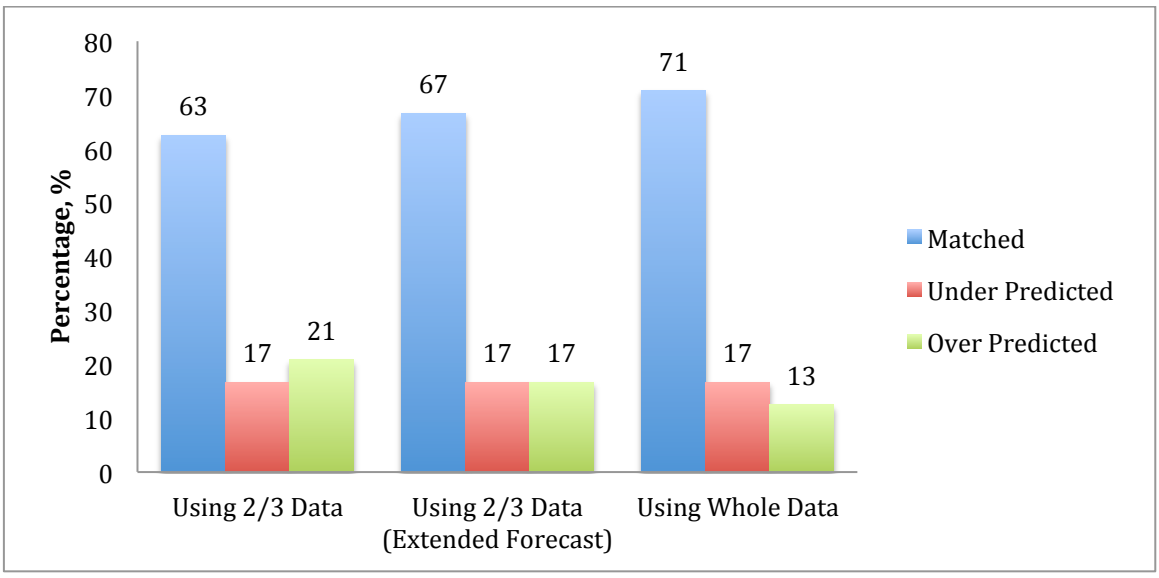

Figure 4.23: Logistic Growth Analysis model predictive performance (LaSalle County)

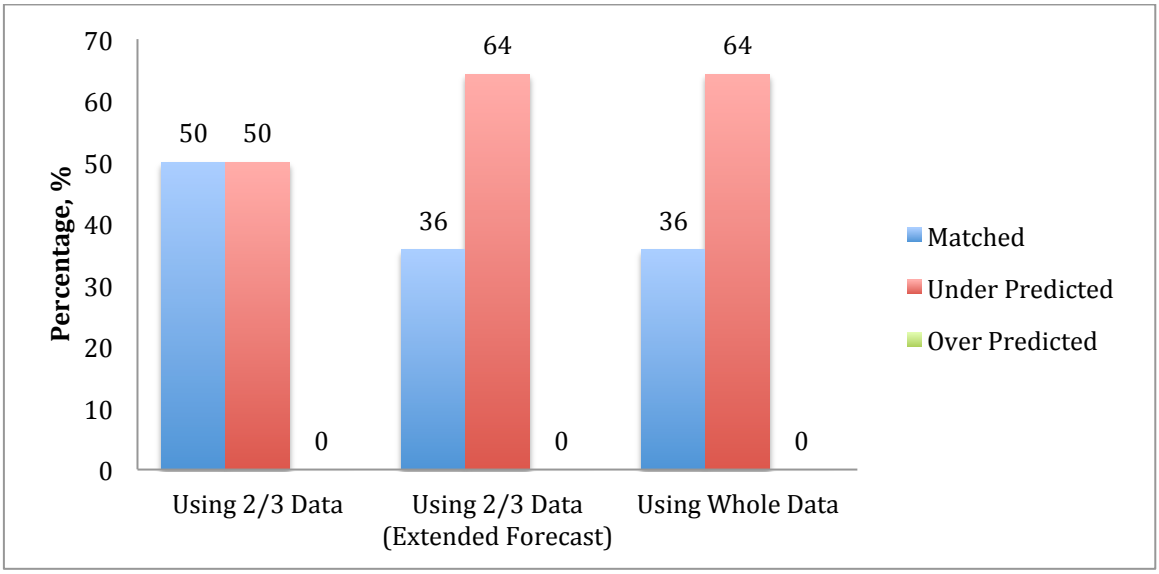

Figure 4.24: Logistic Growth Analysis model predictive performance (Webb County)

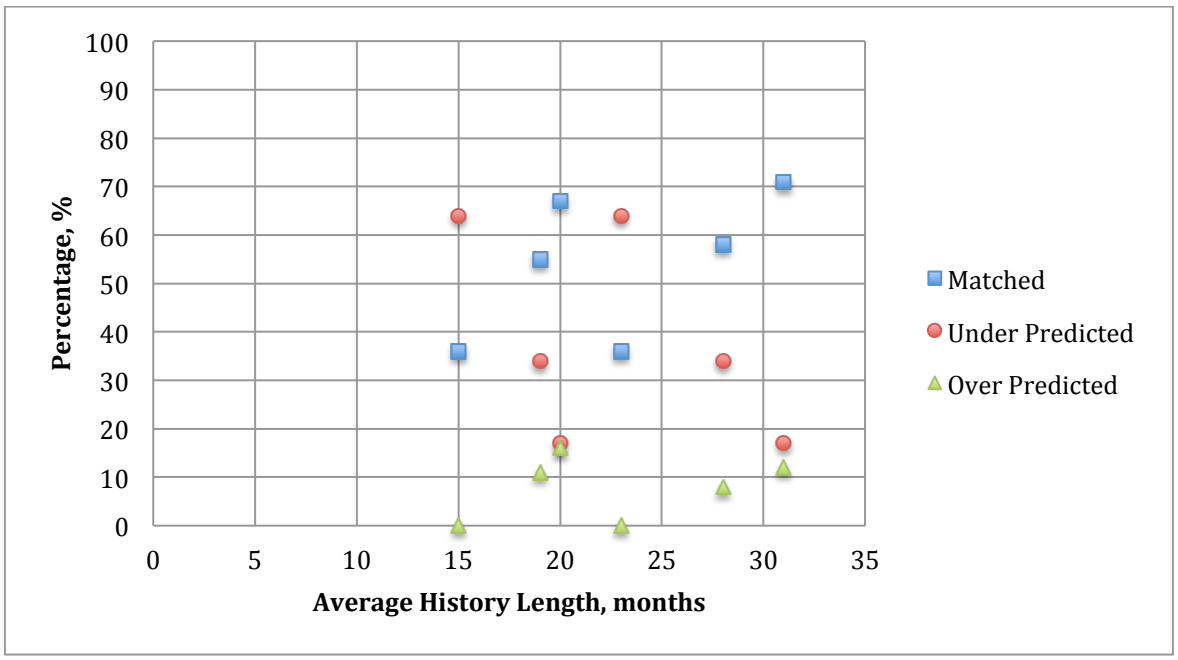

Figure 4.25: Summary of LGA decline model predictive performance based on different production history length

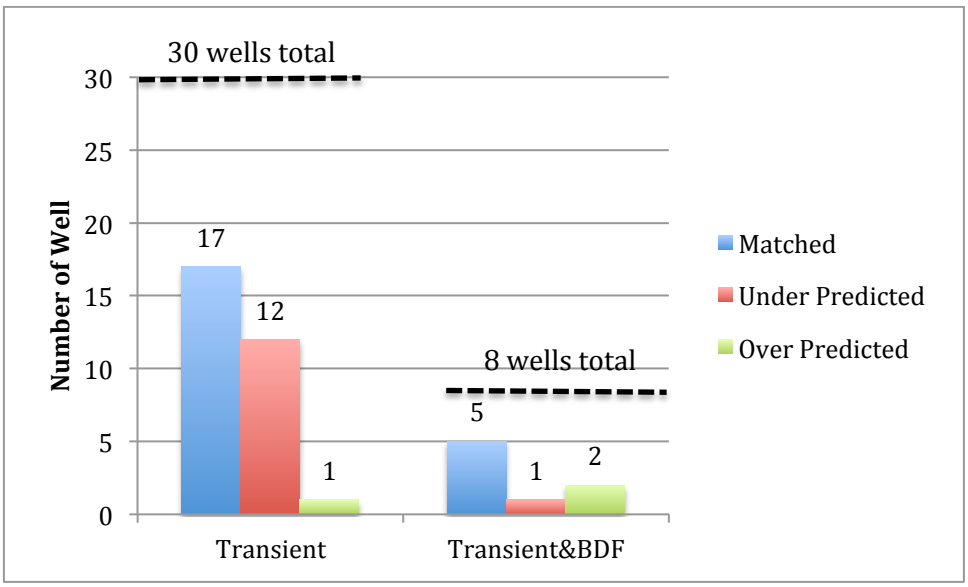

Figure 4.26: Summary of LGA decline model predictive performance based on different types of flow regimes

4.3.10 Observation and Discussion

Production rate history matching resulted from LGA of 24 wells in LaSalle County is showed in **Figure 4.23**. It clearly shows that the majority of predicted outcomes are matched the production history up to 71% and only 13%-21% range of mismatch. When two-third of the data has been used in LGA model to match the rest one-third of the production history, the model could match up to 63%. With more data that has been recently updated to compare, it improved the accuracy of LGA model slightly as matched wells increased from 63% (Using 2/3 Data) to 67% (Using 2/3 Data, Extended Forecast). Moreover, percentage of matched wells also increased from 67% to 71% when longer production history or whole data in this case was used in LGA model. However, the results for 14 wells in Webb County are behaving differently as showed in **Figure 4.24**. Over 50% of the matching results are under-predicted regardless of whether two-third of the data or the whole data was used in LGA model. Matched wells can be as high as 50% but reducing to 36% when having more data to compare. From this observation, it can be implied that LGA model also has a limitation in term of production history length as other DCA model. Lacking of production history down to certain length, 23 months in this case, would impair the predictive performance of LGA model. Overall results in **Figure 4.25** show that the model gives the highest accuracy of 71% compared with the other DCA models when using 31-month production history length. This indicates that LGA model seems to be an appropriate DCA model for prediction of future production trend, remaining reserve and remaining well life.

As a flow regime is concerned, from results in **Figure 4.26** out of the 30 wells that exhibiting only transient flow, the LGA model performed very well matched in 17 wells (57%). Moreover, the model gave a good match of the production history in 5 out of the 8 wells (63%) that showing transient flow at early time followed by BDF. The 3 unmatched wells might be affected by poor quality of their production history, which have no record of a specific activity that may result in

erratic production trend. The overall results indicate that the LGA model seems to be suitable to handle the decline trend of dry gas production that shows both transient flow and BDF.

4.3.11 Duong's Decline Analysis Model

Duong proposed his decline analysis model in 2011 to be used for prediction of ultimate recovery and future production trend specifically with very tight reservoirs, shale formation for example where fluid flow from fractures is dominated. The model has been developed and simplified to be easy to use and produce accurate forecast. **Tables 4.19** and **4.20** are representing the summary of the associated parameters in Duong's model including intercept constant (a), slope (m), rate at day 1 (q_1) and rate at infinite time (q_∞) calculated from dry gas wells in LaSalle and Webb counties respectively. Matching results of the individual well can be found in **Appendix II**, which has been done by the same approach of visual observation between the forecasts from Duong's model and their actual production history as **Section 4.3.3**. **Table 4.21** summarizes the numbers of the wells from the matching results, which are classified into 3 types, matched, under-predicted and over-predicted. For better clarification, the results in **Table 4.21** are calculated as percentage and plotted in 3 bar charts separately based on each county as showed in **Figures 4.27** through **4.29**. **Figure 4.30** also shows the matching results based on different types of flow regimes including the wells showing only transient flow and the wells showing both transient flow and BDF.

Table 4.19: Duong's decline analysis model parameters, LaSalle County wells

Well Number	Model Parameters	Value Calculated Using 2/3 Data	Value Calculated Using Whole Data
1	Intercept Constant, a	2.843	1.9433
	Slope, m	1.281	1.209
	Rate at Day 1, q_1 (Mscf/Day)	911.2	3,215.7
	Rate at Infinite Time, q_∞ (Mscf/Day)	88.9	159.8
2	Intercept Constant, a	2.7777	2.77
	Slope, m	1.287	1.286
	Rate at Day 1, q_1 (Mscf/Day)	881.2	871.3
	Rate at Infinite Time, q_∞ (Mscf/Day)	111.6	78.5
3	Intercept Constant, a	2.1048	1.0732
	Slope, m	1.25	1.121
	Rate at Day 1, q_1 (Mscf/Day)	3,922.7	15,587.0
	Rate at Infinite Time, q_∞ (Mscf/Day)	305.8	431.1
4	Intercept Constant, a	2.4024	2.1106
	Slope, m	1.244	1.219
	Rate at Day 1, q_1 (Mscf/Day)	982.9	1,461.0
	Rate at Infinite Time, q_∞ (Mscf/Day)	101.3	95.7
5	Intercept Constant, a	1.8757	1.348
	Slope, m	1.23	1.167
	Rate at Day 1, q_1 (Mscf/Day)	6,826.5	13,585.0
	Rate at Infinite Time, q_∞ (Mscf/Day)	480.2	458.0
6	Intercept Constant, a	1.7752	1.5525
	Slope, m	1.198	1.171
	Rate at Day 1, q_1 (Mscf/Day)	5,265.3	6,890.6
	Rate at Infinite Time, q_∞ (Mscf/Day)	421.1	361.9
7	Intercept Constant, a	2.5895	2.7182
	Slope, m	1.283	1.291
	Rate at Day 1, q_1 (Mscf/Day)	1,726.3	1,394.3
	Rate at Infinite Time, q_∞ (Mscf/Day)	190.6	112.9
8	Intercept Constant, a	3.1492	5.8005
	Slope, m	1.309	1.429
	Rate at Day 1, q_1 (Mscf/Day)	674.2	23.54
	Rate at Infinite Time, q_∞ (Mscf/Day)	101.3	0

Table 4.19: Continued

Well Number	Model Parameters	Value Calculated Using 2/3 Data	Value Calculated Using Whole Data
9	Intercept Constant, a	2.2728	2.0275
	Slope, m	1.234	1.212
	Rate at Day 1, q_1 (Mscf/Day)	2,803.5	3,884.6
	Rate at Infinite Time, q_∞ (Mscf/Day)	359.7	298.7
10	Intercept Constant, a	3.3232	3.2834
	Slope, m	1.318	1.317
	Rate at Day 1, q_1 (Mscf/Day)	251.5	270.0
	Rate at Infinite Time, q_∞ (Mscf/Day)	46.9	41.3
11	Intercept Constant, a	2.3722	2.3427
	Slope, m	1.248	1.245
	Rate at Day 1, q_1 (Mscf/Day)	1,696.5	1,713.4
	Rate at Infinite Time, q_∞ (Mscf/Day)	241.0	171.0
12	Intercept Constant, a	2.0194	1.9774
	Slope, m	1.22	1.215
	Rate at Day 1, q_1 (Mscf/Day)	2,816.3	2,866.9
	Rate at Infinite Time, q_∞ (Mscf/Day)	324.6	241.2
13	Intercept Constant, a	1.3193	1.1552
	Slope, m	1.132	1.105
	Rate at Day 1, q_1 (Mscf/Day)	5,547.9	6,624.1
	Rate at Infinite Time, q_∞ (Mscf/Day)	415.6	348.8
14	Intercept Constant, a	1.9721	1.5737
	Slope, m	1.209	1.163
	Rate at Day 1, q_1 (Mscf/Day)	1,709.6	2,862.7
	Rate at Infinite Time, q_∞ (Mscf/Day)	185.9	192.0
15	Intercept Constant, a	1.7744	1.6879
	Slope, m	1.179	1.169
	Rate at Day 1, q_1 (Mscf/Day)	1,632.1	1,790.0
	Rate at Infinite Time, q_∞ (Mscf/Day)	149.2	111.5
16	Intercept Constant, a	2.4434	2.4663
	Slope, m	1.234	1.236
	Rate at Day 1, q_1 (Mscf/Day)	1,143.9	1,106.6
	Rate at Infinite Time, q_∞ (Mscf/Day)	72.1	55.6

Table 4.19: Continued

Well Number	Model Parameters	Value Calculated Using 2/3 Data	Value Calculated Using Whole Data
17	Intercept Constant, a	1.8906	1.4241
	Slope, m	1.194	1.137
	Rate at Day 1, q_1 (Mscf/Day)	2,010.0	3,771.4
	Rate at Infinite Time, q_∞ (Mscf/Day)	192.1	228.0
18	Intercept Constant, a	2.3935	2.6773
	Slope, m	1.236	1.259
	Rate at Day 1, q_1 (Mscf/Day)	1,396.7	949.6
	Rate at Infinite Time, q_∞ (Mscf/Day)	127.1	66.3
19	Intercept Constant, a	3.0935	2.1677
	Slope, m	1.327	1.252
	Rate at Day 1, q_1 (Mscf/Day)	1,865.1	5,778.2
	Rate at Infinite Time, q_∞ (Mscf/Day)	433.2	557.7
20	Intercept Constant, a	1.9762	1.8376
	Slope, m	1.207	1.192
	Rate at Day 1, q_1 (Mscf/Day)	4,076.1	4,778.3
	Rate at Infinite Time, q_∞ (Mscf/Day)	466.0	372.5
21	Intercept Constant, a	3.0557	1.9062
	Slope, m	1.297	1.2
	Rate at Day 1, q_1 (Mscf/Day)	1,453.6	6,600.3
	Rate at Infinite Time, q_∞ (Mscf/Day)	179.2	530.1
22	Intercept Constant, a	2.0898	1.6637
	Slope, m	1.233	1.185
	Rate at Day 1, q_1 (Mscf/Day)	6,020.6	10,056.0
	Rate at Infinite Time, q_∞ (Mscf/Day)	895.3	816.2
23	Intercept Constant, a	2.3424	2.4825
	Slope, m	1.233	1.245
	Rate at Day 1, q_1 (Mscf/Day)	1,375.2	1,125.5
	Rate at Infinite Time, q_∞ (Mscf/Day)	184.1	120.9
24	Intercept Constant, a	6.9057	7.3893
	Slope, m	1.516	1.53
	Rate at Day 1, q_1 (Mscf/Day)	19.4	11.5
	Rate at Infinite Time, q_∞ (Mscf/Day)	24.4	19.8

Table 4.20: Duong's decline analysis model parameters, Webb County wells

Well Number	Model Parameters	Value Calculated Using 2/3 Data	Value Calculated Using Whole Data
25	Intercept Constant, a	3.2669	3.4547
	Slope, m	1.342	1.354
	Rate at Day 1, q_1 (Mscf/Day)	426.3	333.1
	Rate at Infinite Time, q_∞ (Mscf/Day)	121.1	70.9
26	Intercept Constant, a	2.4092	2.7551
	Slope, m	1.221	1.249
	Rate at Day 1, q_1 (Mscf/Day)	656.0	417.4
	Rate at Infinite Time, q_∞ (Mscf/Day)	9.0	0
27	Intercept Constant, a	2.5279	2.3343
	Slope, m	1.266	1.249
	Rate at Day 1, q_1 (Mscf/Day)	815.0	1,021.7
	Rate at Infinite Time, q_∞ (Mscf/Day)	127.3	109.6
28	Intercept Constant, a	3.8278	3.1347
	Slope, m	1.365	1.324
	Rate at Day 1, q_1 (Mscf/Day)	501.6	1,180.1
	Rate at Infinite Time, q_∞ (Mscf/Day)	136.3	189.1
29	Intercept Constant, a	2.0072	2.0072
	Slope, m	1.225	1.225
	Rate at Day 1, q_1 (Mscf/Day)	1,934.7	1,934.7
	Rate at Infinite Time, q_∞ (Mscf/Day)	143.8	143.8
30	Intercept Constant, a	2.6286	2.4104
	Slope, m	1.304	1.287
	Rate at Day 1, q_1 (Mscf/Day)	1,440.0	1,834.3
	Rate at Infinite Time, q_∞ (Mscf/Day)	277.7	192.6
31	Intercept Constant, a	3.8342	3.9047
	Slope, m	1.375	1.379
	Rate at Day 1, q_1 (Mscf/Day)	275.3	250.2
	Rate at Infinite Time, q_∞ (Mscf/Day)	109.2	71.8
32	Intercept Constant, a	3.1728	3.132
	Slope, m	1.311	1.309
	Rate at Day 1, q_1 (Mscf/Day)	1,056.2	1,114.2
	Rate at Infinite Time, q_∞ (Mscf/Day)	231.6	181.7

Table 4.20: Continued

Well Number	Model Parameters	Value Calculated Using 2/3 Data	Value Calculated Using Whole Data
33	Intercept Constant, a	5.2756	4.7555
	Slope, m	1.429	1.407
	Rate at Day 1, q_1 (Mscf/Day)	109.6	200.0
	Rate at Infinite Time, q_∞ (Mscf/Day)	0	24.4
34	Intercept Constant, a	3.7193	4.4315
	Slope, m	1.362	1.398
	Rate at Day 1, q_1 (Mscf/Day)	333.0	138.3
	Rate at Infinite Time, q_∞ (Mscf/Day)	111.4	39.7
35	Intercept Constant, a	3.1957	2.6309
	Slope, m	1.33	1.288
	Rate at Day 1, q_1 (Mscf/Day)	1,649.2	3,204.0
	Rate at Infinite Time, q_∞ (Mscf/Day)	594.1	571.1
36	Intercept Constant, a	2.4326	2.9389
	Slope, m	1.283	1.324
	Rate at Day 1, q_1 (Mscf/Day)	1,062.4	552.1
	Rate at Infinite Time, q_∞ (Mscf/Day)	203.9	95.7
37	Intercept Constant, a	2.6624	2.8855
	Slope, m	1.287	1.305
	Rate at Day 1, q_1 (Mscf/Day)	1,199.5	894.5
	Rate at Infinite Time, q_∞ (Mscf/Day)	252.7	138.9
38	Intercept Constant, a	2.2929	1.979
	Slope, m	1.251	1.221
	Rate at Day 1, q_1 (Mscf/Day)	1,416.4	2,078.3
	Rate at Infinite Time, q_∞ (Mscf/Day)	237.1	196.9

Table 4.21: Result summary of Duong's decline analysis model predictive performance

Well Number	Predictive Performance	Number of Wells		
		Using 2/3 Data	Using 2/3 Data (Compared with recently updated data)	Using Whole Data
LaSalle	Matched	9	11	4
	Under Predicted	1	0	0
	Over Predicted	14	13	20
Webb	Matched	4	4	6
	Under Predicted	0	2	2
	Over Predicted	10	8	6
Total	Matched	13	15	10
	Under Predicted	1	2	2
	Over Predicted	24	21	26

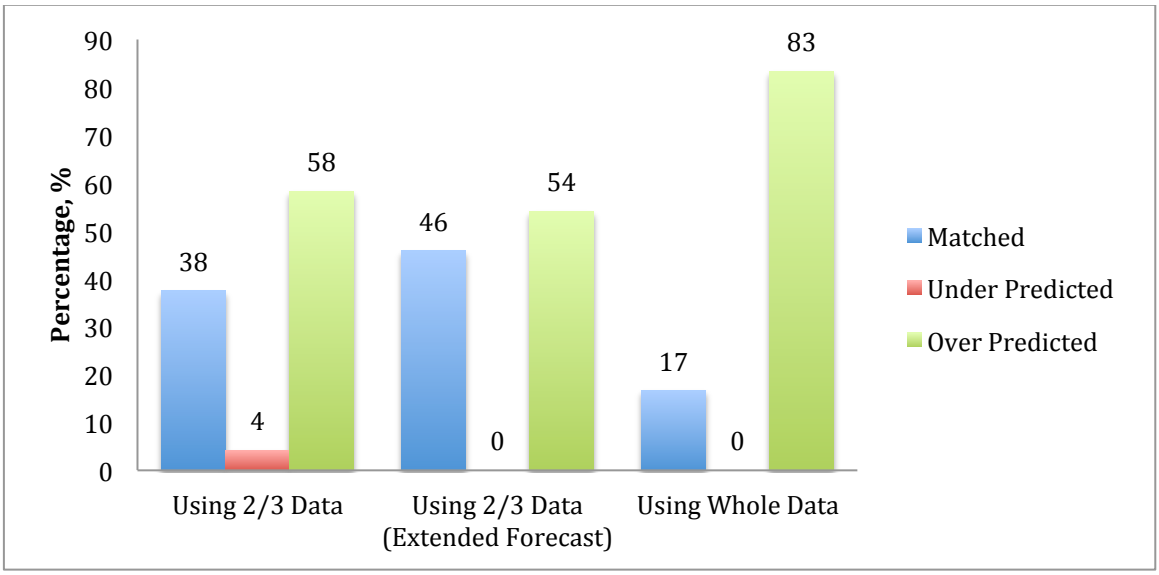

Figure 4.27: Duong's decline analysis model predictive performance (LaSalle County)

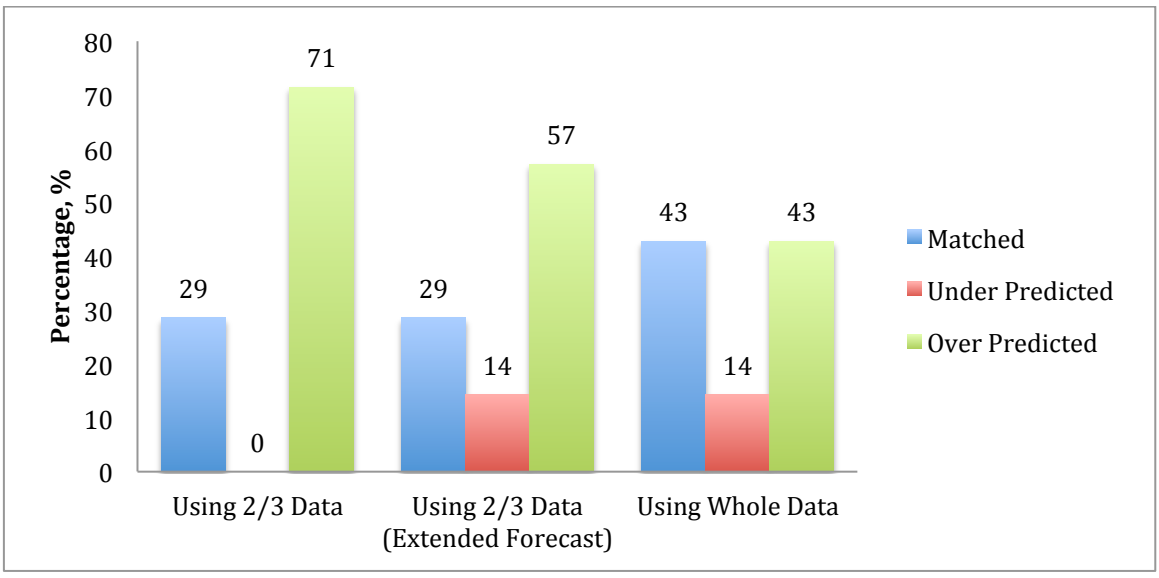

Figure 4.28: Duong's decline analysis model predictive performance (Webb County)

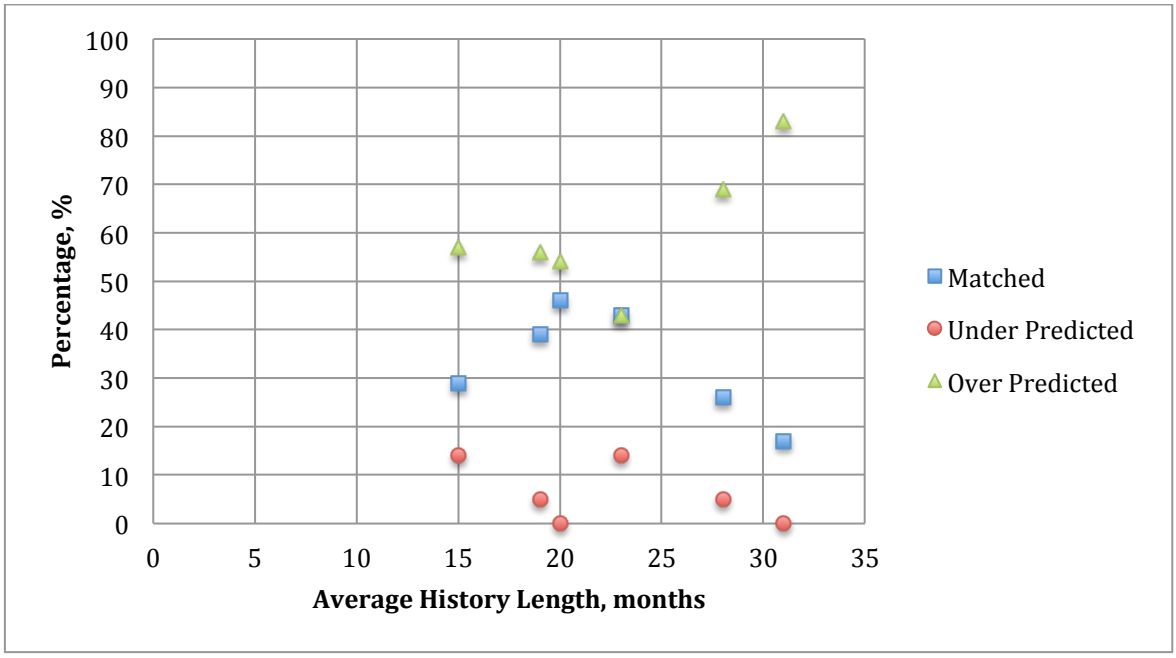

Figure 4.29: Summary of Duong's decline model predictive performance based on different production history length

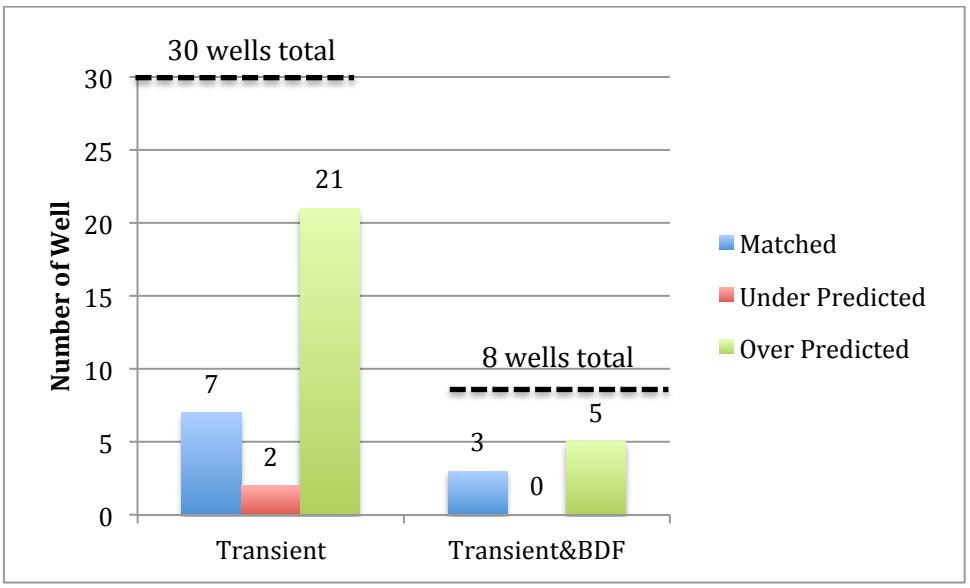

Figure 4.30: Summary of Duong's decline model predictive performance based on different types of flow regimes

4.3.12 Observation and Discussion

Obvious observations that can be drawn from **Figure 4.27** is that over 50% and up to 83% of the forecasted production trends generated by Duong's model are over-predicted and only maximum 46% of matched wells. Not like the other DCA models in this study, when longer production data (whole data) was used in Duong's model, percentage of matched wells decreased significantly from 46% to 17%. On the other hand for the wells in Webb County as showed in **Figure 4.28**, when the whole production data was applied in Duong's model instead of the two-third of the data, percentage of matched wells increased from 29% to 43%. However, the majority of the forecast outcomes are over-predicted. According to overall result in **Figure 4.29**, Duong's model does not seem to be a good decline analysis model for prediction of future production trend in these particular regions due to high percentage (43%-83%) of future production trend mismatch (over-predicted) and low percentage of matched wells (17%-46%).

When looked into the possible effect of the flow regime on the predictive accuracy of Duong's model, the results in **Figure 4.30** show that 7 out of the 30 wells (23%) that exhibiting only transient flow and 3 out of the 8 wells (38%) that showing the transient flow followed by BDF are matched with the production history when Duong's model is applied. The majority of the matching results are 70% over-predicted and 63% over-predicted for transient flow wells and transient-BDF wells respectively. Due to very low percentage of matching accuracy in both cases, it indicates that Duong's model does not seem to be a reliable DCA model for predicting future production trend.

4.4 Simulation Models

4 wells were selected (2 wells from in each county) based on available information of well completion and reservoir characteristics. The selected wells include

- Well#1 - HENDERSON-CENIZO, Lease No.251105 located in LaSalle County (43-month production history)
- Well#16 - APPLING 695, Lease No.258036 located in LaSalle County (31-month production history)
- Well#26 - GALVAN RANCH, Lease No.257683 located in Webb County (28-month production history)
- Well#31 - ROSA VELA BENAVIDES, Lease No.260047 located in Webb County (23-month production history)

It must be mentioned again that these simulation models are for one quarter of one hydraulic fracture based on the assumption of identical hydraulic fractures along a horizontal wellbore. Therefore, the total rate is the rate for the simulation model multiplied by four and then by number of hydraulic fractures of each particular well. The assumption of identical fractures is not correct but is used because of lack of data related to the fractures in a well as well as to simplify the study

by using less number of grid blocks. The models also included the effects of the presence of the hydraulic fracturing fluid prior the production, gas desorption, non-Darcy flow and hydraulic fracture distribution as described in **Sections 3.1.4** and **3.2.2.**

The simulation models of these wells were built by using the actual parameters officially reported on TRRC database. However, 3 main parameters including matrix permeability, matrix porosity and hydraulic fracture un-propped zone permeability were adjusted during the history matching since broad ranges of values were given for them. The matrix permeability and matrix porosity were obtained from Eagle Ford shale core analysis by Inamdar et al. in 2010 in the ranges of 1-800 nD and 5-18% respectively. Moreover, the fracture design software, FracPro, does not provide the result of the conductivity of un-propped zone in the hydraulic fracture plain thus the un-propped zone permeability was also used as matching parameter in the range of 1 nD (as low as minimum matrix permeability) to 10 mD (minimum permeability of hydraulic fracture in propped zone).

The 3 main parameters were varied in pre-simulation of well#1 model to observe their effects on production trend and gas recovery factor. The results were used as a general guideline for adjusting the parameters to be able to obtain a reasonable match between actual production history and simulated production result on plots of production rate versus time and cumulative production versus time. The matching results were done by visual observation and final values of the variables were listed in **Table 3.8** in **Section 3.2.2**.

The matrix permeability plays a big role on production decline trend as showed in **Figure 4.31**. When the permeability increase one order of magnitude from 10 nD to 100 nD, it shifts up the whole production trend with initial rate increased from 7,200 Mscf/day to 10,000 Mscf/day and fairly high rates at late production time, at 1,310 days for instance, the production rate of 100nD matrix permeability is 2,568 Mscf/day but only 790 Mscf/day for 10 nD matrix permeability. Moreover, the gas recovery factor relatively increases significantly from 6.6% to 21.2% when the

permeability increases from 10 nD to 100 nD. The increase may not be as high for higher values of permeability, e.g. 1,000 versus 100 nD.

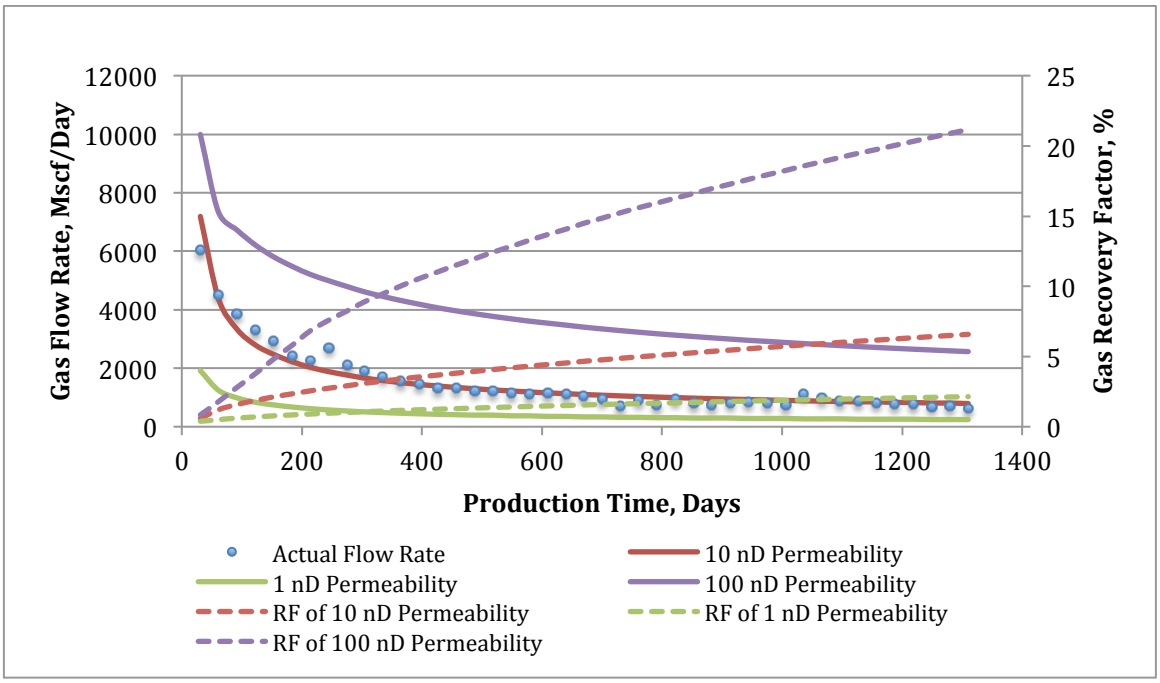

Figure 4.31: Effect of matrix permeability on production trend and gas recovery factor of well#1

The effect of the matrix porosity is showed in **Figure 4.32**. The result clearly indicates that the porosity also influences the production decline trend, unlike the matrix permeability that shifts the entire trend; the porosity contributes much on initial rate and rates during early production time. The initial rate relatively increases from 7,200 Mscf/day to 8,800 Mscf/day when the matrix porosity increases from 6% to 10%. However, the gas recovery factor decreases when the porosity increases. This is because when the porosity increases, the original gas in place will increase thus the well will have to spend more time to produce up to a given recovery factor.

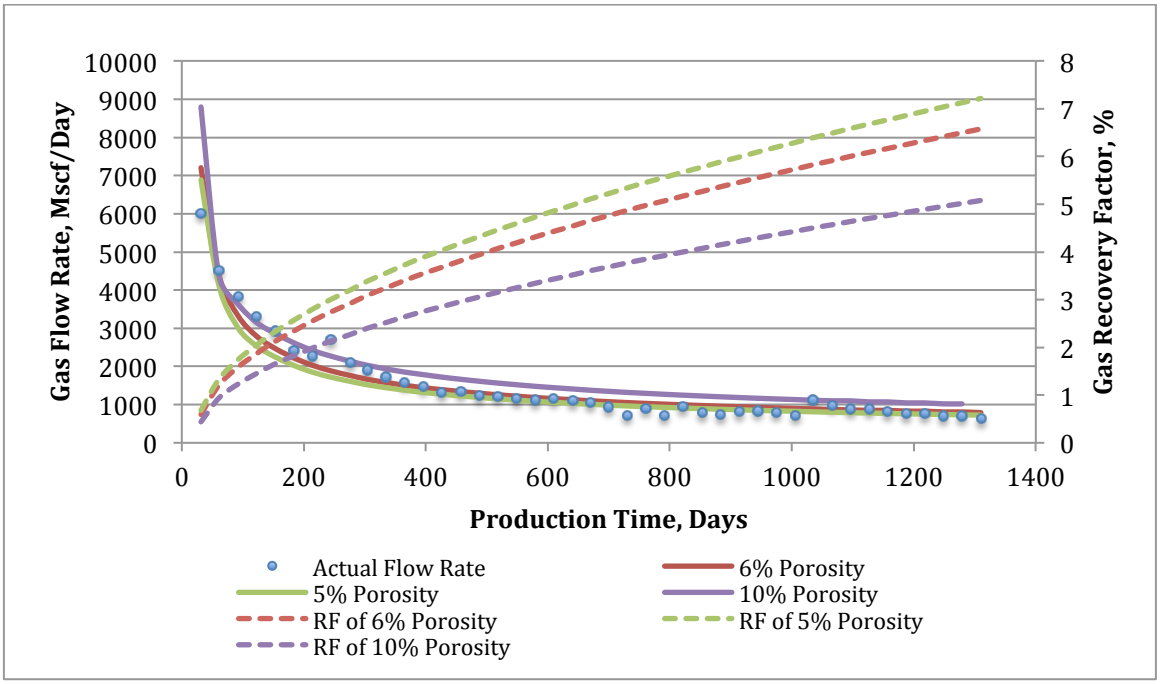

Figure 4.32: Effect of matrix porosity on production trend and gas recovery factor of well#1

The permeability of un-propped zone also affects the behavior of the production decline trend. The result in **Figure 4.33** shows that when the permeability of un-propped zone increases, the production rates of the entire trend slightly increase compared to the effects of the other two factors. The gas recovery factor result also corresponds to the production rates.

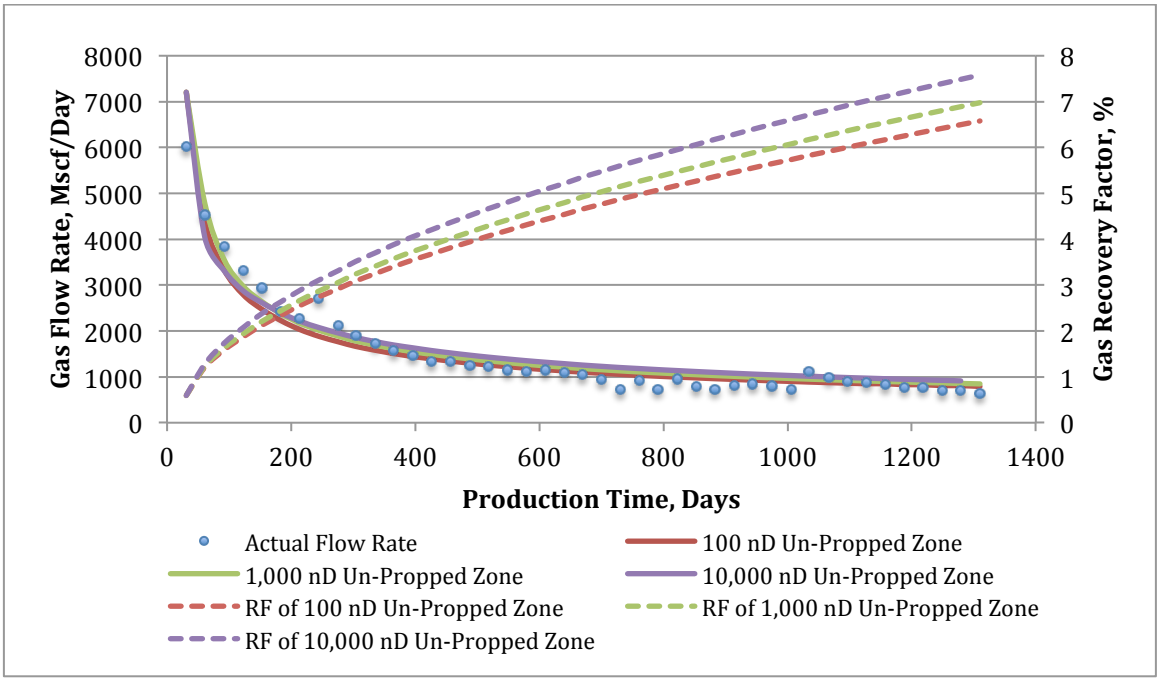

Figure 4.33: Effect of un-propped zone permeability on production trend and gas recovery factor of well#1

The past production history of each well was matched by adjusting the three unknown parameters. History-matched simulation model of each well was used to predict the remaining reserve and remaining well life to abandonment rate of 100 Mscf/day. The predictions from the simulation will be served as a benchmark to compare remaining reserve and remaining life forecasted by each DCA model. This is in light of a real fact that history matching is not unique but this is the best that can be done considering the limitation of data.

4.4.1 Well#1, HENDERSON-CENIZO, Lease No. 251105

Well#1 in this study is a dry gas well located in LaSalle County. The well was drilled and completed horizontally in Eagle Ford shale stratum at depth of 11,000 feet. Petrohawk Operating Company started the production in April 2009 by utilizing the hydraulic fracturing technique with 10 fracturing stages in 4,000 ft long lateral. The highest gas production rate reached in May 2009, which was 6,022 Mscf/Day. Cumulative gas production up to Dec 2012 is 1,975 MMscf. Based on the production data reported on the TRRC website, this well has 43 months of production history (end of Dec 2012) available when firstly collected and 11 more months for recently updated production history (end of Nov 2013). Out of 24 wells in LaSalle County and 38 total wells in this study, this well has the longest production history.

4.4.2 Observation and Discussion

The history matching results of this well can be found in **Table 4.3**. Future production rate trend generated from Arps' Harmonic and LGA models fit production rate history regardless whether whole or two-third of the data is used in the models. PLE and Arps' Hyperbolic models match the history only when using whole production data in the models. On the other hand, Duong's model fit the history only when using two-third of the data.

A fair fit between a half slope line and the actual production history in **Figure 4.34** indicates a transient flow behavior of well#1 up to the end of the available production history. However, sudden increase of the production rate at around 900 days of the producing time can imply that there most likely was an additional operation took place during the production but was not reported on the database. By that operation, it might extend the transient flow behavior instead of starting to follow BDF behavior. Moreover, the decrease in production rate at 1,600 days seems to be a starting point of BDF behavior. More actual production data is needed to draw any reasonable conclusion.

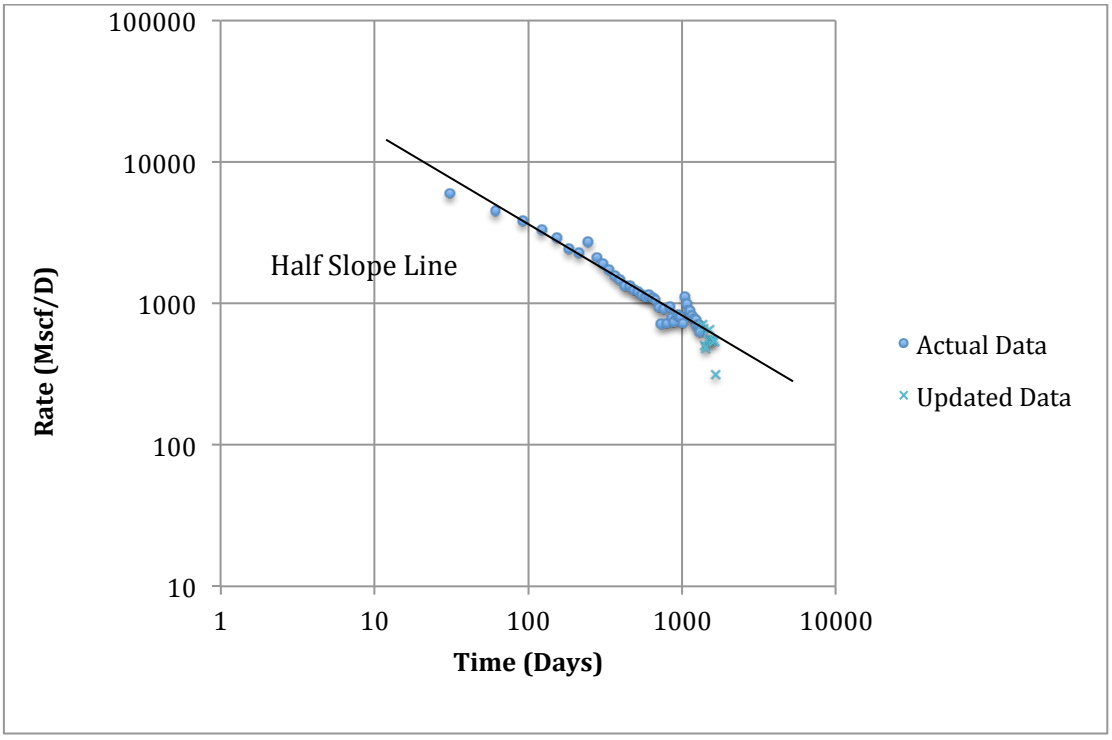

Figure 4.34: Flow regime diagnostic plot of well#1

Figure 4.35 (a-b) shows a reasonable match of the actual production history. The simulation model then was used for prediction of remaining reserve and remaining well life which are 1,308 MMscf and 12 years respectively. From the summary of the predicted remaining reserve and remaining well life in **Figures 4.36** and **4.37** in general, Aprs' Harmonic model gives very high estimates of both remaining reserve and remaining life which are 2,305 MMscf and 23 years respectively when 29 month production history is used. However, when applying longer data, 43 months, the remaining reserve reduces significantly to 1,586 MMscf, which is close to the simulation result, and its remaining well life decreases slightly to 20 years. On the other hand, the rest of the DCA models give the estimates of both remaining reserve and remaining life lower than the simulation results when 29-month production history is used. The estimates are getting higher and closer to the simulation results when 43 months of the production history is used. This observation is in-line with the fact that when a longer production history is matched by simulation or DCA, the predictions are expected to be more accurate. When considering both remaining reserve and remaining life together, LGA model seems to be the most acceptable model for prediction in this case since it predicted 1,081 MMscf of remaining reserve which is slightly lower than the simulation result but its remaining life is 13 years which is very close to the result from the simulation.

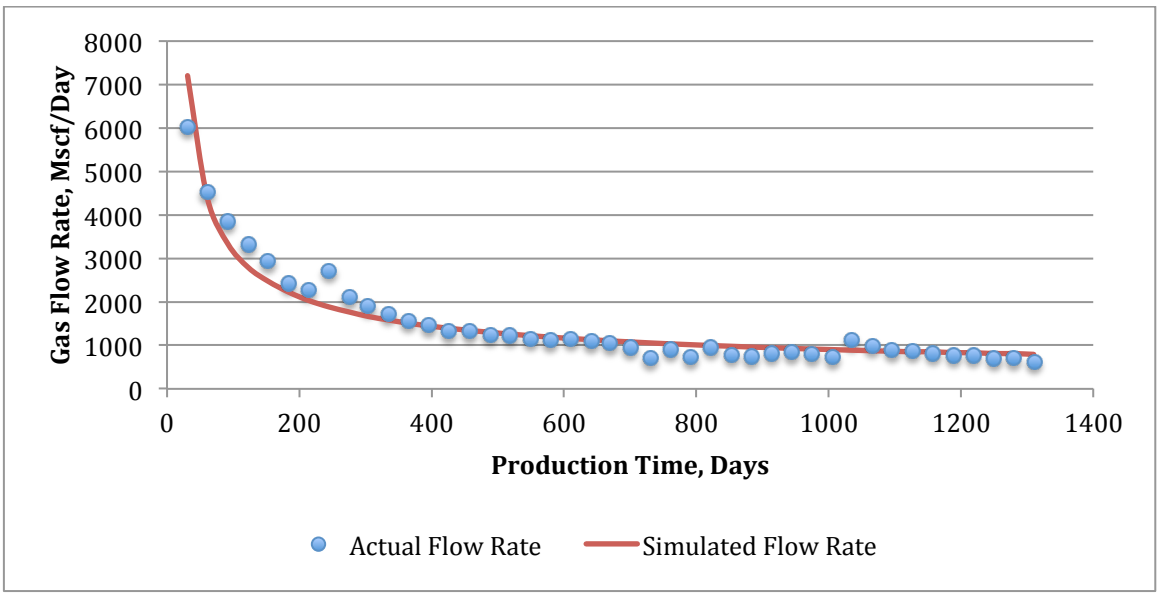

(a)

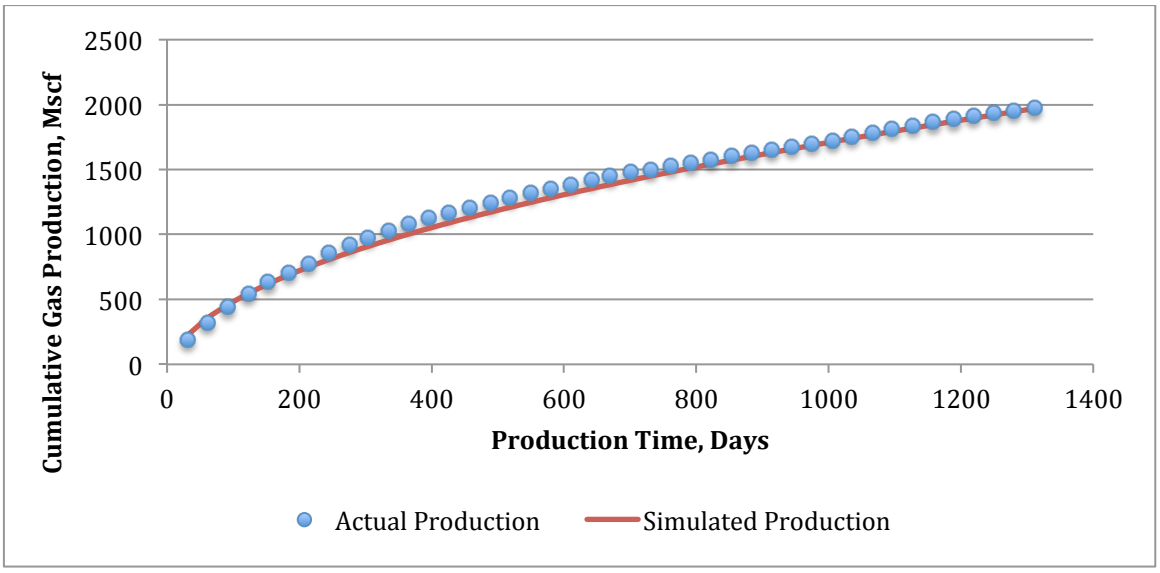

(b)

Figure 4.35 (a-b): Matching results of well#1 between actual production data and simulated outcomes of (a) production rate and (b) cumulative production

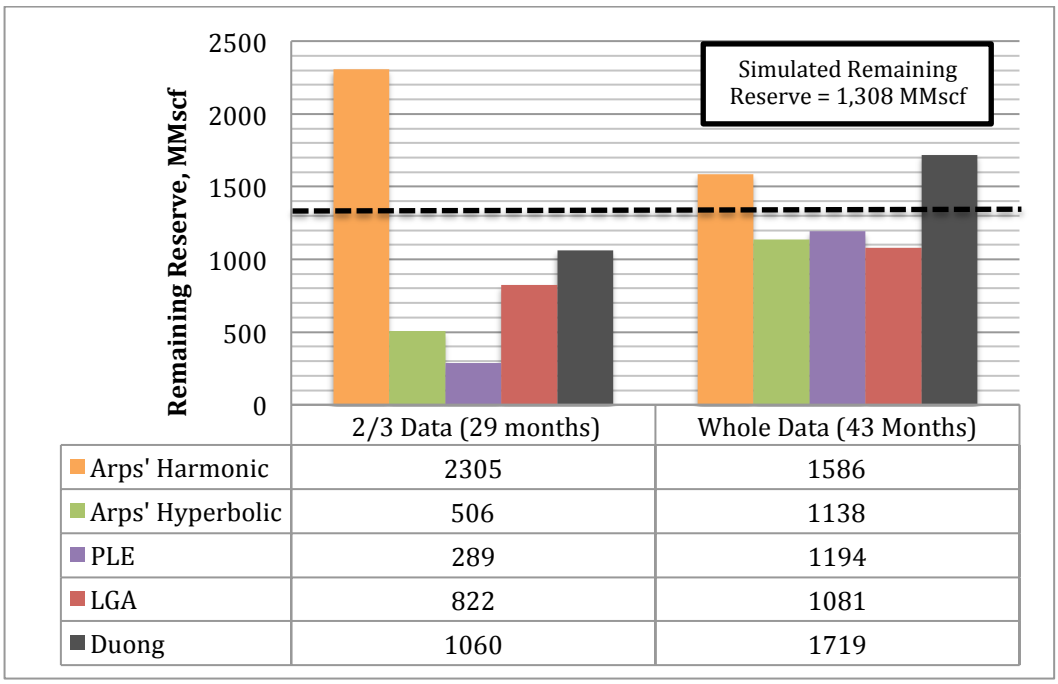

	2/3 Data (29 months)	Whole Data (43 Months)
Arps' Harmonic	2305	1586
Arps' Hyperbolic	506	1138
PLE	289	1194
LGA	822	1081
Duong	1060	1719

Figure 4.36: Comparison of remaining reserve predicted by 5 DCA models using different length of production data of well#1

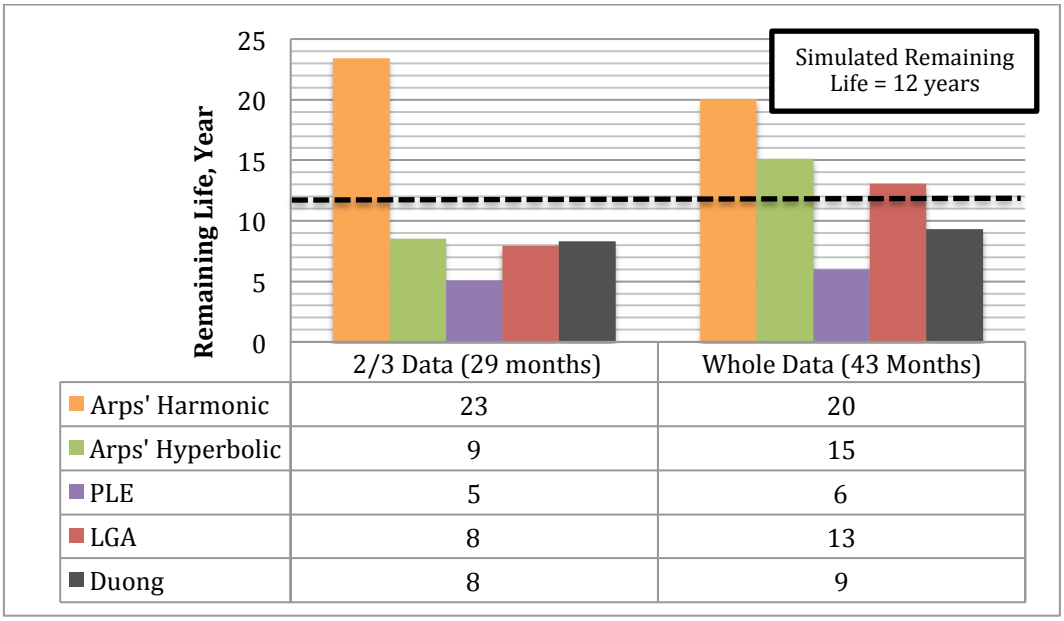

	2/3 Data (29 months)	Whole Data (43 Months)
Arps' Harmonic	23	20
Arps' Hyperbolic	9	15
PLE	5	6
LGA	8	13
Duong	8	9

Figure 4.37: Comparison of remaining well life predicted by 5 DCA models using different length of production data of well#1

The future production trends predicted up to 10,000 days by different DCA models using 29 months and 43 months of the actual production histories are plotted and showed in **Figure 4.38** and **Figure 4.39**. When using 43 months of the data, Duong's model predicts the highest production rate until 10,000 days. Beside Duong's model, the trends calculated by the rest of DCA models follow very close to each other until they start to split at approximately 2,400 days. In case of using 29 months of the data, **Figure 4.39**, results from all models follow the same trend until splitting at around 900 days. Duong's model seems to have more fit of the production trend when compared with the predicted trend in the 43-month case. Arps' Harmonic gives relatively higher trend toward 10,000 days. Arp's Hyperbolic, PLE and LGA exhibit very low production rate trend when short data is used. Moreover, PLE seems to be the most sensitive model against available history length since it generates very conservative production rate trend when using 29 months of the data same as the other models. Gas well that exhibiting only transient flow, with longer production history (43 months), all the DCA models in this study seem to follow closely to the half slope line toward abandonment. However, the production history as short as 29 months seems to dictate their forecast behaviors. The decline rates forecasted by Arps' Hyperbolic, LGA and PLE will decrease nonlinearly on a log-log plot of rate versus time at late time toward abandonment.

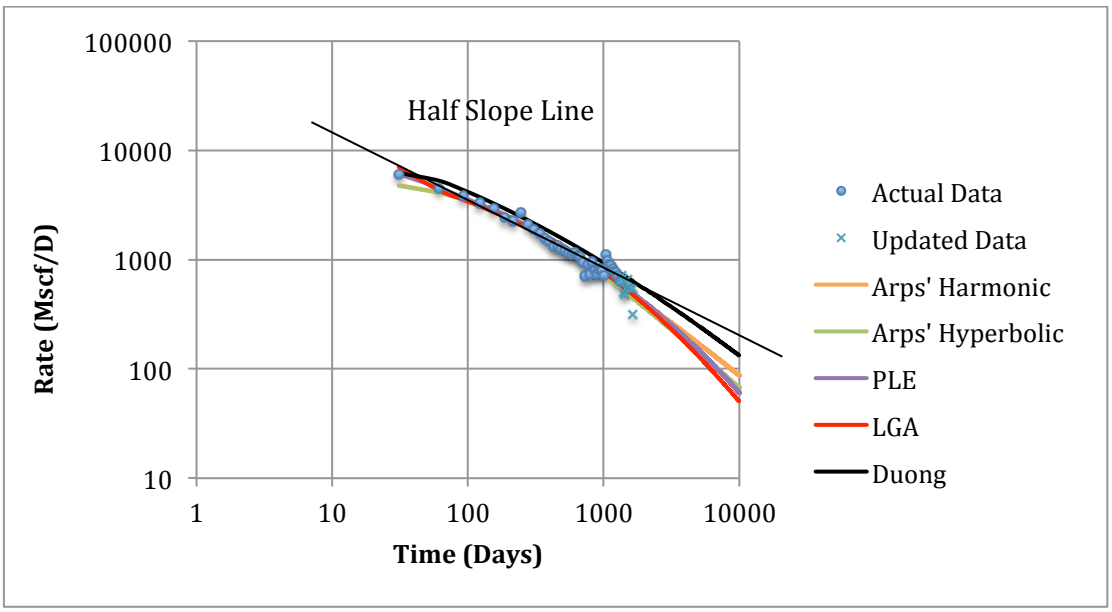

Figure 4.38: Comparison of forecasts calculated using whole data of well#1

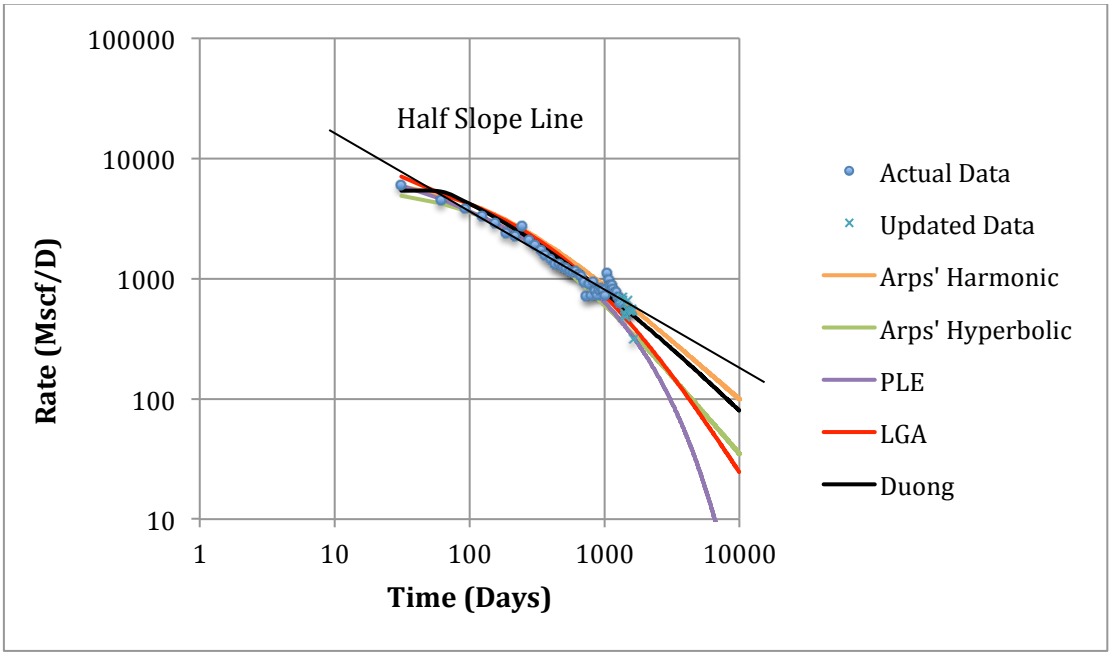

Figure 4.39: Comparison of forecasts calculated using 2/3 data of well#1

4.4.3 Well#16, APPLING 695, Lease No.258036

Well#16 Appling 695, is located in LaSalle County. It was drilled and completed horizontally in Eagle Ford shale stratum at depth of 12,693 feet. Petrohawk Operating Company also has operated this well since May 2010 and the hydraulic fracturing technique again has been employed. 14 fracturing stages were executed to create fractures along 4,200 ft horizontal leg. The well is producing only dry gas with no other heavier hydrocarbon reported. The initial gas rate was 2,125 Mscf/Day in May 2010 and reached 5,109 Mscf/Day, which is the highest rate in June 2010. Cumulative gas production up to date (Dec 2012) is 1,844 MMscf. Based on the production data available on TRRC website, only 31 months of the production history (end of Dec 2012) is available for this well when began collecting the data for this study. 12 more months of the production history has been recently reported up to end of Dec 2013. 31-month data length of this well is considered as the shortest length compared to the other wells in LaSalle County.

4.4.4 Observation and Discussion

The DCA summary of well#16 is presented in **Table 4.3**. The results can be observed clearly that Arps' Harmonic and LGA models well match the production history in both cases of using whole data and two-third of the data. PLE model can fit the history only when using longer production history (whole data). The matching results of Duong's model are over-predicted regardless of how long the history length is used in the model. Arps' Hyperbolic matching results are very erratic. When applying two-third of the data in the model to match the rest one-third, the synthetic trend goes underneath the actual production trend however when compared to the recent update of the data, they are matched. Moreover, the matching result is over-predicted when whole data is used in the model.

The production rate trend of well#16 shows a half slope line indicating transient flow to approximately 400 days and then starts going into BDF that can be observed by a unit slope line as showed in **Figure 4.40**.

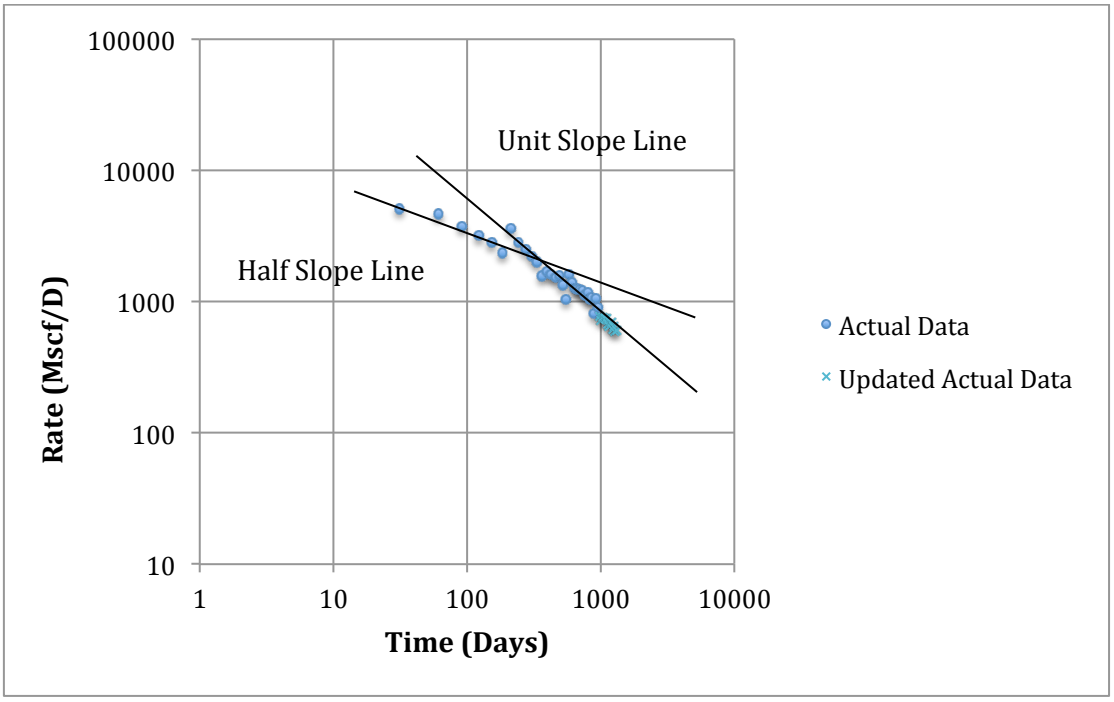

Figure 4.40: Flow regime diagnostic plot of well#16

Figure 4.41 (a-b) shows the matched production history. In **Figure 4.41 (a)**, it is noted that there might be an additional operation that took place during the production causing the sudden increase of the production rates at approximately 200 days. As a result, that phenomenon might contribute to higher cumulative production trend showing in **Figure 4.41 (b)**. The history-matched simulation model predicted that the well will take approximately 8 years to produce the remaining reserve of 1,422 MMscf based on abandonment rate of 100 Mscf/day.

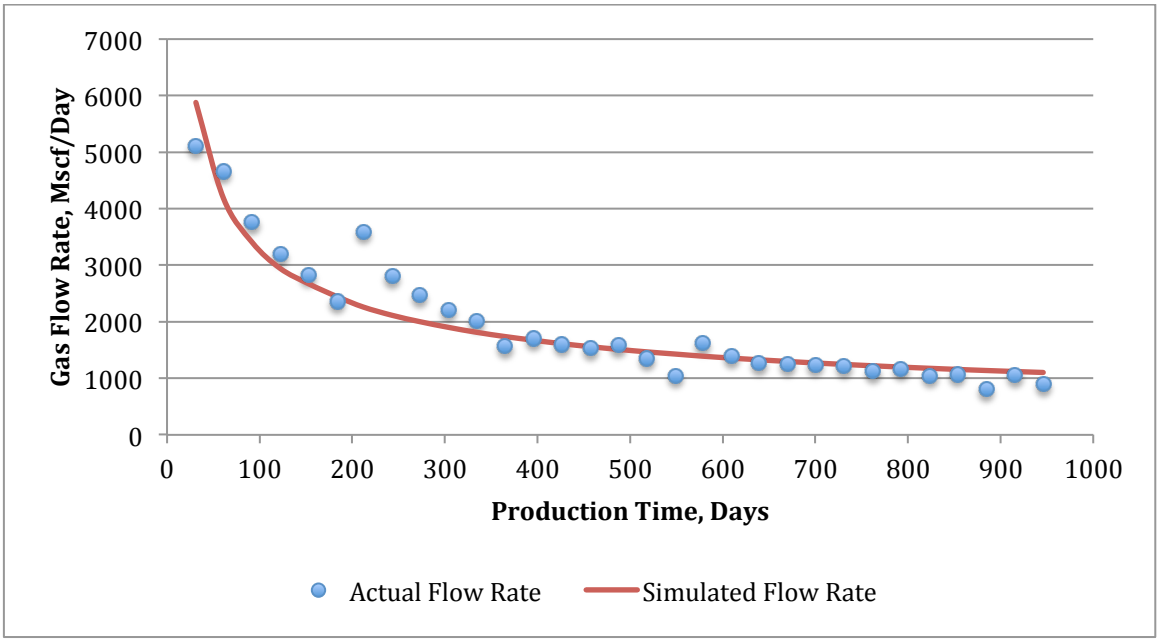

(a)

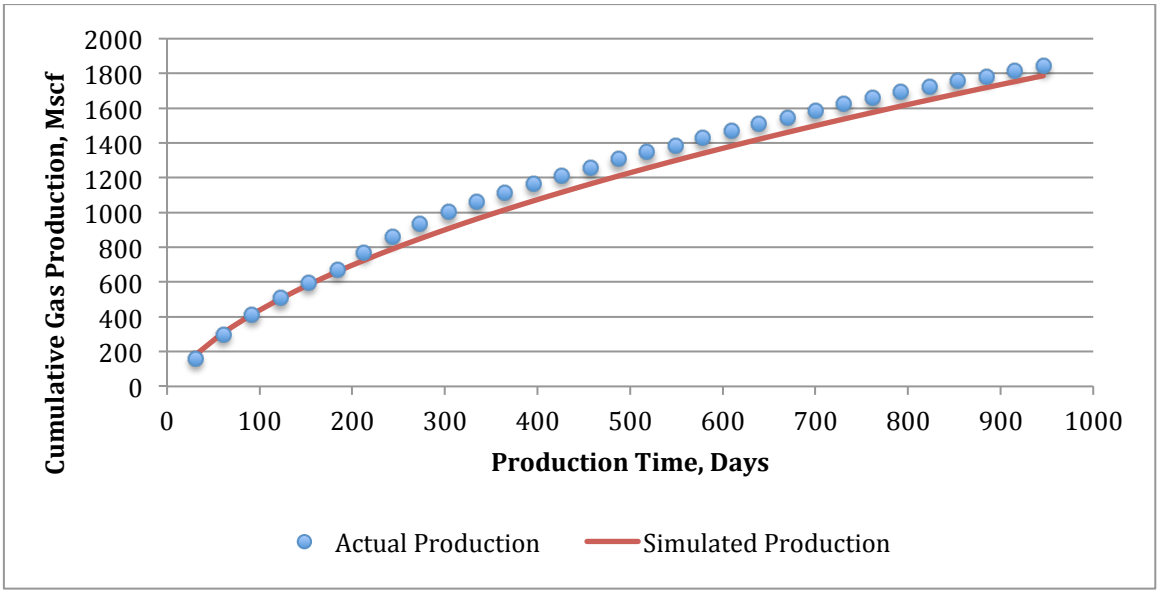

(b)

Figure 4.41 (a-b): Matching results of well#16 between actual production data and simulated outcomes of (a) production rate and (b) cumulative production

In the case of this transient flow with BDF behavior, the remaining reserve predicted by LGA model is the closest estimate when compared to the simulation result as showed in **Figure 4.42**. The remaining reserve by LGA slightly increases from 959 MMscf to 1145 MMscf when 31 months of the production data is used in the model over 21 month data. Duong's model overestimates the remaining reserve in this case. It also follows the same behavior as LGA as it gives slightly higher value of the remaining reserve when longer production history is used. Arps' Harmonic model still exhibits the similar result trend as well#1. It gives fairly high value of the estimated remaining reserve and it decreases (only slight decrease in this case) when longer production history is used in the model. PLE predicts the most conservative values of the remaining reserve in both cases of using whole or two-third of the production data. Unreasonably high value of the remaining reserve predicted by Arps' Hyperbolic happens when the model parameters specifically *b* value are strictly adjusted to fit the actual production data. Even though the *b* value of Arps' Hyperbolic in this case was adjusted to be 1.313, the synthetic production trend still does not match the real data. From **Figure 4.43**, the remaining life by Arps' Hyperbolic also corresponds the same phenomenon as remaining reserve. The overall results of the remaining life predicted by different DCA models follow the same behavior as the remaining reserve as showed in **Figure 4.43**. However, LGA predicted 11 years of the remaining life of this well, which is the closest estimate, compared to the simulation result.

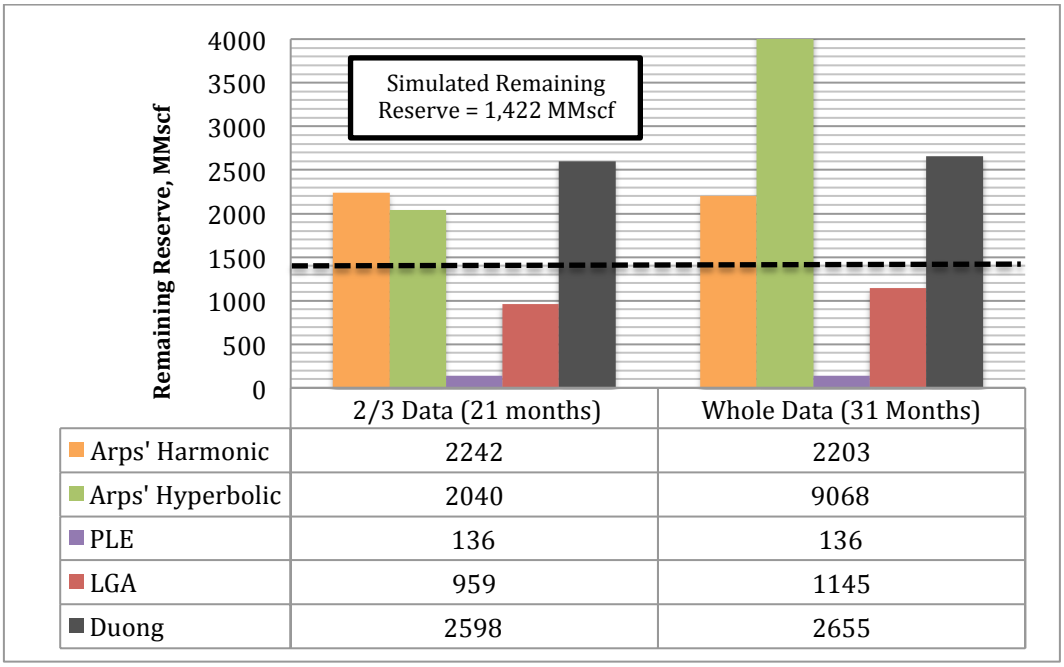

	2/3 Data (21 months)	Whole Data (31 Months)
Arps' Harmonic	2242	2203
Arps' Hyperbolic	2040	9068
PLE	136	136
LGA	959	1145
Duong	2598	2655

Figure 4.42: Comparison of remaining reserve predicted by 5 DCA models using different length of production data of well#16

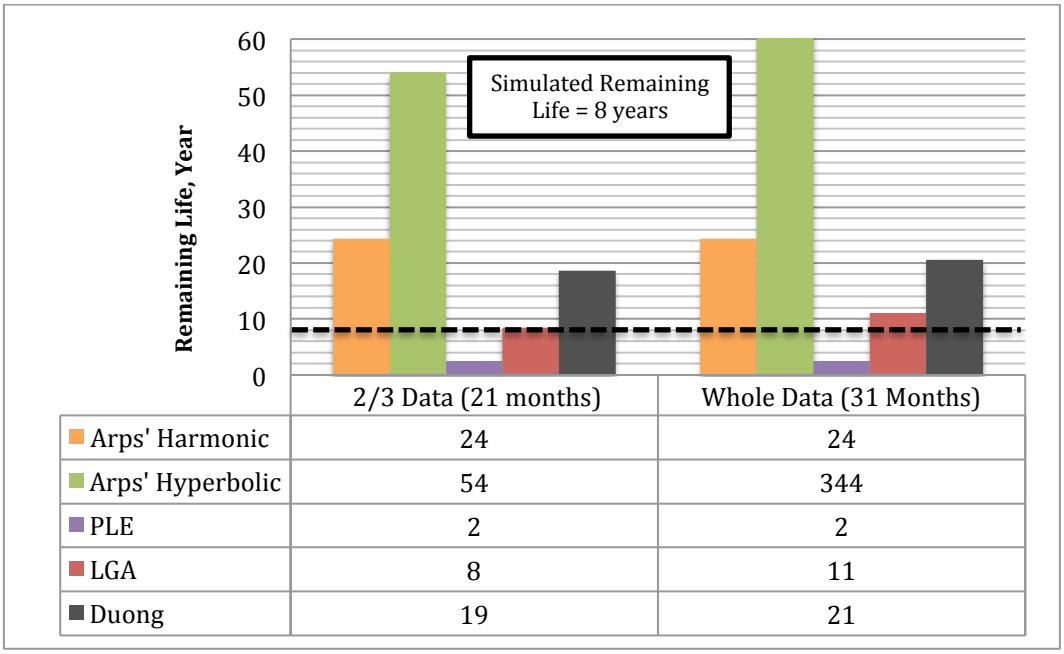

	2/3 Data (21 months)	Whole Data (31 Months)
Arps' Harmonic	24	24
Arps' Hyperbolic	54	344
PLE	2	2
LGA	8	11
Duong	19	21

Figure 4.43: Comparison of remaining well life predicted by 5 DCA models using different length of production data of well#16

The comparison of the production trends predicted up to 10,000 days by different DCA models using 21 months and 31 months of the actual production histories from well#16 are shown in **Figures 4.44** and **4.45**. From both figures, all synthetic production trends seem to closely follow the actual production trend until they start to split at approximately 500 days. Only LGA model continues showing a very good match until the end of the actual data. PLE and LGA model tend to curve down very quickly toward abandonment compared to Duong's and Arps' Harmonic models which are showing almost straight lines until abandonment. The production trend by Arps' Hyperbolic also corresponds to the results of the predicted remaining reserve and remaining life. When *b* value is forced to be greater than unity, it gives an out-of-the-place high value of the future production trend. In general, when the production history length is more limited from 29-43 month range of well#1 to 21-31 month range, there is only slight difference between the results predicted by applying whole and two-third of the data in the DCA models.

When sufficient amount of the production history during BDF is available, Arps' Harmonic, Arps' Hyperbolic and Duong's models seem to be suitable for modelling a production rate trend in a dry gas well in this case if its flow regime is expected to show transient flow and BDF until 10,000-day abandonment since their results very well follow the unit slope line. However, the production rate trends forecasted by LGA and PLE are still behaving the same fashion as the well#1. They will decrease nonlinearly at late time toward the abandonment and will decrease even more quickly when the production history is very limited.

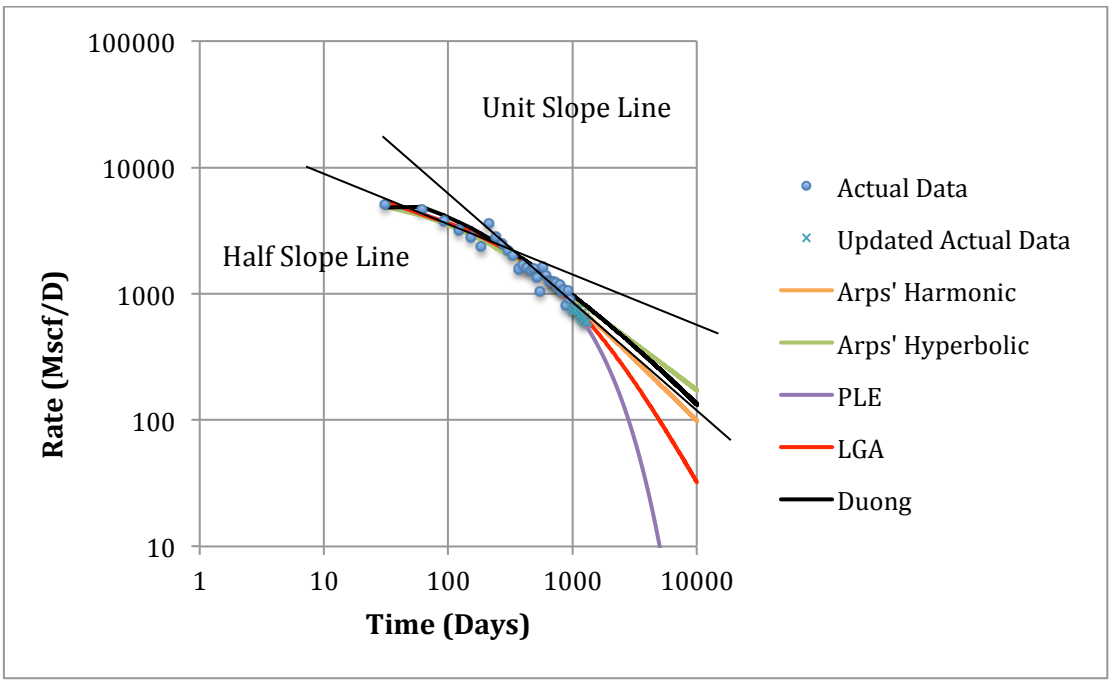

Figure 4.44: Comparison of forecasts calculated using whole data of well#16

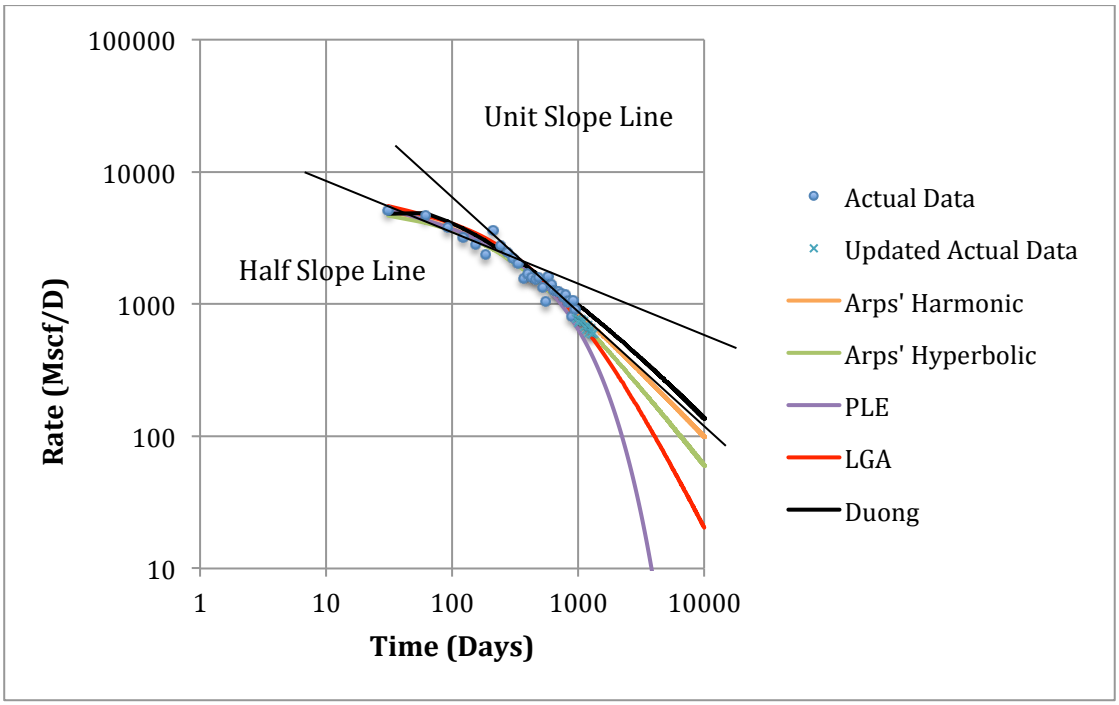

Figure 4.45: Comparison of forecasts calculated using 2/3 data of well#16

4.4.5 Well#26, GALVAN RANCH, Lease No.257683

Galvan Range is a dry gas well located in Webb County operated by Lewis Petro Properties, Inc since Oct 2009 with initial gas production rate of 1,423 Mscf/Day. The well was drilled and completed horizontally in 10,847 ft deep Eagle Ford shale stratum. 14 stages of hydraulic fracturing were executed to create fractures along 3,920 ft long lateral. The highest gas rate of 3,109 Mscf/Day reached in Nov 2009 and total gas produced up to date (Feb 2012) is 1,211 MMscf. 28 months of the production history (end of Feb 2012) is available for this well when stared data mining for this study. 11 more months of the production history has been recently reported up to end of Dec 2013. 28-month production history of this well is the longest history length of all dry gas wells in Webb County.

4.3.6 Observation and Discussion

DCA result summary of Well#26 can be found in **Table 4.4**. The results exhibit good matches between predicted production trend and actual production history generated from PLE and LGA models in both cases of using whole and two-third of the data. However, results calculated from Arps' Harmonic and Duong's models show over-predicted trends compared to actual production history regardless how long the data is used in the models. Arps' Hyperbolic's result again exhibits unpredictable trends. The model underestimates future production rate trend when two-third of the data is used and overestimates the future trend when the whole data is applied in the model.

The production rate of well#26 shows a fairly short half-slope line that indicates the transient flow behavior until approximately 400 days then the trend appears to go into BDF that can be observed by a unit slope line as showed in **Figure 4.46**.

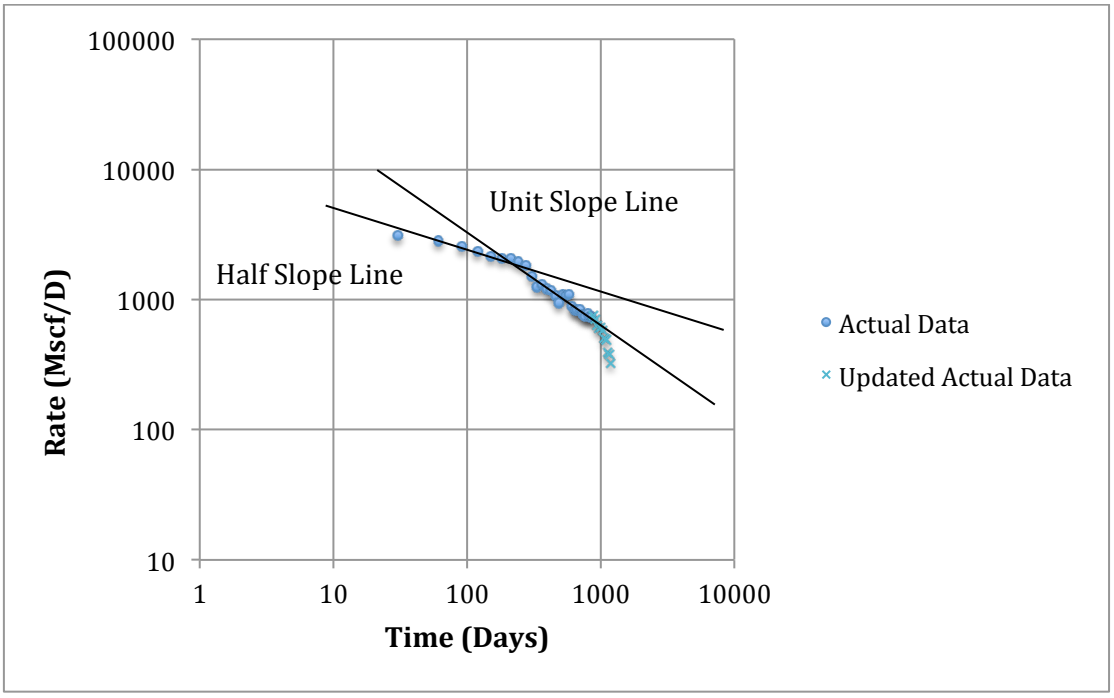

Figure 4.46: Flow regime diagnostic plot of well#26

Figure 4.47 (a-b) shows the simulated history matching. In **Figure 4.47 (a)** again, the fluctuation of the production decline trend might be caused by an additional operation took place during the production. However, there is no official report regarding such an operation. The history-matched simulation model predicted that the well will take approximately 5 years to produce the remaining reserve of 1,089 MMscf based on abandonment rate of 100 Mscf/day. The result summary of the remaining reserves and remaining well life predicted by each DCA model are consolidated in **Figures 4.48** and **4.49** showing that LGA predicted the closest estimates of remaining reserve and remaining well life, 562 MMscf and 6 years respectively. The results in **Figures 4.48** and **4.49** also indicate that length of the production history used in the DCA models still plays an important role affecting a prediction outcome. Longer production history used in LGA model makes its forecast higher (slightly) and more accurate. Arps' Harmonic and Duong exhibit a reverse behavior compared to well#1 and well#16. Their remaining reserve and remaining life estimates decrease when using the whole data of 28 months instead of 19 months. PLE is still the most conservative DCA model in this study as its results are the lowest and they do not change even using different length of the production history. Arps' Hyperbolic model with *b* value greater than unity also gives the ridiculously high values of the estimates.

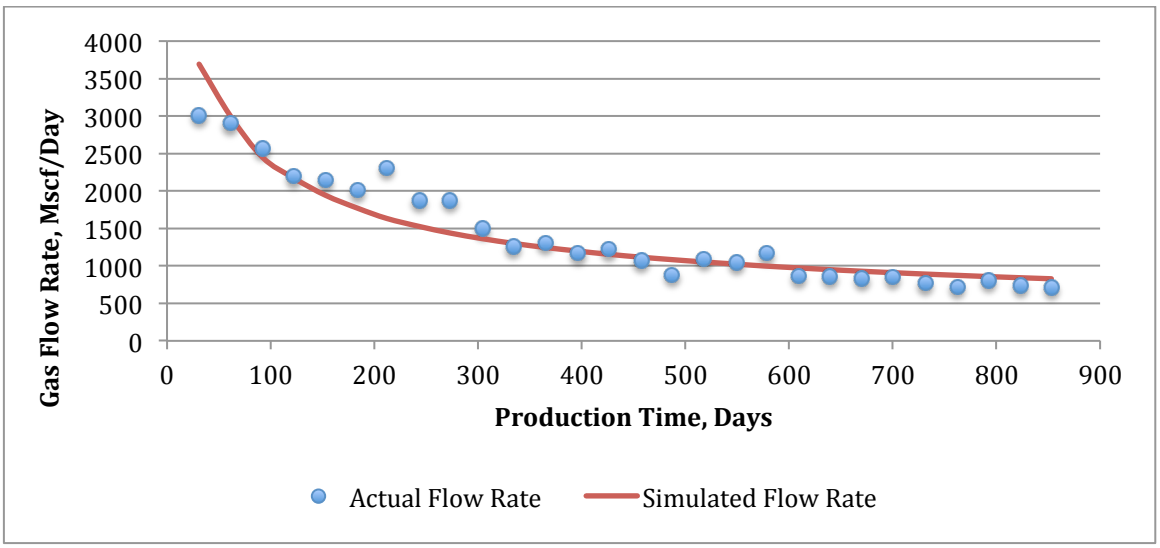

(a)

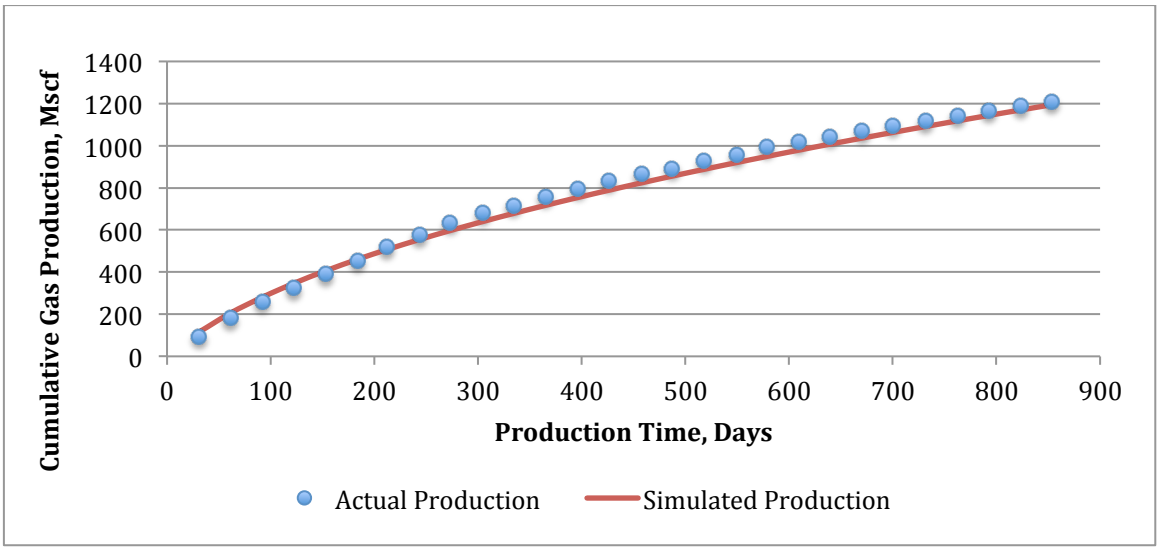

(b)

Figure 4.47 (a-b): Matching results of well#26 between actual production data and simulated outcomes of (a) production rate and (b) cumulative production

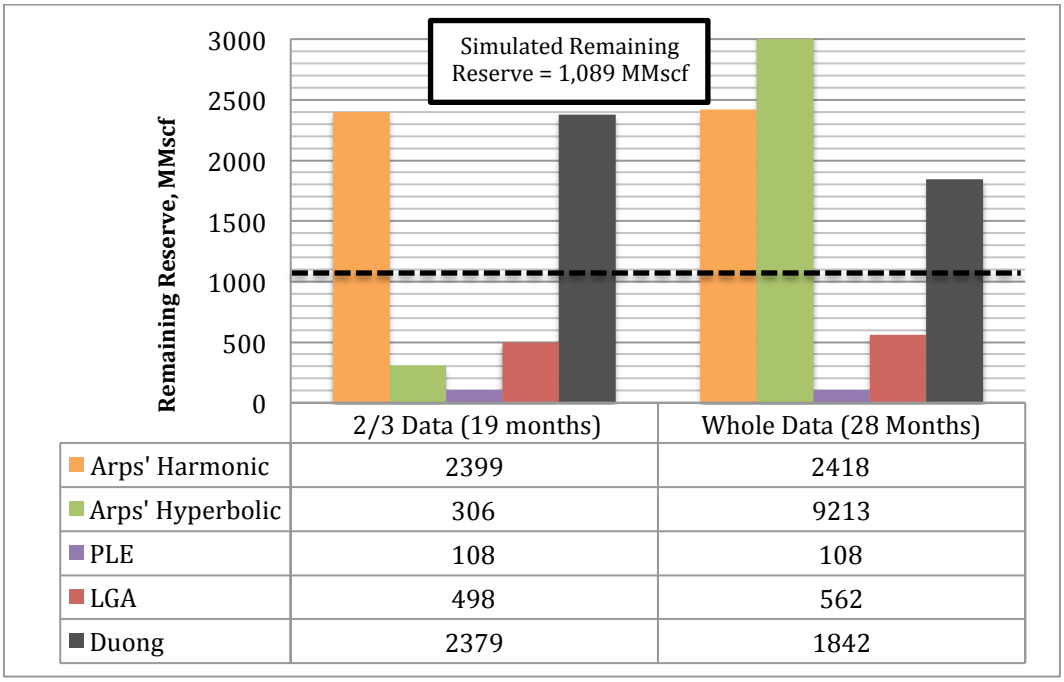

	2/3 Data (19 months)	Whole Data (28 Months)
Arps' Harmonic	2399	2418
Arps' Hyperbolic	306	9213
PLE	108	108
LGA	498	562
Duong	2379	1842

Figure 4.48: Comparison of remaining reserve predicted by 5 DCA models using different length of production data of well#26

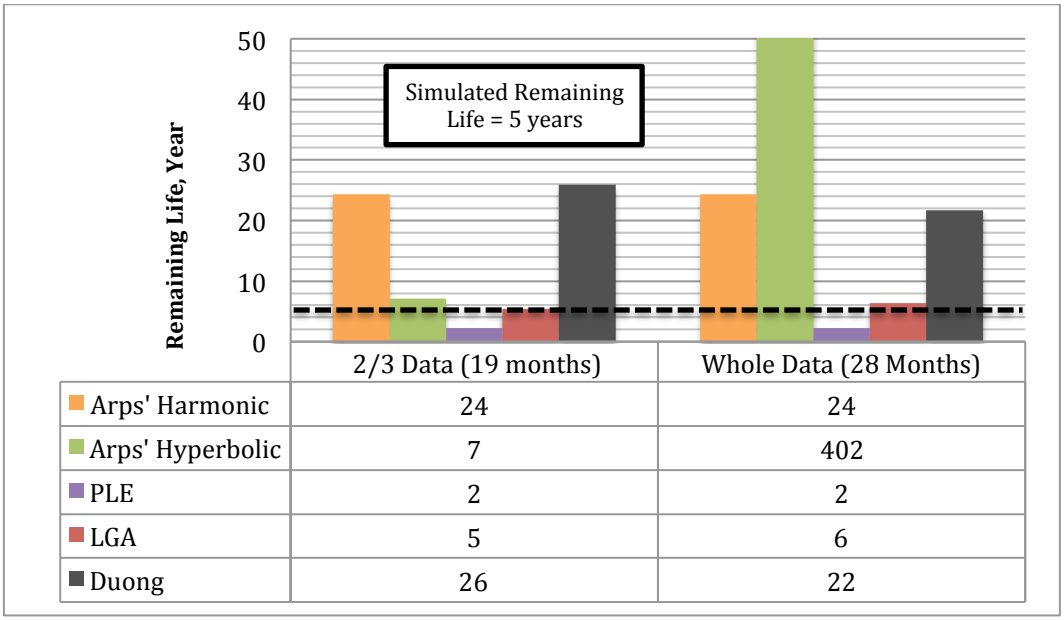

	2/3 Data (19 months)	Whole Data (28 Months)
Arps' Harmonic	24	24
Arps' Hyperbolic	7	402
PLE	2	2
LGA	5	6
Duong	26	22

Figure 4.49: Comparison of remaining well life predicted by 5 DCA models using different length of production data of well#26

The behaviors of the production trends forecasted by different DCA models up to 10,000-day abandonment using 28 months and 19 months of the actual production histories from well#26 are showed in **Figures 4.50** and **4.51** respectively. From both figures, Arps' Harmonic and Duong's models follow the same straight line at late times along the unit slope line toward abandonment regardless of how long the production history is used, this behavior may be implied that Arps' Harmonic and Duong are more applicable to a well that showing long transient-BDF flow. Arps' Hyperbolic with *b* value less than unity, when using such a short production history as 19 months, it predicts very conservative trend of the future production rate. On the contrary, with *b* value greater than 1, the model produces very unreasonable trends as showed in both figures. The synthetic trends by PLE and LGA tend to steeply decrease at late time when using 19 months of the data. The overall results in this case are almost similar to the case of well#16 except for Arps' Hyperbolic model. When its *b* value is forced to be greater than unity to fit production history of a well exhibiting transient-BDF flow, the forecast of late time production rate trend may result in unreasonable values.

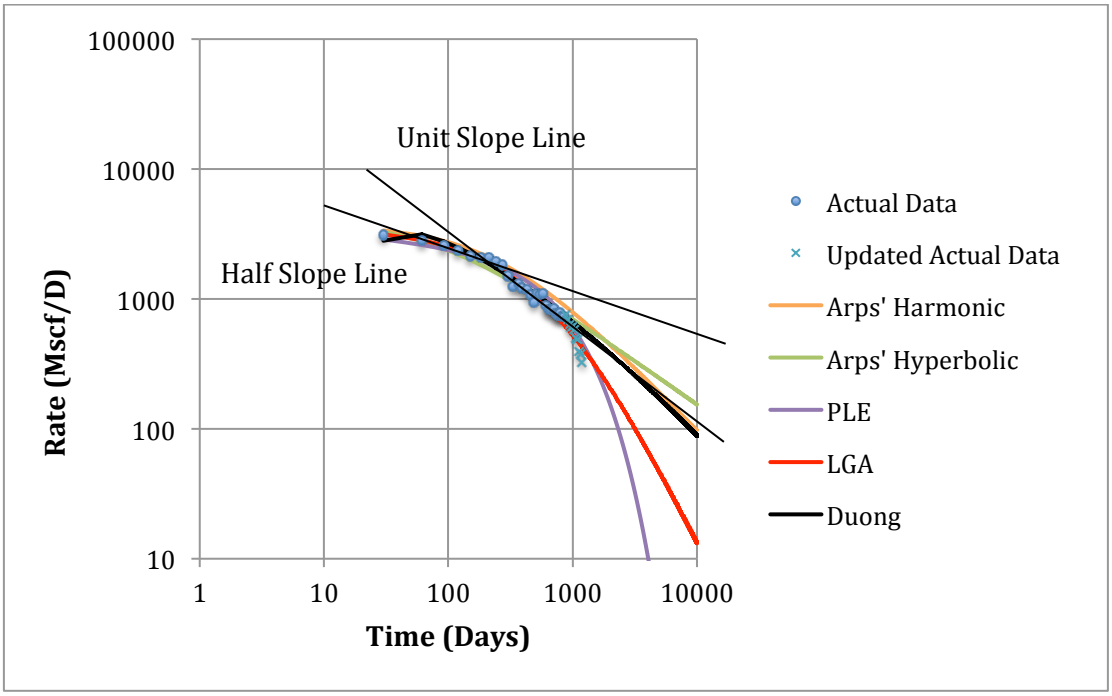

Figure 4.50: Comparison of forecasts calculated using whole data of well#26

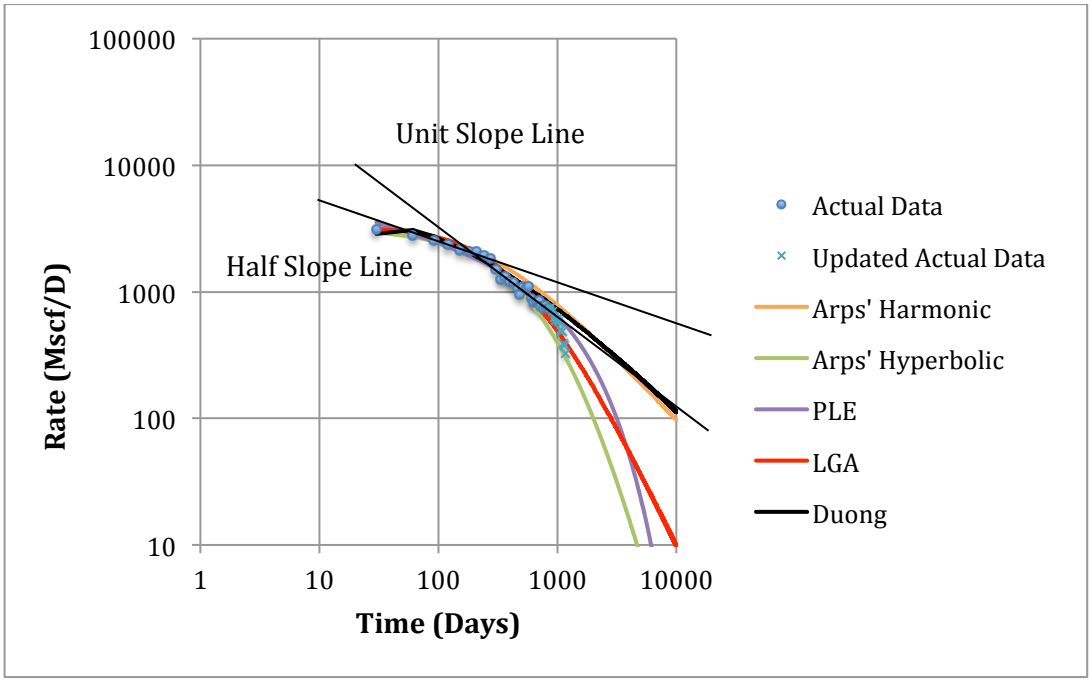

Figure 4.51: Comparison of forecasts calculated using 2/3 data of well#26

4.4.7 Well#31, ROSA VELA BENAVIDES, Lease No.260047

Well#31 in this study is Rosa Vela Benavides located in Webb County and operated by Laredo Energy. The well was drilled and completed horizontally in very deep Eagle Ford shale layer at 13,160 ft depth. Production of dry gas commenced in Oct 2010 with gas rate of 1,406 Mscf/Day in the first month by an assist of hydraulic fracturing method. 13 stages of fracturing were placed along 4,160 ft long horizontal leg to create fractures at designated sweet spots in the shale layer. The highest gas rate of 3,909 Mscf/Day reached in the second month of the production (Nov 2010). Total gas produced so far up to date (Oct 2012) is 715 MMscf and declining. The whole data when firstly collected includes 23 months of the production history (end of Oct 2012) and 10 additional months have been recently updated (end of Nov 2013). This particular well is considered in this study as the youngest well that has sufficient information of completion practices and reservoir characteristics available to be modeled in the simulation.

4.4.8 Observation and Discussion

DCA results of well#31 generated by 5 different models are summarized in **Table 4.4**. With very short production history of this well, synthetic production trend calculated from Arps' Harmonic and LGA models are still being able to match very well with actual history when whole data or two-third of the data is applied in the models. On the contrary, PLE and Arps' Hyperbolic model underestimate the future production trends in both whole data and two-third of the data cases. Moreover, the result from Duong's model shows over-predicted production trend when compared with actual production history regardless how long the production data is used in the model.

Figure 4.52 shows a very short period of the transient flow (less than 100 days). The rest of the production rate trend after approximately 100 days is following a unit slope line indicating that this well goes into BDF at very early time and still in BDF until the end of production history.

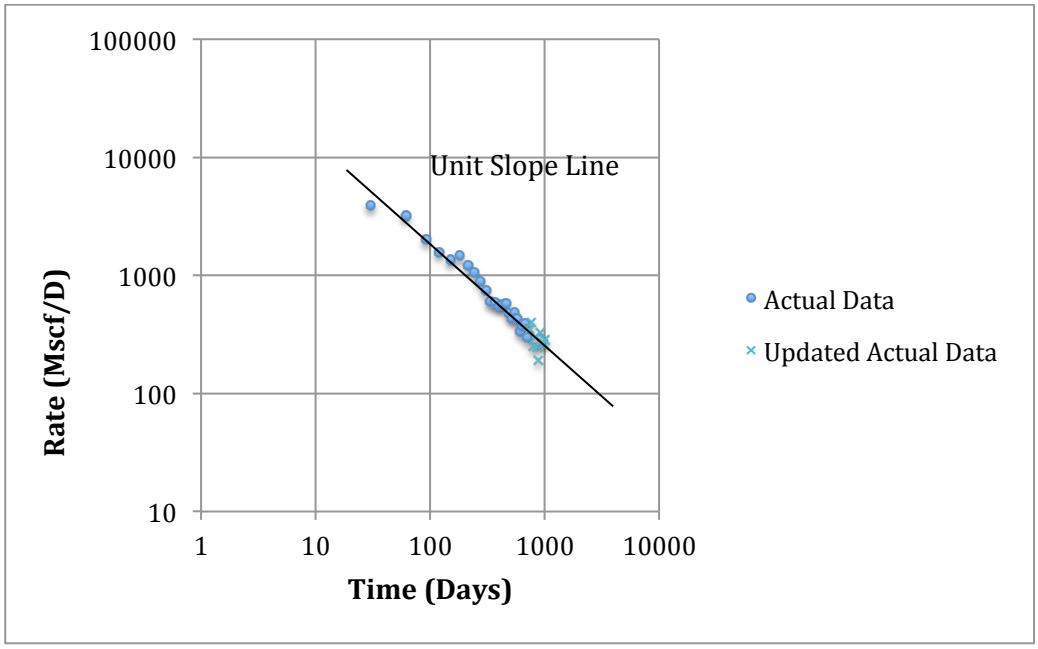

Figure 4.52: Flow regime diagnostic plot of well#31

Figure 4.53 (a-b) shows the simulation history match results. In **Figure 4.53 (a)**, it is noted that there might be an additional operation executed or problem occurred during the production causing the fluctuation of the production rates during the first 200 days of the production, which might contribute to higher cumulative production trend showing in **Figure 4.53 (b)**. The history-matched simulation model predicted that the well will spend approximately 1.5 years to produce the remaining reserve of 182 MMscf based on abandonment rate of 100 Mscf/day.

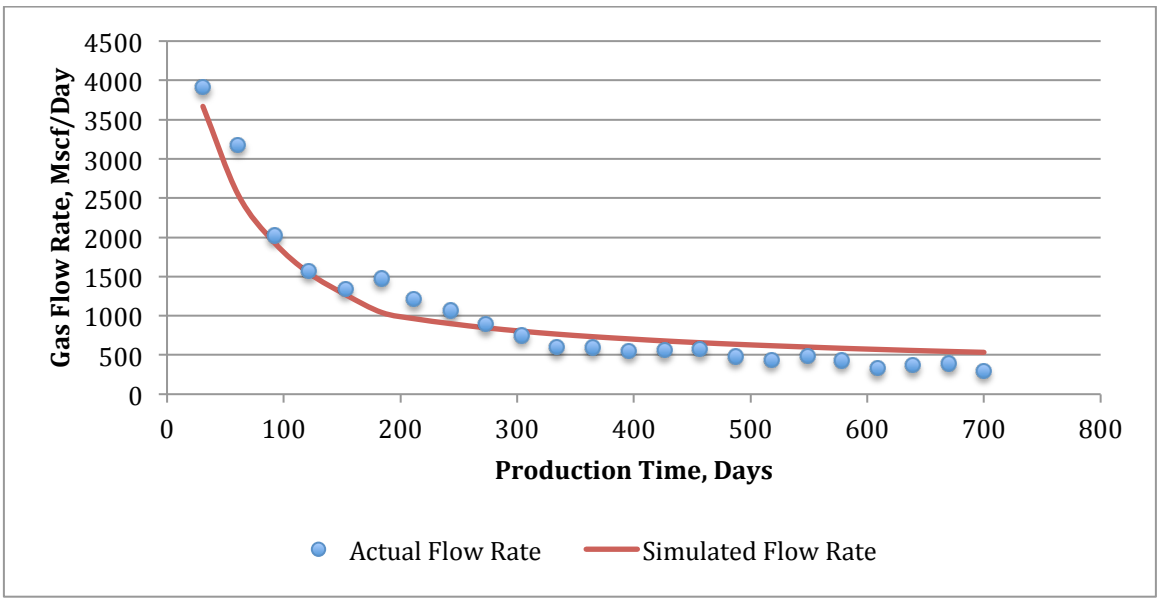

(a)

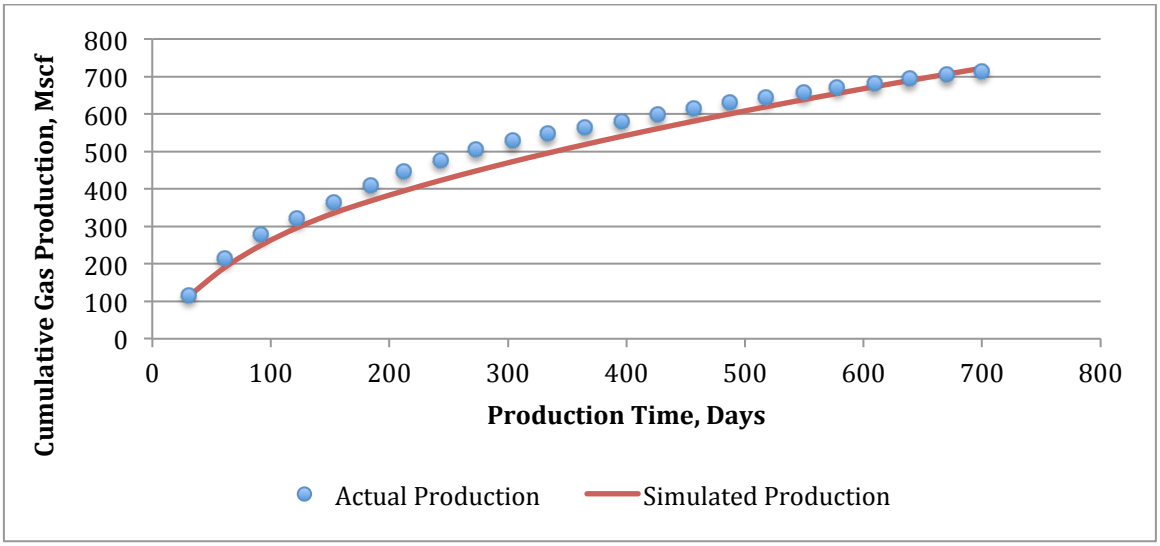

(b)

Figure 4.53 (a-b): Matching results of well#31 between actual production data and simulated outcomes of (a) production rate and (b) cumulative production

Figures 4.54 and **4.55** show that the overall forecasts of both remaining reserve and remaining life from 5 different DCA models will slightly increase when 23 months of the data is used over 15 month history except the Arps' Hyperbolic model that its forecasts decrease when using longer production history. The results clearly show that Arps' Harmonic model gives the highest values of the estimates compared to the other models. On the other hand, PLE is still being the most conservative DCA model for this well and also almost all of the wells in this study, which predicts the lowest remaining reserve and remaining life in general. Duong's model gives the second highest of the remaining reserve. The mid-range remaining reserves are from Arps' Hyperbolic, LGA and PLE models. When considering both remaining reserve and remaining life together, LGA model again seems to be the most appropriate model for prediction in this case because it predicted 135 MMscf of remaining reserve which is slightly lower than the simulation result but its remaining life is 2 years which is very close to the result from the simulation.

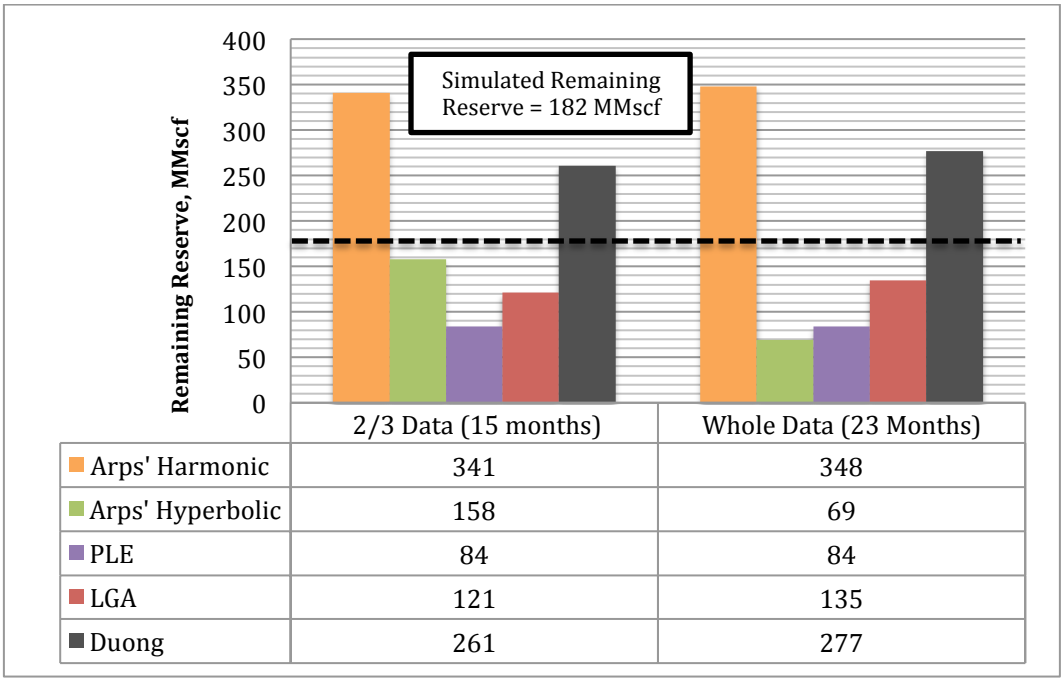

	2/3 Data (15 months)	Whole Data (23 Months)
Arps' Harmonic	341	348
Arps' Hyperbolic	158	69
PLE	84	84
LGA	121	135
Duong	261	277

Figure 4.54: Comparison of remaining reserve predicted by 5 DCA models using different length of production data of well#31

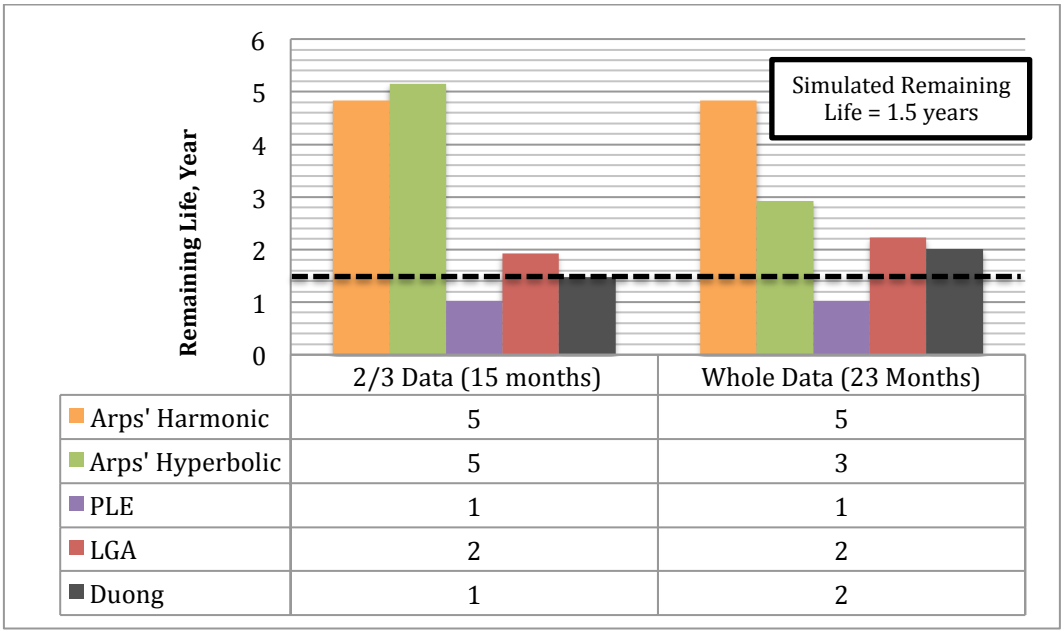

	2/3 Data (15 months)	Whole Data (23 Months)
Arps' Harmonic	5	5
Arps' Hyperbolic	5	3
PLE	1	1
LGA	2	2
Duong	1	2

Figure 4.55: Comparison of remaining well life predicted by 5 DCA models using different length of production data of well#31

The future production trends predicted up to abandonment of 10,000 days by different DCA models using 23 months and 15 months of the actual production histories are plotted and showed in **Figures 4.56** and **4.57** respectively. The results from both figures show that Arps' Harmonic and Duong's models seem to fit well with BDF as they exhibit straight lines matched with the unit slope line on the log-log rate plots until abandonment. However, Aprs' Harmonic model gives higher production trend at late time compared to Duong's model. LGA, PLE and Arps' Hyperbolic models tend to follow a conservative curve started curving down at approximately 400 days of the production. LGA and PLE models when using short production history as short as 15 months show quicker reduction of the production rate specifically with PLE that gives the most conservative trend of the future production rate. The overall results in this case of a dry gas well with BDF (very short period of linear flow) indicate that a decline rate is more rapid compared to the other 3 cases. Arps' Harmonic and Duong's models may be suitable for predicting future production trend if a well showing BDF at early time.

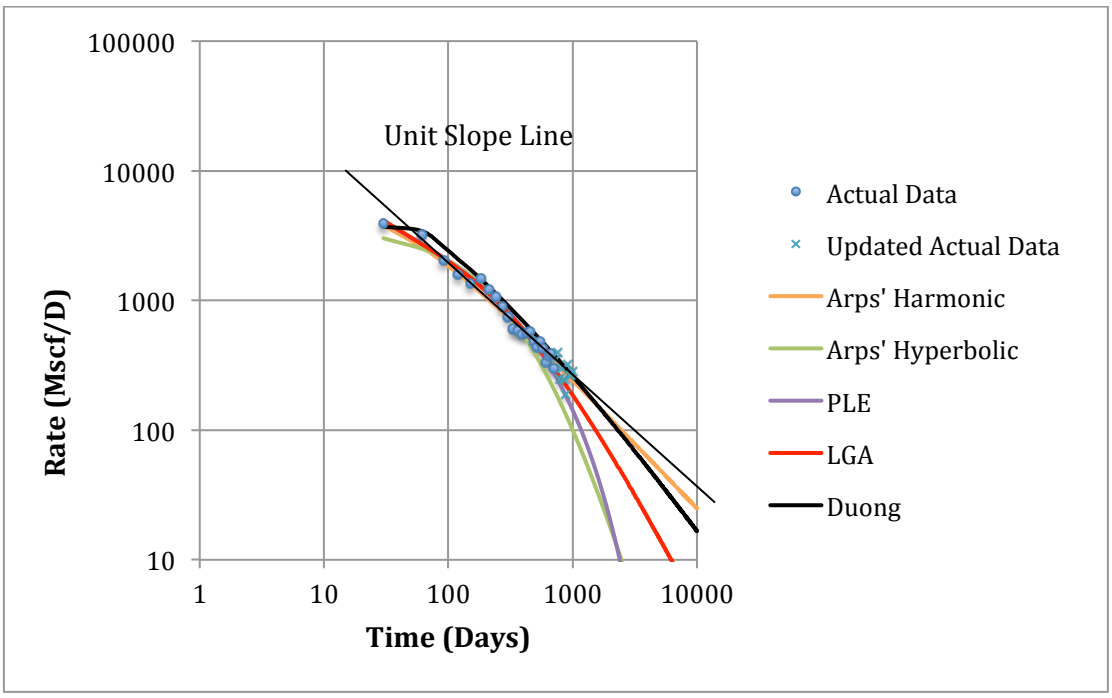

Figure 4.56: Comparison of forecasts calculated using whole data of well#31

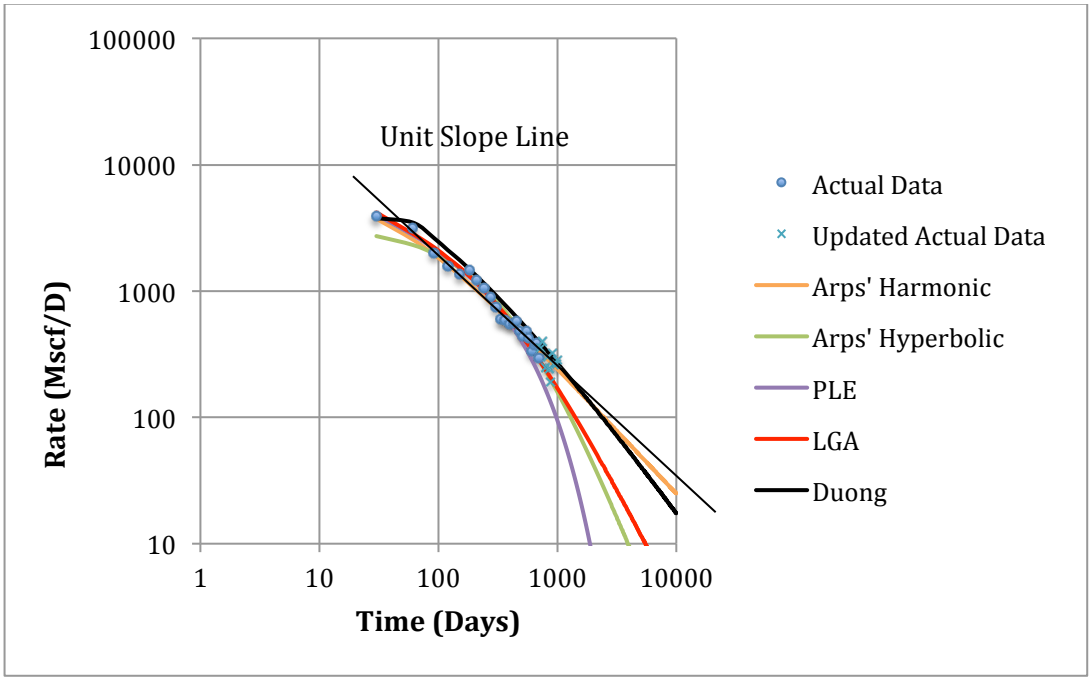

Figure 4.57: Comparison of forecasts calculated using 2/3 data of well#31

CHAPTER 5

CONCLUSIONS AND RECOMMENDATIONS

5.1 Conclusions

Based upon the reported information of the actual completion practices provided on TRRC database, the plots of the average production rate in the first 12 months from 38 different dry gas wells versus various lengths of horizontal wellbore and various numbers of hydraulic fracturing stages indicate slightly positive trends in well performance when longer horizontal wellbore and higher number of fracturing stages are employed along with the hydraulic fracturing technique indicating that the reservoir matrix is very heterogeneous. Longer length of the horizontal leg raises higher opportunity of finding the sweet spots in the reservoirs that is the zone most conductive to fracturing. Higher number of fracturing stages also allows greater formation exposure, which may lead to higher production rate.

Approximately 83% of the wells in LaSalle County are still in the linear flow until the end of 2012 and only 17% exhibiting transient flow at early time and BDF at late time. For Webb County, 71% of the production trends show only linear flow regime and the remaining 29% shows transient flow and BDF. The flow regimes of total 38 wells in both counties in general are 79% exhibiting only transient flow, they may either continue exhibiting the linear flow until abandonment or go into BDF if boundary is established. The rest 21% is showing transient flow at early time and BDF at late time of the production.

The diagnostic plots that are utilized in Arps' Exponential model including semi-log production rate versus production time and production rate versus cumulative production do not show a straight line for all 38 wells. The results indicate that Arps' Exponential model is not applicable for

forecasting future production trend of the dry gas wells in this study since their production rates are not declining exponentially.

From the production rate history matching results, LGA model seems to be the best DCA model for predicting future production rate trend of dry gas wells in Eagle Ford since it can match the production history up to 71% of the total 38 wells in this study. Arps' Harmonic and PLE models have the maximum matching accuracy of 63% followed by 46% matched by Duong's model (important parameters associated with PLE and Duong's models such as D_∞ and q_∞ are not forced to be equal to zero). The least accurate DCA model is Arps' Hyperbolic, which match only 21% maximum. Even though b values are allowed to be greater than unity, the accuracy does not increase beyond 28%. Length of the production data used also plays a significant role in dictating the predictive accuracy of each DCA model. When using 28 months of the production history instead of 23 months, forecasting accuracy of LGA, PLE, Arps' Hyperbolic and Arps' Harmonic relatively increase by 22%, 21%, 21%, and 17% respectively. However, predictive accuracy of Duong's model reached the limit of 46% accuracy when using 20-month history. Its accuracy is decreasing when using longer history.

Forecasted results of the remaining reserve and the remaining life from history-matched simulated wells show that the LGA is the most appropriate DCA model that predicts very reasonable values of the remaining reserve and remaining well life compared to the results estimated by the reservoir simulations in 4 cases. Arps' Harmonic model estimates very high values of the remaining reserve and the remaining well life in general. On the other hand, PLE model is the most conservative model since it gives the lowest estimates. b value in Arps' Hyperbolic model when is allowed to be higher than unity to fit well with the actual production data results in unreasonably high values of the estimates. Duong's model seems to always overestimate the remaining reserve and remaining life as the results can be observed as the second highest estimates.

5.2 Recommendations

To obtain more applicable guideline in term of EUR and well life predictions for the Shublik Shale, it is recommended to conduct the production decline analysis and reservoir simulation using actual data from the Shublik field whenever it is available.

Economic analysis must be done in parallel by utilizing the information acquired from the production decline analysis and reservoir simulations since the associated costs of the entire operations from drilling, completion, production and transportation etc. are different depending upon many factors such as location and available resources.

Fluctuation of the actual production history clearly suggests that filtering the data is needed to obtain more reasonable decline trends of the production rate by giving each data point the same weight through normalizing it. Error can be defined as the summation of $(1-\frac{q}{q_{act}})^2$. Using moving average may help to some degree while the best practice is to know if the fluctuations were due to changes in operating conditions or not.

Recently updated production data of at least 4 out of 38 wells in this study indicates BDF behavior is present. Re-running the calculations of each DCA model with the new data would provide more understanding of their predictive limit and capability when dealing with a dry gas well exhibiting both transient flow and BDF.

Uncertainty of simulation parameters and reservoir conditions defined in the reservoir simulation can be greatly reduced by applying more updated and precise data in the model, porosity and matrix permeability for instance. The presence of natural fractures and heterogeneity of the reservoir also need to be taken into account in the simulation. Moreover, since the hydraulic fracturing process was not accurately simulated in this study, stepwise simulation of the process is

recommended for further development. This helps better modeling of water flow back that affects the fluid saturations near the fracture face and therefore the well production performance.

NOMENCLATURE

a = model constant (LGA), y-intercept (Duong)

b = decline exponent (Arps)

D = decline constant (Arps), 1/day

D_1 = decline constant intercept at one time (PLE), 1/day

D_i = initial decline constant (Arps), 1/day

$\widehat{D}_i$ = decline constant (PLE), 1/day

D_∞ = decline constant at infinite time (PLE), 1/day

G_p = cumulative production, MMscf

K = carrying capacity (LGA), Mscf

k_f = hydraulic fracture permeability, nD, mD

n = time exponent (PLE), hyperbolic exponent (LGA)

m = slope (Duong)

$m(p)$ = pseudopressure (gas), psi^2/cp

P_i = initial reservoir pressure, psi

P_{wf} = wellbore flowing pressure, psi

q = production rate at time t, Mscf/day

q_1 = rate at day one, Mscf/day

q_i = initial production rate, Mscf/day

$\hat{q}_i$ = rate intercept (PLE), Mscf/day

q_g = gas rate, Mscf/day

t = production time, day, year

$t\ (a,m)$ = time function based on equation (14)

W_f = hydraulic fracture width, ft

REFERENCES

Agrawal, A., Wei, Y., Cheng, K., and Holditch, S.A. 2010. A Technical and Economic Study of Completion Techniques in Five Emerging US Gas Shales. Paper SPE 135396 presented at the SPE Annual Technical Conference and Exhibition, Florence, Italy, 19–22 September 2010.

Arps, J.J. 1944. Analysis of Decline Curves. Trans. A.I.M.E 160 228-247.

Baihly, J., Altman, R., Malpani, R., and Luo, F. 2010. Shale Gas Production Decline Trend Comparison Over Time and Basins. Paper SPE 135555 presented at the SPE Annual Technical Conference and Exhibition, Florence, Italy, 19–22 September 2010.

Boulis, A., Jayakumar, R., Nyaaba, C., Rai, R., and Sahai, V. 2013. Challenges Evaluating Shale Gas Well Performance: How Do We Account For What We Don't Know? Paper SPE 16396 presented at the International Petroleum Technology Conference, Beijing, China, 26–28 March 2013.

Clark, A.J., Lake, L.W., and Patzek, T.W. 2011. Production Forecasting with Logistic Growth Models. Paper SPE 144790 presented at the SPE Annual Technical Conference and Exhibition, Denver, Colorado, USA, 30 October-2 November.

CMG, Advanced Black Oil/Gas Reservoir Simulator Version 2012, By Computer Modelling Group Ltd.

Duong, A.N. 2011. Rate-Decline Analysis for Fracture-Dominated Shale Reservoirs. SPE Reservoir Evaluation & Engineering (3): pp. 377-387.

Daniels, J., Waters, G., LeCalvez, J., Lassek, J., and Bentley, D. 2007. Contacting More of the Barnett Shale Through an Integration of Real-TimeMicroseismic Monitoring, Petrophysics and Hydraulic Fracture Design. Paper SPE 110562 presented at the SPE Annual Technical Conference and Exhibition, Anaheim, California, 12–14 October 2007.

Dong, Z., Holditch, S.A., McVay, D.A., and Ayers, W.B. 2012. Global Unconventional Gas Resource Assessment. Paper SPE 148365 presented at the Canadian Unconventional Resources Conference, Calgary, Alberta, 15–17 November 2011.

Economides, M.J., and Martin, T. 2007. Modern Fracturing Enhancing Natural Gas Production. BJ Services Company, Houston, Texas, 2007.

EIA (U.S. Energy Information Administration). 2011. Review of Emerging Resources: U.S. Shale Gas and Shale Oil Plays. Independent Statistics and Analysis.

EIA (U.S. Energy Information Administration). 2013. Annual Energy Outlook 2013 Early Release Overview. Independent Statistics and Analysis.

Fetkovich, M.J. 1971. A Simplified Approach to Water Influx Calculations-Finite Aquifer Systems. SPE Journal of Petroleum Technology 23 (7): 814-828.

Fetkovich, M.J. 1980. Decline Curve Analysis Using Type Curves. SPE Journal of Petroleum Technology 32 (6): 1065-1077.

Fetkovich, M.J., Bradley, M.D., and Works, A.M. 1990. Depletion Performance of Layered Reservoirs without Crossflow. SPE Formation Evaluation 5 (3): 310-318.

Fisher, K., and Warpinski, N. 2011. Hydraulic Fracture-Height Growth: Real Data. Paper SPE 145949 presented at the SPE Annual Technical Conference and Exhibition, Denver, Colorado, 30 October–2 November 2011.

Frederick, D.C. Jr. and Graves, R.M. 1994. New Correlations To Predict Non-Darcy Flow Coefficients at Immobile and Mobile Water Saturation. Paper SPE 28451 presented at the SPE Annual Technical Conference and Exhibition, New Orleans, 25-28 September 1994

Freeman, C.M., Moridis, G.J., Ilk, D. and Blasingame, T.A. 2009. A Numerical Study of Performance for Tight Gas and Shale Gas Reservoir Systems. Paper SPE 124961 presented at the SPE Annual Technical Conference and Exhibition, New Orleans, Louisiana, 4-7 October 2009.

Geertsma, J. 1974. Estimating the Coefficient of Inertial resistance in Fluid Flow Through Porous Media. SPEJ 445.

Gidley, J.L., Holditch, S.A., Nierode, D.E., and Veatch, R.W. 1989. Recent Advances in Hydraulic Fracturing. SPE Monograph Series, Volume 12, 1989.

Hanks, C. 2012. Petroleum Geology (PowerPoint Slides). University of Alaska Fairbanks.

Hassanpoor, D., Hayatdavoudi, A., and Boukadi, F. 2013. The Effect of Shale Chemistry on Gas Production Decline in Hydraulically Fractured Shale Gas Wells. Paper SPE 164093 presented at the SPE International Symposium on Oilfield Chemistry, Woodlands, Texas, USA, 8–10 April 2013.

Hubbert, M.K. 1956. Nuclear Energy and the Fossil Fuel. American Petroleum Institute API-56-007.

Ikewun, P.O. 2012. Production Optimization and Forecasting of Shale Gas Wells Using Simulation Models and Decline Curve Analysis. Master of Science, University of Alaska Fairbanks.

Ilk, D., Rushing, J.A., and Perego, A.D. 2008. Exponential Vs. Hyperbolic Decline in Tight Gas Sands - Understanding the Origin and Implications for Reserve Estimates Using Arps' Decline Curves. Paper SPE 116731 presented at the SPE Annual Technical Conference and Exhibition, Denver, Colorado, USA, 21-24 September.

Inamdar, A., Malpani, R., and Atwood, K., 2010. Evaluation of Stimulation Techniques Using Microseismic Mapping in the Eagle Ford Shale. Paper SPE 136873 presented at the SPE Tight Gas Completions Conference, San Antonio, Texas, USA, 2–3 November.

Jellison, M., Brock, J., Muradov, A., Morgan, D., Prideco, N.G., and Rowell, J. 2013. Shale Play Drilling Challenges: Case Histories and Lessons Learned. Paper SPE/IADC 163447 presented at the SPE/IADC Drilling Conference and Exhibition, Amsterdam, The Netherlands, 5–7 March 2013.

Jenkins, C.D., and Boyer, C.M. 2008. Coalbed - and Shale - Gas Reservoirs. Paper SPE 103514, Distinguished Author Series, JPT, February 2008.

Kanfar, M.S., and Wattenbarger, R.A. 2012. Comparison of Empirical Decline Curve Methods for Shale Wells. Paper SPE 162648 presented at the SPE Canadian Unconventional Resources Conference, Calgary, Alberta, Canada, 30 October–1 November 2012.

Kennedy, R.L., Knecht, W.N., and Georgi, D.T. 2012. Comparisons and Contrasts of Shale Gas and Tight Gas Developments, North American Experience and Trends. Paper SPE 160855 presented at the SPE Saudi Arabia Section Technical Symposium and Exhibition, Al-Khobar, Saudi Arabia, 8–11 April 2012.

King, G.E. 2010. Thirty Years of Gas Shale Fracturing: What Have We Learned? Paper SPE 133456 presented at the SPE Annual Technical Conference and Exhibition, Florence, Italy, 19–22 September 2010.

Li, N., Ran, Q., Li, J., Yuan, J., Wang, C., and Wu, W.S. 2013. A Multiple-Continuum Model for Simulation of Gas Production from Shale Gas Reservoirs. Paper SPE 165991 presented at the SPE Reservoir Characterization and Simulation Conference and Exhibition, Abu Dhabi, UAE, 16–18 September 2013.

Liu, J., Liu, J., Liu, K., Elsworth, D. and Wang, J. 2009. Hydromechanics of a Virtual Rock Core. Paper SPE ARMA-09-035 presented at the 28 June-1 July 2009.

Liu, S., Ren, S., and Zhao, J. 1998. The Fracturing Technique to Limit Hydraulic Fracture Height Growth Put into Effect Successfully in Xinjiang Oil Field. Paper SPE 39516 presented at the 1998 SPE India Oil and Gas Conference and Exhibition, New Delhi, India, 17-19 February 1998.

Lolon, E.P., McVay, D.A., and Schubarth, S.K. 2003. Effect of Fracture Conductivity on Effective Fracture Length. Paper SPE 84311 presented at the SPE Annual Technical Conference and Exhibition, Denver, Colorado, 5-8 October 2003.

Manchanda, R., Roussel, N.P., Sharma, M.M. 2012. Factors Influencing Fractures Trajectories and Fracturing Pressure Data in a Horizontal Completion. Paper ARMA 12-633 presented at the US Rock Mechanics/Geomechanics Symposium, Chicago.

Masters, J.A. 1979. Deep Basin Gas Trap, Western Canada. AAPG Bull. 63(2): 152–181.

McGuire, W.J., and Sikora, V.J. 1960. The Effect of Vertical Fractures on Well Productivity. Paper SPE 1618-G, Technical Note 2068, 1960.

McNeil, R., Jeje, O., and Renaud, A. 2009. Application of the Power Law Loss-Ratio Method of Decline Analysis. Petroleum Society Paper 2009-159 presented at Canadian International Petroleum Conference (CIPC) 2009, Calgary, Alberta, Canada, 16-18 June 2009.

Meyet, M., Dutta, R., and Burns, C. 2013. Comparison of Decline Curve Analysis Methods with Analytical Models in Unconventional Plays. Paper SPE 166365 presented at the SPE Annual Technical Conference and Exhibition, New Orleans, Louisiana, 30 September-2 October 2013.

Mullen, J. 2010. Petrophysical Characterization of the Eagle Ford Shale in South Texas. Paper CSUG/SPE 138145 presented at the Canadian Unconventional Resources & International Petroleum Conference, Calgary, Alberta, Canada, 19-21 October 2010.

Okouma, V., Symmons, D., Hosseinpour-Zonoozi, N., Ilk, D. and Blasingame, T. 2012. Practical Considerations for Decline Curve Analysis in Unconventional Reservoirs – Application of Recently Developed Time-Rate Relations. Paper SPE 162910 presented at the SPE Hydrocarbon, Economics, and Evaluation Symposium, Calgary, Alberta, Canada, 24–25 September 2012.

Old, S., Holditch, S.A., Ayers, W.B., and McVay, D.A. 2008. Prise: Petroleum Resource Investigation Summary and Evaluation. Paper SPE 117703 presented at the SPE Eastern Regional/AAPG Eastern Section Joint Meeting, Pittsburgh, Pennsylvania, 11–15 October 2008.

Orangi, A., Nagarajan, N.R., Honarpour, M.M. and Rosenzweig, J.J. 2011. Unconventional Shale Oil and Gas-Condensate Reservoir Production, Impact of Rock, Fluid, and Hydraulic Fractures. Paper SPE 140536 presented at the SPE Hydraulic Fracturing Technology Conference, Woodlands, Texas, USA, 1 January 2011.

Passey, Q.R., Bohacs, K.M., Esch, W.L., Klimentidis, R., and Sinha, S. 2010. From Oil-Prone Source Rock to Gas-Producing Shale Reservoir – Geologic and Petrophysical Characterization of Unconventional Shale-Gas Reservoirs. Paper SPE 131350 presented at the CPS/SPE International Oil & Gas Conference and Exhibition, Beijing, China, 8–10 June 2010.

Pearson, C.M. 2001. Dimensionless Fracture Conductivity: Better Input Values Make Better Wells. Paper SPE 60184, Technology Today Series, 2001.

Ramurthy, M., Barree, R.D., Kundert, D.P., Petre, E., and Mullen, M. 2011. Surface Area vs Conductivity Type Fracture Treatments in Shale Reservoirs. Paper SPE 140169 presented at the SPE Hydraulic Fracturing Technology Conference and Exhibition held in The Woodlands, Texas, 24–26 January 2011.

Sahai, V., Jackson, G., and Rai, R. 2013. Effect of Non-uniform Fracture Spacing and Fracture Half-length on Well Spacing for Unconventional Gas Reservoirs. Paper SPE 164927 presented at the EAGE Annual Conference & Exhibition incorporating SPE Europec, London, United Kingdom, 10–13 June 2013.

Sondhi, N. 2011. Petrophysical Characterization of Eagle Ford Shale. Master of Science, University of Oklahoma, 2011.

Stegent, N.A., Wagner, A.L., and Mullen, J., 2010. Engineering a Successful Fracture-Stimulation Treatment in the Eagle Ford Shale. Paper SPE 136183 presented at the SPE Tight Gas Completions Conference, San Antonio, Texas, USA, 2–3 November.

The Railroad Commission of Texas. 2013. http://www.rrc.state.tx.us/data/online

Thompson, J.M., Laing P., and Mattar L. 2012. What's Positive about Negative Intercepts? Paper SPE 162647 presented at the Canadian Unconventional Resources Conference, Calgary, Alberta, Canada, 30 October – 1 November.

Tian, Y., Ayers, W.B., William, D., and McCain, Jr. 2013. The Eagle Ford Shale Play, South Texas: Regional Variations in Fluid Types, Hydrocarbon Production and Reservoir Properties. Paper IPTC 16808 presented at the International Petroleum Technology Conference, Beijing, China, 26–28 March 2013.

Vanorsdale, C.R. 2013. Production Decline Analysis Lessons from Classic Shale Gas Wells. Paper SPE 166205 presented at the SPE Annual Technical Conference and Exhibition, New Orleans, Louisiana, USA, 30 September–2 October 2013.

Warpinski, N.R. 2011. Hydraulic Fracture Height in Gas Shale Reservoirs. Paper SPE 3705 presented at SEG Annual Meeting, San Antonio, Texas, 2011.

Yu, W., and Sepehrnoori, K. 2013. Simulation of Gas Desorption and Geomechanics Effects for Unconventional Gas Reservoirs. Paper SPE 165377 presented at the SPE Western Regional & AAPG Pacific Section Meeting, 2013 Joint Technical Conference, Monterey, California, USA, 19–25 April 2013.

Zanganeh, B. 2014. Understanding Reservoir Engineering Aspects of Shale Oil Development on The Alaska North Slope. Master of Science, University of Alaska Fairbanks.

Zhang, J., Kamenov, A., Zhu, D., and Hill, A.D. 2013. Laboratory Measurement of Hydraulic Fracture Conductivities in the Barnett Shale. Paper SPE 163839 presented at the SPE Hydraulic Fracturing Technology Conference, The Woodlands, Texas, 4–6 February 2013.

Zhang, X., Du, C., Deimbacher, F., Crick, M., and Harikesavanallur, A. 2009. Sensitivity Studies of Horizontal Wells with Hydraulic Fractures in Shale Gas Reservoirs. Paper IPTC 13338 presented at the International Petroleum Technology Conference, Doha, Qatar, 7–9 December 2009.

APPENDIX I

Table I – 1: Production History of Well#1 HENDERSON-CENIZO, Lease No. 251105

Month	Well days Online	Producing times (days)	Gas (MCF)	Gp (Mscf)	qg (Mscf/D)
Apr-09	30	30	34,816	34,816	1,161
May-09	31	61	186,694	221,510	6,022
Jun-09	30	91	135,884	357,394	4,529
Jul-09	31	122	119,126	476,520	3,843
Aug-09	31	153	103,012	579,532	3,323
Sep-09	30	183	87,901	667,433	2,930
Oct-09	31	214	75,033	742,466	2,420
Nov-09	30	244	68,188	810,654	2,273
Dec-09	31	275	84,085	894,739	2,712
Jan-10	31	306	65,406	960,145	2,110
Feb-10	28	334	53,456	1,013,601	1,909
Mar-10	31	365	53,551	1,067,152	1,727
Apr-10	30	395	47,141	1,114,293	1,571
May-10	31	426	45,444	1,159,737	1,466
Jun-10	30	456	39,766	1,199,503	1,326
Jul-10	31	487	41,348	1,240,851	1,334
Aug-10	31	518	38,569	1,279,420	1,244
Sep-10	30	548	36,608	1,316,028	1,220
Oct-10	31	579	35,825	1,351,853	1,156
Nov-10	30	609	33,788	1,385,641	1,126
Dec-10	31	640	35,809	1,421,450	1,155
Jan-11	31	671	33,973	1,455,423	1,096
Feb-11	28	699	29,582	1,485,005	1,057
Mar-11	31	730	29,207	1,514,212	942
Apr-11	30	760	21,413	1,535,625	714
May-11	31	791	28,178	1,563,803	909
Jun-11	30	821	21,730	1,585,533	724
Jul-11	31	852	29,434	1,614,967	949
Aug-11	31	883	24,492	1,639,459	790

Table I – 1: Continued

Month	Well days Online	Producing times (days)	Gas (MCF)	Gp (Mscf)	qg (Mscf/D)
Sep-11	30	913	22,102	1,661,561	737
Oct-11	31	944	25,173	1,686,734	812
Nov-11	30	974	25,128	1,711,862	838
Dec-11	31	1,005	24,841	1,736,703	801
Jan-12	31	1,036	22,423	1,759,126	723
Feb-12	28	1,064	32,398	1,791,524	1,157
Mar-12	31	1,095	30,544	1,822,068	985
Apr-12	30	1,125	26,785	1,848,853	893
May-12	31	1,156	27,242	1,876,095	879
Jun-12	30	1,186	24,667	1,900,762	822
Jul-12	31	1,217	50,369	1,951,131	1,625
Aug-12	31	1,248	24,020	1,975,151	775
Sep-12	30	1,278	23,165	1,998,316	772
Oct-12	31	1,309	21,597	2,019,913	697
Nov-12	30	1,339	21,180	2,041,093	706
Dec-12	31	1,370	19,507	2,060,600	629
Jan-13	31	1,401	21,880	2,082,480	706
Feb-13	28	1,429	18,706	2,101,186	668
Mar-13	31	1,460	15,661	2,116,847	505
Apr-13	30	1,490	14,423	2,131,270	481
May-13	31	1,521	17,132	2,148,402	553
Jun-13	30	1,551	19,604	2,168,006	653
Jul-13	31	1,582	17,037	2,185,043	550
Aug-13	31	1,613	16,798	2,201,841	542
Sep-13	30	1,643	16,703	2,218,544	557
Oct-13	31	1,674	16,814	2,235,358	542
Nov-13	30	1,704	9,426	2,244,784	314
Dec-13	31	1,735	21,633	2,266,417	698

Table I – 2: Production History of Well#2 STS-A, Lease No. 252769

Month	Well days Online	Producing times (days)	Gas (MCF)	Gp (Mscf)	qg (Mscf/D)
Jun-09	30	30	66,127	66,127	2,204
Jul-09	31	61	146,310	212,437	4,720
Aug-09	31	92	109,492	321,929	3,532
Sep-09	30	122	80,649	402,578	2,688
Oct-09	31	153	70,186	472,764	2,264
Nov-09	30	183	51,253	524,017	1,708
Dec-09	31	214	53,617	577,634	1,730
Jan-10	31	245	54,790	632,424	1,767
Feb-10	28	273	44,417	676,841	1,586
Mar-10	31	304	43,603	720,444	1,407
Apr-10	30	334	38,157	758,601	1,272
May-10	31	365	36,194	794,795	1,168
Jun-10	30	395	32,560	827,355	1,085
Jul-10	31	426	31,475	858,830	1,015
Aug-10	31	457	29,844	888,674	963
Sep-10	30	487	27,878	916,552	929
Oct-10	31	518	27,192	943,744	877
Nov-10	30	548	25,358	969,102	845
Dec-10	31	579	24,518	993,620	791
Jan-11	31	610	23,444	1,017,064	756
Feb-11	28	638	13,771	1,030,835	492
Mar-11	31	669	18,936	1,049,771	611
Apr-11	30	699	17,163	1,066,934	572
May-11	31	730	17,505	1,084,439	565
Jun-11	30	760	20,560	1,104,999	685
Jul-11	31	791	18,532	1,123,531	598
Aug-11	31	822	18,001	1,141,532	581
Sep-11	30	852	16,265	1,157,797	542
Oct-11	31	883	16,125	1,173,922	520
Nov-11	30	913	15,229	1,189,151	508

Table I – 2: Continued

Month	Well days Online	Producing times (days)	Gas (MCF)	Gp (Mscf)	qg (Mscf/D)
Dec-11	31	944	16,684	1,205,835	538
Jan-12	31	975	15,486	1,221,321	500
Feb-12	28	1,003	13,886	1,235,207	496
Mar-12	31	1,034	14,837	1,250,044	479
Apr-12	30	1,064	13,866	1,263,910	462
May-12	31	1,095	14,303	1,278,213	461
Jun-12	30	1,125	13,206	1,291,419	440
Jul-12	31	1,156	14,340	1,305,759	463
Aug-12	31	1,187	13,028	1,318,787	420
Sep-12	30	1,217	12,116	1,330,903	404
Oct-12	31	1,248	12,562	1,343,465	405
Nov-12	30	1,278	9,606	1,353,071	320
Dec-12	31	1,309	9,605	1,362,676	310
Jan-13	31	1,340	11,452	1,374,128	369
Feb-13	28	1,368	8,735	1,382,863	312
Mar-13	31	1,399	8,837	1,391,700	285
Apr-13	30	1,429	8,697	1,400,397	290
May-13	31	1,460	11,891	1,412,288	384
Jun-13	30	1,490	10,838	1,423,126	361
Jul-13	31	1,521	10,691	1,433,817	345
Aug-13	31	1,552	9,617	1,443,434	310
Sep-13	30	1,582	10,309	1,453,743	344
Oct-13	31	1,613	9,122	1,462,865	294
Nov-13	30	1,643	7,888	1,470,753	263
Dec-13	31	1,674	8,533	1,479,286	275

Table I – 3: Production History of Well#3 MARTIN, DORA 1716, Lease No. 251816

Month	Well days Online	Producing times (days)	Gas (MCF)	Gp (Mscf)	qg (Mscf/D)
May-09	31	31	54,842	54,842	1,769
Jun-09	30	61	223,480	278,322	7,449
Jul-09	31	92	152,550	430,872	4,921
Aug-09	31	123	103,228	534,100	3,330
Sep-09	30	153	79,137	613,237	2,638
Oct-09	31	184	69,812	683,049	2,252
Nov-09	30	214	56,851	739,900	1,895
Dec-09	31	245	60,125	800,025	1,940
Jan-10	31	276	55,413	855,438	1,788
Feb-10	28	304	44,404	899,842	1,586
Mar-10	31	335	45,699	945,541	1,474
Apr-10	30	365	40,550	986,091	1,352
May-10	31	396	38,316	1,024,407	1,236
Jun-10	30	426	34,565	1,058,972	1,152
Jul-10	31	457	33,066	1,092,038	1,067
Aug-10	31	488	34,423	1,126,461	1,110
Sep-10	30	518	32,284	1,158,745	1,076
Oct-10	31	549	28,957	1,187,702	934
Nov-10	30	579	29,086	1,216,788	970
Dec-10	31	610	31,796	1,248,584	1,026
Jan-11	31	641	30,598	1,279,182	987
Feb-11	28	669	28,017	1,307,199	1,001
Mar-11	31	700	24,600	1,331,799	794
Apr-11	30	730	23,640	1,355,439	788
May-11	31	761	25,646	1,381,085	827
Jun-11	30	791	20,076	1,401,161	669
Jul-11	31	822	18,572	1,419,733	599
Aug-11	31	853	19,158	1,438,891	618
Sep-11	30	883	12,219	1,451,110	407
Oct-11	31	914	25,103	1,476,213	810
Nov-11	30	944	29,569	1,505,782	986

Table I – 3: Continued

Month	Well days Online	Producing times (days)	Gas (MCF)	Gp (Mscf)	qg (Mscf/D)
Dec-11	31	975	34,146	1,539,928	1,101
Jan-12	31	1,006	29,379	1,569,307	948
Feb-12	28	1,034	22,901	1,592,208	818
Mar-12	31	1,065	27,137	1,619,345	875
Apr-12	30	1,095	26,042	1,645,387	868
May-12	31	1,126	24,371	1,669,758	786
Jun-12	30	1,156	21,946	1,691,704	732
Jul-12	31	1,187	24,485	1,716,189	790
Aug-12	31	1,218	22,872	1,739,061	738
Sep-12	30	1,248	22,102	1,761,163	737
Oct-12	31	1,279	20,027	1,781,190	646
Nov-12	30	1,309	20,711	1,801,901	690
Dec-12	31	1,340	19,159	1,821,060	618
Jan-13	31	1,371	21,093	1,842,153	680
Feb-13	28	1,399	15,470	1,857,623	553
Mar-13	31	1,430	13,838	1,871,461	446
Apr-13	30	1,460	14,253	1,885,714	475
May-13	31	1,491	4,608	1,890,322	149
Jun-13	30	1,521	25,389	1,915,711	846
Jul-13	31	1,552	17,048	1,932,759	550
Aug-13	31	1,583	14,846	1,947,605	479
Sep-13	30	1,613	15,586	1,963,191	520
Oct-13	31	1,644	18,148	1,981,339	585
Nov-13	30	1,674	11,866	1,993,205	396
Dec-13	31	1,705	21,701	2,014,906	700

Table I – 4: Production History of Well#4 NUECES MINERALS COMPANY, Lease No. 251773

Month	Well days Online	Producing times (days)	Gas (MCF)	Gp (Mscf)	qg (Mscf/D)
Nov-09	30	30	115,045	115,045	3,835
Dec-09	31	61	80,499	195,544	2,597
Jan-10	31	92	78,732	274,276	2,540
Feb-10	28	120	58,993	333,269	2,107
Mar-10	31	151	57,353	390,622	1,850
Apr-10	30	181	50,015	440,637	1,667
May-10	31	212	47,166	487,803	1,521
Jun-10	30	242	41,976	529,779	1,399
Jul-10	31	273	40,222	570,001	1,297
Aug-10	31	304	37,877	607,878	1,222
Sep-10	30	334	34,275	642,153	1,143
Oct-10	31	365	34,373	676,526	1,109
Nov-10	30	395	31,148	707,674	1,038
Dec-10	31	426	30,140	737,814	972
Jan-11	31	457	28,628	766,442	923
Feb-11	28	485	24,578	791,020	878
Mar-11	31	516	25,792	816,812	832
Apr-11	30	546	23,753	840,565	792
May-11	31	577	17,212	857,777	555
Jun-11	30	607	21,862	879,639	729
Jul-11	31	638	21,993	901,632	709
Aug-11	31	669	21,146	922,778	682
Sep-11	30	699	19,693	942,471	656
Oct-11	31	730	18,073	960,544	583
Nov-11	30	760	19,444	979,988	648
Dec-11	31	791	19,024	999,012	614
Jan-12	31	822	18,834	1,017,846	608
Feb-12	28	850	16,790	1,034,636	600
Mar-12	31	881	17,280	1,051,916	557
Apr-12	30	911	19,524	1,071,440	651

Table I – 4: Continued

Month	Well days Online	Producing times (days)	Gas (MCF)	Gp (Mscf)	qg (Mscf/D)
May-12	31	942	19,506	1,090,946	629
Jun-12	30	972	16,457	1,107,403	549
Jul-12	31	1,003	17,126	1,124,529	552
Aug-12	31	1,034	16,648	1,141,177	537
Sep-12	30	1,064	15,775	1,156,952	526
Oct-12	31	1,095	15,906	1,172,858	513
Nov-12	30	1,125	13,986	1,186,844	466
Dec-12	31	1,156	12,539	1,199,383	404
Jan-13	31	1,187	14,684	1,214,067	474
Feb-13	28	1,215	13,202	1,227,269	472
Mar-13	31	1,246	14,247	1,241,516	460
Apr-13	30	1,276	13,486	1,255,002	450
May-13	31	1,307	13,791	1,268,793	445
Jun-13	30	1,337	13,084	1,281,877	436
Jul-13	31	1,368	13,236	1,295,113	427
Aug-13	31	1,399	12,779	1,307,892	412
Sep-13	30	1,429	12,381	1,320,273	413
Oct-13	31	1,460	12,548	1,332,821	405
Nov-13	30	1,490	11,849	1,344,670	395
Dec-13	31	1,521	11,435	1,356,105	369

Table I – 5: Production History of Well#5 HENDERSON-CENIZO, Lease No. 251817

Month	Well days Online	Producing times (days)	Gas (MCF)	Gp (Mscf)	qg (Mscf/D)
Aug-09	31	31	276,112	276,112	8,907
Sep-09	30	61	188,800	464,912	6,293
Oct-09	31	92	128,713	593,625	4,152
Nov-09	30	122	95,405	689,030	3,180
Dec-09	31	153	84,197	773,227	2,716
Jan-10	31	184	73,202	846,429	2,361
Feb-10	28	212	63,499	909,928	2,268
Mar-10	31	243	62,448	972,376	2,014
Apr-10	30	273	54,520	1,026,896	1,817
May-10	31	304	52,221	1,079,117	1,685
Jun-10	30	334	47,311	1,126,428	1,577
Jul-10	31	365	46,122	1,172,550	1,488
Aug-10	31	396	42,215	1,214,765	1,362
Sep-10	30	426	41,232	1,255,997	1,374
Oct-10	31	457	39,680	1,295,677	1,280
Nov-10	30	487	36,335	1,332,012	1,211
Dec-10	31	518	38,167	1,370,179	1,231
Jan-11	31	549	36,210	1,406,389	1,168
Feb-11	28	577	31,494	1,437,883	1,125
Mar-11	31	608	33,735	1,471,618	1,088
Apr-11	30	638	31,140	1,502,758	1,038
May-11	31	669	31,335	1,534,093	1,011
Jun-11	30	699	29,517	1,563,610	984
Jul-11	31	730	28,983	1,592,593	935
Aug-11	31	761	27,915	1,620,508	900
Sep-11	30	791	26,295	1,646,803	877
Oct-11	31	822	25,944	1,672,747	837
Nov-11	30	852	26,073	1,698,820	869
Dec-11	31	883	26,527	1,725,347	856
Jan-12	31	914	23,731	1,749,078	766
Feb-12	28	942	29,531	1,778,609	1,055

Table I – 5: Continued

Month	Well days Online	Producing times (days)	Gas (MCF)	Gp (Mscf)	qg (Mscf/D)
Mar-12	31	973	29,650	1,808,259	956
Apr-12	30	1,003	27,070	1,835,329	902
May-12	31	1,034	27,179	1,862,508	877
Jun-12	30	1,064	25,078	1,887,586	836
Jul-12	31	1,095	49,810	1,937,396	1,607
Aug-12	31	1,126	23,549	1,960,945	760
Sep-12	30	1,156	23,270	1,984,215	776
Oct-12	31	1,187	23,560	2,007,775	760
Nov-12	30	1,217	22,466	2,030,241	749
Dec-12	31	1,248	21,363	2,051,604	689
Jan-13	31	1,279	23,228	2,074,832	749
Feb-13	28	1,307	19,965	2,094,797	713
Mar-13	31	1,338	20,810	2,115,607	671
Apr-13	30	1,368	20,400	2,136,007	680
May-13	31	1,399	20,665	2,156,672	667
Jun-13	30	1,429	19,796	2,176,468	660
Jul-13	31	1,460	19,994	2,196,462	645
Aug-13	31	1,491	19,636	2,216,098	633
Sep-13	30	1,521	18,640	2,234,738	621
Oct-13	31	1,552	19,168	2,253,906	618
Nov-13	30	1,582	12,297	2,266,203	410
Dec-13	31	1,613	23,593	2,289,796	761

Table I – 6: Production History of Well#6 HENDERSON-CENIZO, Lease No. 255994

Month	Well days Online	Producing times (days)	Gas (MCF)	Gp (Mscf)	qg (Mscf/D)
Oct-09	31	31	121,117	121,117	3,907
Nov-09	30	61	229,481	350,598	7,649
Dec-09	31	92	158,389	508,987	5,109
Jan-10	31	123	117,602	626,589	3,794
Feb-10	28	151	94,444	721,033	3,373
Mar-10	31	182	91,771	812,804	2,960
Apr-10	30	212	79,293	892,097	2,643
May-10	31	243	74,514	966,611	2,404
Jun-10	30	273	66,083	1,032,694	2,203
Jul-10	31	304	63,611	1,096,305	2,052
Aug-10	31	335	57,878	1,154,183	1,867
Sep-10	30	365	55,996	1,210,179	1,867
Oct-10	31	396	52,841	1,263,020	1,705
Nov-10	30	426	46,634	1,309,654	1,554
Dec-10	31	457	49,685	1,359,339	1,603
Jan-11	31	488	45,749	1,405,088	1,476
Feb-11	28	516	40,042	1,445,130	1,430
Mar-11	31	547	41,237	1,486,367	1,330
Apr-11	30	577	37,102	1,523,469	1,237
May-11	31	608	40,259	1,563,728	1,299
Jun-11	30	638	37,113	1,600,841	1,237
Jul-11	31	669	36,781	1,637,622	1,186
Aug-11	31	700	36,523	1,674,145	1,178
Sep-11	30	730	34,082	1,708,227	1,136
Oct-11	31	761	35,432	1,743,659	1,143
Nov-11	30	791	33,311	1,776,970	1,110
Dec-11	31	822	33,218	1,810,188	1,072
Jan-12	31	853	34,553	1,844,741	1,115
Feb-12	28	881	30,576	1,875,317	1,092
Mar-12	31	912	31,985	1,907,302	1,032
Apr-12	30	942	30,291	1,937,593	1,010

Table I – 6: Continued

Month	Well days Online	Producing times (days)	Gas (MCF)	Gp (Mscf)	qg (Mscf/D)
May-12	31	973	31,717	1,969,310	1,023
Jun-12	30	1,003	29,755	1,999,065	992
Jul-12	31	1,034	61,216	2,060,281	1,975
Aug-12	31	1,065	28,544	2,088,825	921
Sep-12	30	1,095	28,007	2,116,832	934
Oct-12	31	1,126	27,455	2,144,287	886
Nov-12	30	1,156	26,492	2,170,779	883
Dec-12	31	1,187	23,318	2,194,097	752
Jan-13	31	1,218	24,426	2,218,523	788
Feb-13	28	1,246	23,650	2,242,173	845
Mar-13	31	1,277	24,491	2,266,664	790
Apr-13	30	1,307	9,099	2,275,763	303
May-13	31	1,338	19,862	2,295,625	641
Jun-13	30	1,368	12,697	2,308,322	423
Jul-13	31	1,399	15,363	2,323,685	496
Aug-13	31	1,430	15,312	2,338,997	494
Sep-13	30	1,460	14,154	2,353,151	472
Oct-13	31	1,491	17,807	2,370,958	574
Nov-13	30	1,521	12,603	2,383,561	420
Dec-13	31	1,552	20,350	2,403,911	656

Table I – 7: Production History of Well#7 NUECES MINERALS COMPANY, Lease No. 255435

Month	Well days Online	Producing times (days)	Gas (MCF)	Gp (Mscf)	qg (Mscf/D)
Dec-09	31	31	180,218	180,218	5,813
Jan-10	31	62	211,094	391,312	6,809
Feb-10	28	90	110,918	502,230	3,961
Mar-10	31	121	109,690	611,920	3,538
Apr-10	30	151	88,779	700,699	2,959
May-10	31	182	78,062	778,761	2,518
Jun-10	30	212	67,203	845,964	2,240
Jul-10	31	243	61,304	907,268	1,978
Aug-10	31	274	55,806	963,074	1,800
Sep-10	30	304	49,394	1,012,468	1,646
Oct-10	31	335	46,590	1,059,058	1,503
Nov-10	30	365	44,025	1,103,083	1,468
Dec-10	31	396	42,983	1,146,066	1,387
Jan-11	31	427	40,478	1,186,544	1,306
Feb-11	28	455	34,662	1,221,206	1,238
Mar-11	31	486	35,866	1,257,072	1,157
Apr-11	30	516	32,498	1,289,570	1,083
May-11	31	547	22,271	1,311,841	718
Jun-11	30	577	27,483	1,339,324	916
Jul-11	31	608	26,750	1,366,074	863
Aug-11	31	639	24,856	1,390,930	802
Sep-11	30	669	22,600	1,413,530	753
Oct-11	31	700	18,816	1,432,346	607
Nov-11	30	730	21,548	1,453,894	718
Dec-11	31	761	25,819	1,479,713	833
Jan-12	31	792	25,338	1,505,051	817
Feb-12	28	820	23,808	1,528,859	850
Mar-12	31	851	27,803	1,556,662	897
Apr-12	30	881	23,276	1,579,938	776
May-12	31	912	21,883	1,601,821	706
Jun-12	30	942	16,926	1,618,747	564

Table I –7: Continued

Month	Well days Online	Producing times (days)	Gas (MCF)	Gp (Mscf)	qg (Mscf/D)
Jul-12	31	973	17,017	1,635,764	549
Aug-12	31	1,004	17,945	1,653,709	579
Sep-12	30	1,034	15,801	1,669,510	527
Oct-12	31	1,065	15,250	1,684,760	492
Nov-12	30	1,095	12,604	1,697,364	420
Dec-12	31	1,126	10,115	1,707,479	326
Jan-13	31	1,157	14,230	1,721,709	459
Feb-13	28	1,185	18,488	1,740,197	660
Mar-13	31	1,216	18,954	1,759,151	611
Apr-13	30	1,246	17,428	1,776,579	581
May-13	31	1,277	15,618	1,792,197	504
Jun-13	30	1,307	18,075	1,810,272	603
Jul-13	31	1,338	17,180	1,827,452	554
Aug-13	31	1,369	16,659	1,844,111	537
Sep-13	30	1,399	15,237	1,859,348	508
Oct-13	31	1,430	15,382	1,874,730	496
Nov-13	30	1,460	14,798	1,889,528	493
Dec-13	31	1,491	14,744	1,904,272	476

Table I – 8: Production History of Well#8 GOLLA 7, Lease No. 255730

Month	Well days Online	Producing times (days)	Gas (MCF)	Gp (Mscf)	qg (Mscf/D)
Dec-09	31	31	17,842	17,842	576
Jan-10	31	62	184,624	202,466	5,956
Feb-10	28	90	131,132	333,598	4,683
Mar-10	31	121	113,112	446,710	3,649
Apr-10	30	151	91,061	537,771	3,035
May-10	31	182	87,717	625,488	2,830
Jun-10	30	212	78,029	703,517	2,601
Jul-10	31	243	66,583	770,100	2,148
Aug-10	31	274	65,282	835,382	2,106
Sep-10	30	304	53,968	889,350	1,799
Oct-10	31	335	51,770	941,120	1,670
Nov-10	30	365	46,394	987,514	1,546
Dec-10	31	396	44,667	1,032,181	1,441
Jan-11	31	427	43,545	1,075,726	1,405
Feb-11	28	455	38,673	1,114,399	1,381
Mar-11	31	486	38,615	1,153,014	1,246
Apr-11	30	516	36,310	1,189,324	1,210
May-11	31	547	25,856	1,215,180	834
Jun-11	30	577	20,544	1,235,724	685
Jul-11	31	608	33,175	1,268,899	1,070
Aug-11	31	639	25,669	1,294,568	828
Sep-11	30	669	26,546	1,321,114	885
Oct-11	31	700	25,899	1,347,013	835
Nov-11	30	730	23,308	1,370,321	777
Dec-11	31	761	26,734	1,397,055	862
Jan-12	31	792	25,417	1,422,472	820
Feb-12	28	820	25,136	1,447,608	898
Mar-12	31	851	20,981	1,468,589	677
Apr-12	30	881	14,155	1,482,744	472
May-12	31	912	15,056	1,497,800	486

Table I – 8: Continued

Month	Well days Online	Producing times (days)	Gas (MCF)	Gp (Mscf)	qg (Mscf/D)
Jun-12	30	942	12,708	1,510,508	424
Jul-12	31	973	13,138	1,523,646	424
Aug-12	31	1,004	12,904	1,536,550	416
Sep-12	30	1,034	11,693	1,548,243	390
Oct-12	31	1,065	12,411	1,560,654	400
Nov-12	30	1,095	11,632	1,572,286	388
Dec-12	31	1,126	11,342	1,583,628	366
Jan-13	31	1,157	11,590	1,595,218	374
Feb-13	28	1,185	10,105	1,605,323	361
Mar-13	31	1,216	11,418	1,616,741	368
Apr-13	30	1,246	9,578	1,626,319	319
May-13	31	1,277	10,215	1,636,534	330
Jun-13	30	1,307	7,017	1,643,551	234
Jul-13	31	1,338	7,070	1,650,621	228
Aug-13	31	1,369	14,092	1,664,713	455
Sep-13	30	1,399	11,645	1,676,358	388
Oct-13	31	1,430	10,399	1,686,757	335
Nov-13	30	1,460	10,821	1,697,578	361
Dec-13	31	1,491	8,344	1,705,922	269

Table I – 9: Production History of Well#9 CAROLINE PIELOP, Lease No. 254447

Month	Well days Online	Producing times (days)	Gas (MCF)	Gp (Mscf)	qg (Mscf/D)
Jan-10	31	31	260,229	260,229	8,394
Feb-10	28	59	208,892	469,121	7,460
Mar-10	31	90	163,511	632,632	5,275
Apr-10	30	120	137,044	769,676	4,568
May-10	31	151	127,567	897,243	4,115
Jun-10	30	181	112,920	1,010,163	3,764
Jul-10	31	212	107,466	1,117,629	3,467
Aug-10	31	243	98,023	1,215,652	3,162
Sep-10	30	273	90,878	1,306,530	3,029
Oct-10	31	304	87,859	1,394,389	2,834
Nov-10	30	334	76,622	1,471,011	2,554
Dec-10	31	365	78,501	1,549,512	2,532
Jan-11	31	396	73,077	1,622,589	2,357
Feb-11	28	424	60,126	1,682,715	2,147
Mar-11	31	455	55,210	1,737,925	1,781
Apr-11	30	485	60,534	1,798,459	2,018
May-11	31	516	33,942	1,832,401	1,095
Jun-11	30	546	49,100	1,881,501	1,637
Jul-11	31	577	43,121	1,924,622	1,391
Aug-11	31	608	55,974	1,980,596	1,806
Sep-11	30	638	62,368	2,042,964	2,079
Oct-11	31	669	58,306	2,101,270	1,881
Nov-11	30	699	51,210	2,152,480	1,707
Dec-11	31	730	51,864	2,204,344	1,673
Jan-12	31	761	51,546	2,255,890	1,663
Feb-12	28	789	47,540	2,303,430	1,698
Mar-12	31	820	47,238	2,350,668	1,524
Apr-12	30	850	47,863	2,398,531	1,595
May-12	31	881	49,473	2,448,004	1,596
Jun-12	30	911	45,844	2,493,848	1,528
Jul-12	31	942	46,379	2,540,227	1,496

Table I – 9: Continued

Month	Well days Online	Producing times (days)	Gas (MCF)	Gp (Mscf)	qg (Mscf/D)
Aug-12	31	973	34,351	2,574,578	1,108
Sep-12	30	1,003	42,450	2,617,028	1,415
Oct-12	31	1,034	41,609	2,658,637	1,342
Nov-12	30	1,064	40,838	2,699,475	1,361
Dec-12	31	1,095	38,510	2,737,985	1,242
Jan-13	31	1,126	31,971	2,769,956	1,031
Feb-13	28	1,154	33,343	2,803,299	1,191
Mar-13	31	1,185	34,601	2,837,900	1,116
Apr-13	30	1,215	33,032	2,870,932	1,101
May-13	31	1,246	34,896	2,905,828	1,126
Jun-13	30	1,276	31,651	2,937,479	1,055
Jul-13	31	1,307	35,105	2,972,584	1,132
Aug-13	31	1,338	33,133	3,005,717	1,069
Sep-13	30	1,368	28,590	3,034,307	953
Oct-13	31	1,399	34,161	3,068,468	1,102
Nov-13	30	1,429	25,873	3,094,341	862
Dec-13	31	1,460	38,585	3,132,926	1,245

Table I – 10: Production History of Well#10 MARTIN FAMILY, Lease No. 263658

Month	Well days Online	Producing times (days)	Gas (MCF)	Gp (Mscf)	qg (Mscf/D)
May-11	31	31	70,117	70,117	2,262
Jun-11	30	61	66,427	136,544	2,214
Jul-11	31	92	83,930	220,474	2,707
Aug-11	31	123	67,540	288,014	2,179
Sep-11	30	153	58,014	346,028	1,934
Oct-11	31	184	49,455	395,483	1,595
Nov-11	30	214	41,372	436,855	1,379
Dec-11	31	245	36,918	473,773	1,191
Jan-12	31	276	33,442	507,215	1,079
Feb-12	28	304	28,428	535,643	1,015
Mar-12	31	335	27,483	563,126	887
Apr-12	30	365	24,048	587,174	802
May-12	31	396	22,215	609,389	717
Jun-12	30	426	16,895	626,284	563
Jul-12	31	457	21,194	647,478	684
Aug-12	31	488	15,757	663,235	508
Sep-12	30	518	15,839	679,074	528
Oct-12	31	549	19,681	698,755	635
Nov-12	30	579	17,778	716,533	593
Dec-12	31	610	15,075	731,608	486
Jan-13	31	641	15,811	747,419	510
Feb-13	28	669	9,583	757,002	342
Mar-13	31	700	13,967	770,969	451
Apr-13	30	730	12,832	783,801	428
May-13	31	761	13,843	797,644	447
Jun-13	30	791	11,351	808,995	378
Jul-13	31	822	11,679	820,674	377
Aug-13	31	853	12,222	832,896	394
Sep-13	30	883	11,272	844,168	376
Oct-13	31	914	10,865	855,033	350
Nov-13	30	944	11,313	866,346	377
Dec-13	31	975	10,174	876,520	328

Table I – 11: Production History of Well#11 BROWN DISTRIBUTING, Lease No. 258106

Month	Well days Online	Producing times (days)	Gas (MCF)	Gp (Mscf)	qg (Mscf/D)
Jul-10	31	31	14,876	14,876	480
Aug-10	31	62	173,418	188,294	5,594
Sep-10	30	92	124,466	312,760	4,149
Oct-10	31	123	104,657	417,417	3,376
Nov-10	30	153	99,988	517,405	3,333
Dec-10	31	184	78,837	596,242	2,543
Jan-11	31	215	74,330	670,572	2,398
Feb-11	28	243	58,578	729,150	2,092
Mar-11	31	274	54,154	783,304	1,747
Apr-11	30	304	52,841	836,145	1,761
May-11	31	335	49,212	885,357	1,587
Jun-11	30	365	44,163	929,520	1,472
Jul-11	31	396	42,028	971,548	1,356
Aug-11	31	427	42,786	1,014,334	1,380
Sep-11	30	457	40,348	1,054,682	1,345
Oct-11	31	488	38,196	1,092,878	1,232
Nov-11	30	518	35,529	1,128,407	1,184
Dec-11	31	549	34,850	1,163,257	1,124
Jan-12	31	580	34,050	1,197,307	1,098
Feb-12	28	608	30,390	1,227,697	1,085
Mar-12	31	639	31,434	1,259,131	1,014
Apr-12	30	669	29,383	1,288,514	979
May-12	31	700	29,828	1,318,342	962
Jun-12	30	730	27,625	1,345,967	921
Jul-12	31	761	27,255	1,373,222	879
Aug-12	31	792	25,942	1,399,164	837
Sep-12	30	822	25,308	1,424,472	844
Oct-12	31	853	24,599	1,449,071	794
Nov-12	30	883	23,529	1,472,600	784
Dec-12	31	914	19,807	1,492,407	639
Jan-13	31	945	20,704	1,513,111	668

Table I – 11: Continued

Month	Well days Online	Producing times (days)	Gas (MCF)	Gp (Mscf)	qg (Mscf/D)
Feb-13	28	973	18,959	1,532,070	677
Mar-13	31	1,004	21,113	1,553,183	681
Apr-13	30	1,034	19,167	1,572,350	639
May-13	31	1,065	19,778	1,592,128	638
Jun-13	30	1,095	17,305	1,609,433	577
Jul-13	31	1,126	19,478	1,628,911	628
Aug-13	31	1,157	18,412	1,647,323	594
Sep-13	30	1,187	18,409	1,665,732	614
Oct-13	31	1,218	20,895	1,686,627	674
Nov-13	30	1,248	6,545	1,693,172	218
Dec-13	31	1,279	23,968	1,717,140	773
Jul-10	31	31	14,876	14,876	480
Aug-10	31	62	173,418	188,294	5,594
Sep-10	30	92	124,466	312,760	4,149

Table I – 12: Production History of Well#12 BROWN DISTRIBUTING, Lease No. 258900

Month	Well days Online	Producing times (days)	Gas (MCF)	Gp (Mscf)	qg (Mscf/D)
Aug-10	31	31	24,935	24,935	804
Sep-10	30	61	167,872	192,807	5,596
Oct-10	31	92	130,761	323,568	4,218
Nov-10	30	122	83,285	406,853	2,776
Dec-10	31	153	93,161	500,014	3,005
Jan-11	31	184	77,402	577,416	2,497
Feb-11	28	212	60,406	637,822	2,157
Mar-11	31	243	53,876	691,698	1,738
Apr-11	30	273	52,331	744,029	1,744
May-11	31	304	50,308	794,337	1,623
Jun-11	30	334	45,690	840,027	1,523
Jul-11	31	365	39,504	879,531	1,274

Table I –12: Continued

Month	Well days Online	Producing times (days)	Gas (MCF)	Gp (Mscf)	qg (Mscf/D)
Aug-11	31	396	43,288	922,819	1,396
Sep-11	30	426	40,006	962,825	1,334
Oct-11	31	457	38,553	1,001,378	1,244
Nov-11	30	487	35,958	1,037,336	1,199
Dec-11	31	518	35,135	1,072,471	1,133
Jan-12	31	549	34,252	1,106,723	1,105
Feb-12	28	577	30,725	1,137,448	1,097
Mar-12	31	608	31,821	1,169,269	1,026
Apr-12	30	638	29,071	1,198,340	969
May-12	31	669	29,235	1,227,575	943
Jun-12	30	699	27,462	1,255,037	915
Jul-12	31	730	28,702	1,283,739	926
Aug-12	31	761	26,411	1,310,150	852
Sep-12	30	791	23,823	1,333,973	794
Oct-12	31	822	23,420	1,357,393	755
Nov-12	30	852	24,440	1,381,833	815
Dec-12	31	883	21,961	1,403,794	708
Jan-13	31	914	24,190	1,427,984	780
Feb-13	28	942	20,824	1,448,808	744
Mar-13	31	973	20,639	1,469,447	666
Apr-13	30	1,003	20,265	1,489,712	676
May-13	31	1,034	17,276	1,506,988	557
Jun-13	30	1,064	4,063	1,511,051	135
Jul-13	31	1,095	24,511	1,535,562	791
Aug-13	31	1,126	18,219	1,553,781	588
Sep-13	30	1,156	18,836	1,572,617	628
Oct-13	31	1,187	18,131	1,590,748	585
Nov-13	30	1,217	11,942	1,602,690	398
Dec-13	31	1,248	24,077	1,626,767	777

Table I – 13: Production History of Well#13 MARTIN, DORA, Lease No. 257263

Month	Well days Online	Producing times (days)	Gas (MCF)	Gp (Mscf)	qg (Mscf/D)
Mar-10	31	31	29,695	29,695	958
Apr-10	30	61	144,438	174,133	4,815
May-10	31	92	83,263	257,396	2,686
Jun-10	30	122	61,425	318,821	2,048
Jul-10	31	153	62,025	380,846	2,001
Aug-10	31	184	54,242	435,088	1,750
Sep-10	30	214	48,251	483,339	1,608
Oct-10	31	245	46,769	530,108	1,509
Nov-10	30	275	42,467	572,575	1,416
Dec-10	31	306	41,918	614,493	1,352
Jan-11	31	337	39,474	653,967	1,273
Feb-11	28	365	33,022	686,989	1,179
Mar-11	31	396	34,721	721,710	1,120
Apr-11	30	426	32,257	753,967	1,075
May-11	31	457	33,622	787,589	1,085
Jun-11	30	487	31,525	819,114	1,051
Jul-11	31	518	28,137	847,251	908
Aug-11	31	549	32,942	880,193	1,063
Sep-11	30	579	28,116	908,309	937
Oct-11	31	610	27,427	935,736	885
Nov-11	30	640	21,688	957,424	723
Dec-11	31	671	30,013	987,437	968
Jan-12	31	702	28,510	1,015,947	920
Feb-12	28	730	25,612	1,041,559	915
Mar-12	31	761	26,232	1,067,791	846
Apr-12	30	791	25,011	1,092,802	834
May-12	31	822	25,081	1,117,883	809
Jun-12	30	852	23,665	1,141,548	789
Jul-12	31	883	25,377	1,166,925	819
Aug-12	31	914	22,472	1,189,397	725
Sep-12	30	944	23,271	1,212,668	776

Table I –13: Continued

Month	Well days Online	Producing times (days)	Gas (MCF)	Gp (Mscf)	qg (Mscf/D)
Oct-12	31	975	22,541	1,235,209	727
Nov-12	30	1,005	21,536	1,256,745	718
Dec-12	31	1,036	22,064	1,278,809	712
Jan-13	31	1,067	21,104	1,299,913	681
Feb-13	28	1,095	18,760	1,318,673	670
Mar-13	31	1,126	19,412	1,338,085	626
Apr-13	30	1,156	18,348	1,356,433	612
May-13	31	1,187	19,545	1,375,978	630
Jun-13	30	1,217	18,083	1,394,061	603
Jul-13	31	1,248	18,952	1,413,013	611
Aug-13	31	1,279	17,857	1,430,870	576
Sep-13	30	1,309	17,633	1,448,503	588
Oct-13	31	1,340	18,233	1,466,736	588
Nov-13	30	1,370	15,485	1,482,221	516
Dec-13	31	1,401	22,689	1,504,910	732

Table I – 14: Production History of Well#14 MARTIN, DORA, Lease No. 257862

Month	Well days Online	Producing times (days)	Gas (MCF)	Gp (Mscf)	qg (Mscf/D)
Jun-10	30	30	49,448	49,448	1,648
Jul-10	31	61	107,086	156,534	3,454
Aug-10	31	92	77,575	234,109	2,502
Sep-10	30	122	59,996	294,105	2,000
Oct-10	31	153	51,582	345,687	1,664
Nov-10	30	183	41,596	387,283	1,387
Dec-10	31	214	46,008	433,291	1,484
Jan-11	31	245	41,023	474,314	1,323
Feb-11	28	273	33,427	507,741	1,194
Mar-11	31	304	33,653	541,394	1,086
Apr-11	30	334	30,369	571,763	1,012

Table I –14: Continued

Month	Well days Online	Producing times (days)	Gas (MCF)	Gp (Mscf)	qg (Mscf/D)
May-11	31	365	30,406	602,169	981
Jun-11	30	395	28,628	630,797	954
Jul-11	31	426	25,156	655,953	811
Aug-11	31	457	27,815	683,768	897
Sep-11	30	487	23,105	706,873	770
Oct-11	31	518	22,759	729,632	734
Nov-11	30	548	17,644	747,276	588
Dec-11	31	579	24,503	771,779	790
Jan-12	31	610	21,008	792,787	678
Feb-12	28	638	20,191	812,978	721
Mar-12	31	669	22,924	835,902	739
Apr-12	30	699	19,879	855,781	663
May-12	31	730	22,326	878,107	720
Jun-12	30	760	19,786	897,893	660
Jul-12	31	791	20,092	917,985	648
Aug-12	31	822	18,834	936,819	608
Sep-12	30	852	18,431	955,250	614
Oct-12	31	883	18,189	973,439	587
Nov-12	30	913	17,141	990,580	571
Dec-12	31	944	17,189	1,007,769	554
Jan-13	31	975	17,630	1,025,399	569
Feb-13	28	1,003	15,456	1,040,855	552
Mar-13	31	1,034	15,699	1,056,554	506
Apr-13	30	1,064	14,759	1,071,313	492
May-13	31	1,095	15,078	1,086,391	486
Jun-13	30	1,125	14,330	1,100,721	478
Jul-13	31	1,156	14,790	1,115,511	477
Aug-13	31	1,187	14,459	1,129,970	466
Sep-13	30	1,217	13,258	1,143,228	442
Oct-13	31	1,248	11,695	1,154,923	377
Nov-13	30	1,278	10,883	1,165,806	363
Dec-13	31	1,309	18,252	1,184,058	589

Table I – 15: Production History of Well#15 MARTIN, DORA, Lease No. 254843

Month	Well days Online	Producing times (days)	Gas (MCF)	Gp (Mscf)	qg (Mscf/D)
Mar-10	31	31	42,554	42,554	1,373
Apr-10	30	61	84,785	127,339	2,826
May-10	31	92	61,599	188,938	1,987
Jun-10	30	122	49,280	238,218	1,643
Jul-10	31	153	47,344	285,562	1,527
Aug-10	31	184	42,267	327,829	1,363
Sep-10	30	214	37,229	365,058	1,241
Oct-10	31	245	35,363	400,421	1,141
Nov-10	30	275	31,892	432,313	1,063
Dec-10	31	306	31,044	463,357	1,001
Jan-11	31	337	26,579	489,936	857
Feb-11	28	365	26,198	516,134	936
Mar-11	31	396	26,340	542,474	850
Apr-11	30	426	24,072	566,546	802
May-11	31	457	24,047	590,593	776
Jun-11	30	487	22,430	613,023	748
Jul-11	31	518	22,362	635,385	721
Aug-11	31	549	22,687	658,072	732
Sep-11	30	579	20,193	678,265	673
Oct-11	31	610	18,520	696,785	597
Nov-11	30	640	14,960	711,745	499
Dec-11	31	671	22,303	734,048	719
Jan-12	31	702	19,275	753,323	622
Feb-12	28	730	16,669	769,992	595
Mar-12	31	761	18,588	788,580	600
Apr-12	30	791	17,364	805,944	579
May-12	31	822	17,506	823,450	565
Jun-12	30	852	16,140	839,590	538
Jul-12	31	883	17,024	856,614	549
Aug-12	31	914	15,717	872,331	507
Sep-12	30	944	14,897	887,228	497

Table I –15: Continued

Month	Well days Online	Producing times (days)	Gas (MCF)	Gp (Mscf)	qg (Mscf/D)
Oct-12	31	975	14,855	902,083	479
Nov-12	30	1,005	14,179	916,262	473
Dec-12	31	1,036	13,575	929,837	438
Jan-13	31	1,067	10,435	940,272	337
Feb-13	28	1,095	13,318	953,590	476
Mar-13	31	1,126	13,294	966,884	429
Apr-13	30	1,156	13,746	980,630	458
May-13	31	1,187	13,614	994,244	439
Jun-13	30	1,217	12,866	1,007,110	429
Jul-13	31	1,248	13,200	1,020,310	426
Aug-13	31	1,279	12,265	1,032,575	396
Sep-13	30	1,309	12,469	1,045,044	416
Oct-13	31	1,340	12,879	1,057,923	415
Nov-13	30	1,370	7,835	1,065,758	261
Dec-13	31	1,401	16,122	1,081,880	520

Table I – 16: Production History of Well#16 APPLING 695, Lease No. 258036

Month	Well days Online	Producing times (days)	Gas (MCF)	Gp (Mscf)	qg (Mscf/D)
May-10	31	31	65,885	65,885	2,125
Jun-10	30	61	158,380	224,265	5,279
Jul-10	31	92	139,828	364,093	4,511
Aug-10	31	123	116,623	480,716	3,762
Sep-10	30	153	96,022	576,738	3,201
Oct-10	31	184	87,543	664,281	2,824
Nov-10	30	214	73,296	737,577	2,443
Dec-10	31	245	100,621	838,198	3,246
Jan-11	31	276	87,020	925,218	2,807
Feb-11	28	304	74,336	999,554	2,655
Mar-11	31	335	68,671	1,068,225	2,215

Table I –16: Continued

Month	Well days Online	Producing times (days)	Gas (MCF)	Gp (Mscf)	qg (Mscf/D)
Apr-11	30	365	60,446	1,128,671	2,015
May-11	31	396	48,739	1,177,410	1,572
Jun-11	30	426	52,606	1,230,016	1,754
Jul-11	31	457	48,126	1,278,142	1,552
Aug-11	31	488	47,385	1,325,527	1,529
Sep-11	30	518	47,615	1,373,142	1,587
Oct-11	31	549	41,759	1,414,901	1,347
Nov-11	30	579	32,521	1,447,422	1,084
Dec-11	31	610	47,013	1,494,435	1,517
Jan-12	31	641	43,309	1,537,744	1,397
Feb-12	28	669	38,126	1,575,870	1,362
Mar-12	31	700	38,684	1,614,554	1,248
Apr-12	30	730	37,259	1,651,813	1,242
May-12	31	761	37,534	1,689,347	1,211
Jun-12	30	791	34,907	1,724,254	1,164
Jul-12	31	822	35,180	1,759,434	1,135
Aug-12	31	853	32,280	1,791,714	1,041
Sep-12	30	883	32,089	1,823,803	1,070
Oct-12	31	914	25,119	1,848,922	810
Nov-12	30	944	32,836	1,881,758	1,095
Dec-12	31	975	27,994	1,909,752	903
Jan-13	31	1,006	24,024	1,933,776	775
Feb-13	28	1,034	20,343	1,954,119	727
Mar-13	31	1,065	23,581	1,977,700	761
Apr-13	30	1,095	22,387	2,000,087	746
May-13	31	1,126	22,901	2,022,988	739
Jun-13	30	1,156	20,329	2,043,317	678
Jul-13	31	1,187	20,144	2,063,461	650
Aug-13	31	1,218	21,470	2,084,931	693
Sep-13	30	1,248	18,284	2,103,215	609

Table I –16: Continued

Month	Well days Online	Producing times (days)	Gas (MCF)	Gp (Mscf)	qg (Mscf/D)
Oct-13	31	1,279	20,043	2,123,258	647
Nov-13	30	1,309	18,005	2,141,263	600
Dec-13	31	1,340	18,641	2,159,904	601

Table I – 17: Production History of Well#17 MARTIN UNIT 1, Lease No. 257955

Month	Well days Online	Producing times (days)	Gas (MCF)	Gp (Mscf)	qg (Mscf/D)
Apr-10	30	30	37,877	37,877	1,263
May-10	31	61	121,763	159,640	3,928
Jun-10	30	91	83,319	242,959	2,777
Jul-10	31	122	75,262	318,221	2,428
Aug-10	31	153	64,710	382,931	2,087
Sep-10	30	183	55,945	438,876	1,865
Oct-10	31	214	52,781	491,657	1,703
Nov-10	30	244	45,818	537,475	1,527
Dec-10	31	275	47,030	584,505	1,517
Jan-11	31	306	43,162	627,667	1,392
Feb-11	28	334	37,775	665,442	1,349
Mar-11	31	365	38,321	703,763	1,236
Apr-11	30	395	35,651	739,414	1,188
May-11	31	426	34,527	773,941	1,114
Jun-11	30	456	32,748	806,689	1,092
Jul-11	31	487	24,471	831,160	789
Aug-11	31	518	25,126	856,286	811
Sep-11	30	548	24,421	880,707	814
Oct-11	31	579	28,451	909,158	918
Nov-11	30	609	23,006	932,164	767
Dec-11	31	640	32,199	964,363	1,039
Jan-12	31	671	30,099	994,462	971
Feb-12	28	699	26,155	1,020,617	934

Table I –17: Continued

Month	Well days Online	Producing times (days)	Gas (MCF)	Gp (Mscf)	qg (Mscf/D)
Mar-12	31	730	28,387	1,049,004	916
Apr-12	30	760	27,247	1,076,251	908
May-12	31	791	27,170	1,103,421	876
Jun-12	30	821	25,402	1,128,823	847
Jul-12	31	852	25,772	1,154,595	831
Aug-12	31	883	23,615	1,178,210	762
Sep-12	30	913	23,112	1,201,322	770
Oct-12	31	944	23,583	1,224,905	761
Nov-12	30	974	23,042	1,247,947	768
Dec-12	31	1,005	22,233	1,270,180	717
Jan-13	31	1,036	22,538	1,292,718	727
Feb-13	28	1,064	19,949	1,312,667	712
Mar-13	31	1,095	18,942	1,331,609	611
Apr-13	30	1,125	16,627	1,348,236	554
May-13	31	1,156	23,121	1,371,357	746
Jun-13	30	1,186	19,188	1,390,545	640
Jul-13	31	1,217	19,288	1,409,833	622
Aug-13	31	1,248	20,590	1,430,423	664
Sep-13	30	1,278	19,045	1,449,468	635
Oct-13	31	1,309	20,926	1,470,394	675
Nov-13	30	1,339	12,955	1,483,349	432
Dec-13	31	1,370	27,654	1,511,003	892

Table I – 18: Production History of Well#18 BURKS RANCH EAST, Lease No. 259883

Month	Well days Online	Producing times (days)	Gas (MCF)	Gp (Mscf)	qg (Mscf/D)
Jan-11	31	31	119,236	119,236	3,846
Feb-11	28	59	152,867	272,103	5,460
Mar-11	31	90	143,538	415,641	4,630
Apr-11	30	120	120,442	536,083	4,015
May-11	31	151	110,985	647,068	3,580
Jun-11	30	181	88,289	735,357	2,943
Jul-11	31	212	95,139	830,496	3,069
Aug-11	31	243	79,642	910,138	2,569
Sep-11	30	273	73,428	983,566	2,448
Oct-11	31	304	69,416	1,052,982	2,239
Nov-11	30	334	59,090	1,112,072	1,970
Dec-11	31	365	61,371	1,173,443	1,980
Jan-12	31	396	56,252	1,229,695	1,815
Feb-12	28	424	50,056	1,279,751	1,788
Mar-12	31	455	48,692	1,328,443	1,571
Apr-12	30	485	44,191	1,372,634	1,473
May-12	31	516	43,466	1,416,100	1,402
Jun-12	30	546	41,032	1,457,132	1,368
Jul-12	31	577	38,107	1,495,239	1,229
Aug-12	31	608	39,796	1,535,035	1,284
Sep-12	30	638	36,550	1,571,585	1,218
Oct-12	31	669	35,167	1,606,752	1,134
Nov-12	30	699	32,612	1,639,364	1,087
Dec-12	31	730	32,489	1,671,853	1,048
Jan-13	31	761	31,323	1,703,176	1,010
Feb-13	28	789	27,268	1,730,444	974
Mar-13	31	820	28,513	1,758,957	920
Apr-13	30	850	26,327	1,785,284	878
May-13	31	881	28,277	1,813,561	912
Jun-13	30	911	29,167	1,842,728	972

Table I –18: Continued

Month	Well days Online	Producing times (days)	Gas (MCF)	Gp (Mscf)	qg (Mscf/D)
Jul-13	31	942	30,759	1,873,487	992
Aug-13	31	973	25,477	1,898,964	822
Sep-13	30	1,003	29,229	1,928,193	974
Oct-13	31	1,034	27,821	1,956,014	897
Nov-13	30	1,064	22,857	1,978,871	762
Dec-13	31	1,095	13,595	1,992,466	439

Table I – 19: Production History of Well#19 HENDERSON-CENIZO, Lease No. 259429

Month	Well days Online	Producing times (days)	Gas (MCF)	Gp (Mscf)	qg (Mscf/D)
Jan-11	31	31	10,364	10,364	334
Feb-11	28	59	324,557	334,921	11,591
Mar-11	31	90	277,216	612,137	8,942
Apr-11	30	120	201,473	813,610	6,716
May-11	31	151	124,577	938,187	4,019
Jun-11	30	181	109,975	1,048,162	3,666
Jul-11	31	212	133,173	1,181,335	4,296
Aug-11	31	243	113,998	1,295,333	3,677
Sep-11	30	273	98,728	1,394,061	3,291
Oct-11	31	304	87,642	1,481,703	2,827
Nov-11	30	334	71,482	1,553,185	2,383
Dec-11	31	365	69,543	1,622,728	2,243
Jan-12	31	396	61,066	1,683,794	1,970
Feb-12	28	424	54,115	1,737,909	1,933
Mar-12	31	455	52,628	1,790,537	1,698
Apr-12	30	485	47,953	1,838,490	1,598
May-12	31	516	47,392	1,885,882	1,529
Jun-12	30	546	58,863	1,944,745	1,962
Jul-12	31	577	123,712	2,068,457	3,991
Aug-12	31	608	58,626	2,127,083	1,891

Table I –19: Continued

Month	Well days Online	Producing times (days)	Gas (MCF)	Gp (Mscf)	qg (Mscf/D)
Sep-12	30	638	53,284	2,180,367	1,776
Oct-12	31	669	52,283	2,232,650	1,687
Nov-12	30	699	48,136	2,280,786	1,605
Dec-12	31	730	44,866	2,325,652	1,447
Jan-13	31	761	46,042	2,371,694	1,485
Feb-13	28	789	37,782	2,409,476	1,349
Mar-13	31	820	41,324	2,450,800	1,333
Apr-13	30	850	27,309	2,478,109	910
May-13	31	881	27,181	2,505,290	877
Jun-13	30	911	25,202	2,530,492	840
Jul-13	31	942	25,177	2,555,669	812
Aug-13	31	973	24,790	2,580,459	800
Sep-13	30	1,003	23,621	2,604,080	787
Oct-13	31	1,034	23,863	2,627,943	770
Nov-13	30	1,064	18,008	2,645,951	600
Dec-13	31	1,095	26,326	2,672,277	849

Table I – 20: Production History of Well#20 GUTIERREZ-LEYENDECKER, Lease No. 258903

Month	Well days Online	Producing times (days)	Gas (MCF)	Gp (Mscf)	qg (Mscf/D)
Sep-10	30	30	127,788	127,788	4,260
Oct-10	31	61	264,611	392,399	8,536
Nov-10	30	91	171,834	564,233	5,728
Dec-10	31	122	160,834	725,067	5,188
Jan-11	31	153	140,055	865,122	4,518
Feb-11	28	181	111,484	976,606	3,982
Mar-11	31	212	105,253	1,081,859	3,395
Apr-11	30	242	95,465	1,177,324	3,182
May-11	31	273	95,712	1,273,036	3,087
Jun-11	30	303	87,475	1,360,511	2,916

Table I –20: Continued

Month	Well days Online	Producing times (days)	Gas (MCF)	Gp (Mscf)	qg (Mscf/D)
Jul-11	31	334	76,131	1,436,642	2,456
Aug-11	31	365	78,976	1,515,618	2,548
Sep-11	30	395	73,283	1,588,901	2,443
Oct-11	31	426	62,502	1,651,403	2,016
Nov-11	30	456	47,081	1,698,484	1,569
Dec-11	31	487	70,377	1,768,861	2,270
Jan-12	31	518	64,221	1,833,082	2,072
Feb-12	28	546	55,957	1,889,039	1,998
Mar-12	31	577	58,398	1,947,437	1,884
Apr-12	30	607	46,361	1,993,798	1,545
May-12	31	638	59,180	2,052,978	1,909
Jun-12	30	668	52,285	2,105,263	1,743
Jul-12	31	699	52,136	2,157,399	1,682
Aug-12	31	730	46,914	2,204,313	1,513
Sep-12	30	760	47,073	2,251,386	1,569
Oct-12	31	791	45,805	2,297,191	1,478
Nov-12	30	821	43,845	2,341,036	1,462
Dec-12	31	852	42,633	2,383,669	1,375
Jan-13	31	883	35,360	2,419,029	1,141
Feb-13	28	911	40,321	2,459,350	1,440
Mar-13	31	942	40,349	2,499,699	1,302
Apr-13	30	972	37,720	2,537,419	1,257
May-13	31	1,003	38,731	2,576,150	1,249
Jun-13	30	1,033	35,905	2,612,055	1,197
Jul-13	31	1,064	36,520	2,648,575	1,178
Aug-13	31	1,095	36,980	2,685,555	1,193
Sep-13	30	1,125	35,729	2,721,284	1,191
Oct-13	31	1,156	39,512	2,760,796	1,275
Nov-13	30	1,186	28,353	2,789,149	945
Dec-13	31	1,217	46,145	2,835,294	1,489

Table I – 21: Production History of Well#21 HEIM, Lease No. 260129

Month	Well days Online	Producing times (days)	Gas (MCF)	Gp (Mscf)	qg (Mscf/D)
Oct-10	31	31	825	825	27
Nov-10	30	61	309,619	310,444	10,321
Dec-10	31	92	349,999	660,443	11,290
Jan-11	31	123	284,078	944,521	9,164
Feb-11	28	151	215,898	1,160,419	7,711
Mar-11	31	182	192,966	1,353,385	6,225
Apr-11	30	212	153,889	1,507,274	5,130
May-11	31	243	37,183	1,544,457	1,199
Jun-11	30	273	129,012	1,673,469	4,300
Jul-11	31	304	118,973	1,792,442	3,838
Aug-11	31	335	106,981	1,899,423	3,451
Sep-11	30	365	120,001	2,019,424	4,000
Oct-11	31	396	114,177	2,133,601	3,683
Nov-11	30	426	83,387	2,216,988	2,780
Dec-11	31	457	89,055	2,306,043	2,873
Jan-12	31	488	87,889	2,393,932	2,835
Feb-12	28	516	80,501	2,474,433	2,875
Mar-12	31	547	84,510	2,558,943	2,726
Apr-12	30	577	79,276	2,638,219	2,643
May-12	31	608	83,156	2,721,375	2,682
Jun-12	30	638	78,383	2,799,758	2,613
Jul-12	31	669	81,102	2,880,860	2,616
Aug-12	31	700	79,507	2,960,367	2,565
Sep-12	30	730	77,634	3,038,001	2,588
Oct-12	31	761	88,088	3,126,089	2,842
Nov-12	30	791	85,008	3,211,097	2,834
Dec-12	31	822	76,159	3,287,256	2,457
Jan-13	31	853	81,257	3,368,513	2,621
Feb-13	28	881	66,414	3,434,927	2,372
Mar-13	31	912	37,280	3,472,207	1,203

Table I –21: Continued

Month	Well days Online	Producing times (days)	Gas (MCF)	Gp (Mscf)	qg (Mscf/D)
Apr-13	30	942	42,001	3,514,208	1,400
May-13	31	973	60,777	3,574,985	1,961
Jun-13	30	1,003	53,852	3,628,837	1,795
Jul-13	31	1,034	43,827	3,672,664	1,414
Aug-13	31	1,065	39,399	3,712,063	1,271
Sep-13	30	1,095	35,026	3,747,089	1,168
Oct-13	31	1,126	34,783	3,781,872	1,122
Nov-13	30	1,156	23,958	3,805,830	799
Dec-13	31	1,187	36,449	3,842,279	1,176

Table I – 22: Production History of Well#22 ROBERT GUTIERREZ, Lease No. 260720

Month	Well days Online	Producing times (days)	Gas (MCF)	Gp (Mscf)	qg (Mscf/D)
Feb-11	28	28	83,466	83,466	2,981
Mar-11	31	59	364,551	448,017	11,760
Apr-11	30	89	286,832	734,849	9,561
May-11	31	120	192,286	927,135	6,203
Jun-11	30	150	137,674	1,064,809	4,589
Jul-11	31	181	135,294	1,200,103	4,364
Aug-11	31	212	136,279	1,336,382	4,396
Sep-11	30	242	135,771	1,472,153	4,526
Oct-11	31	273	102,311	1,574,464	3,300
Nov-11	30	303	86,630	1,661,094	2,888
Dec-11	31	334	93,408	1,754,502	3,013
Jan-12	31	365	84,837	1,839,339	2,737
Feb-12	28	393	73,735	1,913,074	2,633
Mar-12	31	424	76,464	1,989,538	2,467
Apr-12	30	454	60,382	2,049,920	2,013
May-12	31	485	98,052	2,147,972	3,163
Jun-12	30	515	84,131	2,232,103	2,804

Table I –22: Continued

Month	Well days Online	Producing times (days)	Gas (MCF)	Gp (Mscf)	qg (Mscf/D)
Jul-12	31	546	80,725	2,312,828	2,604
Aug-12	31	577	72,758	2,385,586	2,347
Sep-12	30	607	67,231	2,452,817	2,241
Oct-12	31	638	64,245	2,517,062	2,072
Nov-12	30	668	58,303	2,575,365	1,943
Dec-12	31	699	55,858	2,631,223	1,802
Jan-13	31	730	55,332	2,686,555	1,785
Feb-13	28	758	46,560	2,733,115	1,663
Mar-13	31	789	48,533	2,781,648	1,566
Apr-13	30	819	45,040	2,826,688	1,501
May-13	31	850	46,530	2,873,218	1,501
Jun-13	30	880	40,433	2,913,651	1,348
Jul-13	31	911	42,061	2,955,712	1,357
Aug-13	31	942	40,851	2,996,563	1,318
Sep-13	30	972	39,702	3,036,265	1,323
Oct-13	31	1,003	42,233	3,078,498	1,362
Nov-13	30	1,033	28,465	3,106,963	949
Dec-13	31	1,064	46,552	3,153,515	1,502

Table I – 23: Production History of Well#23 APPLING 698 GU, Lease No. 261439

Month	Well days Online	Producing times (days)	Gas (MCF)	Gp (Mscf)	qg (Mscf/D)
Mar-11	31	31	127,561	127,561	4,115
Apr-11	30	61	147,901	275,462	4,930
May-11	31	92	119,549	395,011	3,856
Jun-11	30	122	108,297	503,308	3,610
Jul-11	31	153	95,337	598,645	3,075
Aug-11	31	184	85,992	684,637	2,774
Sep-11	30	214	74,137	758,774	2,471
Oct-11	31	245	69,073	827,847	2,228

Table I –23: Continued

Month	Well days Online	Producing times (days)	Gas (MCF)	Gp (Mscf)	qg (Mscf/D)
Nov-11	30	275	61,551	889,398	2,052
Dec-11	31	306	52,934	942,332	1,708
Jan-12	31	337	55,828	998,160	1,801
Feb-12	28	365	48,075	1,046,235	1,717
Mar-12	31	396	46,032	1,092,267	1,485
Apr-12	30	426	43,844	1,136,111	1,461
May-12	31	457	44,513	1,180,624	1,436
Jun-12	30	487	39,910	1,220,534	1,330
Jul-12	31	518	39,050	1,259,584	1,260
Aug-12	31	549	37,687	1,297,271	1,216
Sep-12	30	579	33,704	1,330,975	1,123
Oct-12	31	610	33,152	1,364,127	1,069
Nov-12	30	640	32,804	1,396,931	1,093
Dec-12	31	671	30,705	1,427,636	990
Jan-13	31	702	30,738	1,458,374	992
Feb-13	28	730	26,757	1,485,131	956
Mar-13	31	761	27,639	1,512,770	892
Apr-13	30	791	26,720	1,539,490	891
May-13	31	822	26,140	1,565,630	843
Jun-13	30	852	25,289	1,590,919	843
Jul-13	31	883	24,394	1,615,313	787
Aug-13	31	914	24,618	1,639,931	794
Sep-13	30	944	22,216	1,662,147	741
Oct-13	31	975	20,902	1,683,049	674
Nov-13	30	1,005	19,603	1,702,652	653
Dec-13	31	1,036	23,317	1,725,969	752

Table I – 24: Production History of Well#24 CHALOS MINERALS, Lease No. 260211

Month	Well days Online	Producing times (days)	Gas (MCF)	Gp (Mscf)	qg (Mscf/D)
Feb-11	28	28	16,343	16,343	584
Mar-11	31	59	209,688	226,031	6,764
Apr-11	30	89	156,875	382,906	5,229
May-11	31	120	119,464	502,370	3,854
Jun-11	30	150	91,664	594,034	3,055
Jul-11	31	181	64,380	658,414	2,077
Aug-11	31	212	61,184	719,598	1,974
Sep-11	30	242	49,170	768,768	1,639
Oct-11	31	273	38,735	807,503	1,250
Nov-11	30	303	21,749	829,252	725
Dec-11	31	334	37,170	866,422	1,199
Jan-12	31	365	30,413	896,835	981
Feb-12	28	393	24,627	921,462	880
Mar-12	31	424	23,688	945,150	764
Apr-12	30	454	20,492	965,642	683
May-12	31	485	20,644	986,286	666
Jun-12	30	515	18,187	1,004,473	606
Jul-12	31	546	17,703	1,022,176	571
Aug-12	31	577	14,937	1,037,113	482
Sep-12	30	607	13,874	1,050,987	462
Oct-12	31	638	13,379	1,064,366	432
Nov-12	30	668	11,647	1,076,013	388
Dec-12	31	699	13,084	1,089,097	422
Jan-13	31	730	12,642	1,101,739	408
Feb-13	28	758	9,852	1,111,591	352
Mar-13	31	789	10,138	1,121,729	327
Apr-13	30	819	8,229	1,129,958	274
May-13	31	850	7,685	1,137,643	248
Jun-13	30	880	5,999	1,143,642	200
Jul-13	31	911	10,369	1,154,011	334
Aug-13	31	942	8,508	1,162,519	274

Table I –24: Continued

Month	Well days Online	Producing times (days)	Gas (MCF)	Gp (Mscf)	qg (Mscf/D)
Sep-13	30	972	8,284	1,170,803	276
Oct-13	31	1,003	9,485	1,180,288	306
Nov-13	30	1,033	5,891	1,186,179	196
Dec-13	31	1,064	10,515	1,196,694	339

Table I – 25: Production History of Well#25 BENAVIDES, ROSA VELA, Lease No. 258131

Month	Well days Online	Producing times (days)	Gas (MCF)	Gp (Mscf)	qg (Mscf/D)
Mar-10	31	31	9,433	9,433	304
Apr-10	30	61	32,627	42,060	1,088
May-10	31	92	27,351	69,411	882
Jun-10	30	122	0	69,411	0
Jul-10	31	153	0	69,411	0
Aug-10	31	184	0	69,411	0
Sep-10	30	214	61,771	131,182	2,059
Oct-10	31	245	97,183	228,365	3,135
Nov-10	30	275	68,201	296,566	2,273
Dec-10	31	306	48,633	345,199	1,569
Jan-11	31	337	33,121	378,320	1,068
Feb-11	28	365	30,075	408,395	1,074
Mar-11	31	396	28,889	437,284	932
Apr-11	30	426	29,757	467,041	992
May-11	31	457	24,885	491,926	803
Jun-11	30	487	21,547	513,473	718
Jul-11	31	518	19,263	532,736	621
Aug-11	31	549	16,825	549,561	543
Sep-11	30	579	13,212	562,773	440
Oct-11	31	610	3,880	566,653	125
Nov-11	30	640	13,188	579,841	440
Dec-11	31	671	9,241	589,082	298

Table I –25: Continued

Month	Well days Online	Producing times (days)	Gas (MCF)	Gp (Mscf)	qg (Mscf/D)
Jan-12	31	702	13,848	602,930	447
Feb-12	28	730	13,553	616,483	484
Mar-12	31	761	12,141	628,624	392
Apr-12	30	791	10,365	638,989	346
May-12	31	822	10,928	649,917	353
Jun-12	30	852	10,345	660,262	345
Jul-12	31	883	6,869	667,131	222
Aug-12	31	914	9,375	676,506	302
Sep-12	30	944	9,105	685,611	304
Oct-12	31	975	7,368	692,979	238
Nov-12	30	1,005	8,664	701,643	289
Dec-12	31	1,036	7,927	709,570	256
Jan-13	31	1,067	6,926	716,496	223
Feb-13	28	1,095	7,806	724,302	279
Mar-13	31	1,126	8,697	732,999	281
Apr-13	30	1,156	5,177	738,176	173
May-13	31	1,187	5,650	743,826	182
Jun-13	30	1,217	5,127	748,953	171
Jul-13	31	1,248	5,622	754,575	181
Aug-13	31	1,279	6,693	761,268	216
Sep-13	30	1,309	7,295	768,563	243
Oct-13	31	1,340	5,096	773,659	164
Nov-13	30	1,370	6,476	780,135	216

Table I – 26: Production History of Well#26 GALVAN RANCH, Lease No. 257683

Month	Well days Online	Producing times (days)	Gas (MCF)	Gp (Mscf)	qg (Mscf/D)
Oct-09	31	31	44,119	44,119	1,423
Nov-09	30	61	93,296	137,415	3,110
Dec-09	31	92	87,350	224,765	2,818
Jan-10	31	123	79,539	304,304	2,566
Feb-10	28	151	65,990	370,294	2,357
Mar-10	31	182	66,604	436,898	2,149
Apr-10	30	212	62,405	499,303	2,080
May-10	31	243	64,557	563,860	2,082
Jun-10	30	273	58,207	622,067	1,940
Jul-10	31	304	56,298	678,365	1,816
Aug-10	31	335	46,479	724,844	1,499
Sep-10	30	365	37,641	762,485	1,255
Oct-10	31	396	40,697	803,182	1,313
Nov-10	30	426	36,457	839,639	1,215
Dec-10	31	457	36,724	876,363	1,185
Jan-11	31	488	33,245	909,608	1,072
Feb-11	28	516	26,530	936,138	948
Mar-11	31	547	33,876	970,014	1,093
Apr-11	30	577	32,311	1,002,325	1,077
May-11	31	608	34,077	1,036,402	1,099
Jun-11	30	638	26,719	1,063,121	891
Jul-11	31	669	25,701	1,088,822	829
Aug-11	31	700	25,780	1,114,602	832
Sep-11	30	730	25,353	1,139,955	845
Oct-11	31	761	23,941	1,163,896	772
Nov-11	30	791	22,435	1,186,331	748
Dec-11	31	822	24,069	1,210,400	776
Jan-12	31	853	22,832	1,233,232	737
Feb-12	28	881	21,388	1,254,620	764

Table I –26: Continued

Month	Well days Online	Producing times (days)	Gas (MCF)	Gp (Mscf)	qg (Mscf/D)
Mar-12	31	912	30,144	1,284,764	972
Apr-12	30	942	25,232	1,309,996	841
May-12	31	973	28,134	1,338,130	908
Jun-12	30	1,003	25,165	1,363,295	839
Jul-12	31	1,034	29,746	1,393,041	960
Aug-12	31	1,065	27,000	1,420,041	871
Sep-12	30	1,095	24,521	1,444,562	817
Oct-12	31	1,126	23,429	1,467,991	756
Nov-12	30	1,156	25,632	1,493,623	854
Dec-12	31	1,187	24,733	1,518,356	798
Jan-13	31	1,218	29,018	1,547,374	936
Feb-13	28	1,246	21,131	1,568,505	755
Mar-13	31	1,277	21,669	1,590,174	699
Apr-13	30	1,307	19,055	1,609,229	635
May-13	31	1,338	18,543	1,627,772	598
Jun-13	30	1,368	18,327	1,646,099	611
Jul-13	31	1,399	18,005	1,664,104	581
Aug-13	31	1,430	15,578	1,679,682	503
Sep-13	30	1,460	14,687	1,694,369	490
Oct-13	31	1,491	12,192	1,706,561	393
Nov-13	30	1,521	11,332	1,717,893	378
Dec-13	31	1,552	10,139	1,728,032	327

Table I – 27: Production History of Well#27 STATE OF TEXAS HILL RANCH, Lease No. 257687

Month	Well days Online	Producing times (days)	Gas (MCF)	Gp (Mscf)	qg (Mscf/D)
Jan-10	31	31	14,579	14,579	470
Feb-10	28	59	69,431	84,010	2,480
Mar-10	31	90	117,409	201,419	3,787
Apr-10	30	120	111,404	312,823	3,713
May-10	31	151	8,403	321,226	271
Jun-10	30	181	0	321,226	0
Jul-10	31	212	0	321,226	0
Aug-10	31	243	0	321,226	0
Sep-10	30	273	56,973	378,199	1,899
Oct-10	31	304	98,145	476,344	3,166
Nov-10	30	334	67,573	543,917	2,252
Dec-10	31	365	55,896	599,813	1,803
Jan-11	31	396	45,168	644,981	1,457
Feb-11	28	424	42,232	687,213	1,508
Mar-11	31	455	44,198	731,411	1,426
Apr-11	30	485	34,375	765,786	1,146
May-11	31	516	32,027	797,813	1,033
Jun-11	30	546	26,149	823,962	872
Jul-11	31	577	0	823,962	0
Aug-11	31	608	30,611	854,573	987
Sep-11	30	638	13,686	868,259	456
Oct-11	31	669	21,904	890,163	707
Nov-11	30	699	23,358	913,521	779
Dec-11	31	730	23,711	937,232	765
Jan-12	31	761	22,989	960,221	742
Feb-12	28	789	19,361	979,582	691
Mar-12	31	820	19,082	998,664	616
Apr-12	30	850	16,413	1,015,077	547
May-12	31	881	19,331	1,034,408	624
Jun-12	30	911	14,144	1,048,552	471
Jul-12	31	942	18,056	1,066,608	582

Table I –27: Continued

Month	Well days Online	Producing times (days)	Gas (MCF)	Gp (Mscf)	qg (Mscf/D)
Aug-12	31	973	17,523	1,084,131	565
Sep-12	30	1,003	15,834	1,099,965	528
Oct-12	31	1,034	11,110	1,111,075	358
Nov-12	30	1,064	18,893	1,129,968	630
Dec-12	31	1,095	14,599	1,144,567	471
Jan-13	31	1,126	12,588	1,157,155	406
Feb-13	28	1,154	11,594	1,168,749	414
Mar-13	31	1,185	15,041	1,183,790	485
Apr-13	30	1,215	14,160	1,197,950	472
May-13	31	1,246	14,691	1,212,641	474
Jun-13	30	1,276	11,592	1,224,233	386
Jul-13	31	1,307	14,380	1,238,613	464
Aug-13	31	1,338	13,725	1,252,338	443
Sep-13	30	1,368	12,814	1,265,152	427
Oct-13	31	1,399	13,019	1,278,171	420
Nov-13	30	1,429	11,163	1,289,334	372

Table I – 28: Production History of Well#28 FASKEN "A" EF, Lease No. 257628

Month	Well days Online	Producing times (days)	Gas (MCF)	Gp (Mscf)	qg (Mscf/D)
Mar-10	31	31	6,030	6,030	195
Apr-10	30	61	25,465	31,495	849
May-10	31	92	34,778	66,273	1,122
Jun-10	30	122	20,570	86,843	686
Jul-10	31	153	3,372	90,215	109
Aug-10	31	184	23,208	113,423	749
Sep-10	30	214	17,046	130,469	568
Oct-10	31	245	24,139	154,608	779
Nov-10	30	275	100,430	255,038	3,348
Dec-10	31	306	239,956	494,994	7,741

Table I –28: Continued

Month	Well days Online	Producing times (days)	Gas (MCF)	Gp (Mscf)	qg (Mscf/D)
Jan-11	31	337	188,358	683,352	6,076
Feb-11	28	365	176,307	859,659	6,297
Mar-11	31	396	117,061	976,720	3,776
Apr-11	30	426	87,265	1,063,985	2,909
May-11	31	457	107,596	1,171,581	3,471
Jun-11	30	487	57,380	1,228,961	1,913
Jul-11	31	518	76,774	1,305,735	2,477
Aug-11	31	549	71,016	1,376,751	2,291
Sep-11	30	579	49,993	1,426,744	1,666
Oct-11	31	610	16,332	1,443,076	527
Nov-11	30	640	115,022	1,558,098	3,834
Dec-11	31	671	44,729	1,602,827	1,443
Jan-12	31	702	47,635	1,650,462	1,537
Feb-12	28	730	39,128	1,689,590	1,397
Mar-12	31	761	38,898	1,728,488	1,255
Apr-12	30	791	39,283	1,767,771	1,309
May-12	31	822	41,682	1,809,453	1,345
Jun-12	30	852	33,572	1,843,025	1,119
Jul-12	31	883	33,896	1,876,921	1,093
Aug-12	31	914	33,443	1,910,364	1,079
Sep-12	30	944	30,313	1,940,677	1,010
Oct-12	31	975	32,507	1,973,184	1,049
Nov-12	30	1,005	27,455	2,000,639	915
Dec-12	31	1,036	31,642	2,032,281	1,021
Jan-13	31	1,067	28,995	2,061,276	935
Feb-13	28	1,095	27,888	2,089,164	996
Mar-13	31	1,126	30,198	2,119,362	974
Apr-13	30	1,156	27,258	2,146,620	909
May-13	31	1,187	36,692	2,183,312	1,184
Jun-13	30	1,217	40,807	2,224,119	1,360
Jul-13	31	1,248	32,947	2,257,066	1,063

Table I –28: Continued

Month	Well days Online	Producing times (days)	Gas (MCF)	Gp (Mscf)	qg (Mscf/D)
Aug-13	31	1,279	33,438	2,290,504	1,079
Sep-13	30	1,309	30,373	2,320,877	1,012
Oct-13	31	1,340	30,483	2,351,360	983
Nov-13	30	1,370	28,362	2,379,722	945
Dec-13	31	1,401	22,775	2,402,497	735

Table I – 29: Production History of Well#29 NEEL, Lease No. 257685

Month	Well days Online	Producing times (days)	Gas (MCF)	Gp (Mscf)	qg (Mscf/D)
Jul-10	31	31	108,117	108,117	3,488
Aug-10	31	62	114,682	222,799	3,699
Sep-10	30	92	81,041	303,840	2,701
Oct-10	31	123	52,705	356,545	1,700
Nov-10	30	153	45,328	401,873	1,511
Dec-10	31	184	49,387	451,260	1,593
Jan-11	31	215	47,880	499,140	1,545
Feb-11	28	243	39,913	539,053	1,425
Mar-11	31	274	24,234	563,287	782
Apr-11	30	304	29,797	593,084	993
May-11	31	335	28,909	621,993	933
Jun-11	30	365	26,000	647,993	867
Jul-11	31	396	25,155	673,148	811
Aug-11	31	427	24,447	697,595	789
Sep-11	30	457	19,590	717,185	653
Oct-11	31	488	20,072	737,257	647
Nov-11	30	518	21,491	758,748	716
Dec-11	31	549	18,539	777,287	598
Jan-12	31	580	19,289	796,576	622
Feb-12	28	608	17,314	813,890	618
Mar-12	31	639	17,748	831,638	573

Table I –29: Continued

Month	Well days Online	Producing times (days)	Gas (MCF)	Gp (Mscf)	qg (Mscf/D)
Apr-12	30	669	16,432	848,070	548
May-12	31	700	16,684	864,754	538
Jun-12	30	730	15,415	880,169	514
Jul-12	31	761	15,729	895,898	507
Aug-12	31	792	14,953	910,851	482
Sep-12	30	822	14,138	924,989	471
Oct-12	31	853	13,861	938,850	447
Nov-12	30	883	12,898	951,748	430
Dec-12	31	914	13,566	965,314	438
Jan-13	31	945	13,327	978,641	430
Feb-13	28	973	11,735	990,376	419
Mar-13	31	1,004	12,410	1,002,786	400
Apr-13	30	1,034	11,685	1,014,471	390
May-13	31	1,065	12,124	1,026,595	391
Jun-13	30	1,095	11,496	1,038,091	383
Jul-13	31	1,126	11,755	1,049,846	379
Aug-13	31	1,157	12,347	1,062,193	398
Sep-13	30	1,187	10,814	1,073,007	360
Oct-13	31	1,218	10,637	1,083,644	343
Nov-13	30	1,248	11,701	1,095,345	390
Dec-13	31	1,279	10,363	1,105,708	334

Table I – 30: Production History of Well#30 ROSA V. BENAVIDES, Lease No. 260046

Month	Well days Online	Producing times (days)	Gas (MCF)	Gp (Mscf)	qg (Mscf/D)
Aug-10	31	31	0	0	0
Sep-10	30	61	8,923	8,923	297
Oct-10	31	92	110,061	118,984	3,550
Nov-10	30	122	130,438	249,422	4,348
Dec-10	31	153	99,451	348,873	3,208
Jan-11	31	184	62,425	411,298	2,014
Feb-11	28	212	43,164	454,462	1,542
Mar-11	31	243	41,778	496,240	1,348
Apr-11	30	273	34,087	530,327	1,136
May-11	31	304	30,624	560,951	988
Jun-11	30	334	11,254	572,205	375
Jul-11	31	365	0	572,205	0
Aug-11	31	396	0	572,205	0
Sep-11	30	426	0	572,205	0
Oct-11	31	457	0	572,205	0
Nov-11	30	487	23,567	595,772	786
Dec-11	31	518	28,735	624,507	927
Jan-12	31	549	28,152	652,659	908
Feb-12	28	577	21,365	674,024	763
Mar-12	31	608	21,017	695,041	678
Apr-12	30	638	18,379	713,420	613
May-12	31	669	20,647	734,067	666
Jun-12	30	699	18,472	752,539	616
Jul-12	31	730	18,043	770,582	582
Aug-12	31	761	17,539	788,121	566
Sep-12	30	791	6,833	794,954	228
Oct-12	31	822	18,086	813,040	583
Nov-12	30	852	15,294	828,334	510
Dec-12	31	883	14,414	842,748	465
Jan-13	31	914	13,635	856,383	440
Feb-13	28	942	11,786	868,169	421

Table I –30: Continued

Month	Well days Online	Producing times (days)	Gas (MCF)	Gp (Mscf)	qg (Mscf/D)
Mar-13	31	973	12,980	881,149	419
Apr-13	30	1,003	12,620	893,769	421
May-13	31	1,034	12,229	905,998	394
Jun-13	30	1,064	9,569	915,567	319
Jul-13	31	1,095	12,193	927,760	393
Aug-13	31	1,126	12,020	939,780	388
Sep-13	30	1,156	11,212	950,992	374
Oct-13	31	1,187	10,823	961,815	349
Nov-13	30	1,217	9,499	971,314	317

Table I – 31: Production History of Well#31 ROSA VELA BENAVIDES, Lease No. 260047

Month	Well days Online	Producing times (days)	Gas (MCF)	Gp (Mscf)	qg (Mscf/D)
Oct-10	31	31	43,602	43,602	1,407
Nov-10	30	61	117,298	160,900	3,910
Dec-10	31	92	98,629	259,529	3,182
Jan-11	31	123	62,650	322,179	2,021
Feb-11	28	151	44,058	366,237	1,574
Mar-11	31	182	41,759	407,996	1,347
Apr-11	30	212	44,161	452,157	1,472
May-11	31	243	37,645	489,802	1,214
Jun-11	30	273	31,900	521,702	1,063
Jul-11	31	304	27,829	549,531	898
Aug-11	31	335	23,217	572,748	749
Sep-11	30	365	17,988	590,736	600
Oct-11	31	396	5,234	595,970	169
Nov-11	30	426	17,717	613,687	591
Dec-11	31	457	17,013	630,700	549
Jan-12	31	488	17,371	648,071	560
Feb-12	28	516	16,739	664,810	598

Table I –31: Continued

Month	Well days Online	Producing times (days)	Gas (MCF)	Gp (Mscf)	qg (Mscf/D)
Mar-12	31	547	14,900	679,710	481
Apr-12	30	577	13,085	692,795	436
May-12	31	608	14,974	707,769	483
Jun-12	30	638	12,858	720,627	429
Jul-12	31	669	10,334	730,961	333
Aug-12	31	700	11,539	742,500	372
Sep-12	30	730	11,711	754,211	390
Oct-12	31	761	9,236	763,447	298
Nov-12	30	791	13,030	776,477	434
Dec-12	31	822	11,454	787,931	369
Jan-13	31	853	12,761	800,692	412
Feb-13	28	881	9,854	810,546	352
Mar-13	31	912	12,303	822,849	397
Apr-13	30	942	7,463	830,312	249
May-13	31	973	9,272	839,584	299
Jun-13	30	1,003	7,333	846,917	244
Jul-13	31	1,034	5,872	852,789	189
Aug-13	31	1,065	10,038	862,827	324
Sep-13	30	1,095	7,876	870,703	263
Oct-13	31	1,126	8,169	878,872	264
Nov-13	30	1,156	8,514	887,386	284

Table I – 32: Production History of Well#32 FASKEN "A" EF, Lease No. 260071

Month	Well days Online	Producing times (days)	Gas (MCF)	Gp (Mscf)	qg (Mscf/D)
Dec-10	31	31	33,742	33,742	1,088
Jan-11	31	62	24,773	58,515	799
Feb-11	28	90	90,786	149,301	3,242
Mar-11	31	121	267,659	416,960	8,634
Apr-11	30	151	242,162	659,122	8,072
May-11	31	182	201,165	860,287	6,489
Jun-11	30	212	154,328	1,014,615	5,144
Jul-11	31	243	129,308	1,143,923	4,171
Aug-11	31	274	98,599	1,242,522	3,181
Sep-11	30	304	85,548	1,328,070	2,852
Oct-11	31	335	24,655	1,352,725	795
Nov-11	30	365	107,781	1,460,506	3,593
Dec-11	31	396	98,874	1,559,380	3,189
Jan-12	31	427	82,743	1,642,123	2,669
Feb-12	28	455	66,868	1,708,991	2,388
Mar-12	31	486	68,868	1,777,859	2,222
Apr-12	30	516	57,580	1,835,439	1,919
May-12	31	547	61,252	1,896,691	1,976
Jun-12	30	577	52,486	1,949,177	1,750
Jul-12	31	608	50,220	1,999,397	1,620
Aug-12	31	639	51,812	2,051,209	1,671
Sep-12	30	669	45,507	2,096,716	1,517
Oct-12	31	700	47,470	2,144,186	1,531
Nov-12	30	730	40,598	2,184,784	1,353
Dec-12	31	761	44,186	2,228,970	1,425
Jan-13	31	792	42,866	2,271,836	1,383
Feb-13	28	820	35,884	2,307,720	1,282
Mar-13	31	851	41,693	2,349,413	1,345
Apr-13	30	881	39,432	2,388,845	1,314
May-13	31	912	45,092	2,433,937	1,455
Jun-13	30	942	48,089	2,482,026	1,603

Table I –32: Continued

Month	Well days Online	Producing times (days)	Gas (MCF)	Gp (Mscf)	qg (Mscf/D)
Jul-13	31	973	38,931	2,520,957	1,256
Aug-13	31	1,004	41,202	2,562,159	1,329
Sep-13	30	1,034	38,945	2,601,104	1,298
Oct-13	31	1,065	40,092	2,641,196	1,293
Nov-13	30	1,095	35,301	2,676,497	1,177
Dec-13	31	1,126	32,918	2,709,415	1,062

Table I – 33: Production History of Well#33 FASKEN "A" EF, Lease No. 260182

Month	Well days Online	Producing times (days)	Gas (MCF)	Gp (Mscf)	qg (Mscf/D)
Feb-11	28	28	96,921	96,921	3,461
Mar-11	31	59	276,411	373,332	8,916
Apr-11	30	89	273,567	646,899	9,119
May-11	31	120	257,330	904,229	8,301
Jun-11	30	150	164,386	1,068,615	5,480
Jul-11	31	181	127,643	1,196,258	4,118
Aug-11	31	212	94,299	1,290,557	3,042
Sep-11	30	242	86,637	1,377,194	2,888
Oct-11	31	273	24,837	1,402,031	801
Nov-11	30	303	105,978	1,508,009	3,533
Dec-11	31	334	93,227	1,601,236	3,007
Jan-12	31	365	77,711	1,678,947	2,507
Feb-12	28	393	60,798	1,739,745	2,171
Mar-12	31	424	56,245	1,795,990	1,814
Apr-12	30	454	46,357	1,842,347	1,545
May-12	31	485	49,714	1,892,061	1,604
Jun-12	30	515	42,321	1,934,382	1,411
Jul-12	31	546	40,997	1,975,379	1,322
Aug-12	31	577	42,753	2,018,132	1,379
Sep-12	30	607	37,903	2,056,035	1,263

Table I –33: Continued

Month	Well days Online	Producing times (days)	Gas (MCF)	Gp (Mscf)	qg (Mscf/D)
Oct-12	31	638	38,875	2,094,910	1,254
Nov-12	30	668	30,204	2,125,114	1,007
Dec-12	31	699	40,558	2,165,672	1,308
Jan-13	31	730	36,555	2,202,227	1,179
Feb-13	28	758	32,503	2,234,730	1,161
Mar-13	31	789	36,002	2,270,732	1,161
Apr-13	30	819	34,238	2,304,970	1,141
May-13	31	850	28,755	2,333,725	928
Jun-13	30	880	25,900	2,359,625	863
Jul-13	31	911	25,786	2,385,411	832
Aug-13	31	942	23,145	2,408,556	747
Sep-13	30	972	21,158	2,429,714	705
Oct-13	31	1,003	20,353	2,450,067	657
Nov-13	30	1,033	19,272	2,469,339	642
Dec-13	31	1,064	15,556	2,484,895	502

Table I – 34: Production History of Well#34 HACHAR, Lease No. 261381

Month	Well days Online	Producing times (days)	Gas (MCF)	Gp (Mscf)	qg (Mscf/D)
Feb-11	28	28	116,695	116,695	4,168
Mar-11	31	59	136,885	253,580	4,416
Apr-11	30	89	103,857	357,437	3,462
May-11	31	120	87,079	444,516	2,809
Jun-11	30	150	67,869	512,385	2,262
Jul-11	31	181	57,523	569,908	1,856
Aug-11	31	212	49,454	619,362	1,595
Sep-11	30	242	34,107	653,469	1,137
Oct-11	31	273	29,242	682,711	943
Nov-11	30	303	30,980	713,691	1,033
Dec-11	31	334	38,014	751,705	1,226
Jan-12	31	365	28,118	779,823	907
Feb-12	28	393	21,275	801,098	760
Mar-12	31	424	23,135	824,233	746
Apr-12	30	454	22,076	846,309	736
May-12	31	485	21,581	867,890	696
Jun-12	30	515	19,810	887,700	660
Jul-12	31	546	19,153	906,853	618
Aug-12	31	577	16,950	923,803	547
Sep-12	30	607	15,810	939,613	527
Oct-12	31	638	10,472	950,085	338
Nov-12	30	668	11,340	961,425	378
Dec-12	31	699	15,046	976,471	485
Jan-13	31	730	10,925	987,396	352
Feb-13	28	758	10,616	998,012	379
Mar-13	31	789	17,440	1,015,452	563
Apr-13	30	819	13,011	1,028,463	434
May-13	31	850	14,597	1,043,060	471
Jun-13	30	880	9,481	1,052,541	316
Jul-13	31	911	14,091	1,066,632	455
Aug-13	31	942	13,805	1,080,437	445

Table I –34: Continued

Month	Well days Online	Producing times (days)	Gas (MCF)	Gp (Mscf)	qg (Mscf/D)
Sep-13	30	972	11,242	1,091,679	375
Oct-13	31	1,003	10,436	1,102,115	337
Nov-13	30	1,033	8,986	1,111,101	300

Table I – 35: Production History of Well#35 FASKEN A5, Lease No. 260379

Month	Well days Online	Producing times (days)	Gas (MCF)	Gp (Mscf)	qg (Mscf/D)
Feb-11	28	28	195,145	195,145	6,969
Mar-11	31	59	380,029	575,174	12,259
Apr-11	30	89	331,730	906,904	11,058
May-11	31	120	348,625	1,255,529	11,246
Jun-11	30	150	282,131	1,537,660	9,404
Jul-11	31	181	225,340	1,763,000	7,269
Aug-11	31	212	76,163	1,839,163	2,457
Sep-11	30	242	102,972	1,942,135	3,432
Oct-11	31	273	28,582	1,970,717	922
Nov-11	30	303	139,072	2,109,789	4,636
Dec-11	31	334	137,800	2,247,589	4,445
Jan-12	31	365	114,906	2,362,495	3,707
Feb-12	28	393	92,355	2,454,850	3,298
Mar-12	31	424	92,904	2,547,754	2,997
Apr-12	30	454	82,043	2,629,797	2,735
May-12	31	485	80,057	2,709,854	2,582
Jun-12	30	515	73,868	2,783,722	2,462
Jul-12	31	546	70,977	2,854,699	2,290
Aug-12	31	577	69,606	2,924,305	2,245
Sep-12	30	607	61,562	2,985,867	2,052
Oct-12	31	638	61,629	3,047,496	1,988
Nov-12	30	668	52,772	3,100,268	1,759
Dec-12	31	699	57,775	3,158,043	1,864

Table I –35: Continued

Month	Well days Online	Producing times (days)	Gas (MCF)	Gp (Mscf)	qg (Mscf/D)
Jan-13	31	730	53,613	3,211,656	1,729
Feb-13	28	758	48,159	3,259,815	1,720
Mar-13	31	789	51,440	3,311,255	1,659
Apr-13	30	819	50,551	3,361,806	1,685
May-13	31	850	53,882	3,415,688	1,738
Jun-13	30	880	62,277	3,477,965	2,076
Jul-13	31	911	53,979	3,531,944	1,741
Aug-13	31	942	54,264	3,586,208	1,750
Sep-13	30	972	48,733	3,634,941	1,624
Oct-13	31	1,003	49,191	3,684,132	1,587
Nov-13	30	1,033	46,877	3,731,009	1,563
Dec-13	31	1,064	39,189	3,770,198	1,264

Table I – 36: Production History of Well#36 ST OF TX-LA CRUZ TRES LAND, Lease No. 261320

Month	Well days Online	Producing times (days)	Gas (MCF)	Gp (Mscf)	qg (Mscf/D)
Apr-11	30	30	82,990	82,990	2,766
May-11	31	61	90,316	173,306	2,913
Jun-11	30	91	41,428	214,734	1,381
Jul-11	31	122	19,890	234,624	642
Aug-11	31	153	33,451	268,075	1,079
Sep-11	30	183	34,157	302,232	1,139
Oct-11	31	214	27,872	330,104	899
Nov-11	30	244	25,180	355,284	839
Dec-11	31	275	25,034	380,318	808
Jan-12	31	306	19,294	399,612	622
Feb-12	28	334	15,654	415,266	559
Mar-12	31	365	15,859	431,125	512
Apr-12	30	395	13,360	444,485	445
May-12	31	426	13,810	458,295	445

Table I –36: Continued

Month	Well days Online	Producing times (days)	Gas (MCF)	Gp (Mscf)	qg (Mscf/D)
Jun-12	30	456	11,981	470,276	399
Jul-12	31	487	11,069	481,345	357
Aug-12	31	518	10,581	491,926	341
Sep-12	30	548	9,430	501,356	314
Oct-12	31	579	6,178	507,534	199
Nov-12	30	609	11,053	518,587	368
Dec-12	31	640	7,838	526,425	253
Jan-13	31	671	8,410	534,835	271
Feb-13	28	699	6,256	541,091	223
Mar-13	31	730	8,735	549,826	282
Apr-13	30	760	9,680	559,506	323
May-13	31	791	7,102	566,608	229
Jun-13	30	821	6,486	573,094	216
Jul-13	31	852	7,820	580,914	252
Aug-13	31	883	7,550	588,464	244
Sep-13	30	913	7,406	595,870	247
Oct-13	31	944	6,548	602,418	211
Nov-13	30	974	6,482	608,900	216

Table I – 37: Production History of Well#37 LA CRUZ LAND GAS UNIT, Lease No. 261632

Month	Well days Online	Producing times (days)	Gas (MCF)	Gp (Mscf)	qg (Mscf/D)
May-11	31	31	9,419	9,419	304
Jun-11	30	61	140,231	149,650	4,674
Jul-11	31	92	114,778	264,428	3,703
Aug-11	31	123	87,318	351,746	2,817
Sep-11	30	153	59,787	411,533	1,993
Oct-11	31	184	41,613	453,146	1,342
Nov-11	30	214	49,385	502,531	1,646
Dec-11	31	245	60,275	562,806	1,944
Jan-12	31	276	45,051	607,857	1,453
Feb-12	28	304	35,006	642,863	1,250
Mar-12	31	335	34,655	677,518	1,118
Apr-12	30	365	30,125	707,643	1,004
May-12	31	396	30,835	738,478	995
Jun-12	30	426	26,278	764,756	876
Jul-12	31	457	24,501	789,257	790
Aug-12	31	488	24,584	813,841	793
Sep-12	30	518	21,884	835,725	729
Oct-12	31	549	15,387	851,112	496
Nov-12	30	579	23,823	874,935	794
Dec-12	31	610	20,496	895,431	661
Jan-13	31	641	19,380	914,811	625
Feb-13	28	669	18,574	933,385	663
Mar-13	31	700	20,060	953,445	647
Apr-13	30	730	22,698	976,143	757
May-13	31	761	22,483	998,626	725
Jun-13	30	791	17,717	1,016,343	591
Jul-13	31	822	20,215	1,036,558	652
Aug-13	31	853	19,394	1,055,952	626
Sep-13	30	883	17,289	1,073,241	576
Oct-13	31	914	17,609	1,090,850	568
Nov-13	30	944	15,880	1,106,730	529

Table I – 38: Production History of Well#38 STATE OF TEXAS - A.E. PUIG, Lease No. 26144

Month	Well days Online	Producing times (days)	Gas (MCF)	Gp (Mscf)	qg (Mscf/D)
Mar-11	31	31	17,893	17,893	577
Apr-11	30	61	110,914	128,807	3,697
May-11	31	92	86,967	215,774	2,805
Jun-11	30	122	64,166	279,940	2,139
Jul-11	31	153	52,041	331,981	1,679
Aug-11	31	184	52,090	384,071	1,680
Sep-11	30	214	34,676	418,747	1,156
Oct-11	31	245	29,422	448,169	949
Nov-11	30	275	33,390	481,559	1,113
Dec-11	31	306	35,914	517,473	1,159
Jan-12	31	337	30,096	547,569	971
Feb-12	28	365	24,932	572,501	890
Mar-12	31	396	27,554	600,055	889
Apr-12	30	426	24,036	624,091	801
May-12	31	457	23,376	647,467	754
Jun-12	30	487	20,905	668,372	697
Jul-12	31	518	21,669	690,041	699
Aug-12	31	549	19,809	709,850	639
Sep-12	30	579	19,935	729,785	665
Oct-12	31	610	14,392	744,177	464
Nov-12	30	640	24,200	768,377	807
Dec-12	31	671	18,974	787,351	612
Jan-13	31	702	18,640	805,991	601
Feb-13	28	730	16,072	822,063	574
Mar-13	31	761	17,147	839,210	553
Apr-13	30	791	20,009	859,219	667
May-13	31	822	15,502	874,721	500
Jun-13	30	852	14,792	889,513	493
Jul-13	31	883	19,720	909,233	636
Aug-13	31	914	18,482	927,715	596
Sep-13	30	944	14,422	942,137	481
Oct-13	31	975	15,517	957,654	501
Nov-13	30	1,005	11,891	969,545	396

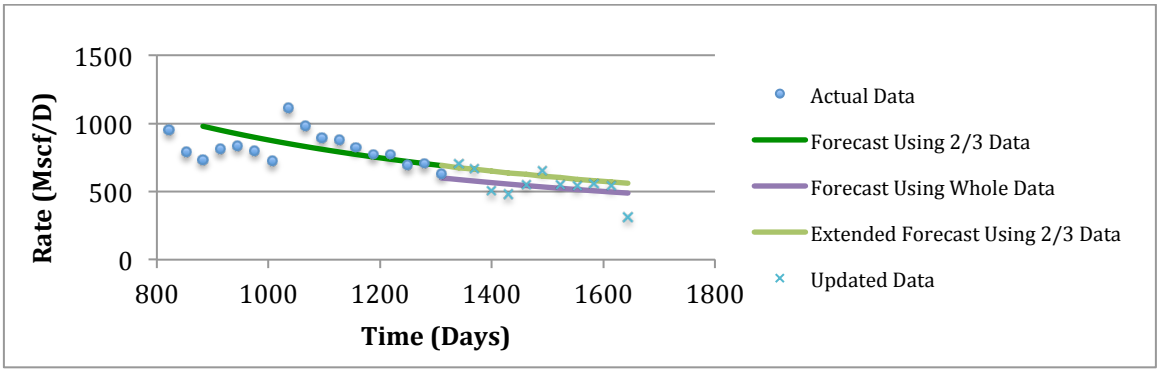

Figure II - 1: History Matching of Well#1, No.251105 Generated by Arps' Harmonic Model

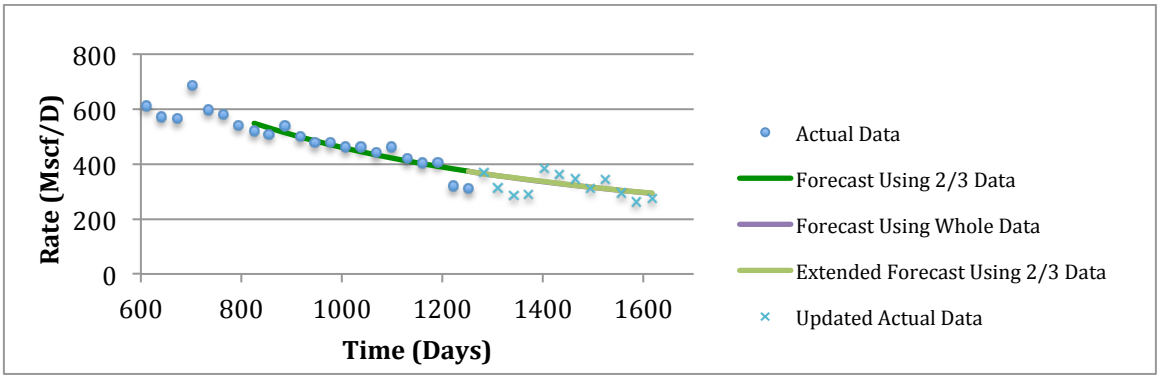

Figure II - 2: History Matching of Well#2, No.252769 Generated by Arps' Harmonic Model

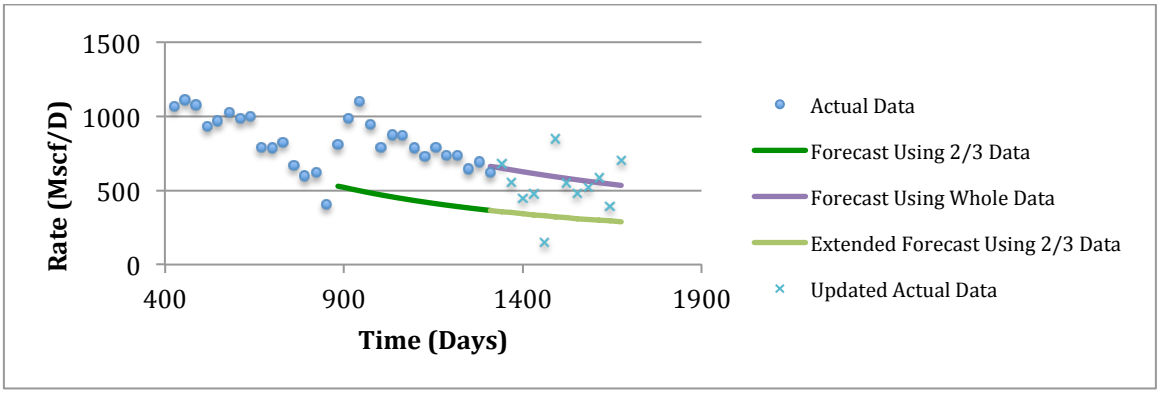

Figure II - 3: History Matching of Well#3, No.251816 Generated by Arps' Harmonic Model

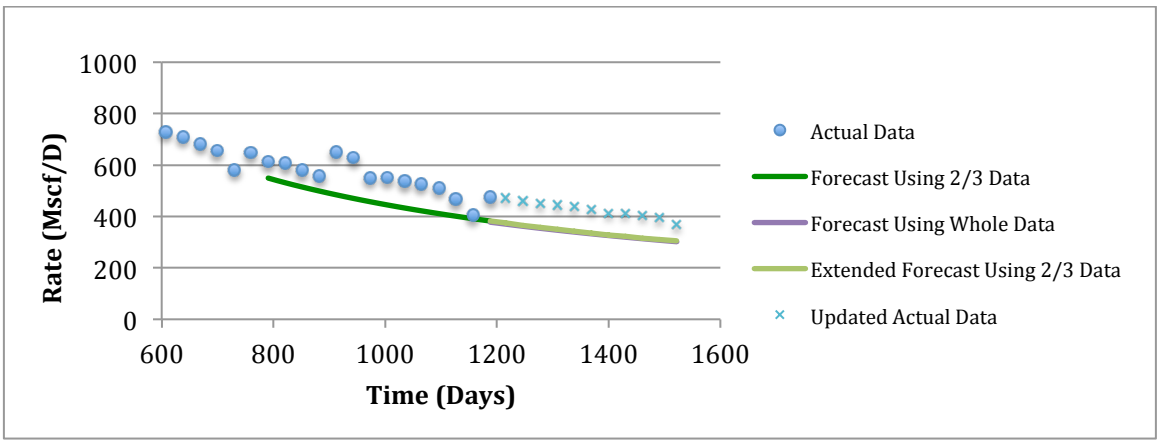

Figure II - 4: History Matching of Well#4, No.251773 Generated by Arps' Harmonic Model

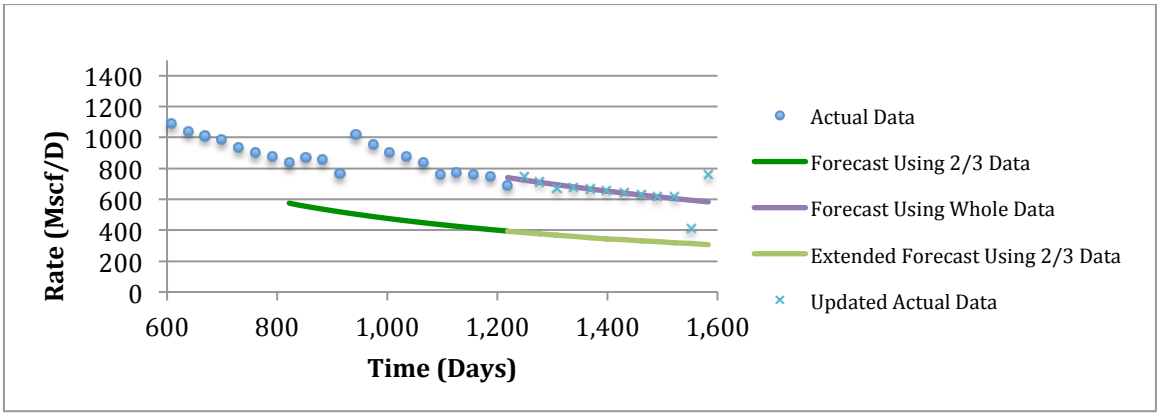

Figure II - 5: History Matching of Well#5, No.251817 Generated by Arps' Harmonic Model

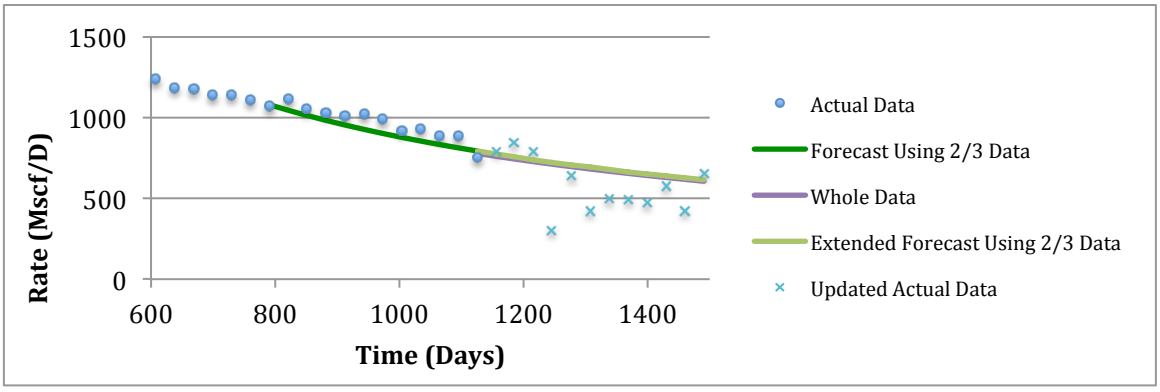

Figure II - 6: History Matching of Well#6, No.255994 Generated by Arps' Harmonic Model

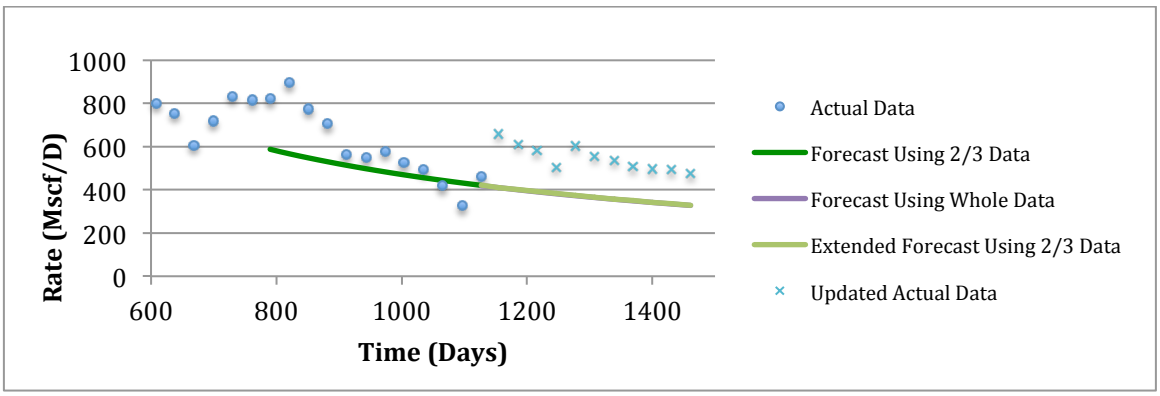

Figure II - 7: History Matching of Well#7, No.255435 Generated by Arps' Harmonic Model

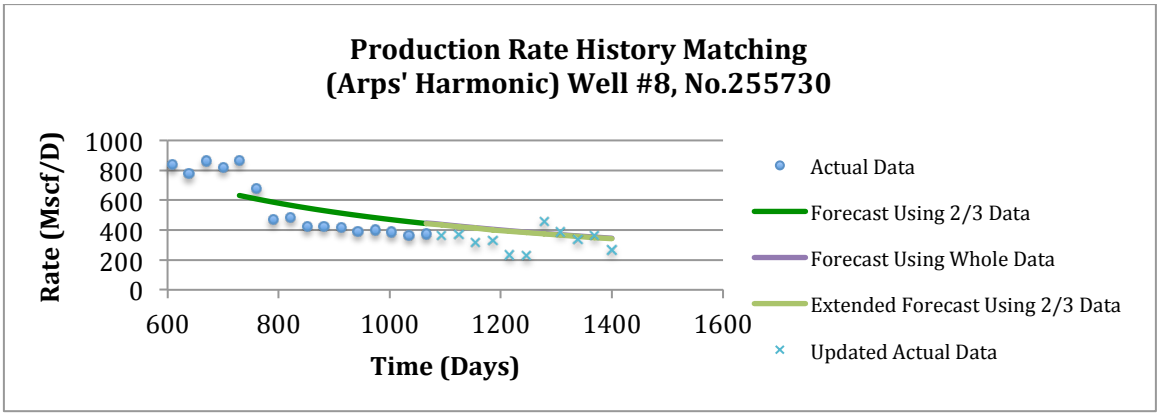

Figure II - 8: History Matching of Well#8, No.255730 Generated by Arps' Harmonic Model

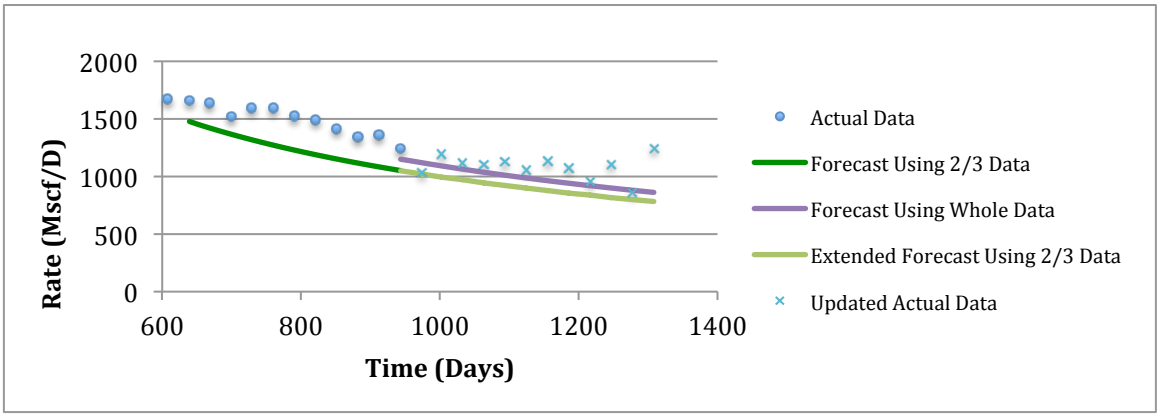

Figure II - 9: History Matching of Well#9, No.254447 Generated by Arps' Harmonic Model

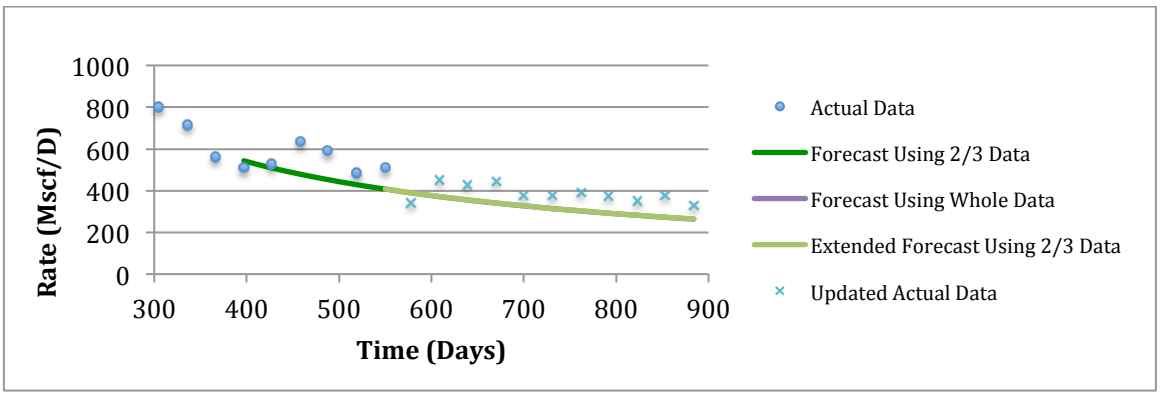

Figure II - 10: History Matching of Well#10, No.263658 Generated by Arps' Harmonic Model

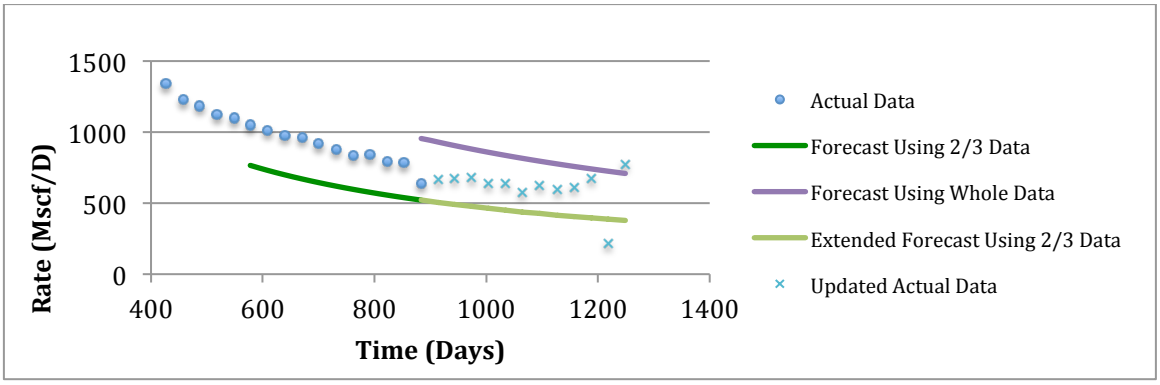

Figure II - 11: History Matching of Well#11, No.258106 Generated by Arps' Harmonic Model

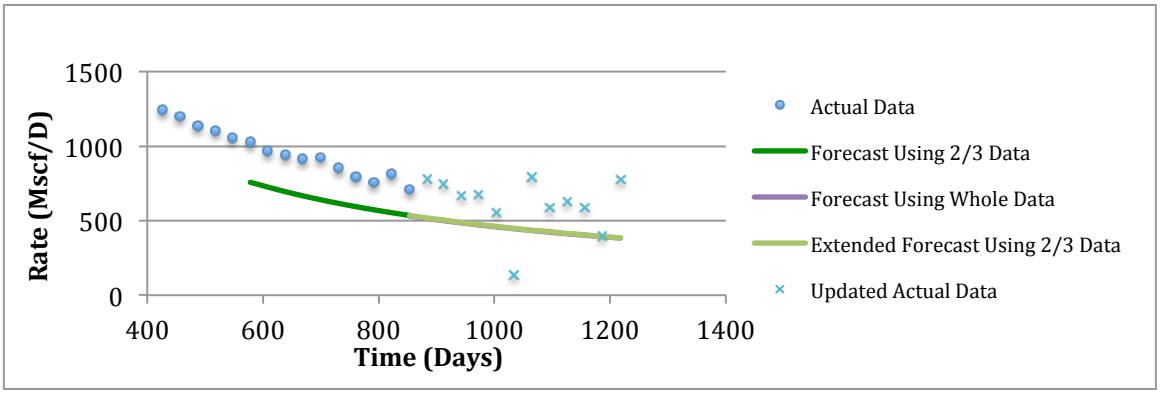

Figure II - 12: History Matching of Well#12, No.258900 Generated by Arps' Harmonic Model

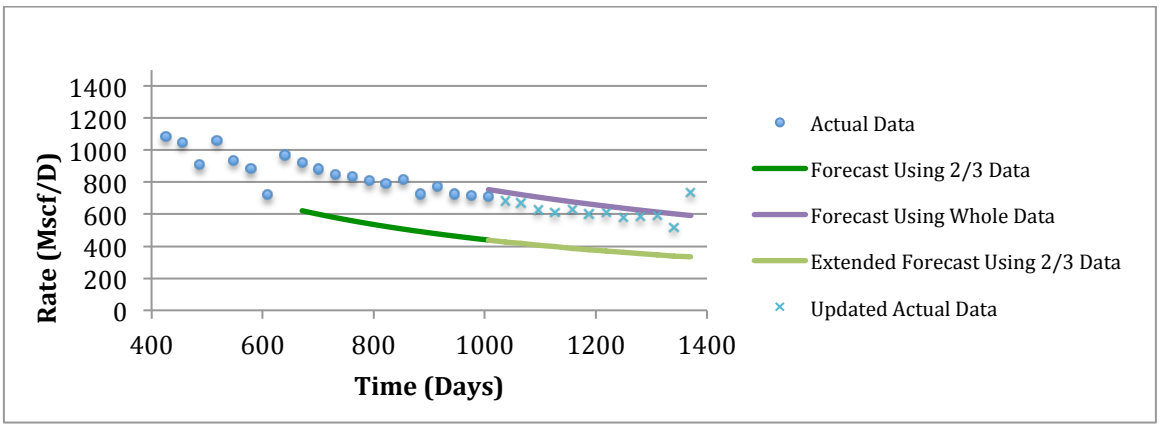

Figure II - 13: History Matching of Well#13, No.257263 Generated by Arps' Harmonic Model

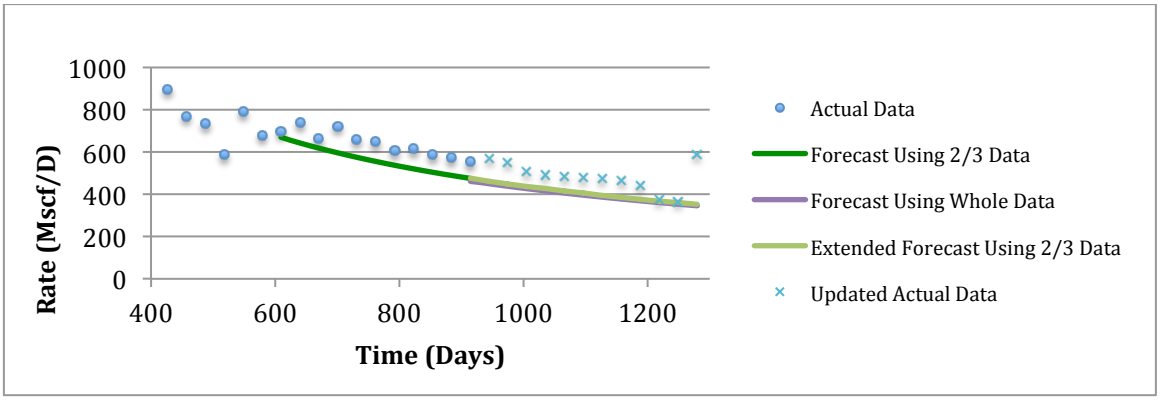

Figure II - 14: History Matching of Well#14, No.257862 Generated by Arps' Harmonic Model

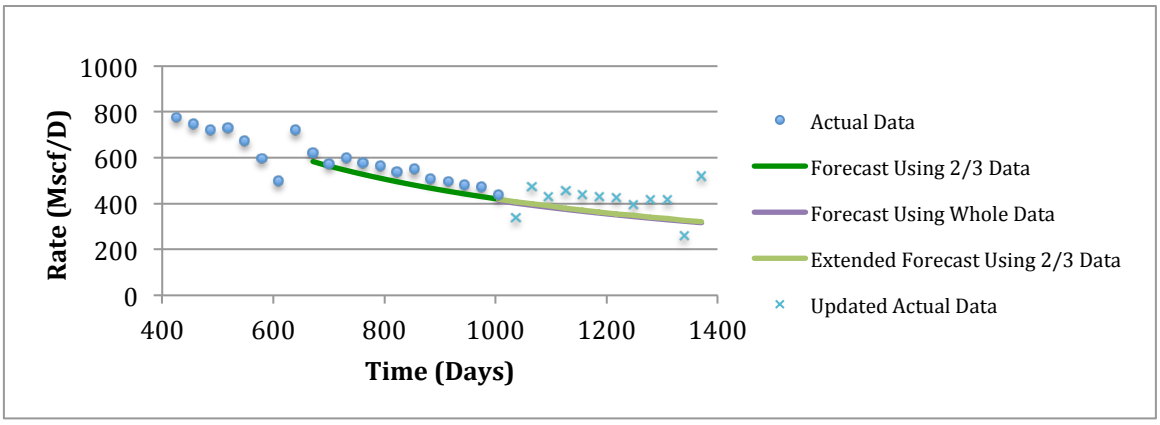

Figure II - 15: History Matching of Well#15, No.254843 Generated by Arps' Harmonic Model

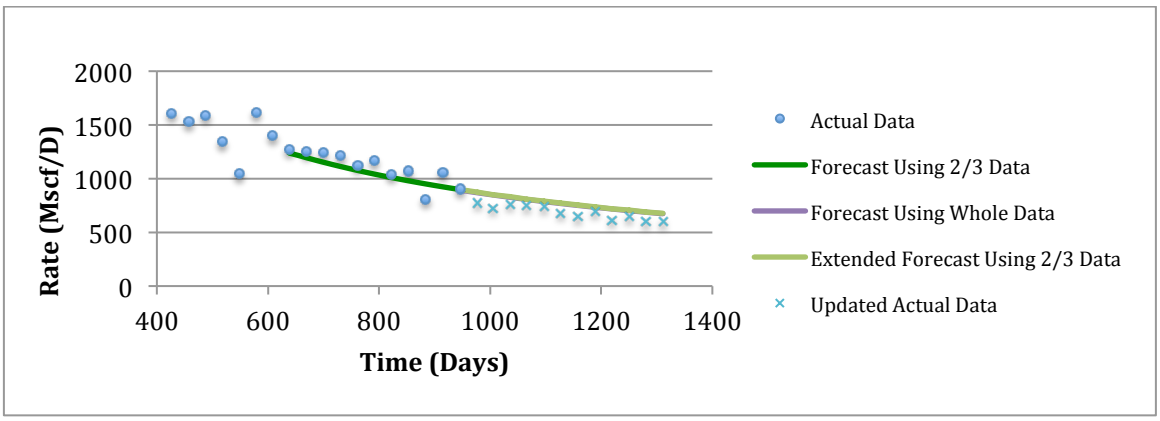

Figure II - 16: History Matching of Well#16, No.258036 Generated by Arps' Harmonic Model

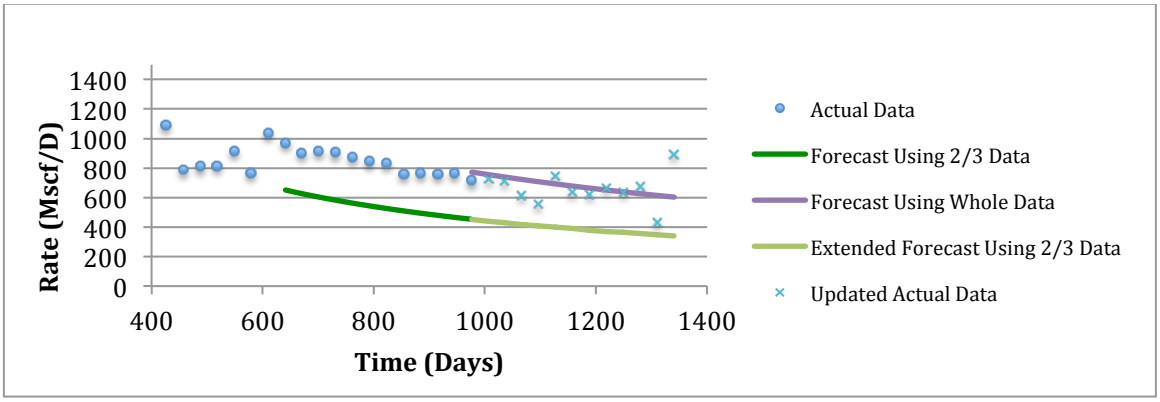

Figure II - 17: History Matching of Well#17, No.257955 Generated by Arps' Harmonic Model

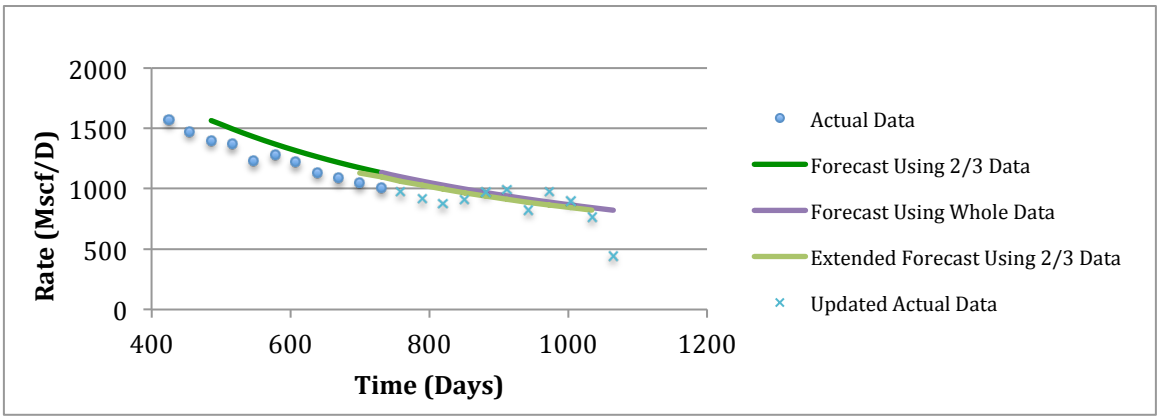

Figure II - 18: History Matching of Well#18, No.259883 Generated by Arps' Harmonic Model

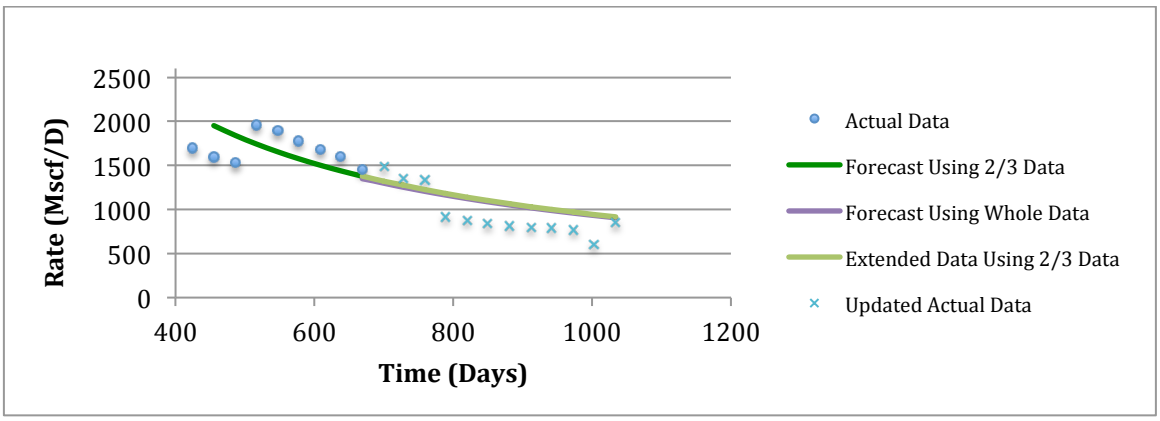

Figure II - 19: History Matching of Well#19, No.259429 Generated by Arps' Harmonic Model

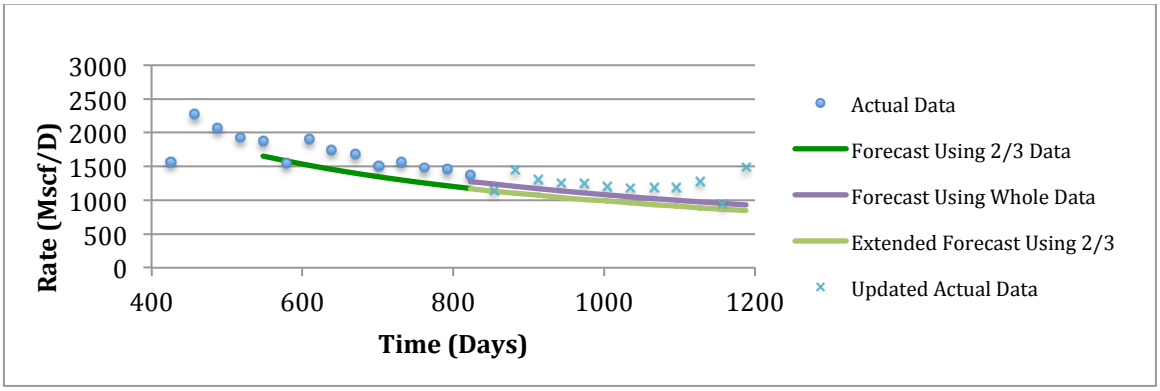

Figure II - 20: History Matching of Well#20, No.258903 Generated by Arps' Harmonic Model

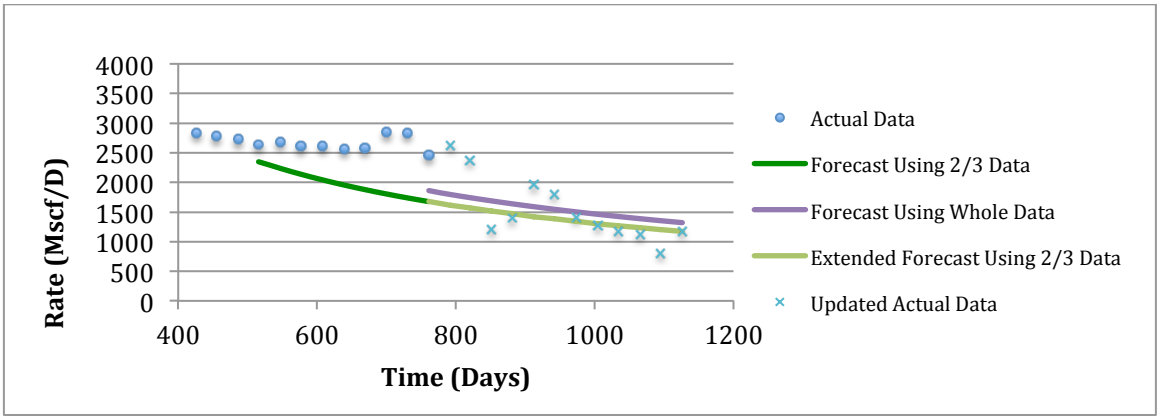

Figure II - 21: History Matching of Well#21, No.260129 Generated by Arps' Harmonic Model

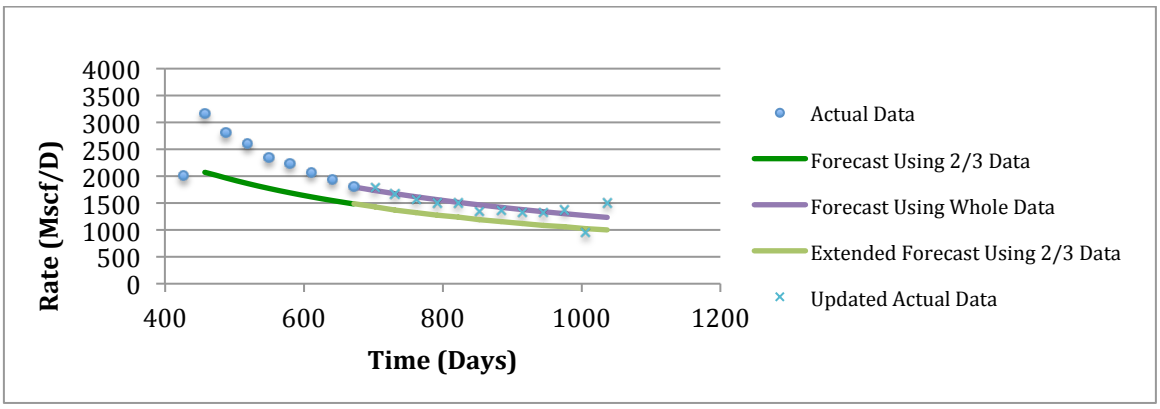

Figure II - 22: History Matching of Well#22, No.260720 Generated by Arps' Harmonic Model

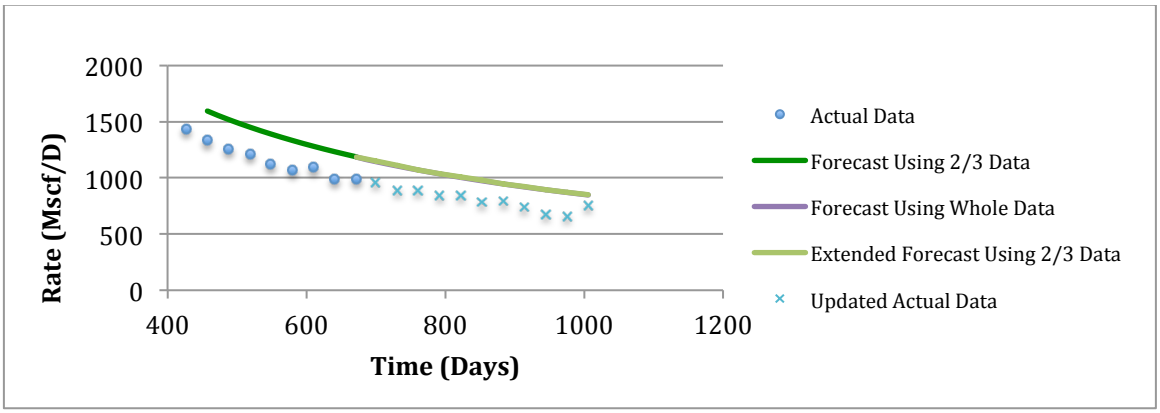

Figure II - 23: History Matching of Well#23, No.261439 Generated by Arps' Harmonic Model

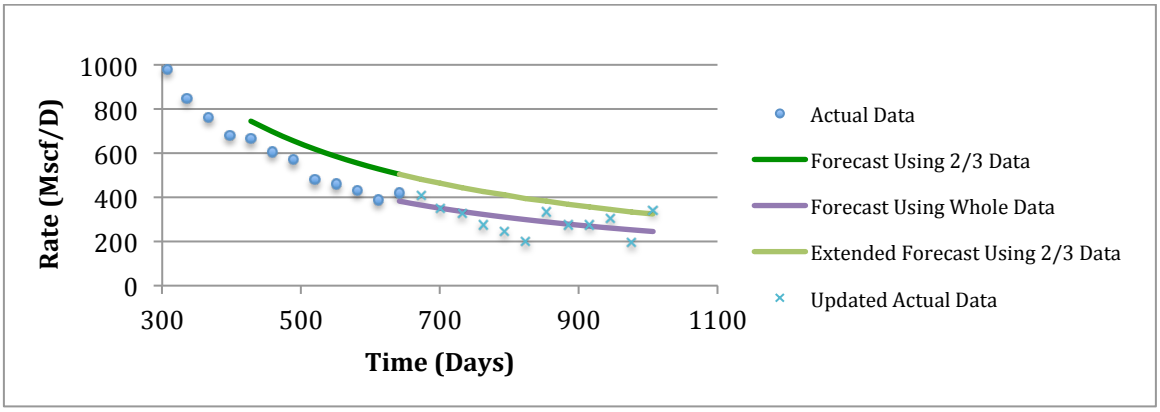

Figure II - 24: History Matching of Well#24, No.260211 Generated by Arps' Harmonic Model

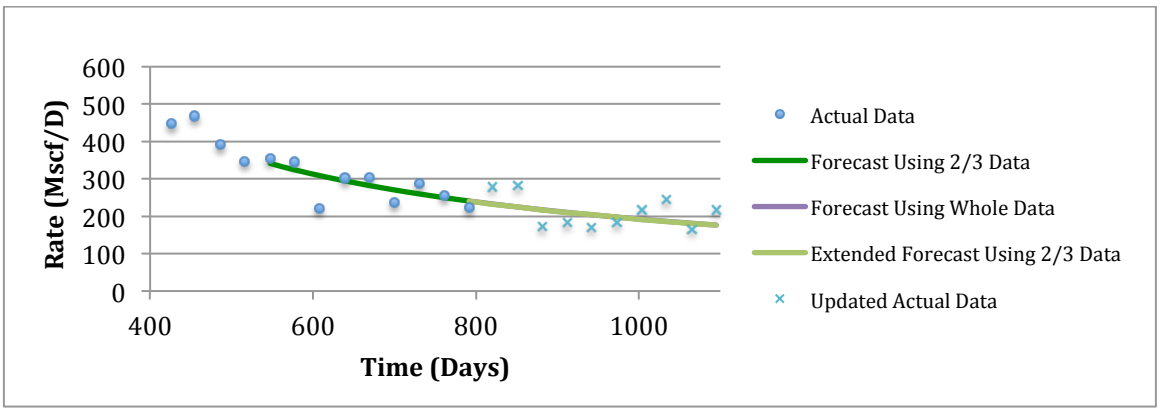

Figure II - 25: History Matching of Well#26, No.258131 Generated by Arps' Harmonic Model

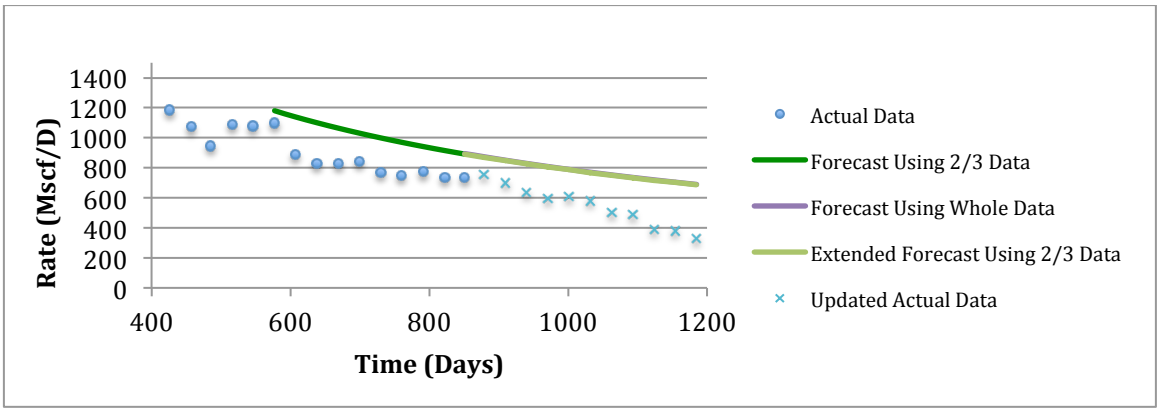

Figure II - 26: History Matching of Well#27, No.257683 Generated by Arps' Harmonic Model

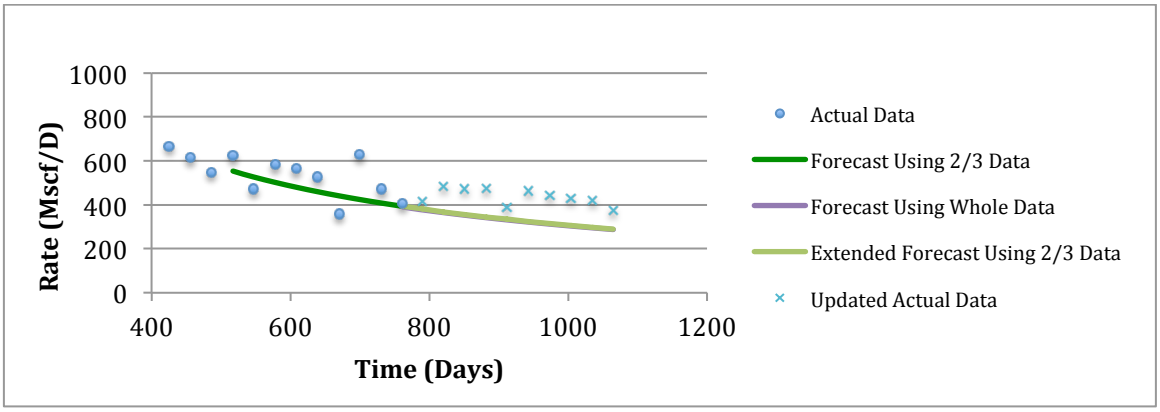

Figure II - 27: History Matching of Well#28, No.257687 Generated by Arps' Harmonic Model

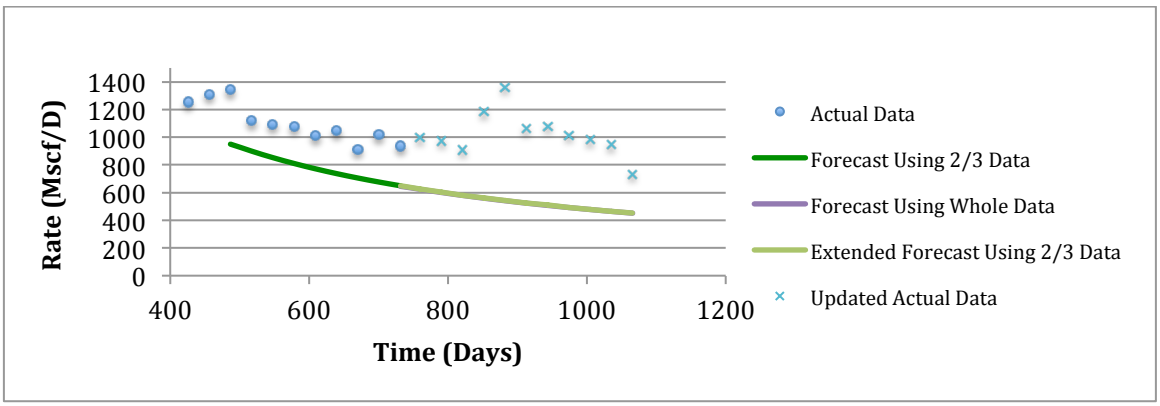

Figure II - 28: History Matching of Well#29, No.257628 Generated by Arps' Harmonic Model

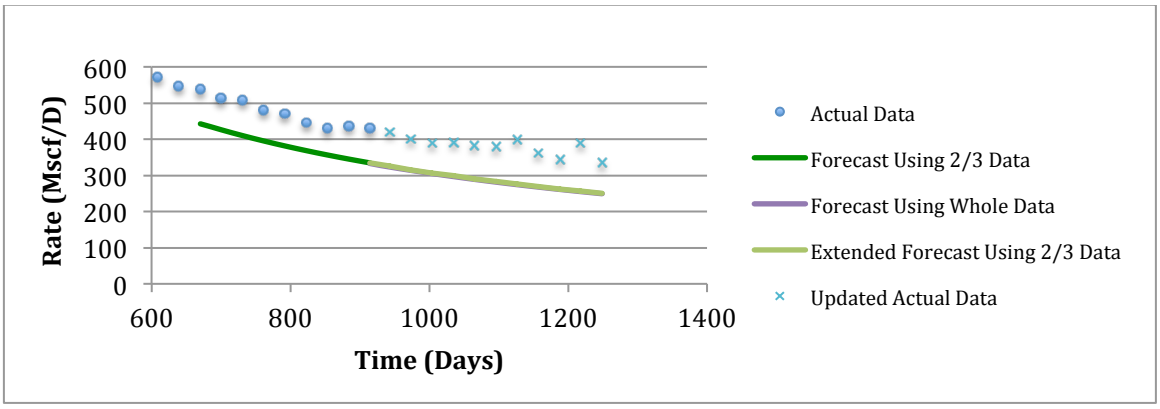

Figure II - 29: History Matching of Well#30, No.257685 Generated by Arps' Harmonic Model

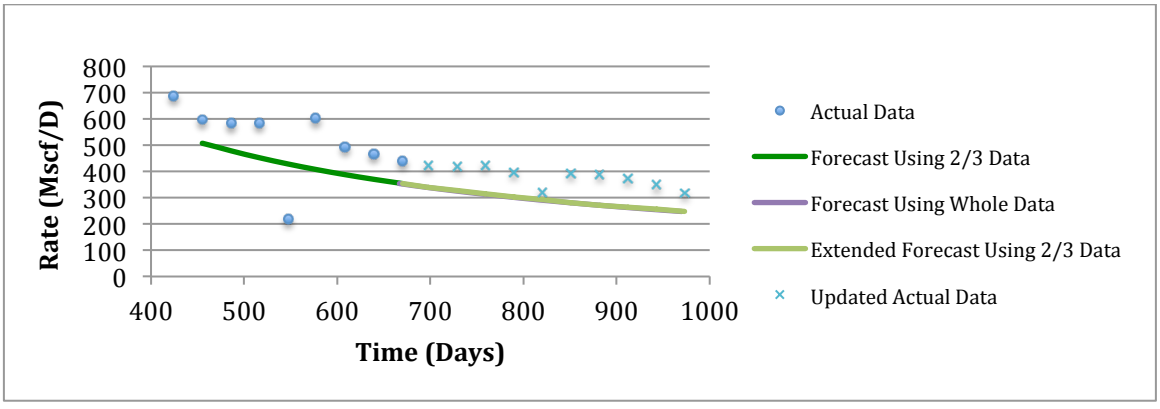

Figure II - 30: History Matching of Well#31, No.260046 Generated by Arps' Harmonic Model

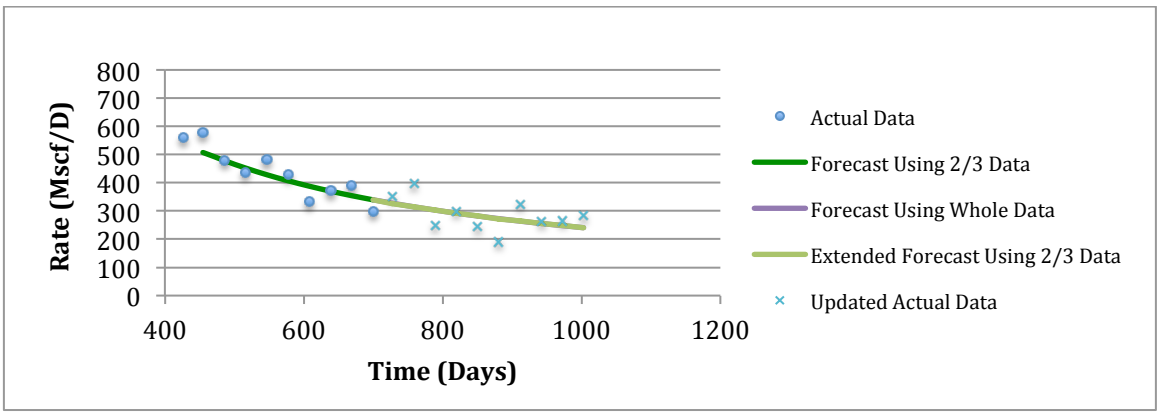

Figure II - 31: History Matching of Well#32, No.260047 Generated by Arps' Harmonic Model

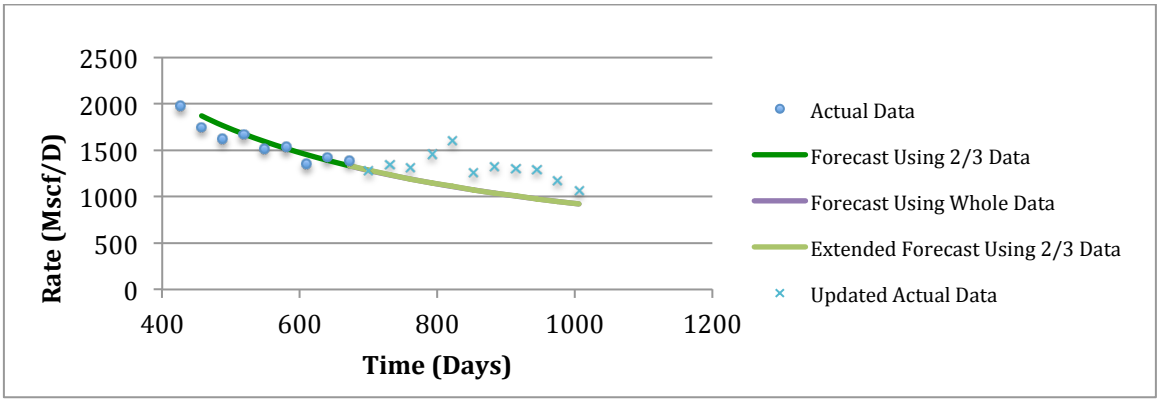

Figure II - 32: History Matching of Well#33, No.260071 Generated by Arps' Harmonic Model

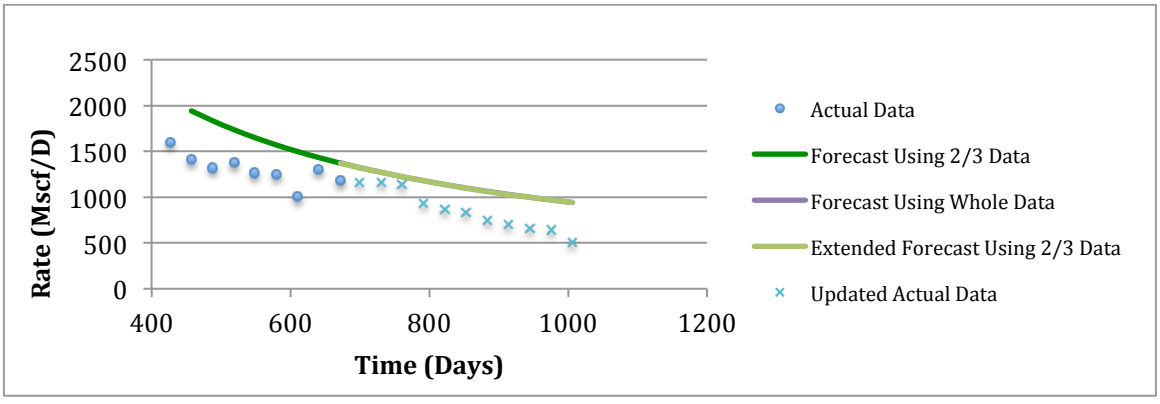

Figure II - 33: History Matching of Well#34, No.260182 Generated by Arps' Harmonic Model

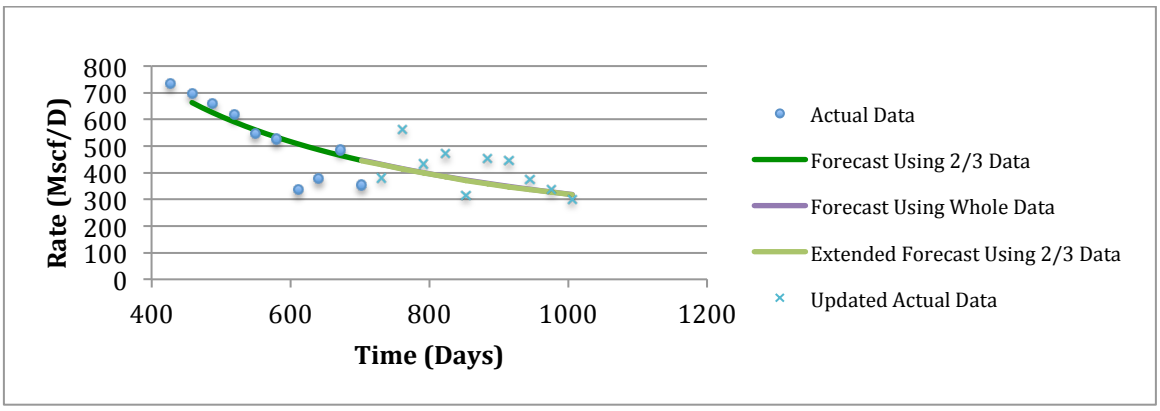

Figure II - 34: History Matching of Well#35, No.261381 Generated by Arps' Harmonic Model

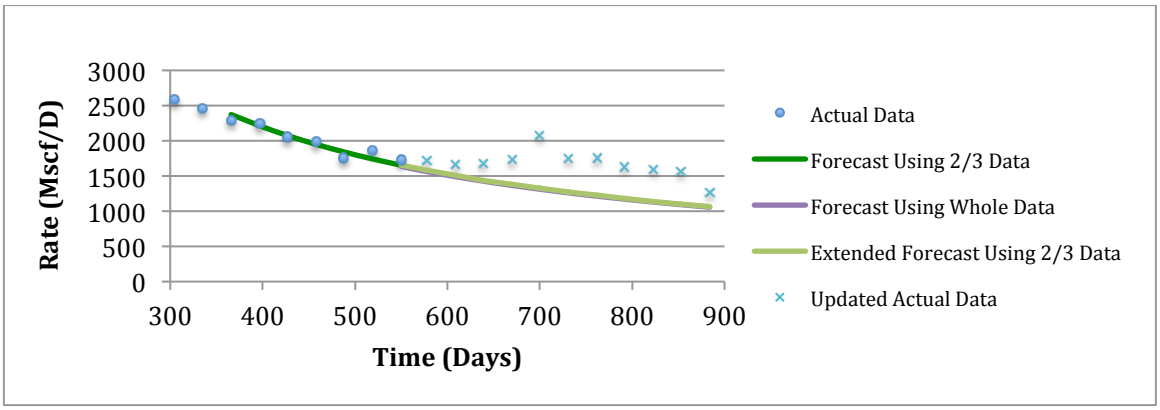

Figure II - 35: History Matching of Well#36, No.260379 Generated by Arps' Harmonic Model

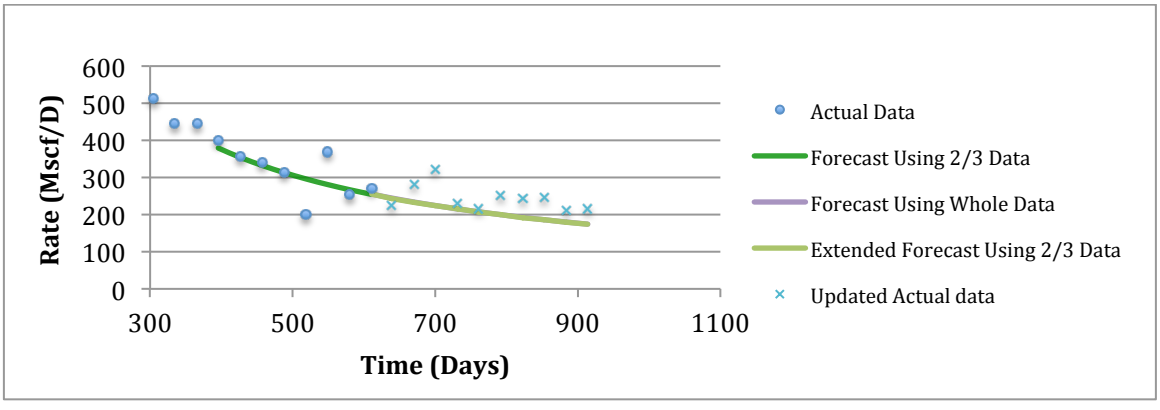

Figure II - 36: History Matching of Well#37, No.261320 Generated by Arps' Harmonic Model

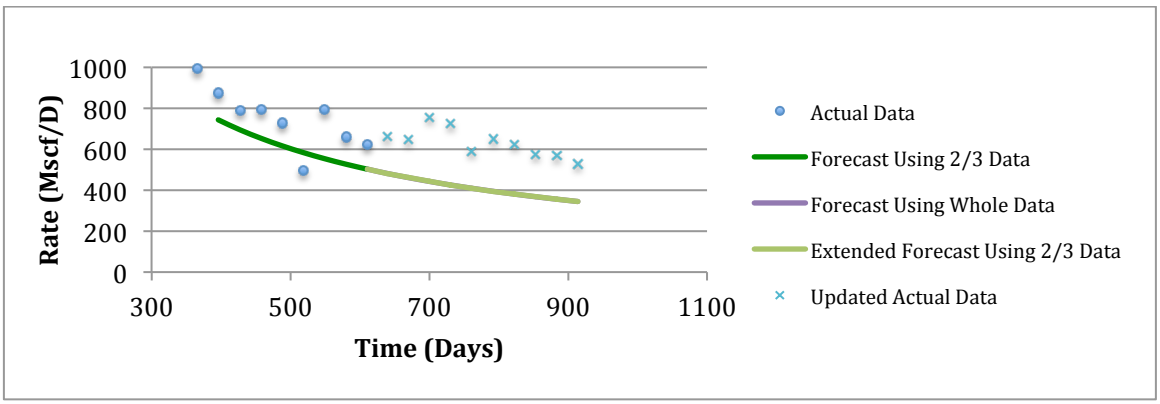

Figure II - 37: History Matching of Well#38, No.261632 Generated by Arps' Harmonic Model

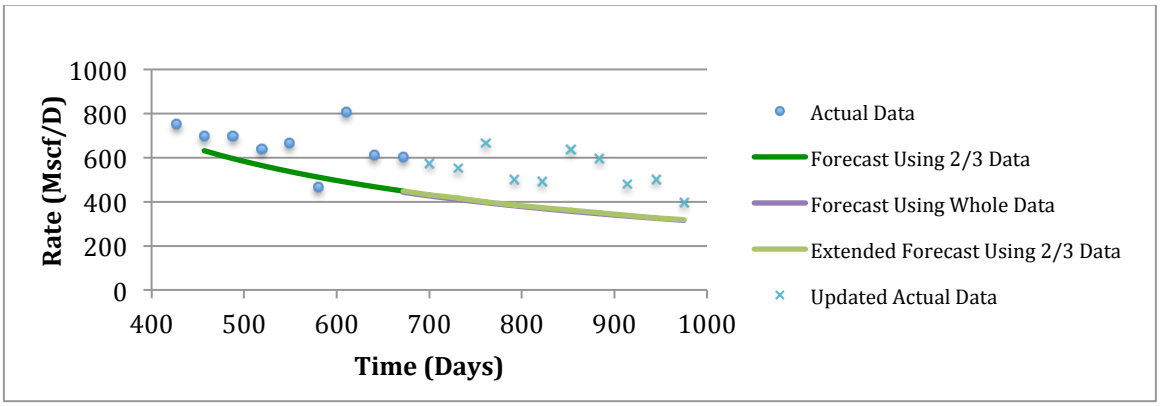

Figure II - 38: History Matching of Well#39, No.261443 Generated by Arps' Harmonic Model

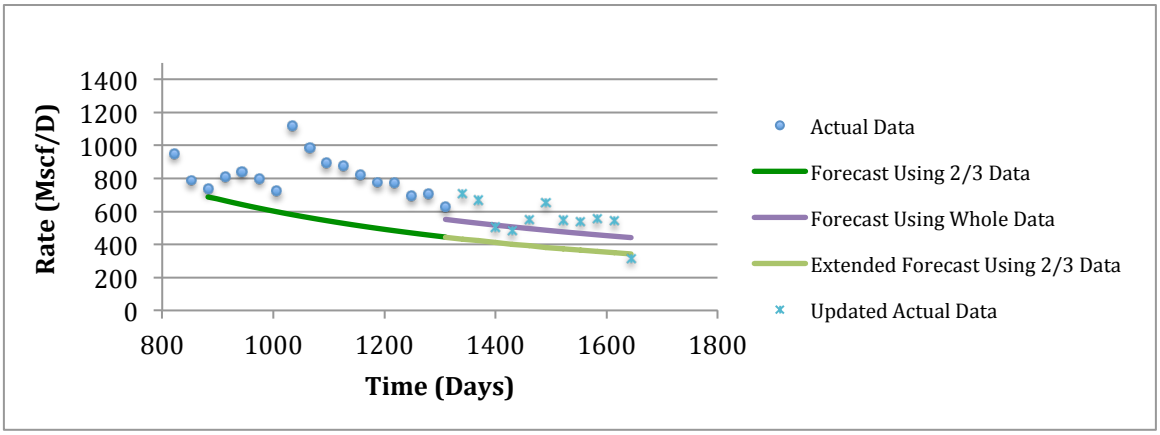

Figure II - 39: History Matching of Well#1, No.251105 Generated by Arps' Hyperbolic Model

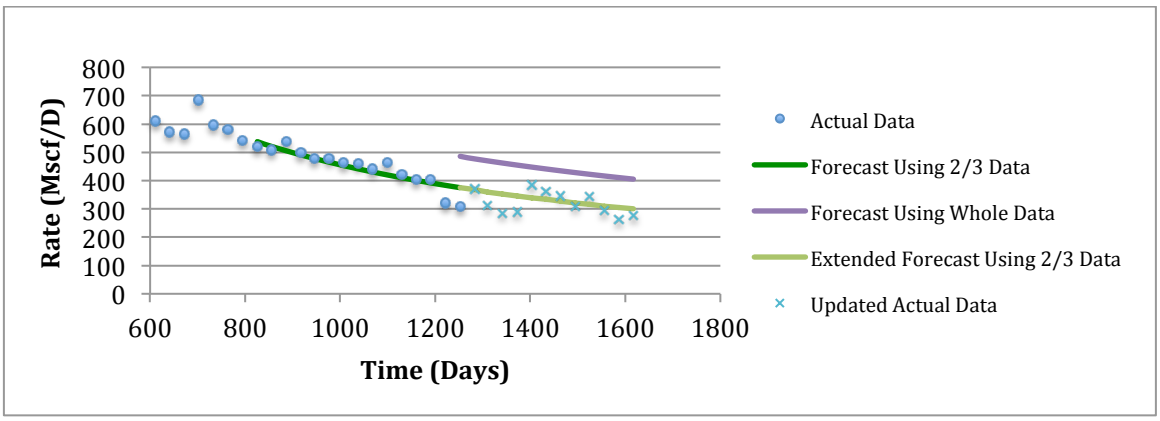

Figure II - 40: History Matching of Well#2, No.252769 Generated by Arps' Hyperbolic Model

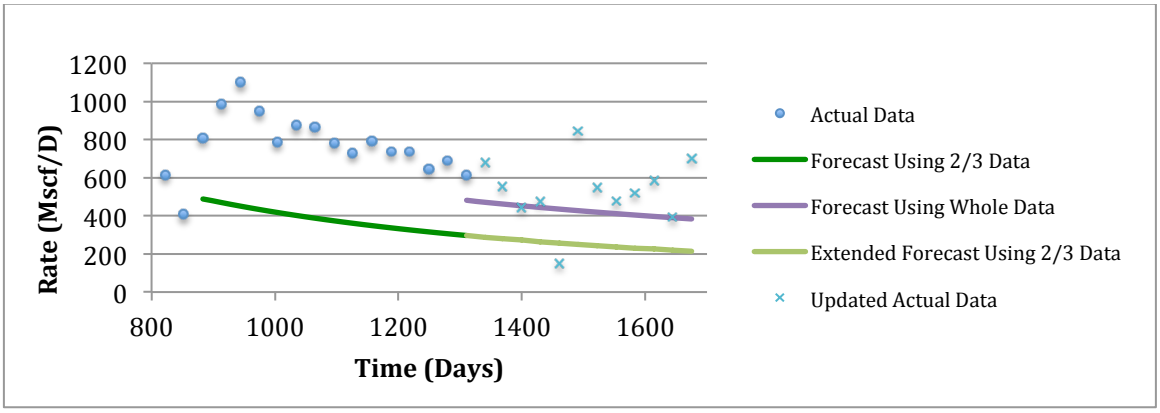

Figure II - 41: History Matching of Well#3, No.251816 Generated by Arps' Hyperbolic Model

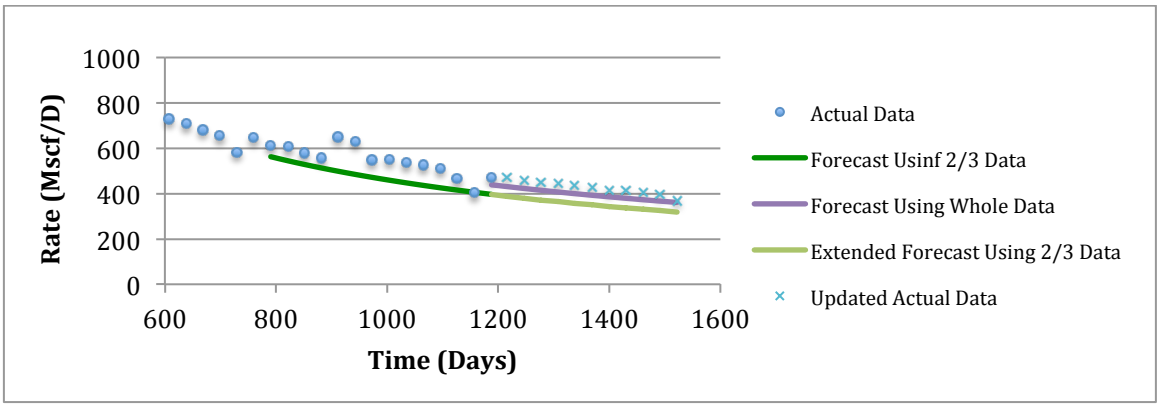

Figure II - 42: History Matching of Well#4, No.251773 Generated by Arps' Hyperbolic Model

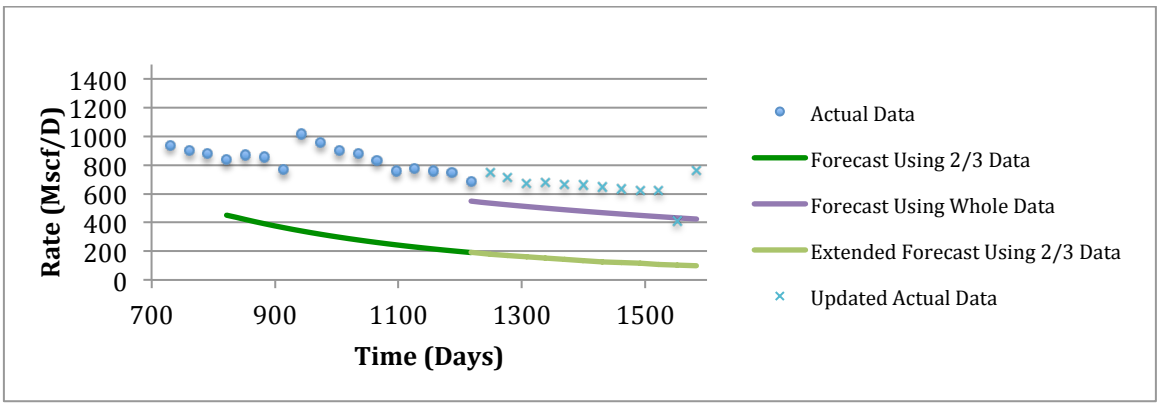

Figure II - 43: History Matching of Well#5, No.251817 Generated by Arps' Hyperbolic Model

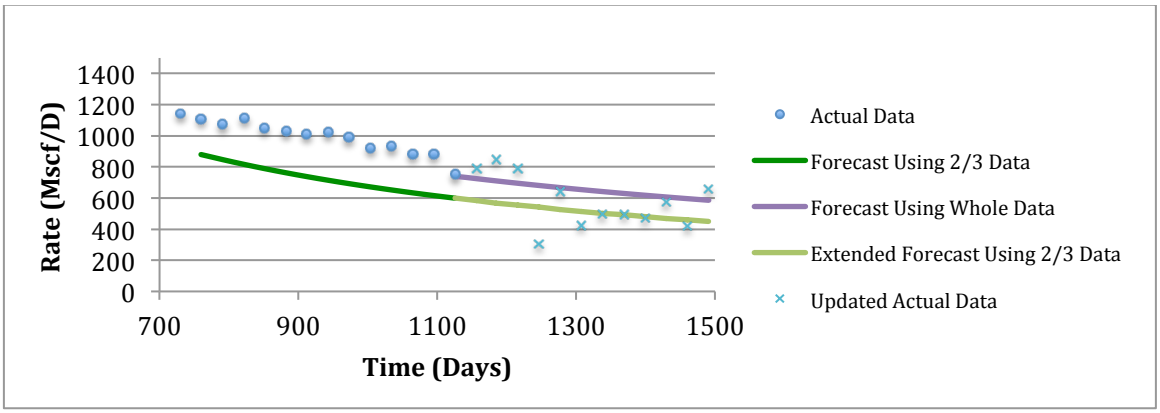

Figure II - 44: History Matching of Well#6, No.255994 Generated by Arps' Hyperbolic Model

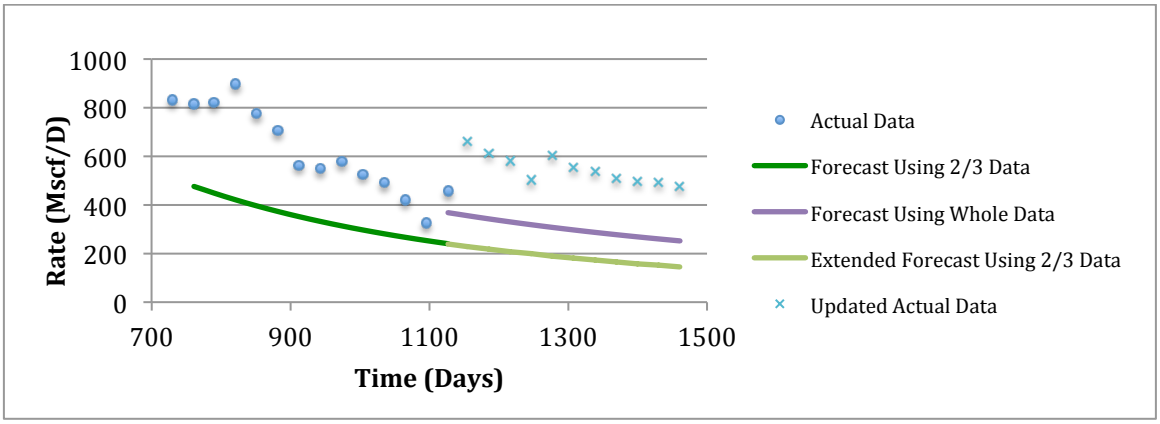

Figure II - 45: History Matching of Well#7, No.255435 Generated by Arps' Hyperbolic Model

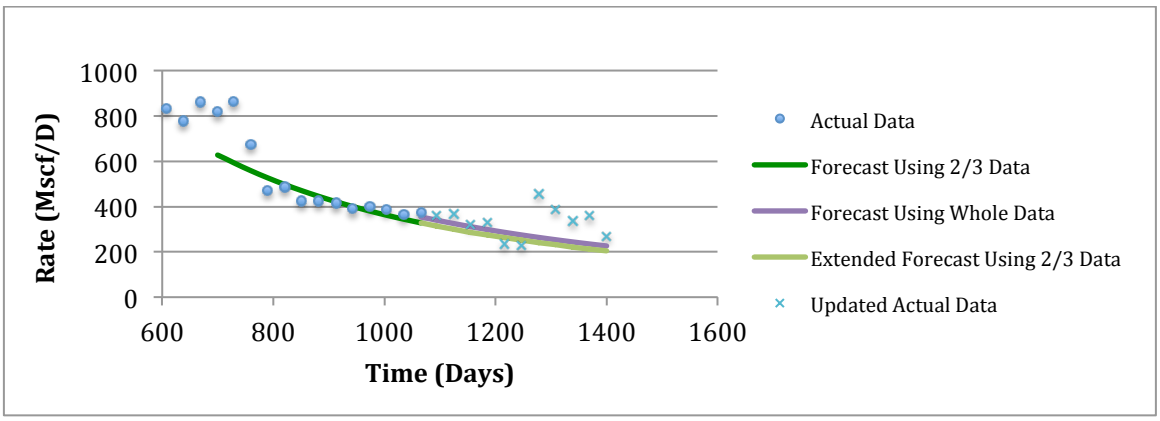

Figure II - 46: History Matching of Well#8, No.255730 Generated by Arps' Hyperbolic Model

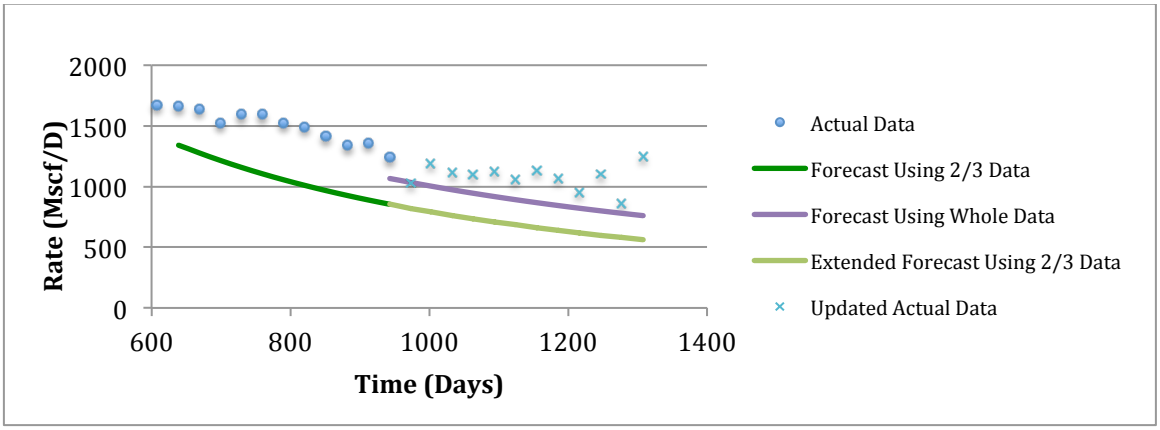

Figure II - 47: History Matching of Well#9, No.254447 Generated by Arps' Hyperbolic Model

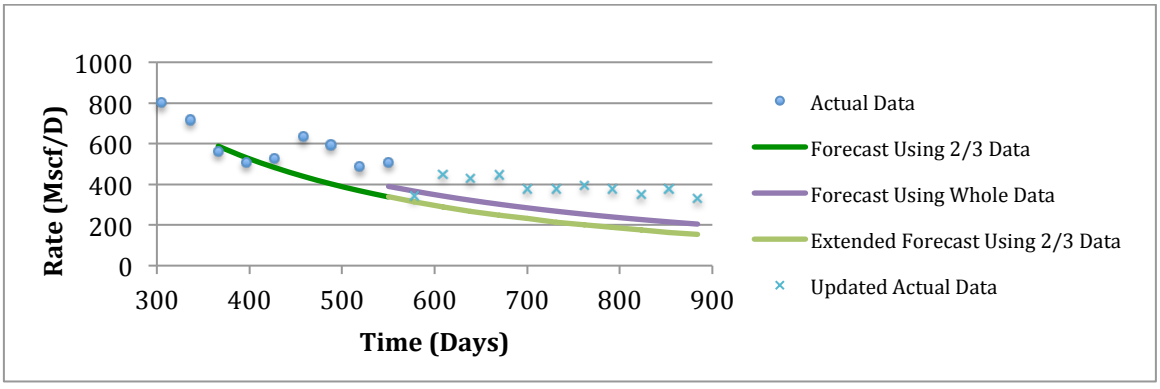

Figure II - 48: History Matching of Well#10, No.263658 Generated by Arps' Hyperbolic Model

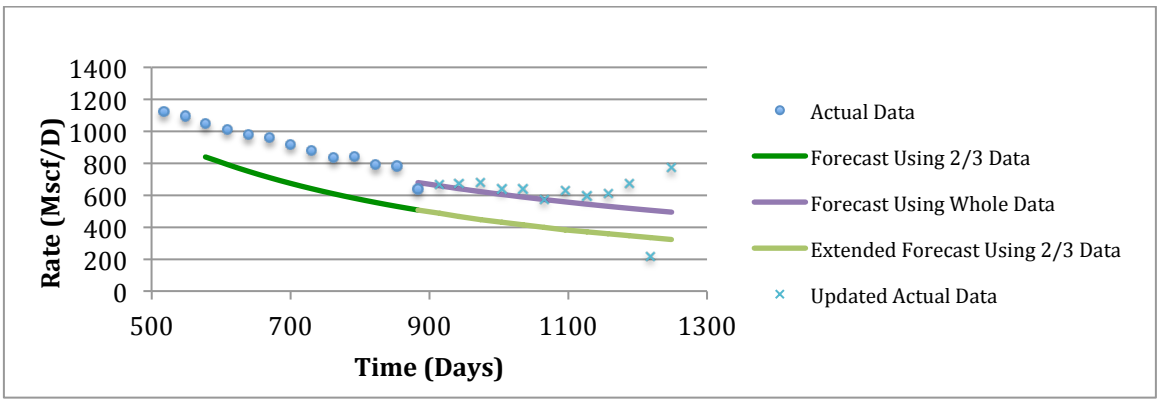

Figure II - 49: History Matching of Well#11, No.258106 Generated by Arps' Hyperbolic Model

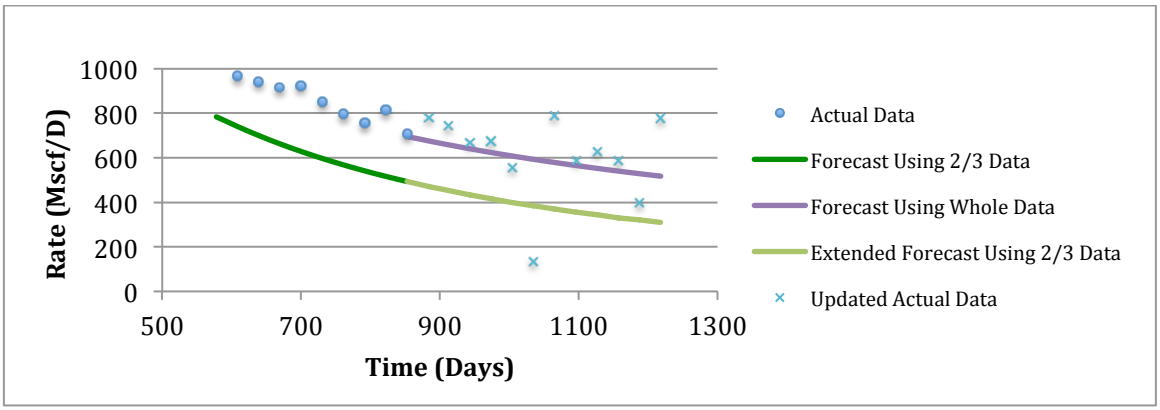

Figure II - 50: History Matching of Well#12, No.258900 Generated by Arps' Hyperbolic Model

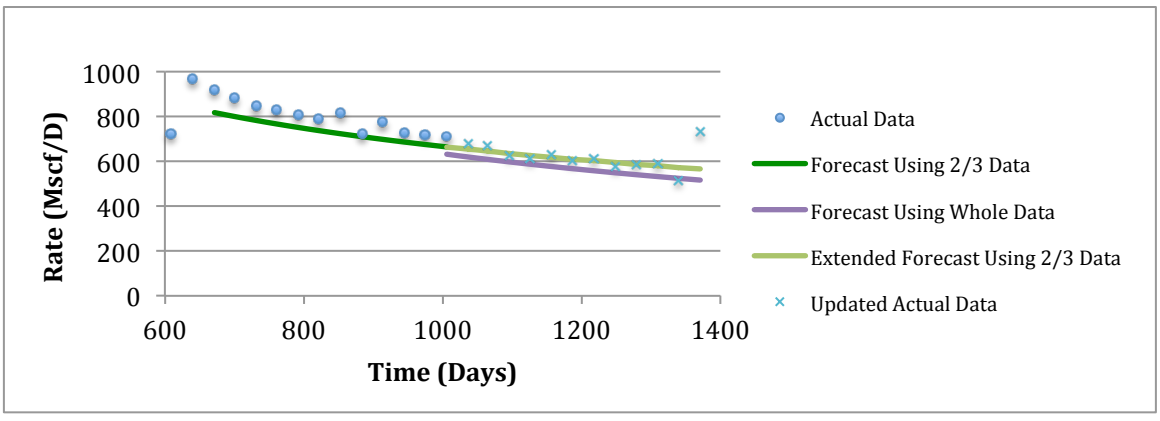

Figure II - 51: History Matching of Well#13, No.257263 Generated by Arps' Hyperbolic Model

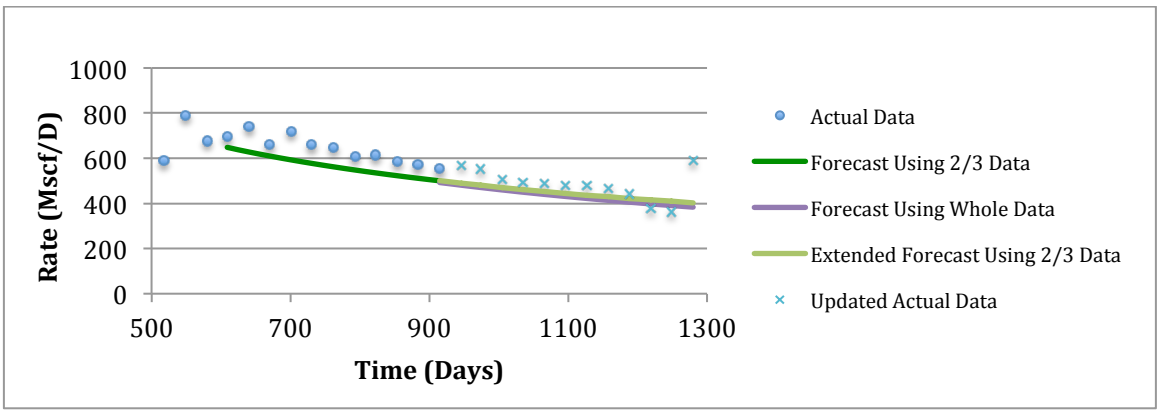

Figure II - 52: History Matching of Well#14, No.257862 Generated by Arps' Hyperbolic Model

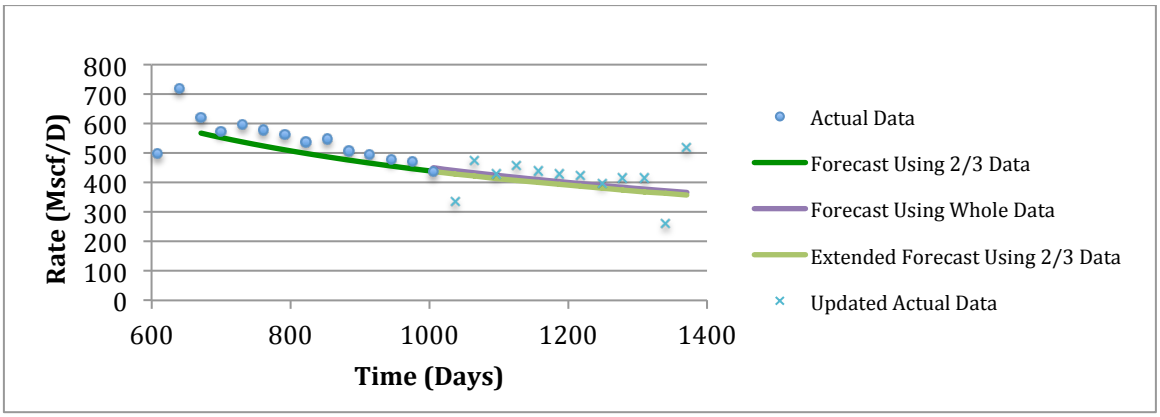

Figure II - 53: History Matching of Well#15, No.254843 Generated by Arps' Hyperbolic Model

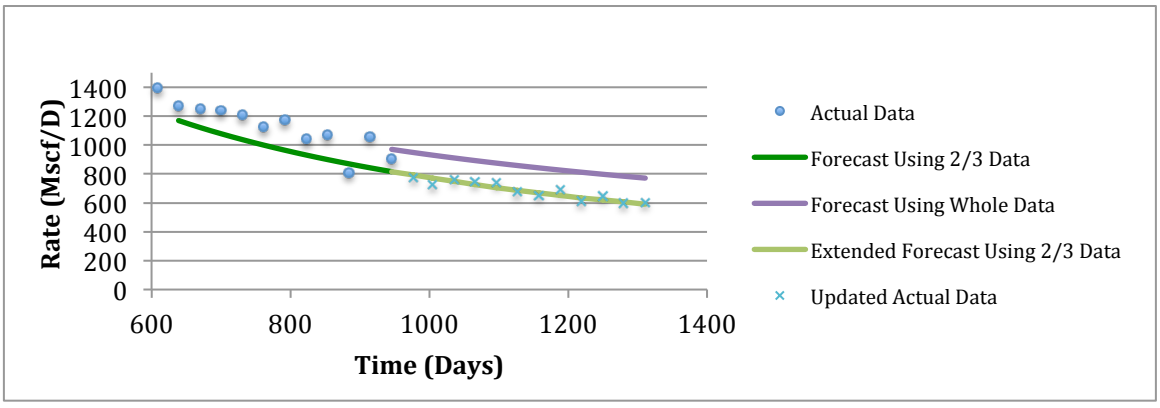

Figure II - 54: History Matching of Well#16, No.258036 Generated by Arps' Hyperbolic Model

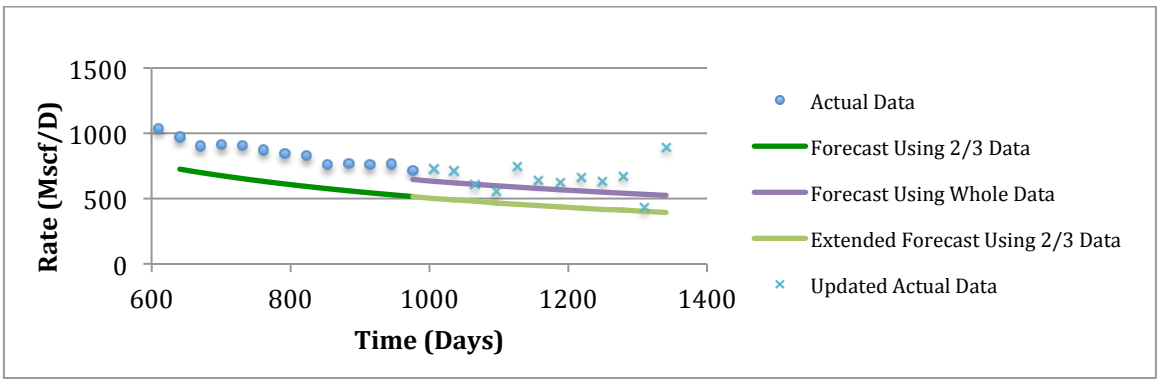

Figure II - 55: History Matching of Well#17, No.257955 Generated by Arps' Hyperbolic Model

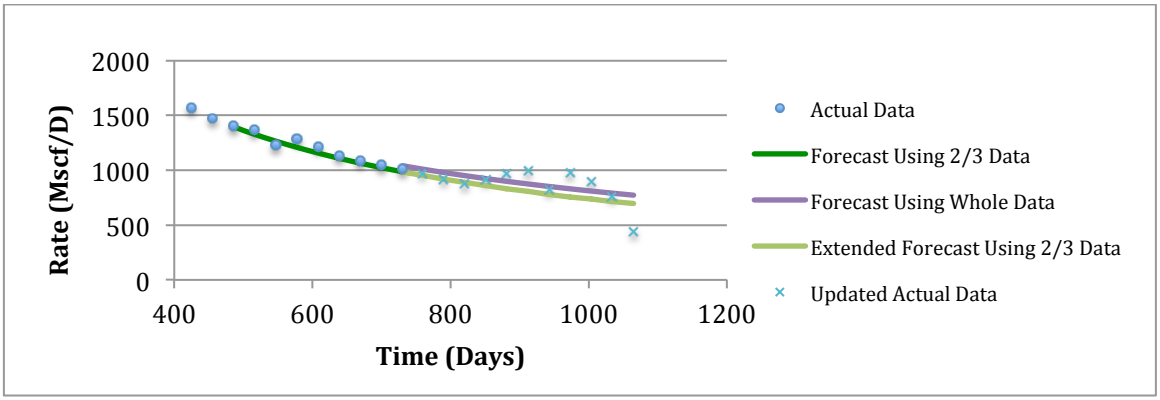

Figure II - 56: History Matching of Well#18, No.259883 Generated by Arps' Hyperbolic Model

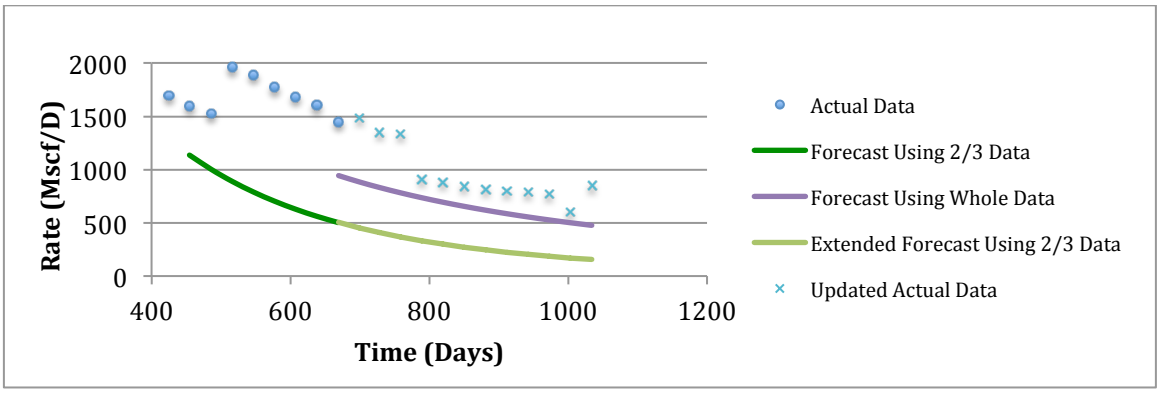

Figure II - 57: History Matching of Well#19, No.259429 Generated by Arps' Hyperbolic Model

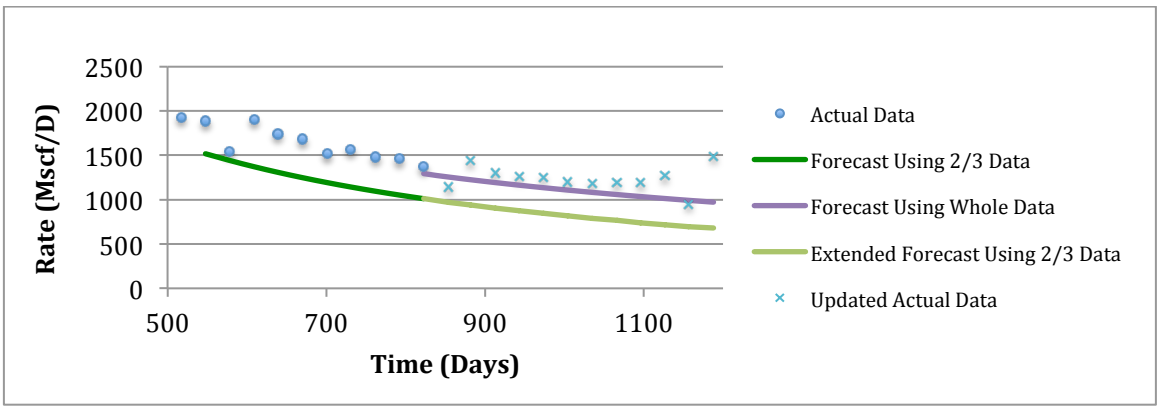

Figure II - 58: History Matching of Well#20, No.258903 Generated by Arps' Hyperbolic Model

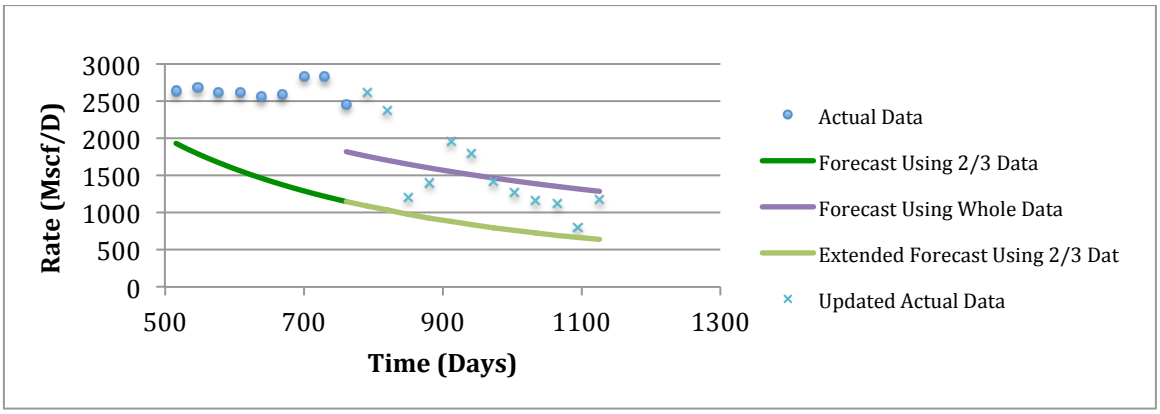

Figure II - 59: History Matching of Well#21, No.260129 Generated by Arps' Hyperbolic Model

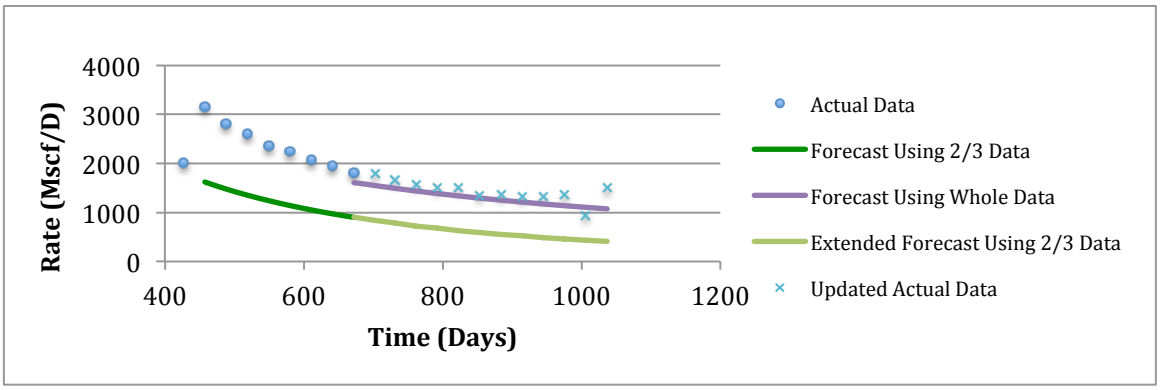

Figure II - 60: History Matching of Well#22, No.260720 Generated by Arps' Hyperbolic Model

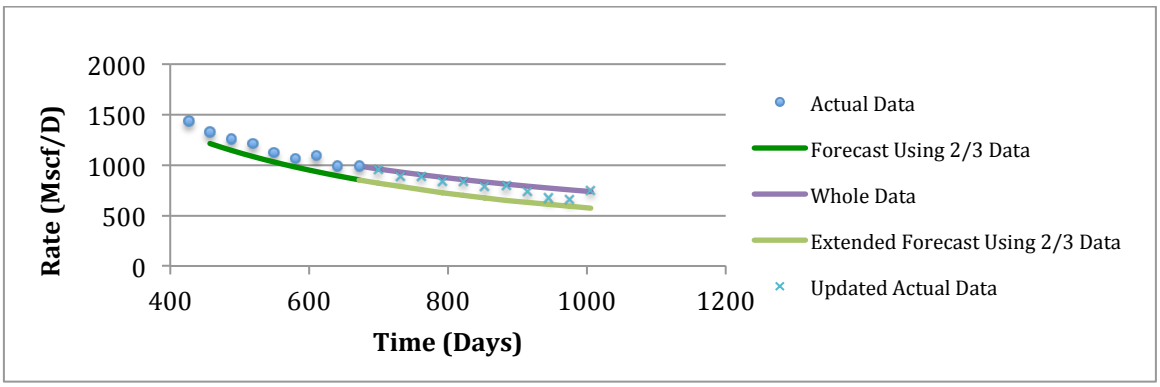

Figure II - 61: History Matching of Well#23, No.261439 Generated by Arps' Hyperbolic Model

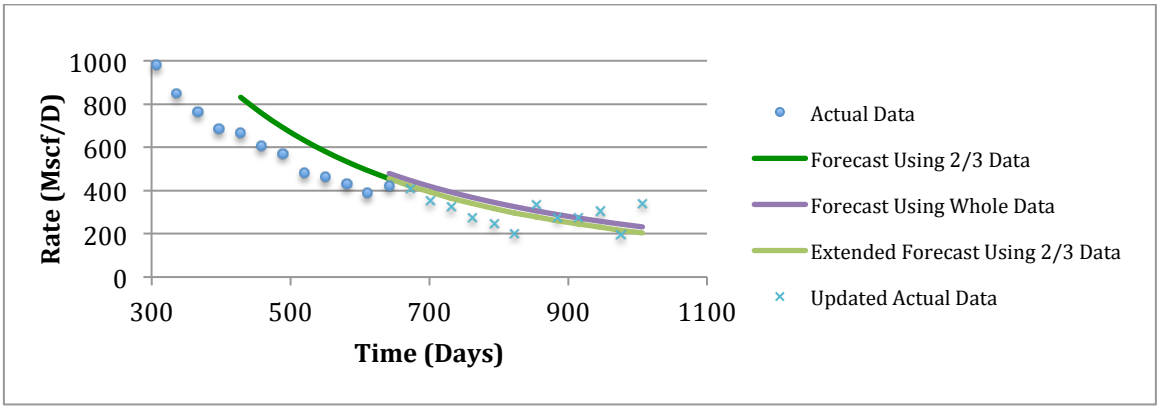

Figure II - 62: History Matching of Well#24, No.260211 Generated by Arps' Hyperbolic Model

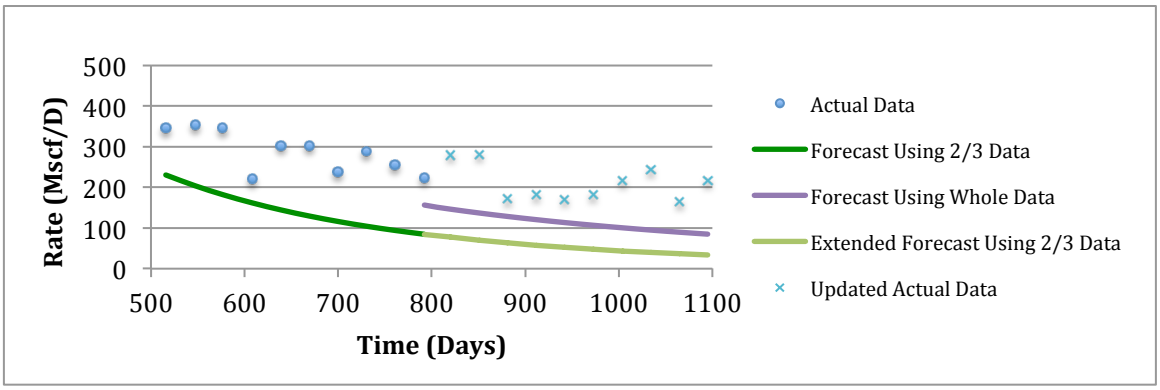

Figure II - 63: History Matching of Well#26, No.258131 Generated by Arps' Hyperbolic Model

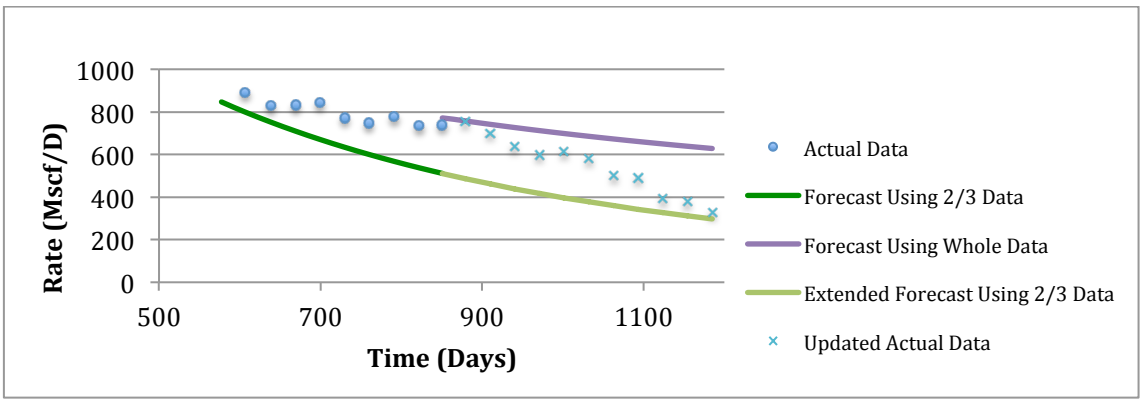

Figure II - 64: History Matching of Well#27, No.257683 Generated by Arps' Hyperbolic Model

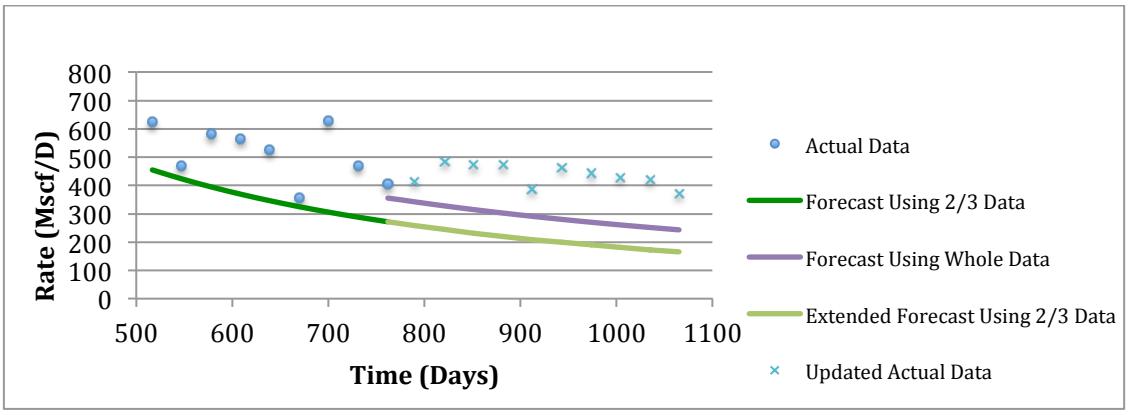

Figure II - 65: History Matching of Well#28, No.257687 Generated by Arps' Hyperbolic Model

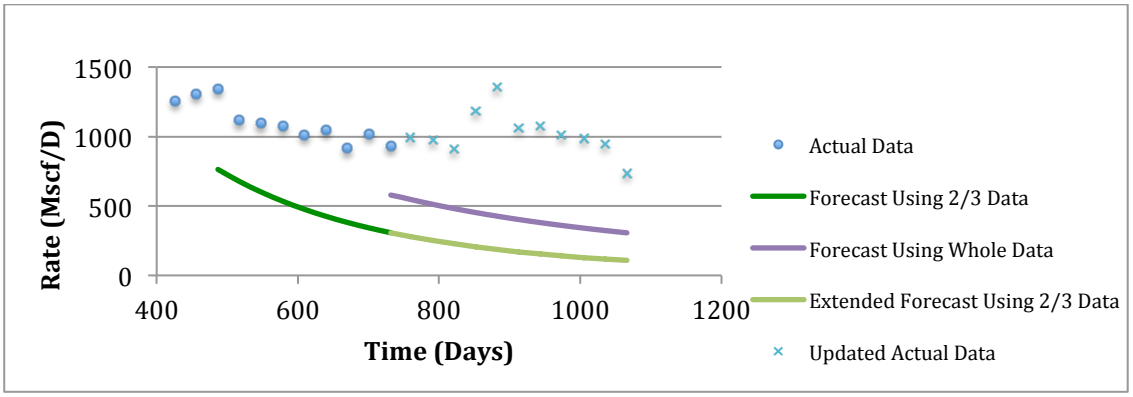

Figure II - 66: History Matching of Well#29, No.257628 Generated by Arps' Hyperbolic Model

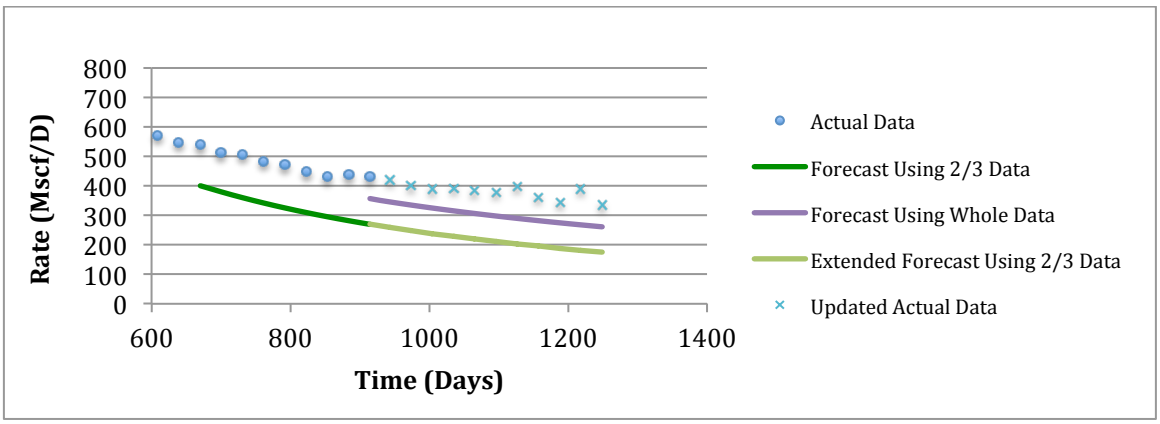

Figure II - 67: History Matching of Well#30, No.257685 Generated by Arps' Hyperbolic Model

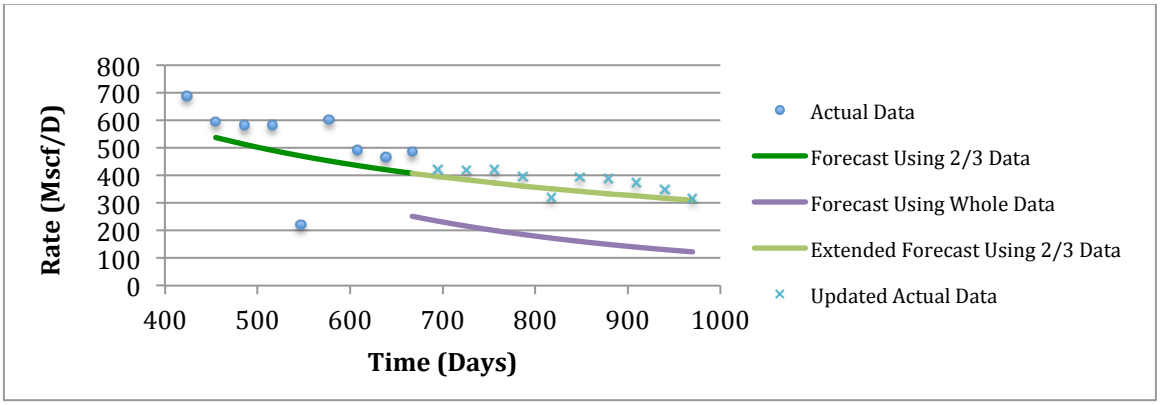

Figure II - 68: History Matching of Well#31, No.260046 Generated by Arps' Hyperbolic Model

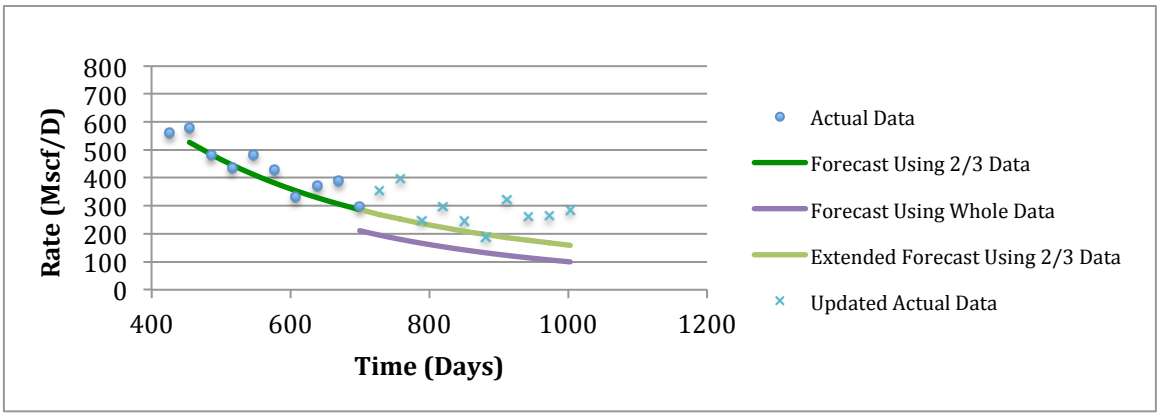

Figure II - 69: History Matching of Well#32, No.260047 Generated by Arps' Hyperbolic Model

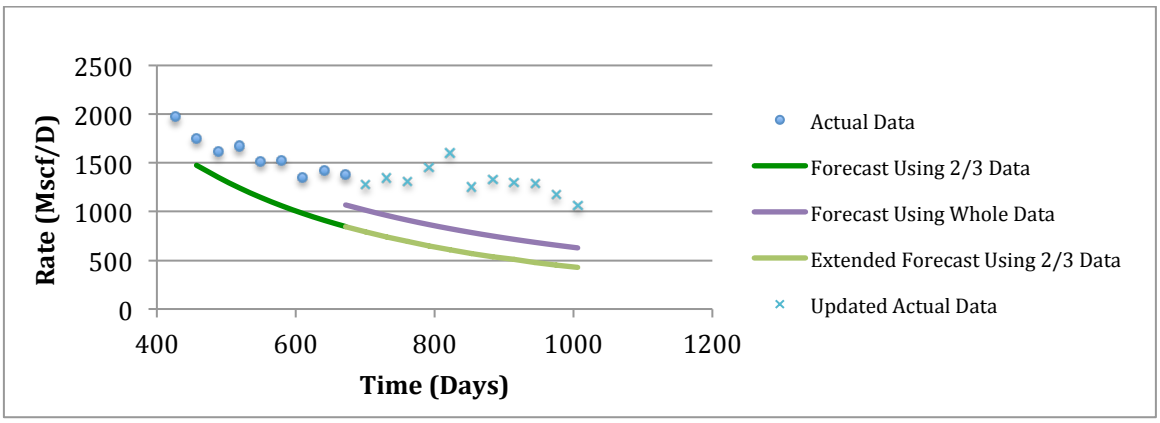

Figure II - 70: History Matching of Well#33, No.260071 Generated by Arps' Hyperbolic Model

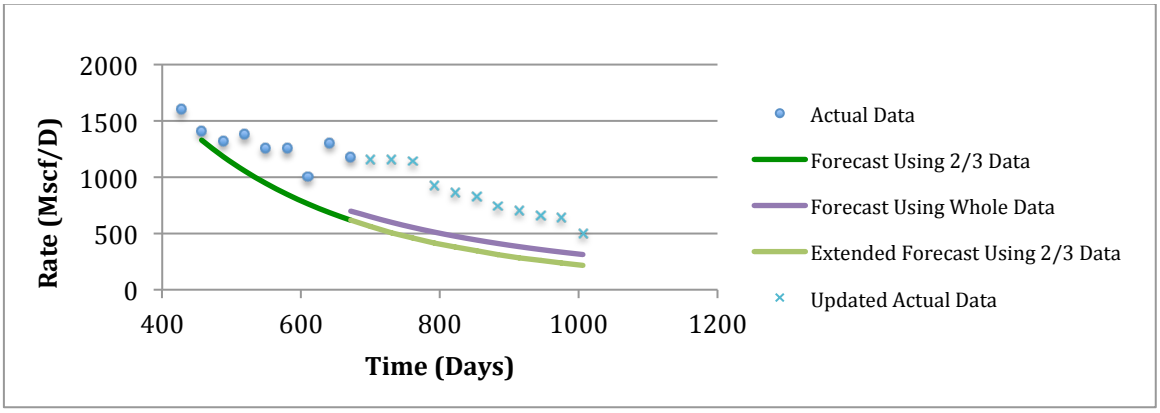

Figure II - 71: History Matching of Well#34, No.260182 Generated by Arps' Hyperbolic Model

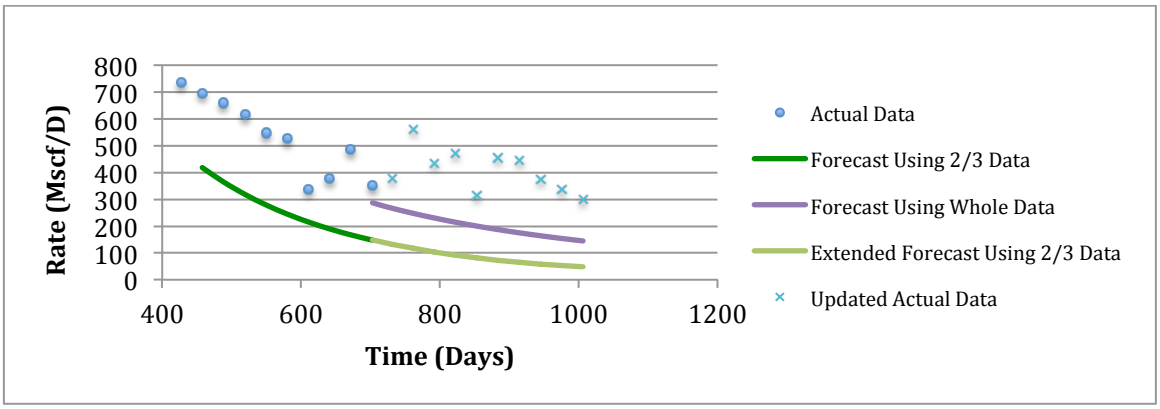

Figure II - 72: History Matching of Well#35, No.261381 Generated by Arps' Hyperbolic Model

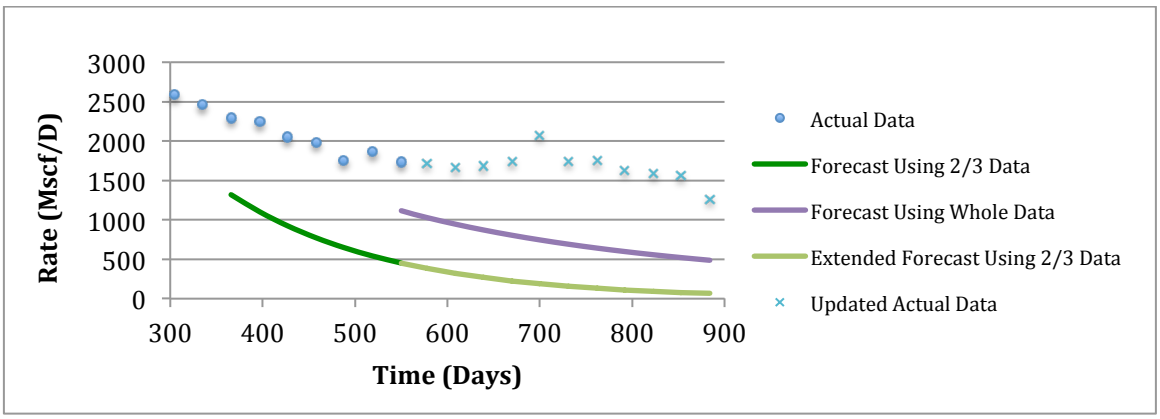

Figure II - 73: History Matching of Well#36, No.260379 Generated by Arps' Hyperbolic Model

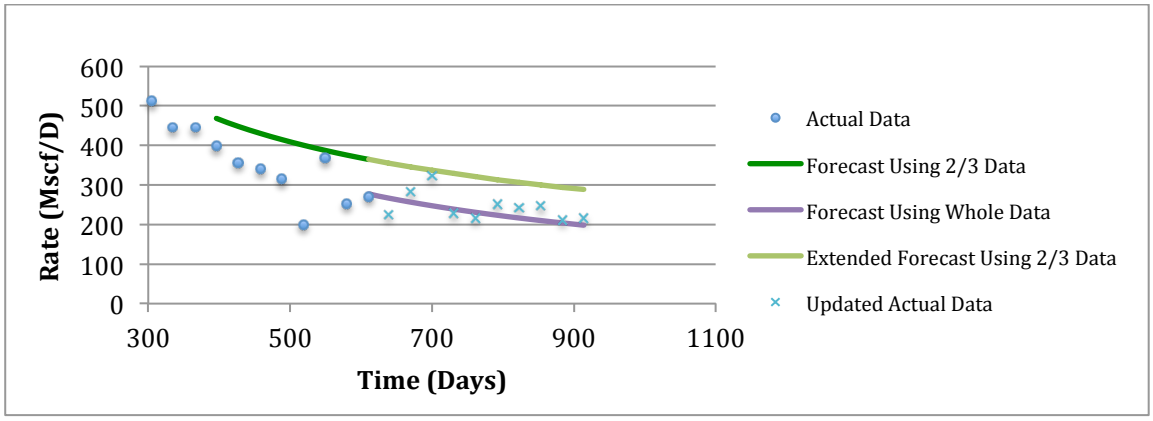

Figure II - 74: History Matching of Well#37, No.261320 Generated by Arps' Hyperbolic Model

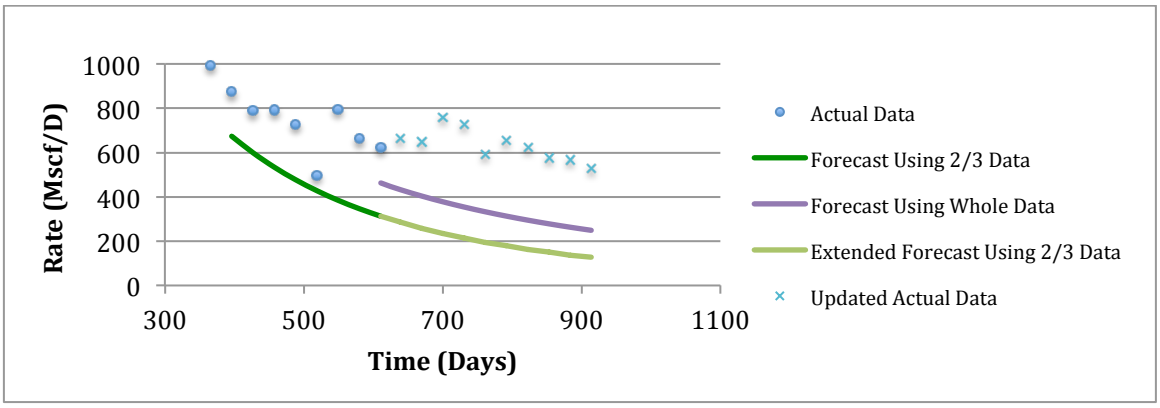

Figure II - 75: History Matching of Well#38, No.261632 Generated by Arps' Hyperbolic Model

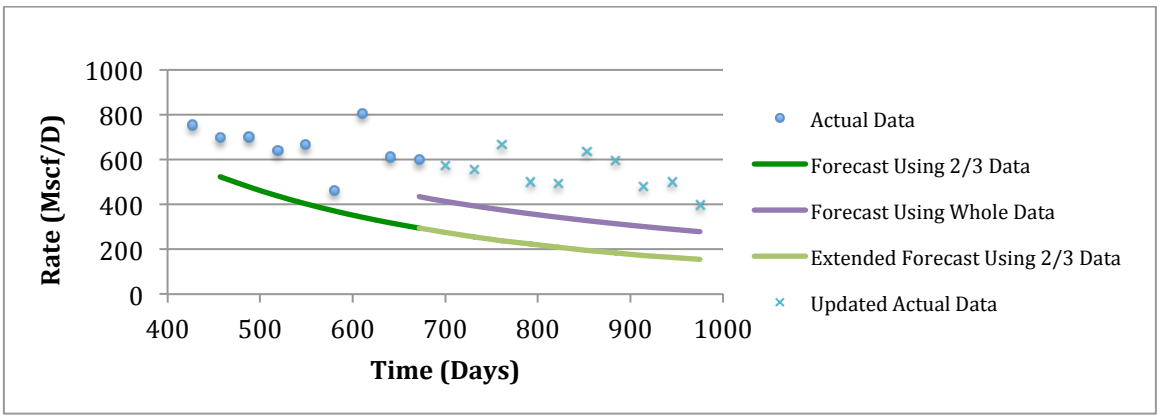

Figure II - 76: History Matching of Well#39, No.261443 Generated by Arps' Hyperbolic Model

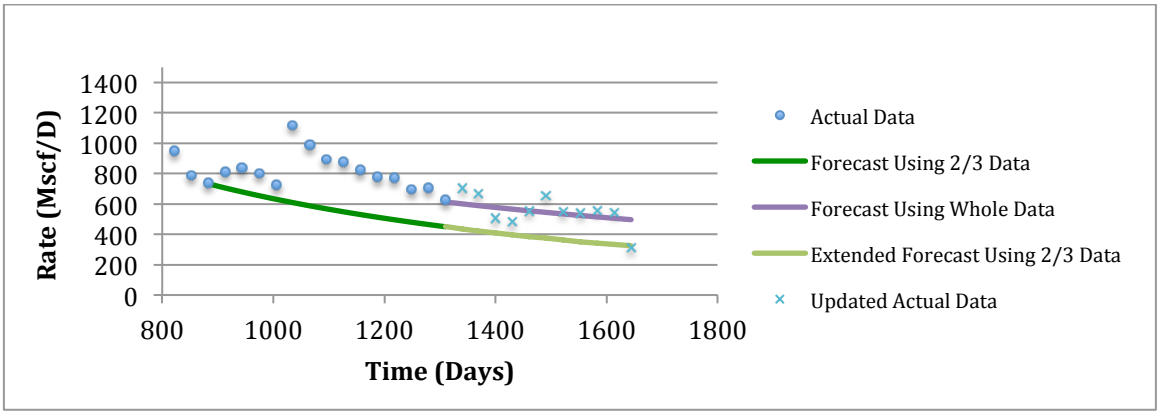

Figure II - 77: History Matching of Well#1, No.251105 Generated by PLE Model

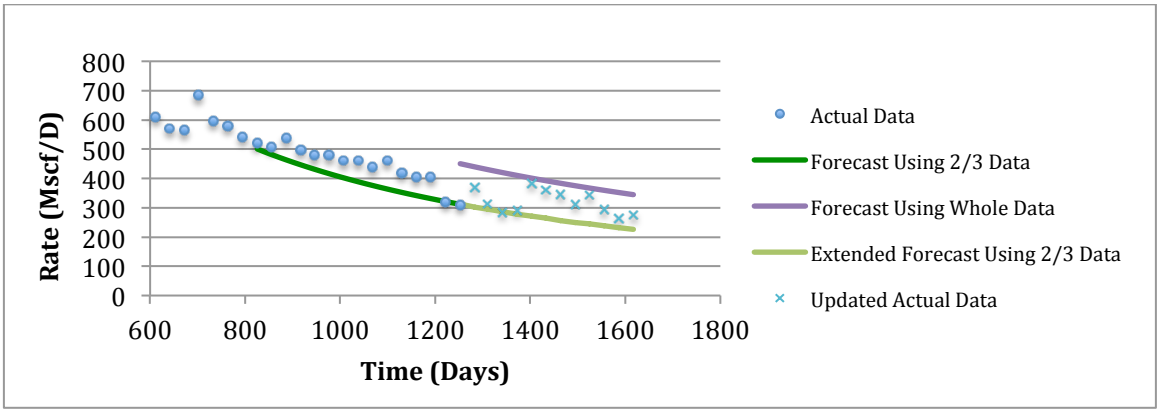

Figure II - 78: History Matching of Well#2, No.252769 Generated by PLE Model

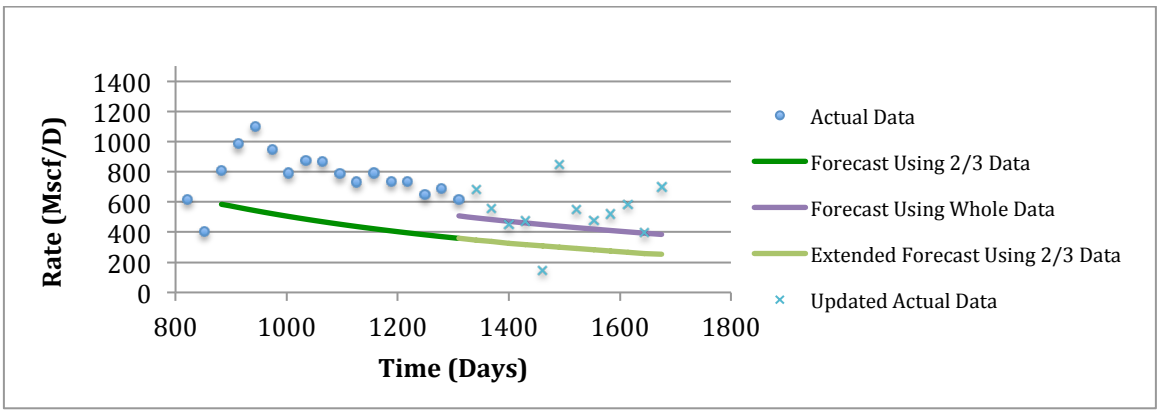

Figure II - 79: History Matching of Well#3, No.251816 Generated by PLE Model

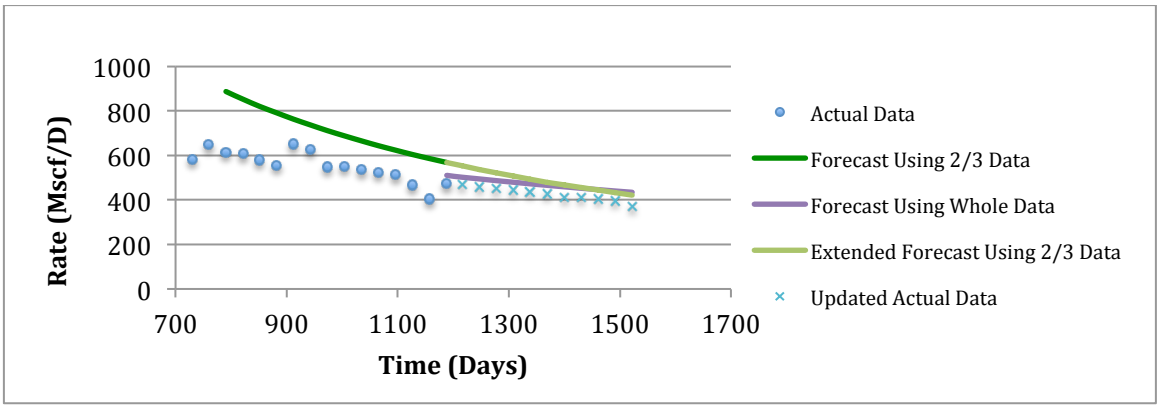

Figure II - 80: History Matching of Well#4, No.251773 Generated by PLE Model

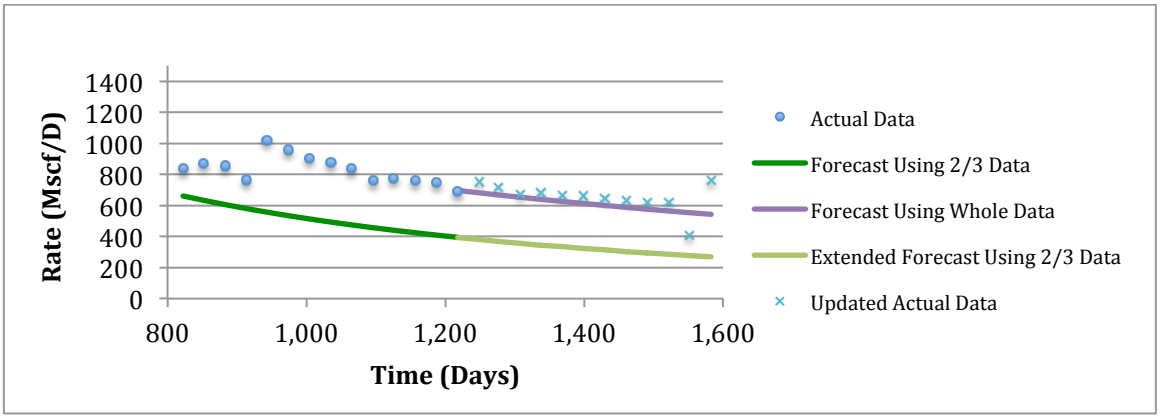

Figure II - 81: History Matching of Well#5, No.251817 Generated by PLE Model

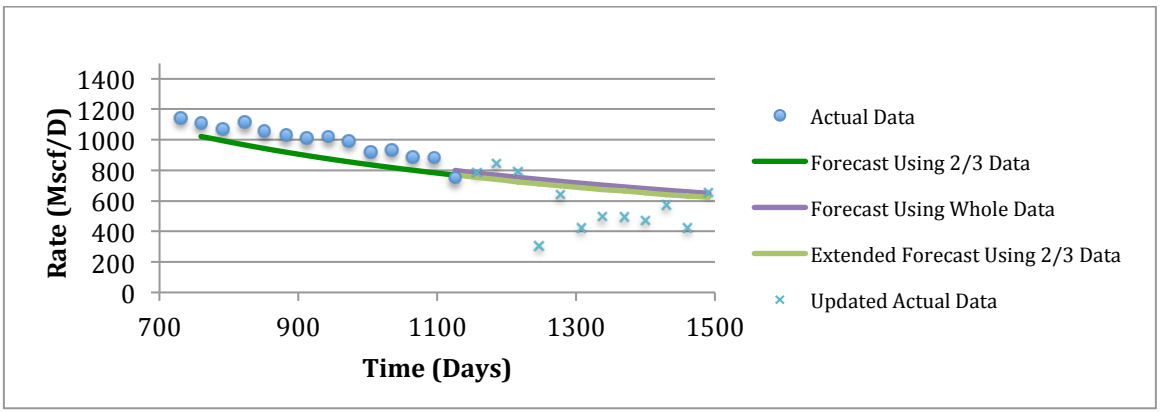

Figure II - 82: History Matching of Well#6, No.255994 Generated by PLE Model

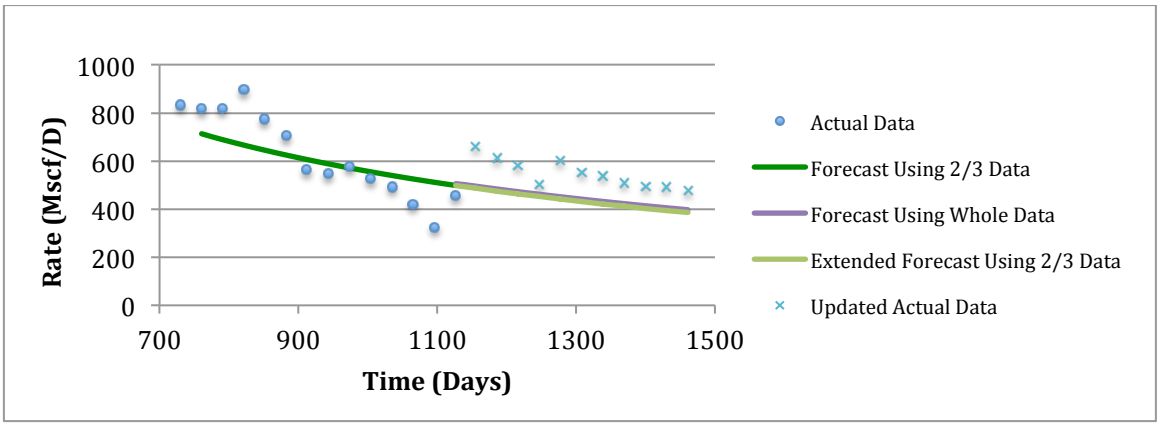

Figure II - 83: History Matching of Well#7, No.255435 Generated by PLE Model

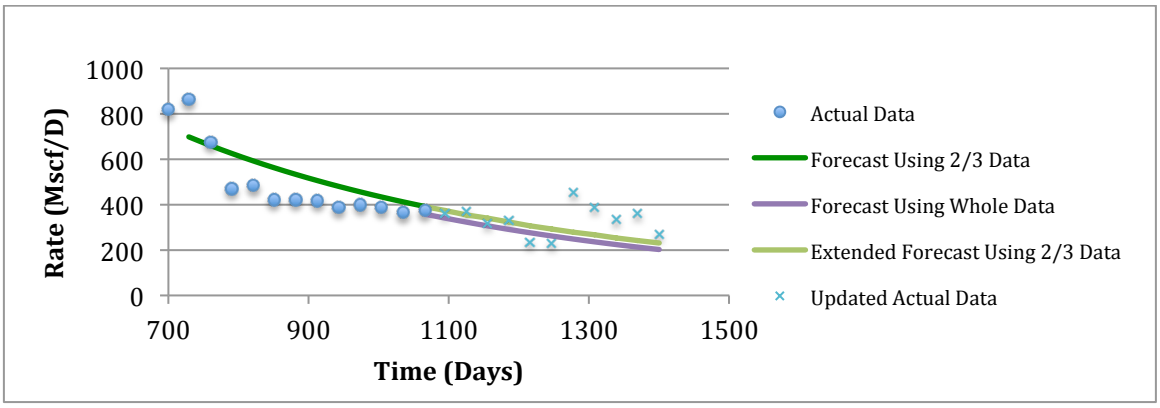

Figure II - 84: History Matching of Well#8, No.255730 Generated by PLE Model

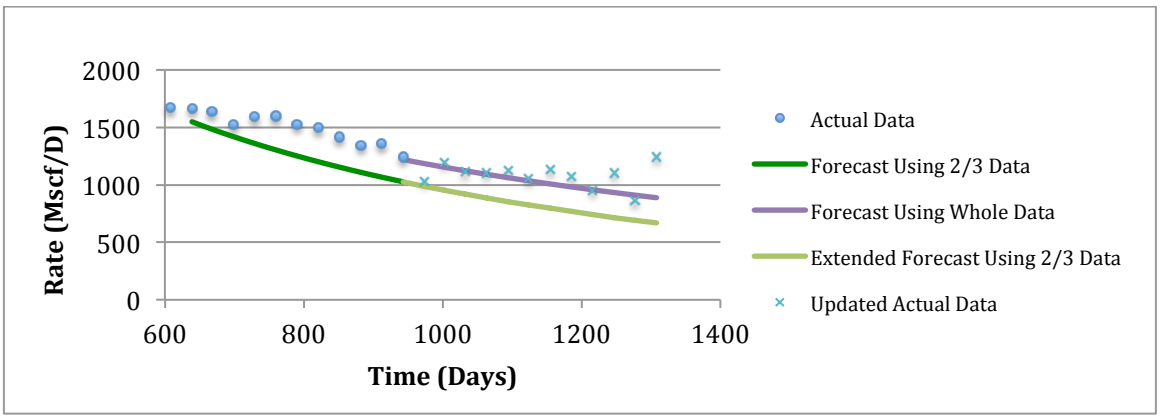

Figure II - 85: History Matching of Well#9, No.254447 Generated by PLE Model

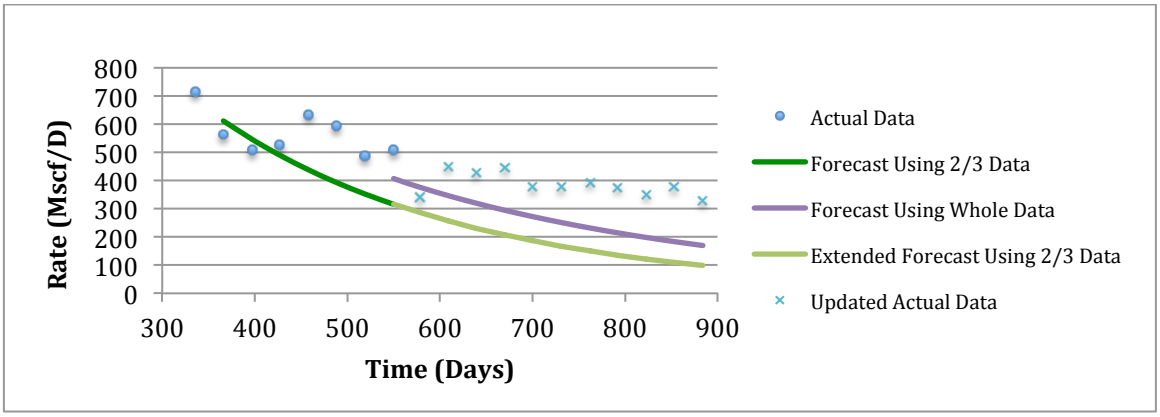

Figure II - 86: History Matching of Well#10, No.263658 Generated by PLE Model

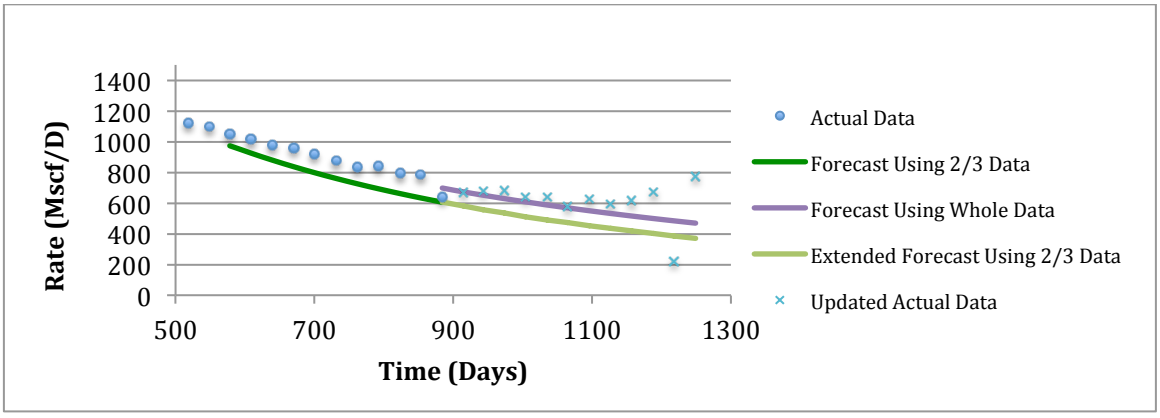

Figure II - 87: History Matching of Well#11, No.258106 Generated by PLE Model

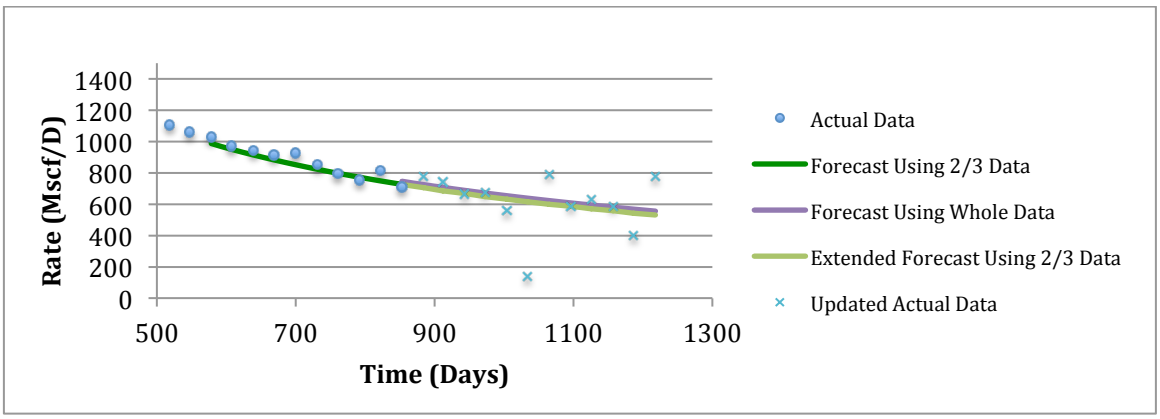

Figure II - 88: History Matching of Well#12, No.258900 Generated by PLE Model

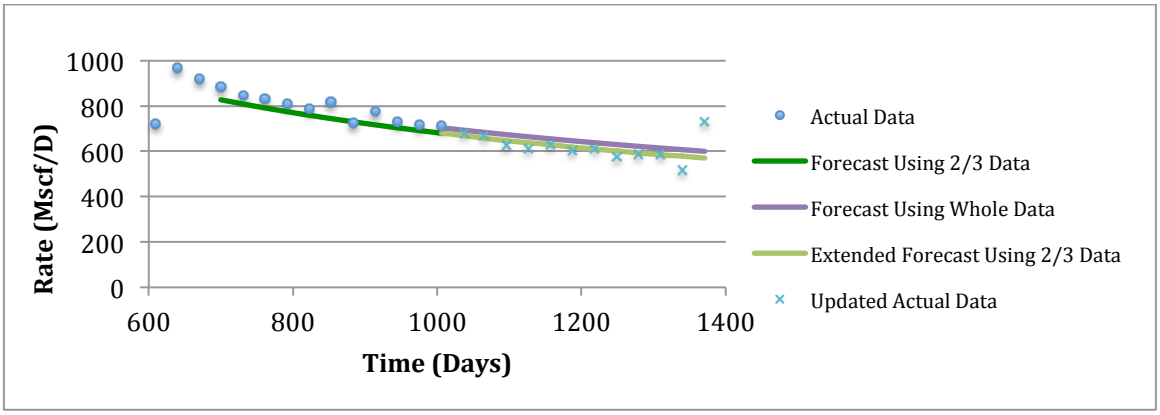

Figure II - 89: History Matching of Well#13, No.257263 Generated by PLE Model

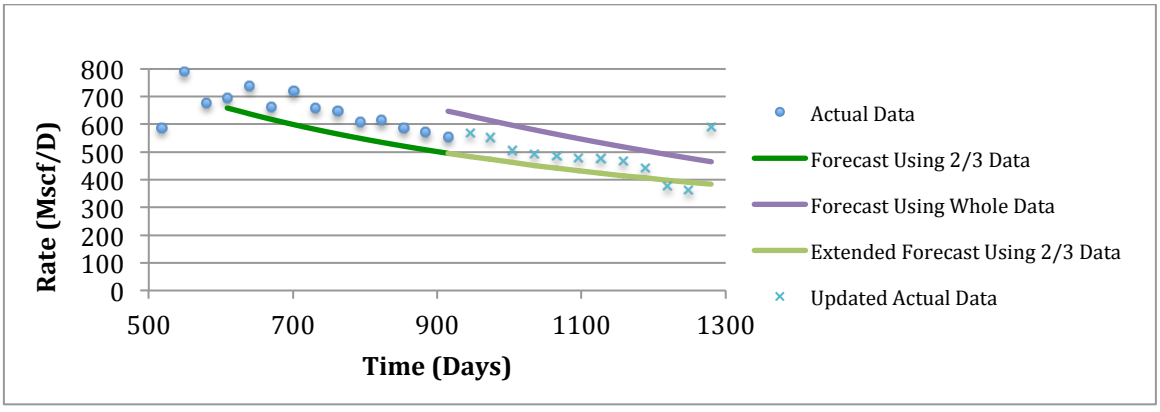

Figure II - 90: History Matching of Well#14, No.257826 Generated by PLE Model

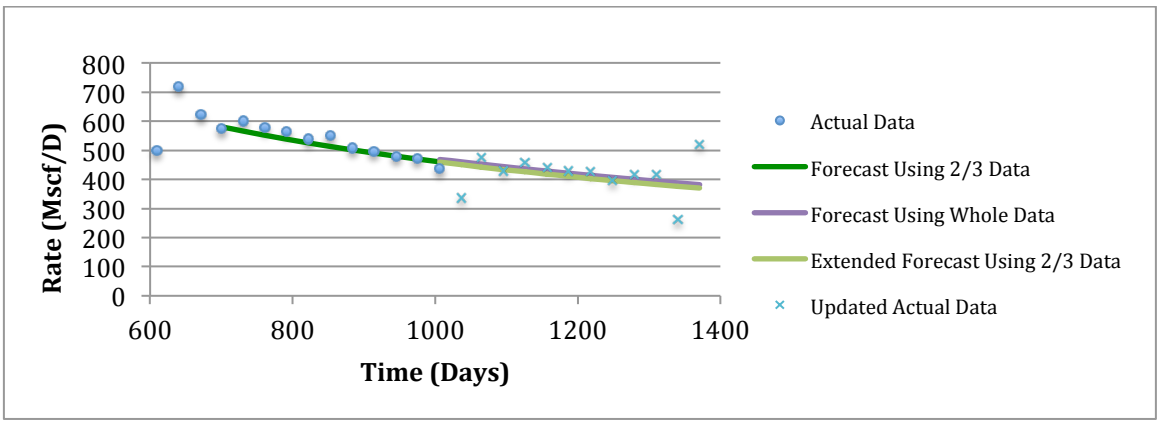

Figure II - 91: History Matching of Well#15, No.254843 Generated by PLE Model

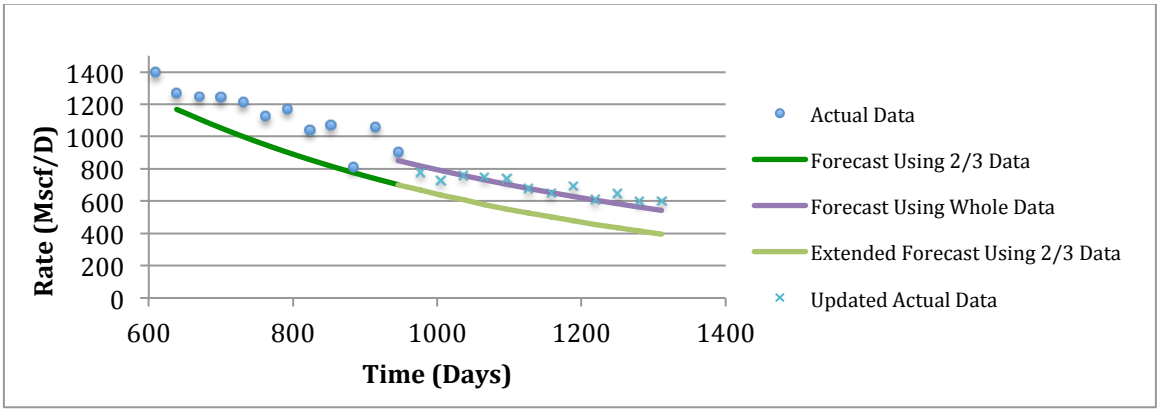

Figure II - 92: History Matching of Well#16, No.258036 Generated by PLE Model

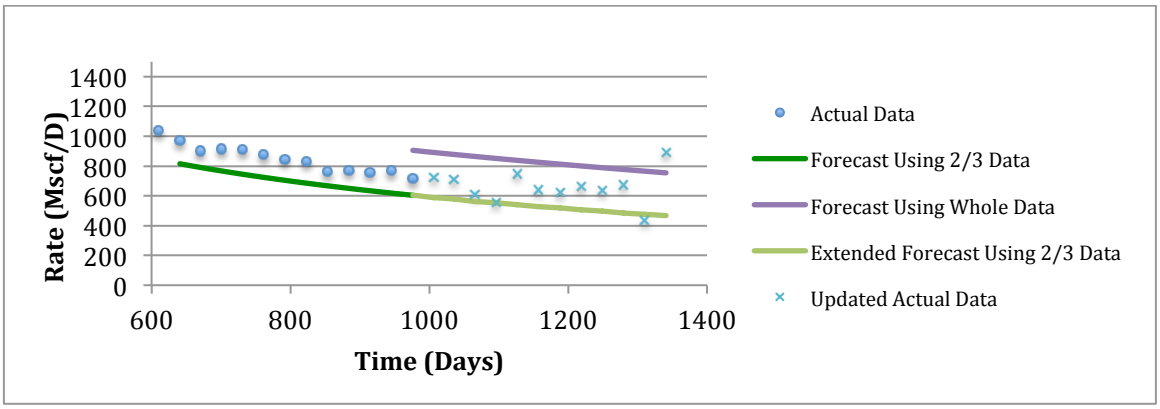

Figure II - 93: History Matching of Well#17, No.257955 Generated by PLE Model

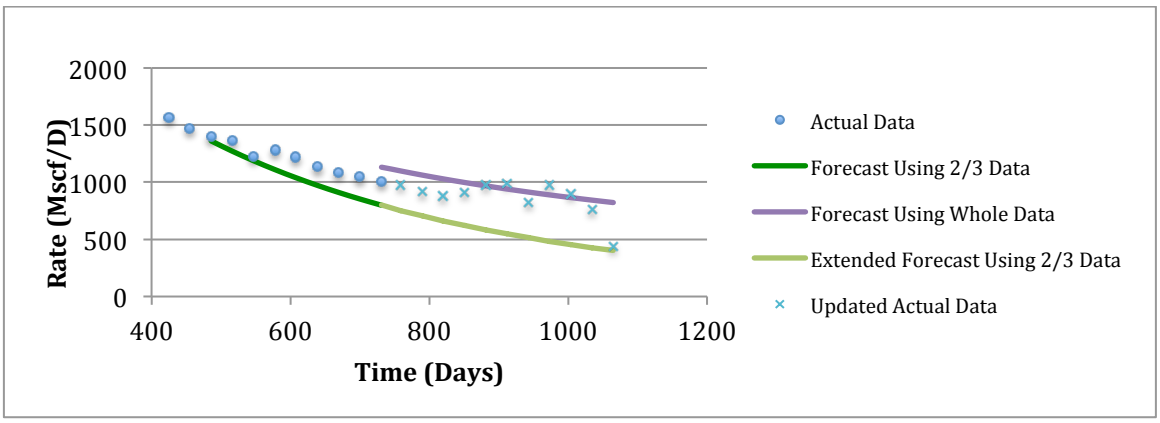

Figure II - 94: History Matching of Well#18, No.259883 Generated by PLE Model

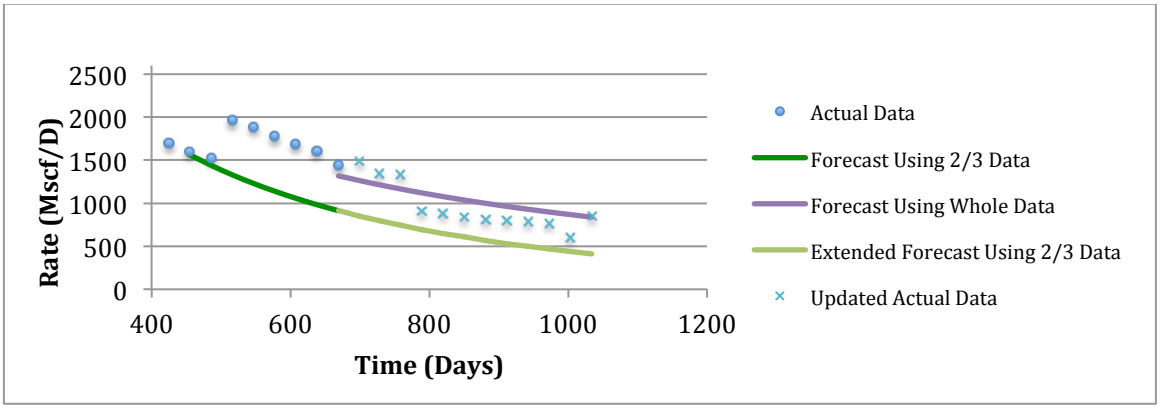

Figure II - 95: History Matching of Well#19, No.259429 Generated by PLE Model

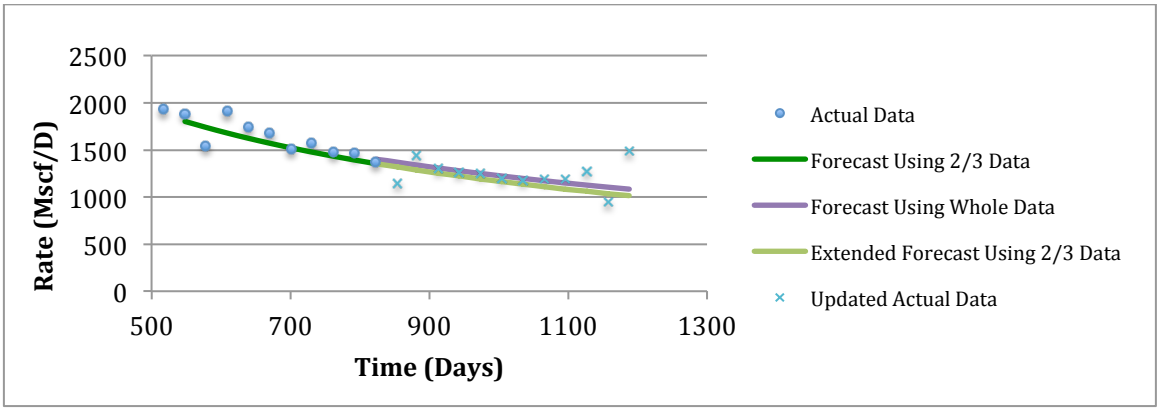

Figure II - 96: History Matching of Well#20, No.258903 Generated by PLE Model

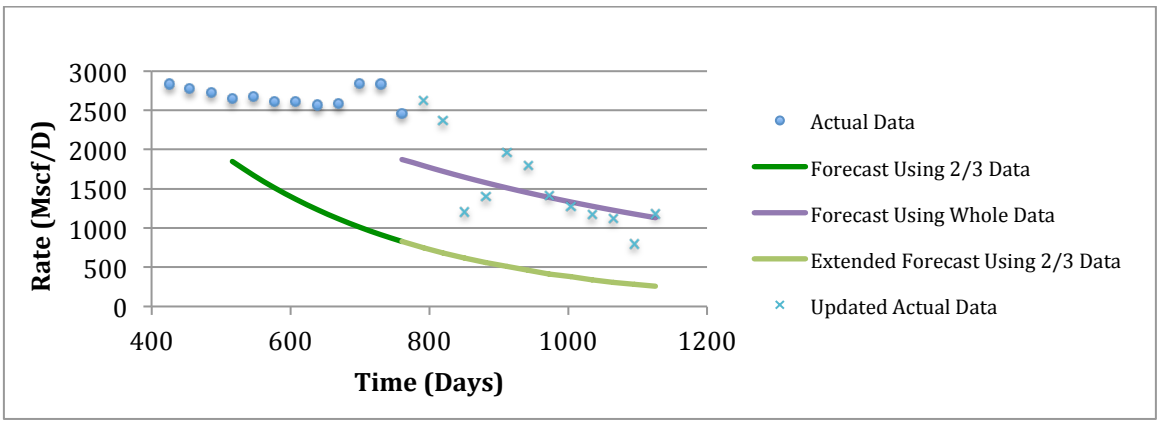

Figure II - 97: History Matching of Well#21, No.260129 Generated by PLE Model

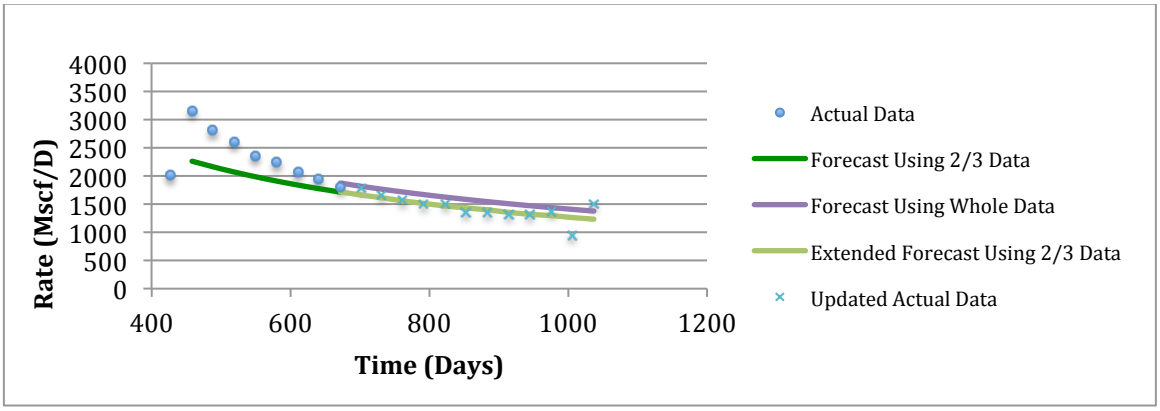

Figure II - 98: History Matching of Well#22, No.260720 Generated by PLE Model

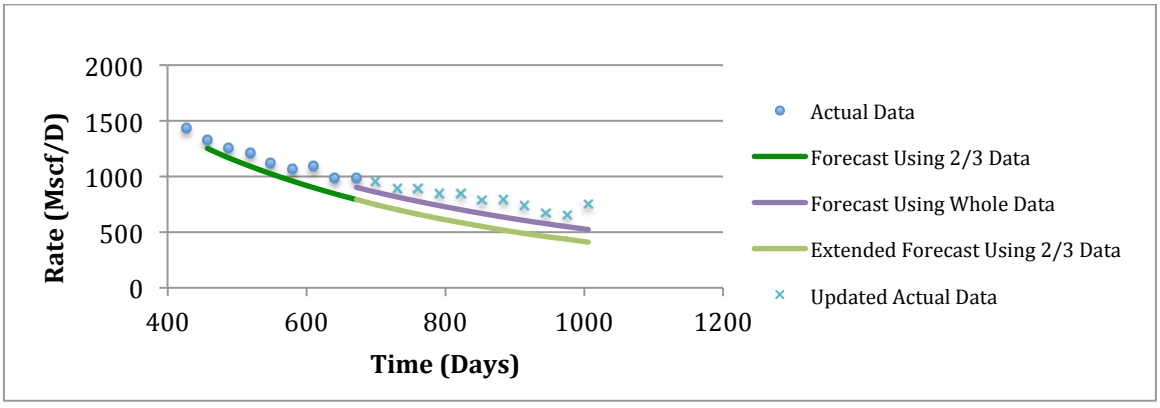

Figure II - 99: History Matching of Well#23, No.261439 Generated by PLE Model

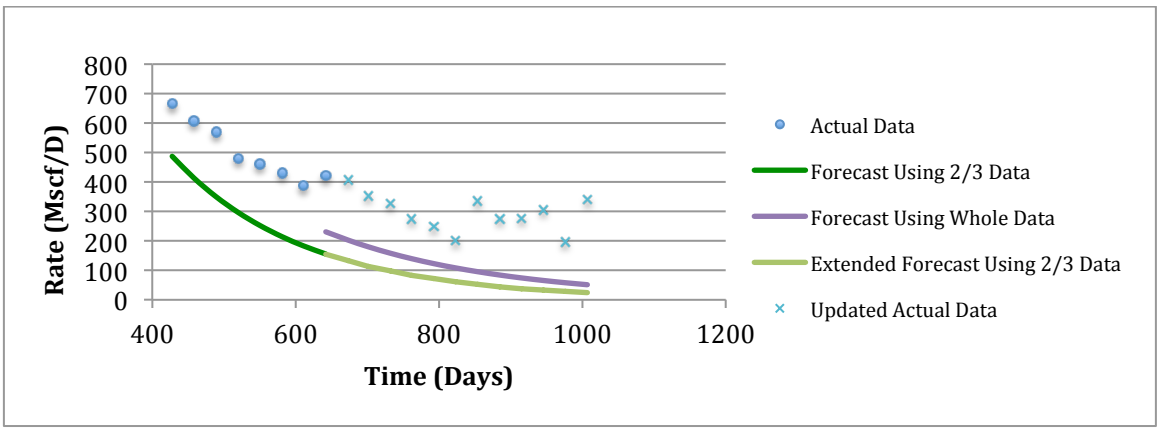

Figure II - 100: History Matching of Well#24, No.260211 Generated by PLE Model

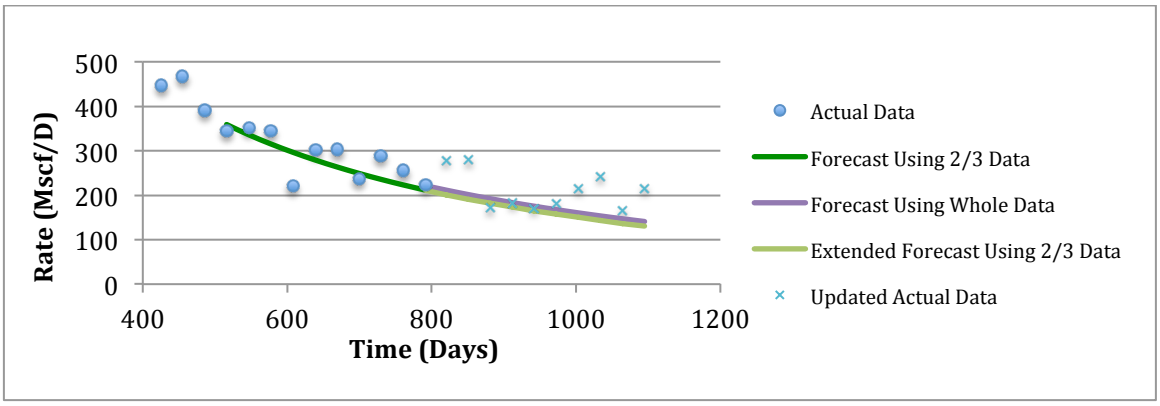

Figure II - 101: History Matching of Well#26, No.258131 Generated by PLE Model

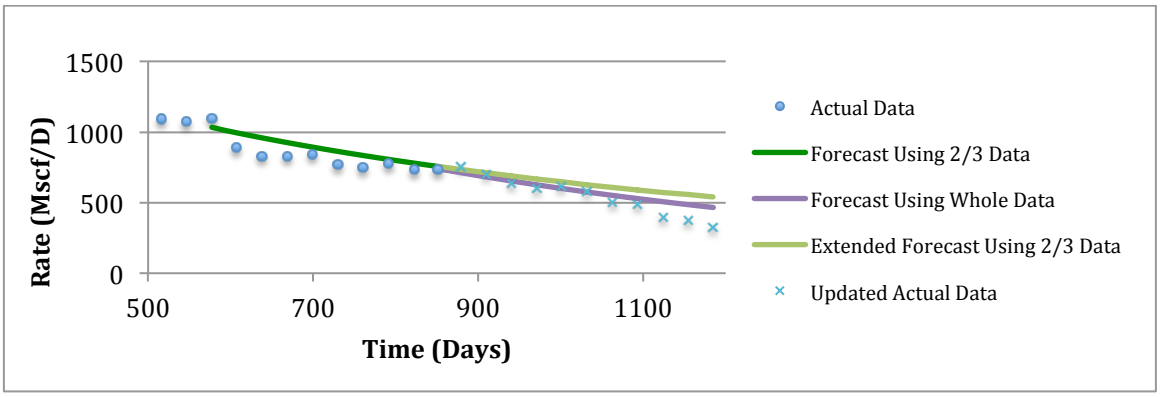

Figure II - 102: History Matching of Well#27, No.257683 Generated by PLE Model

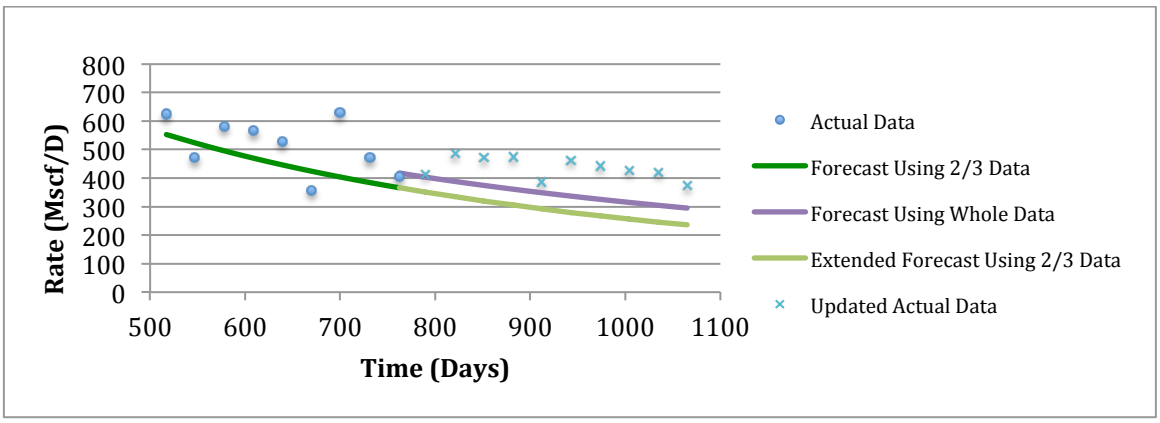

Figure II - 103: History Matching of Well#28, No.257687 Generated by PLE Model

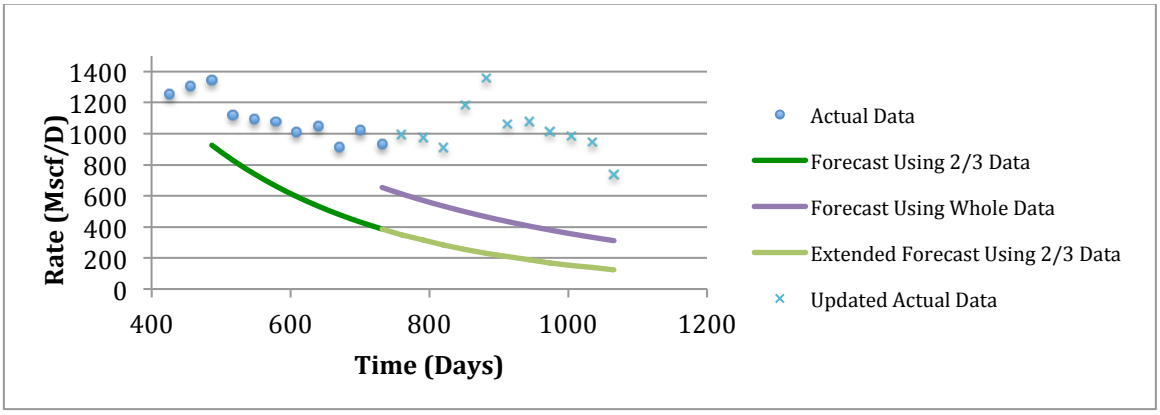

Figure II - 104: History Matching of Well#29, No.257628 Generated by PLE Model

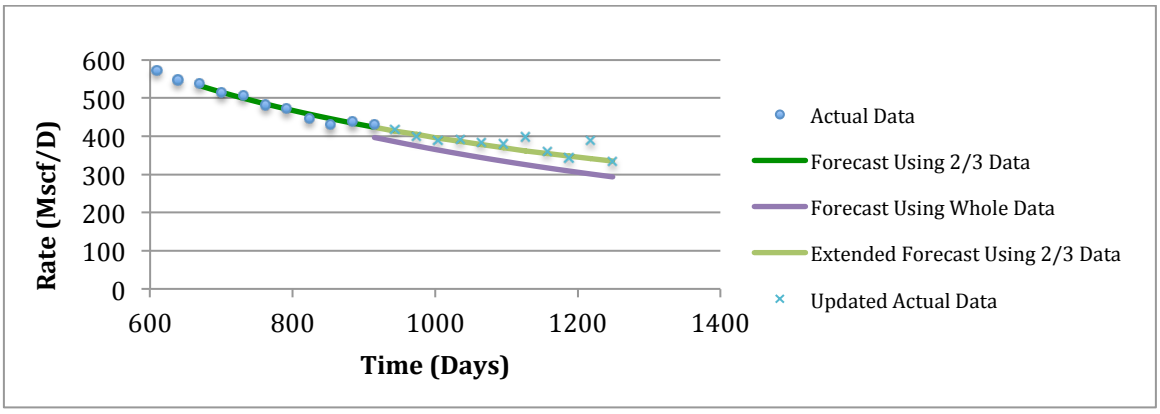

Figure II - 105: History Matching of Well#30, No.257685 Generated by PLE Model

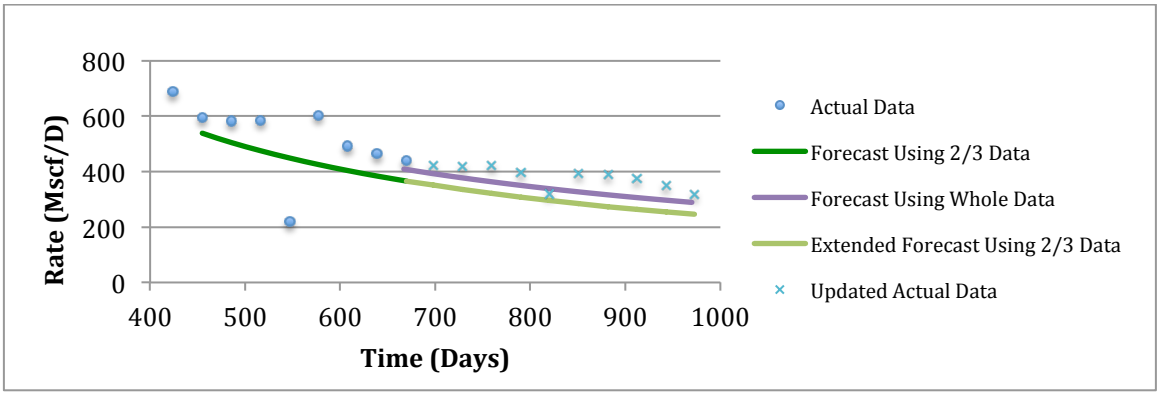

Figure II - 106: History Matching of Well#31, No.260046 Generated by PLE Model

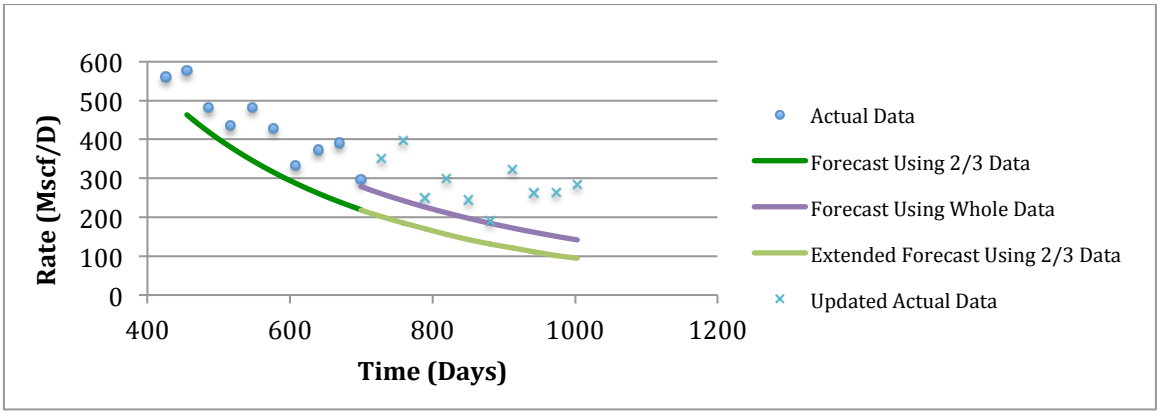

Figure II - 107: History Matching of Well#32, No.260047 Generated by PLE Model

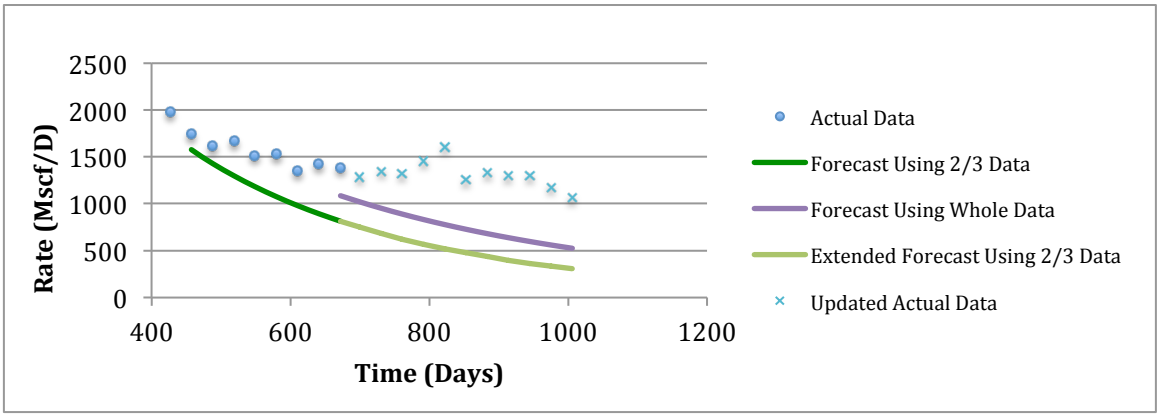

Figure II - 108: History Matching of Well#33, No.260071 Generated by PLE Model

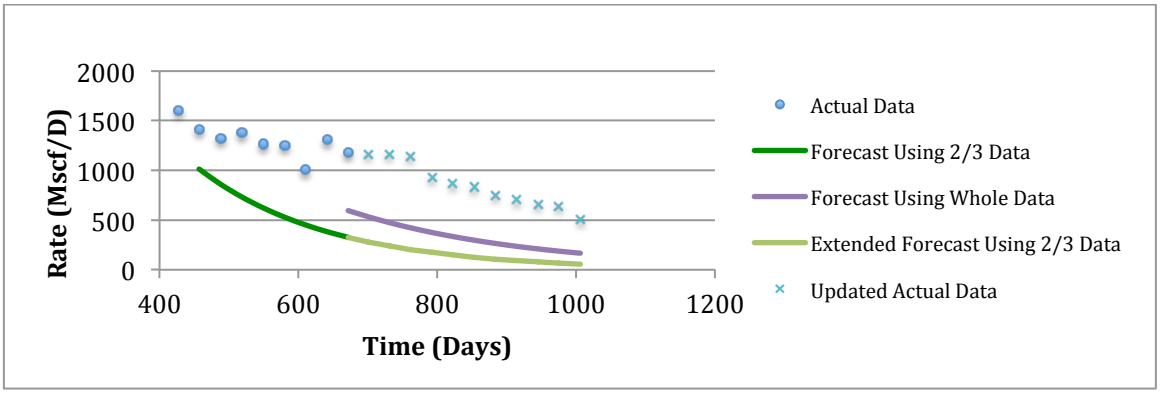

Figure II - 109: History Matching of Well#34, No.260182 Generated by PLE Model

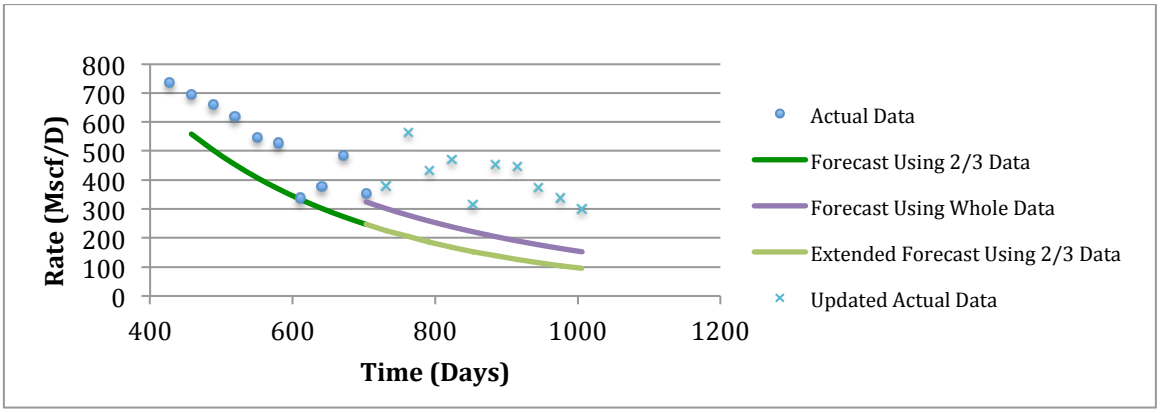

Figure II - 110: History Matching of Well#35, No.261381 Generated by PLE Model

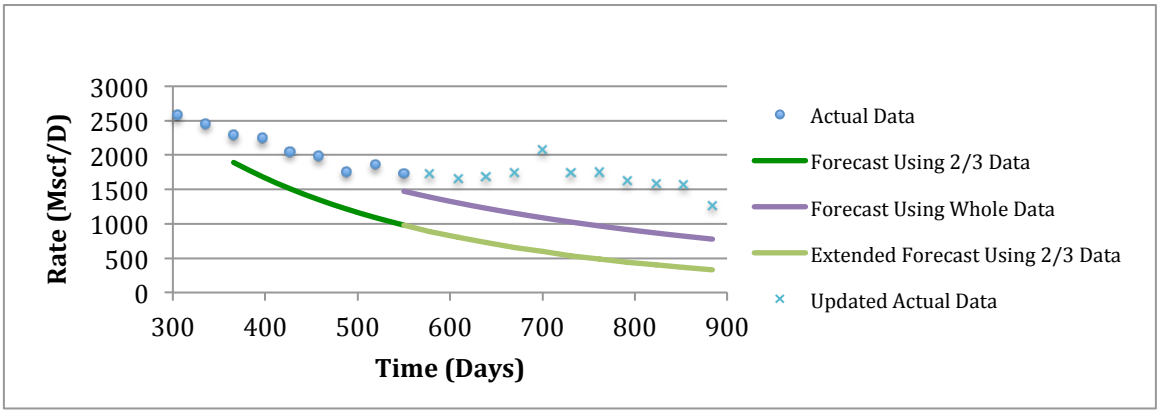

Figure II - 111: History Matching of Well#36, No.260379 Generated by PLE Model

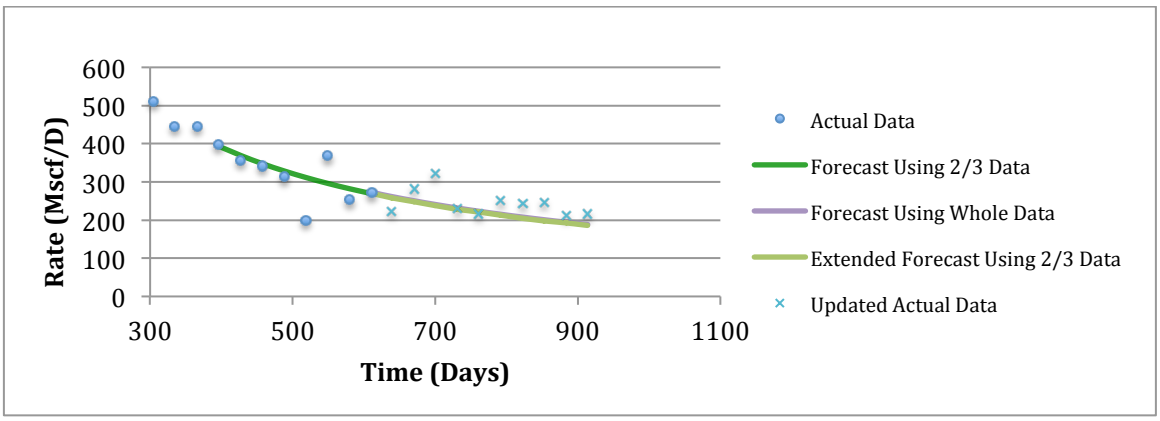

Figure II - 112: History Matching of Well#37, No.261320 Generated by PLE Model

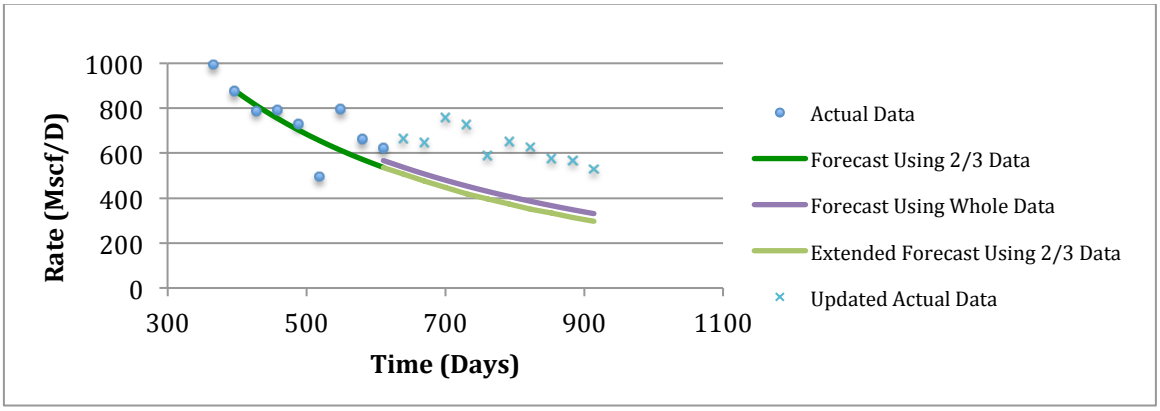

Figure II - 113: History Matching of Well#38, No.261632 Generated by PLE Model

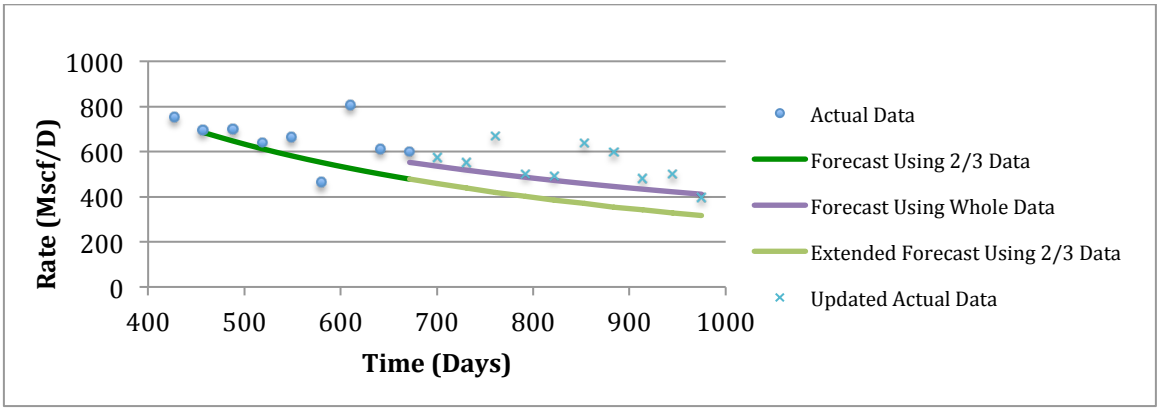

Figure II - 114: History Matching of Well#39, No.261443 Generated by PLE Model

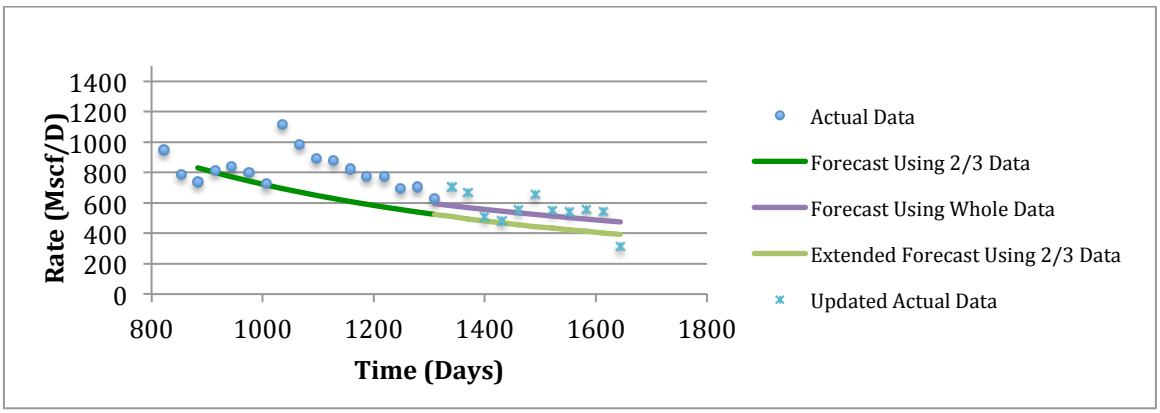

Figure II - 115: History Matching of Well#1, No.251105 Generated by LGA Model

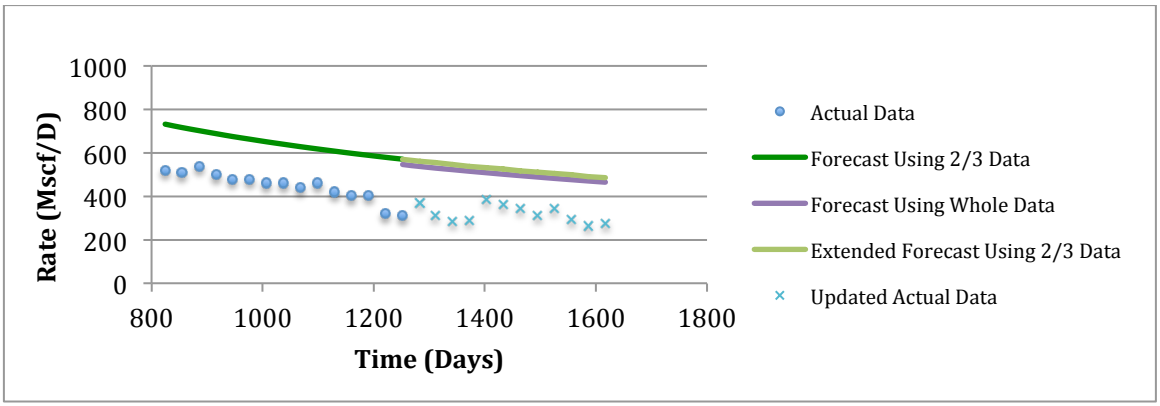

Figure II - 116: History Matching of Well#2, No.252769 Generated by LGA Model

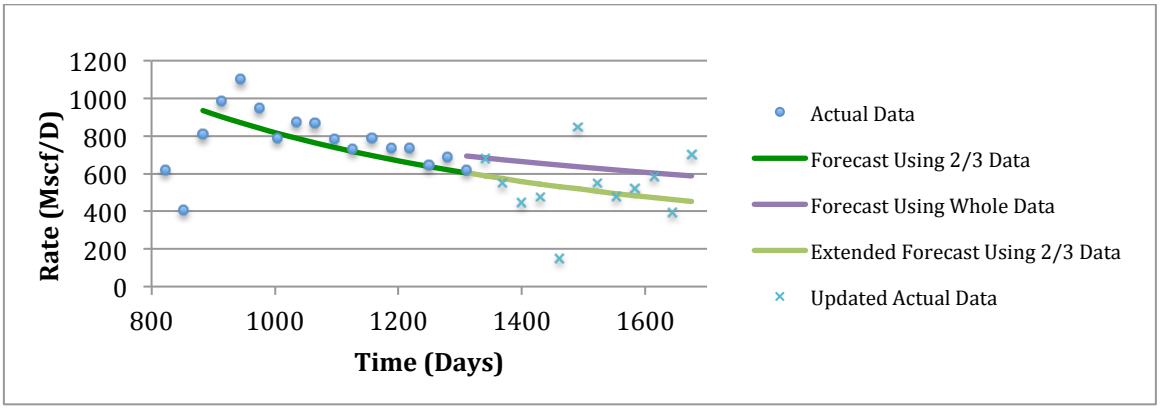

Figure II - 117: History Matching of Well#3, No.251816 Generated by LGA Model

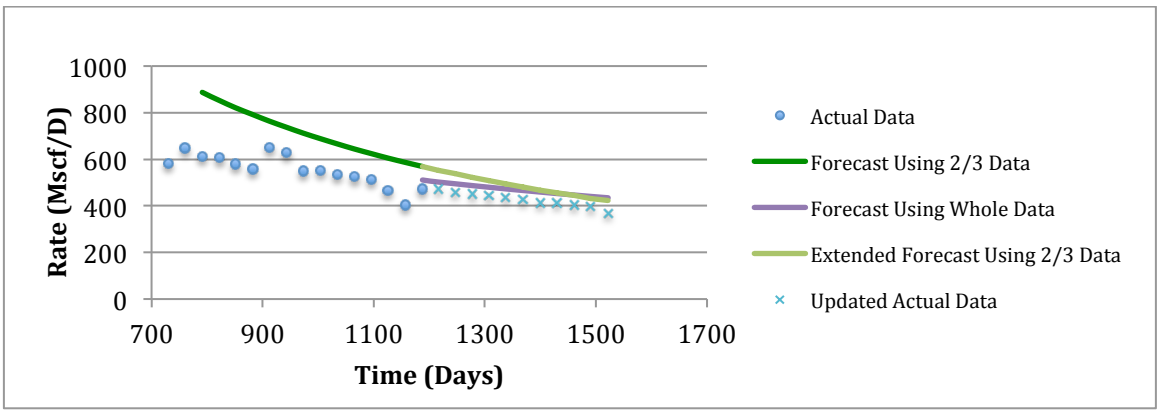

Figure II - 118: History Matching of Well#4, No.251773 Generated by LGA Model

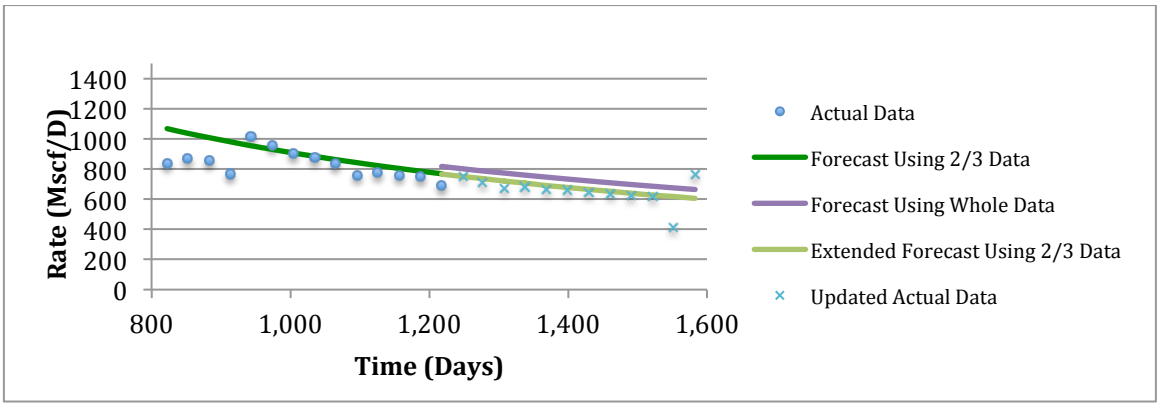

Figure II - 119: History Matching of Well#5, No.251817 Generated by LGA Model

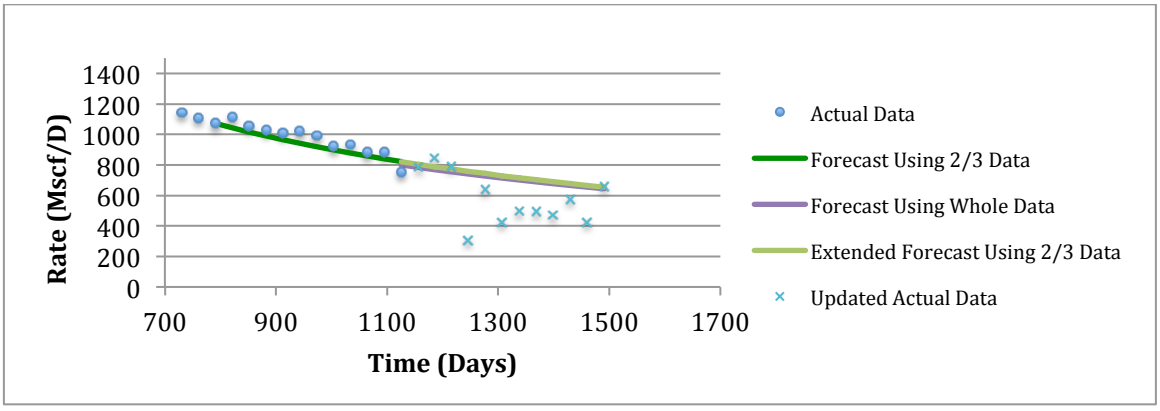

Figure II - 120: History Matching of Well#6, No.255994 Generated by LGA Model

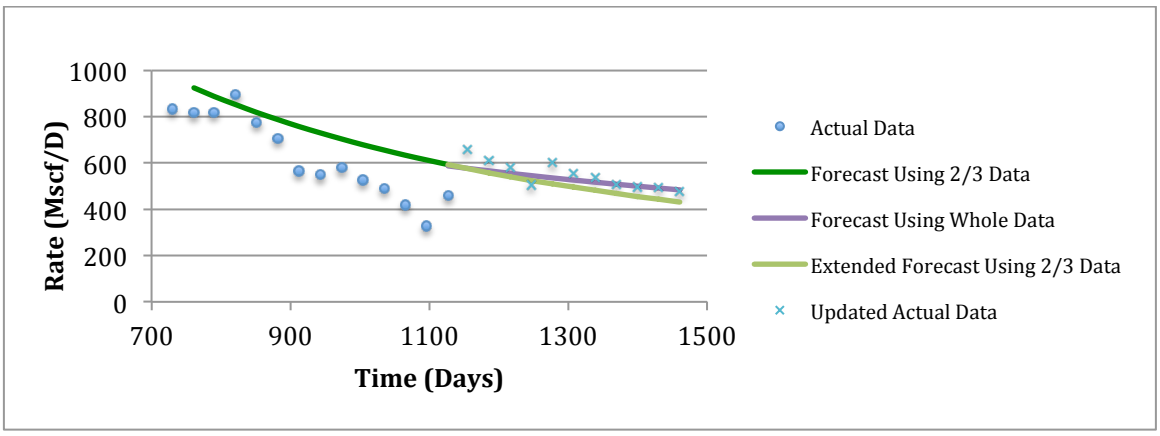

Figure II - 121: History Matching of Well#7, No.255435 Generated by LGA Model

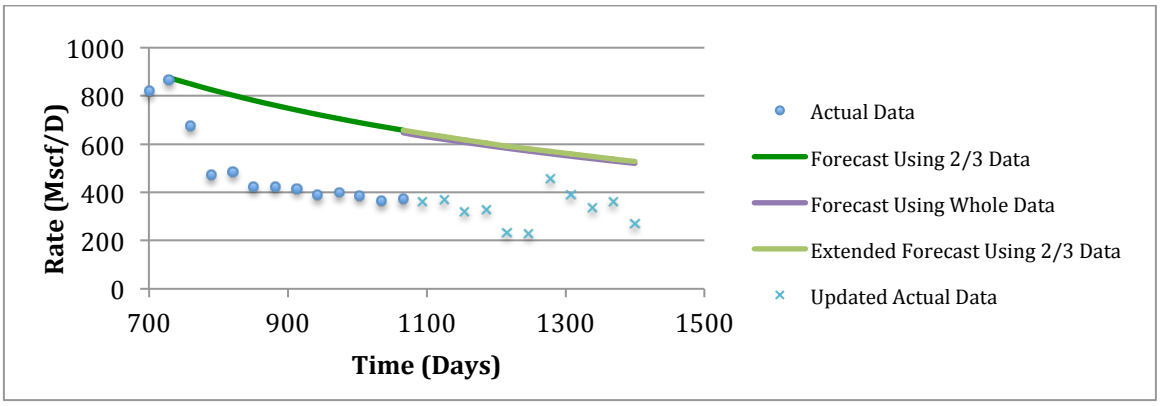

Figure II - 122: History Matching of Well#8, No.255730 Generated by LGA Model

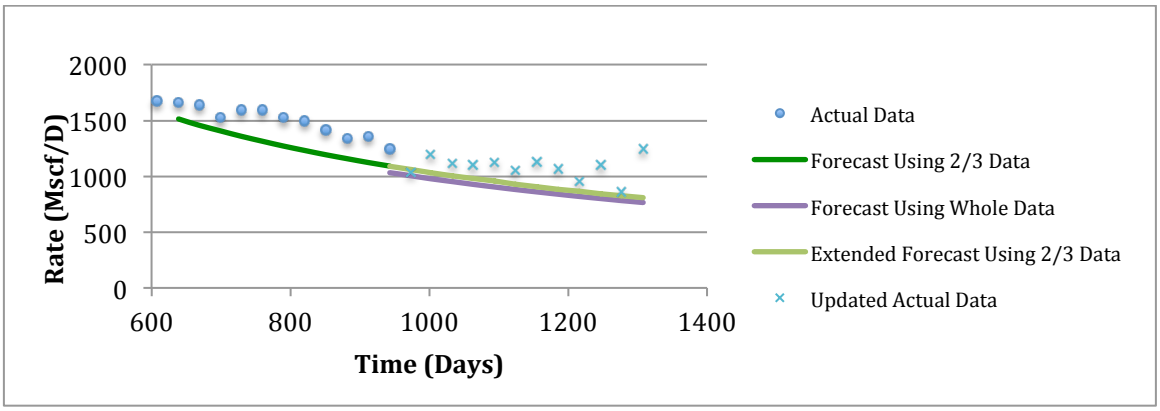

Figure II - 123: History Matching of Well#9, No.254447 Generated by LGA Model

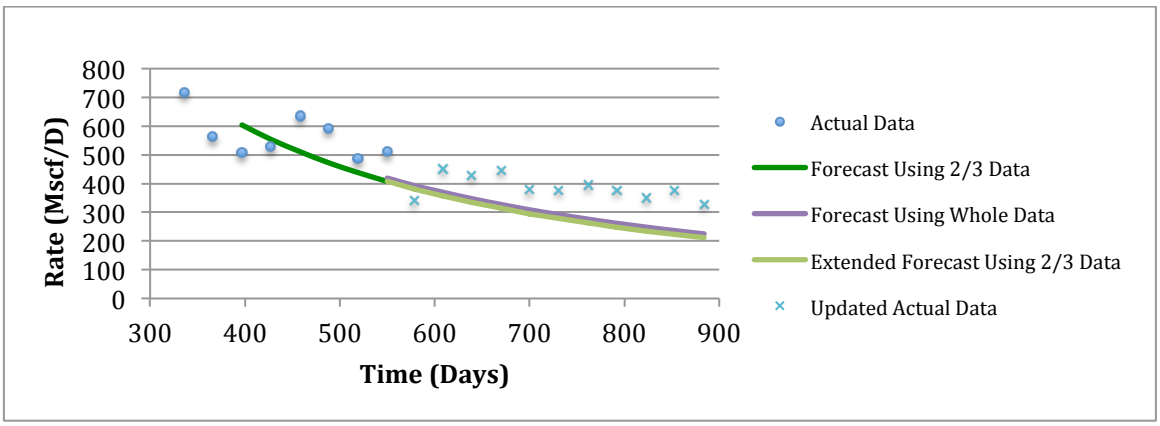

Figure II - 124: History Matching of Well#10, No.263658 Generated by LGA Model

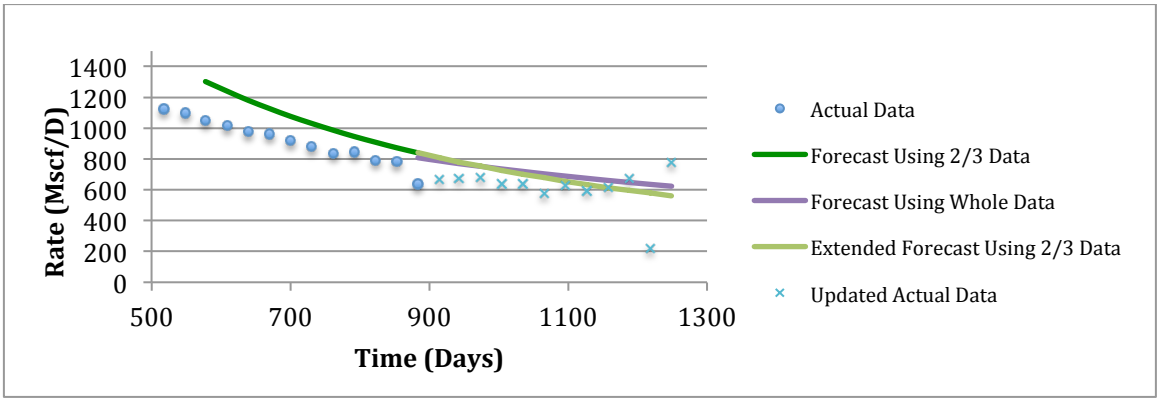

Figure II - 125: History Matching of Well#11, No.258106 Generated by LGA Model

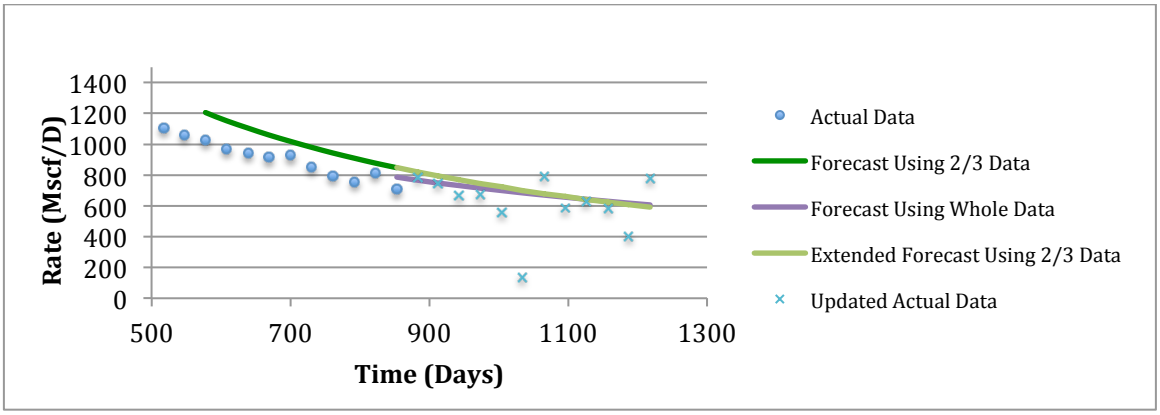

Figure II - 126: History Matching of Well#12, No.258900 Generated by LGA Model

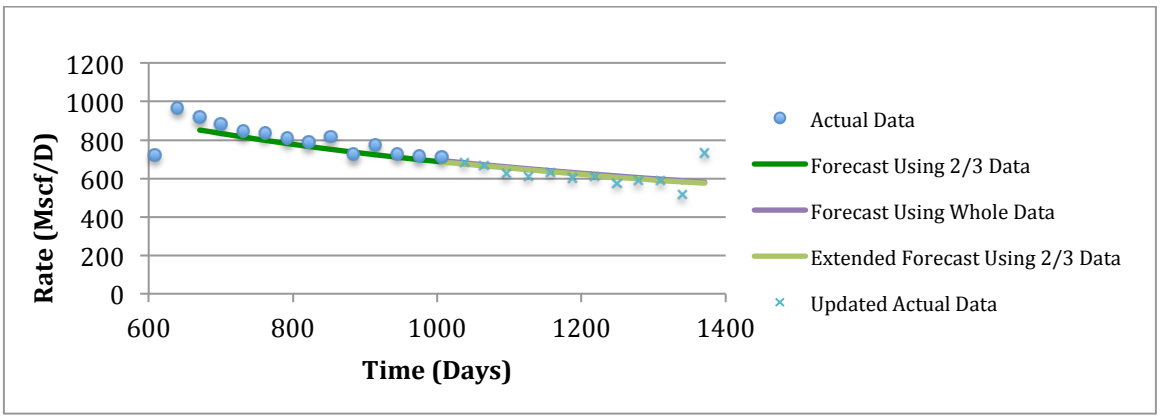

Figure II - 127: History Matching of Well#13, No.257263 Generated by LGA Model

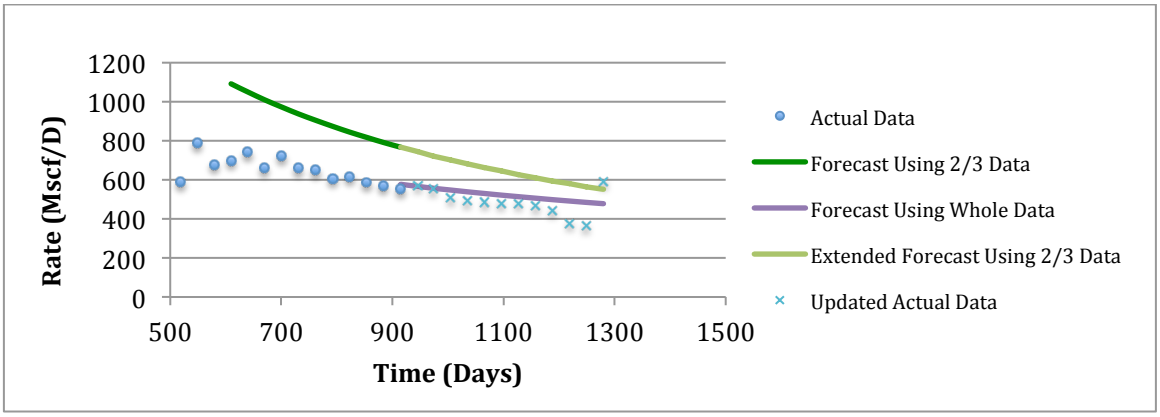

Figure II - 128: History Matching of Well#14, No.257862 Generated by LGA Model

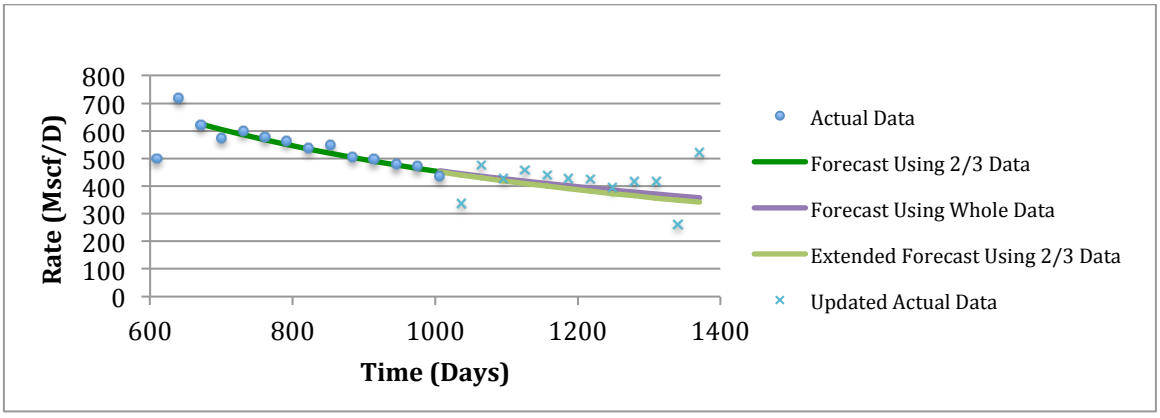

Figure II - 129: History Matching of Well#15, No.254843 Generated by LGA Model

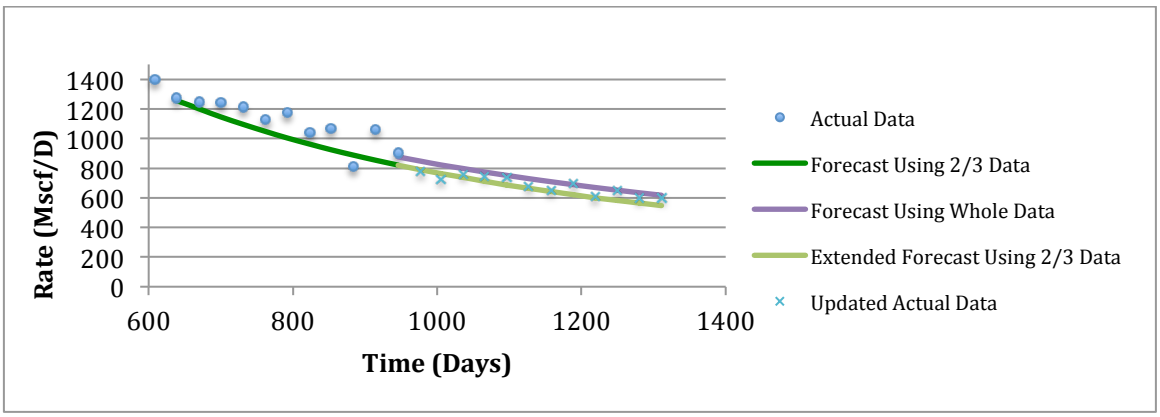

Figure II - 130: History Matching of Well#16, No.258036 Generated by LGA Model

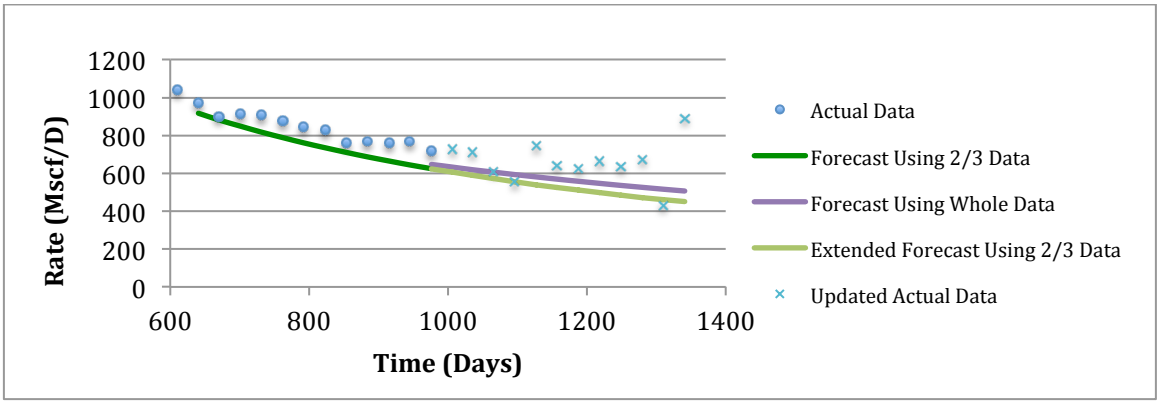

Figure II - 131: History Matching of Well#17, No.257955 Generated by LGA Model

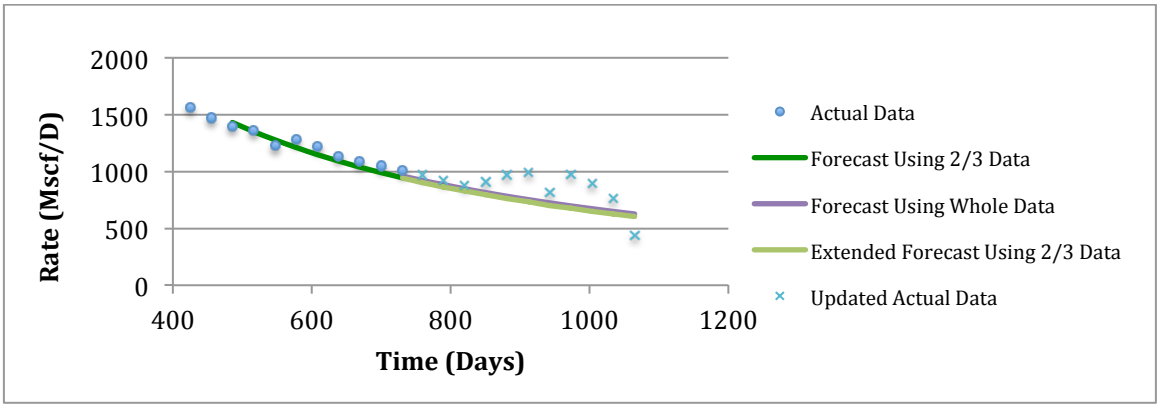

Figure II - 132: History Matching of Well#18, No.259883 Generated by LGA Model

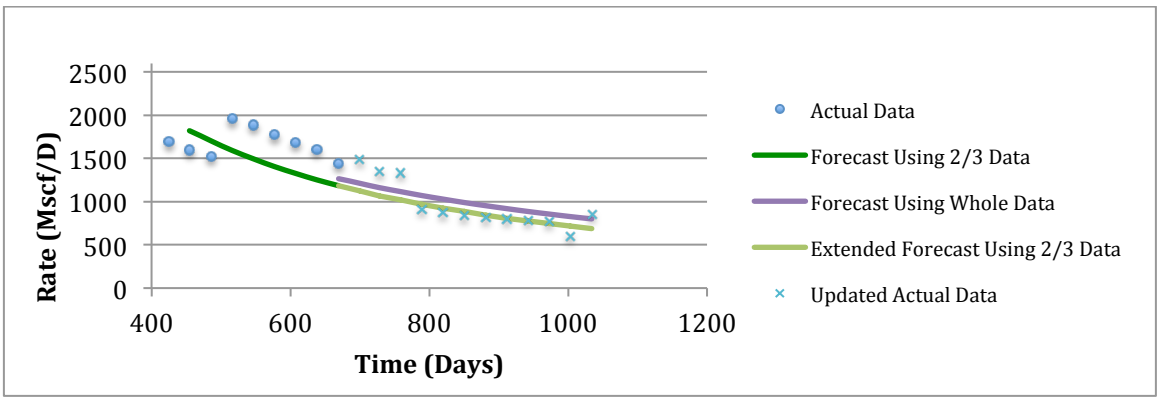

Figure II - 133: History Matching of Well#19, No.259429 Generated by LGA Model

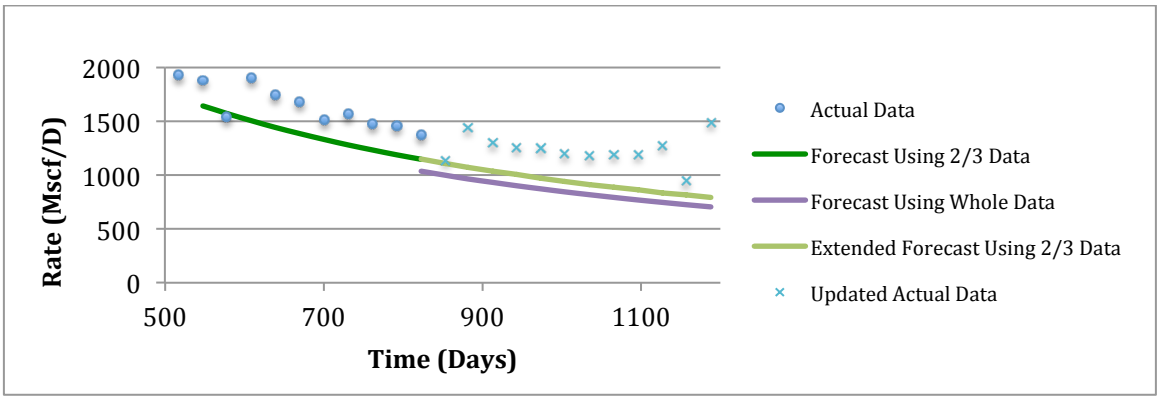

Figure II - 134: History Matching of Well#20, No.258903 Generated by LGA Model

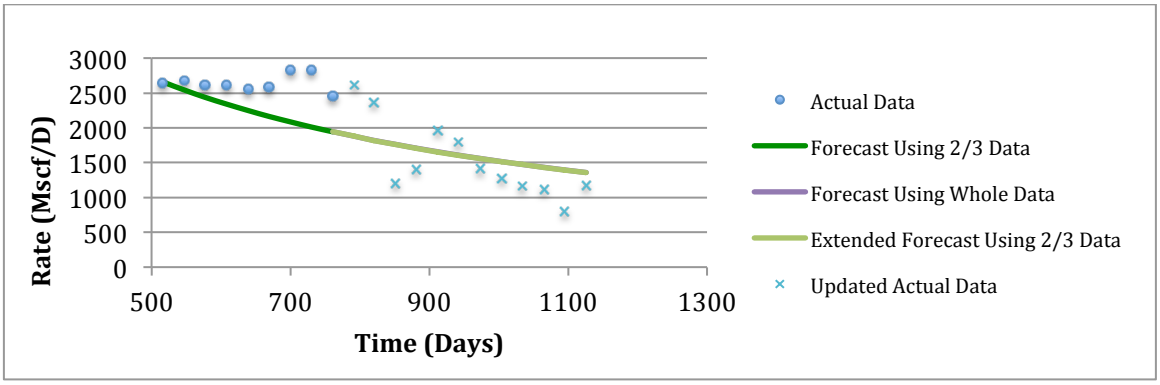

Figure II - 135: History Matching of Well#21, No.260129 Generated by LGA Model

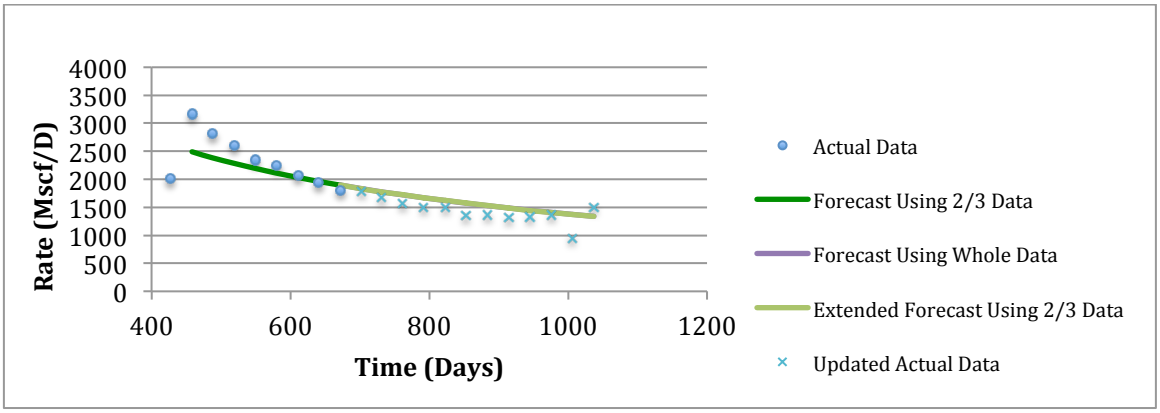

Figure II - 136: History Matching of Well#22, No.260720 Generated by LGA Model

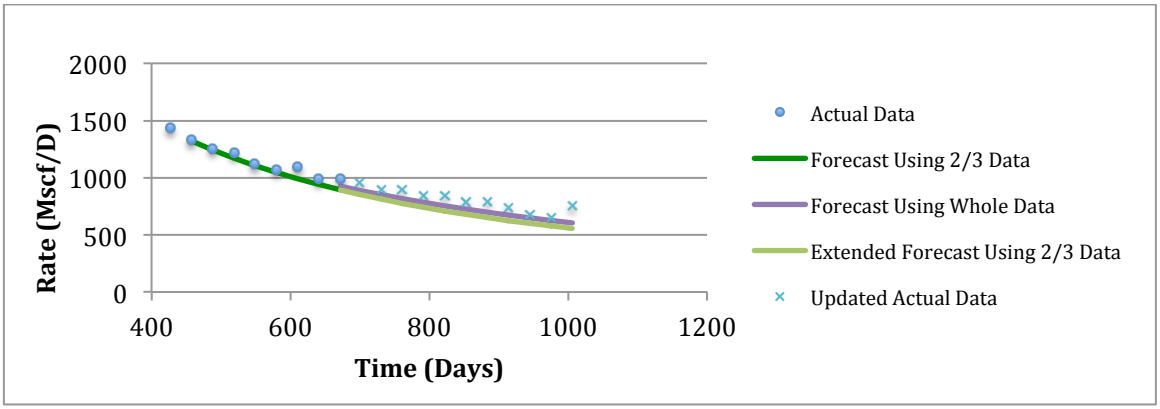

Figure II - 137: History Matching of Well#23, No.261439 Generated by LGA Model

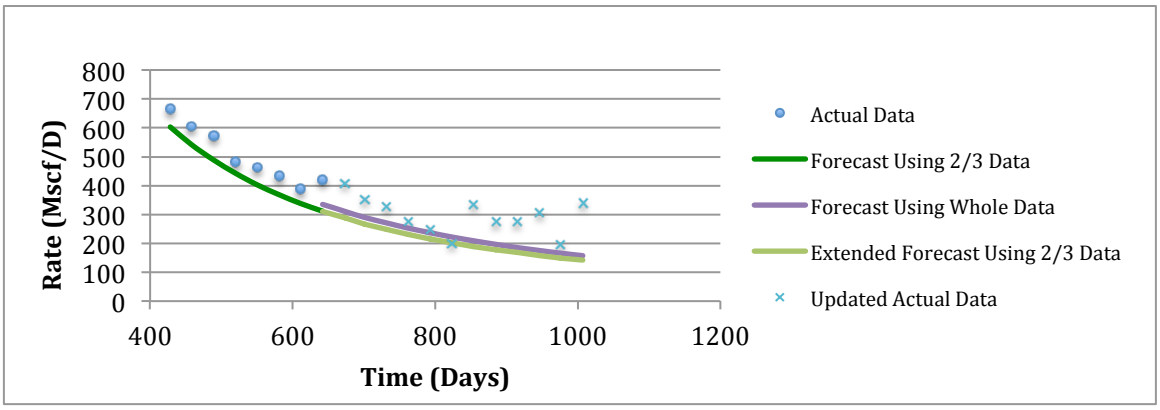

Figure II - 138: History Matching of Well#24, No.260211 Generated by LGA Model

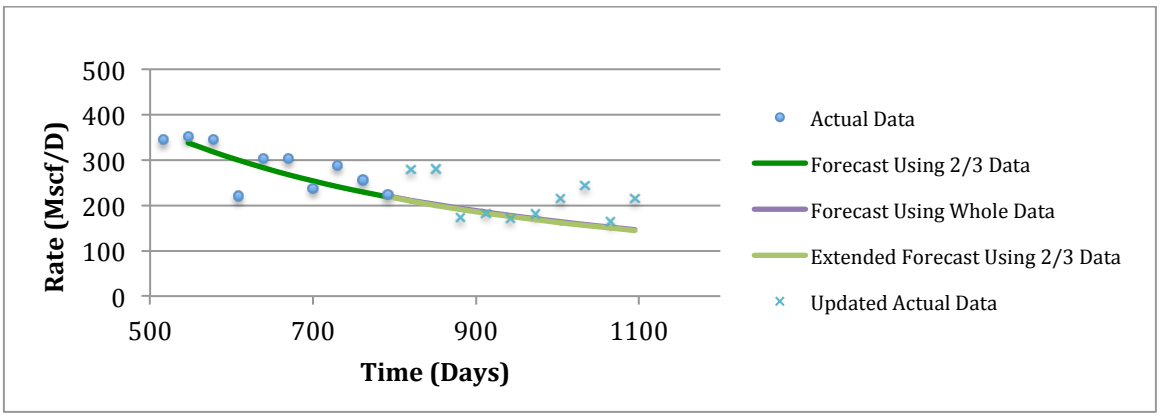

Figure II - 139: History Matching of Well#26, No.258131 Generated by LGA Model

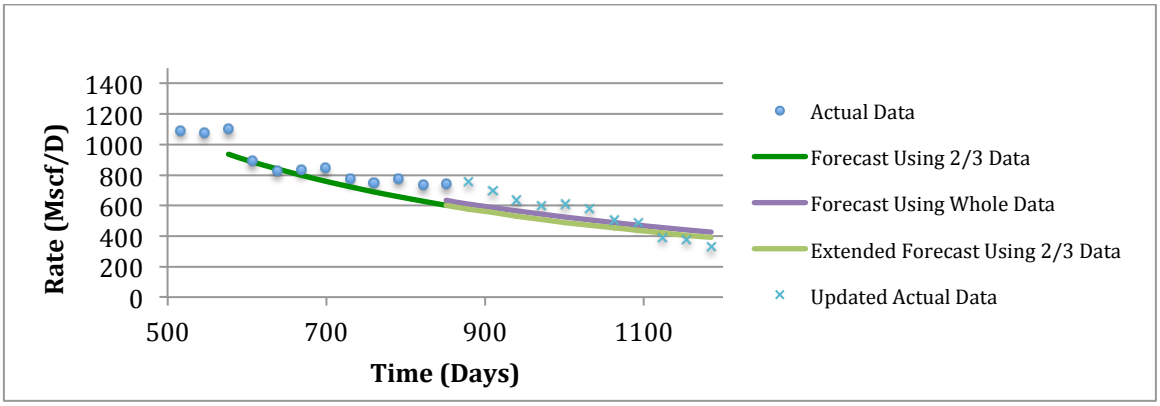

Figure II - 140: History Matching of Well#27, No.257683 Generated by LGA Model

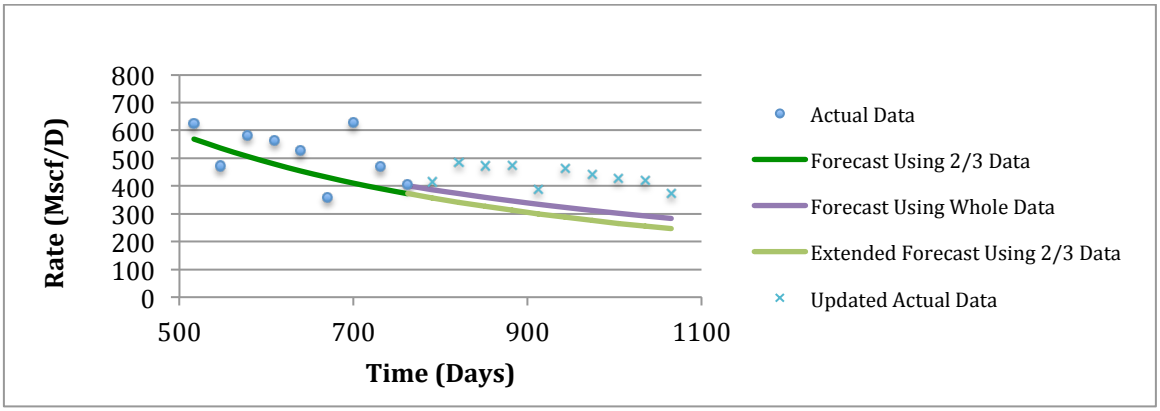

Figure II - 141: History Matching of Well#28, No.257687 Generated by LGA Model

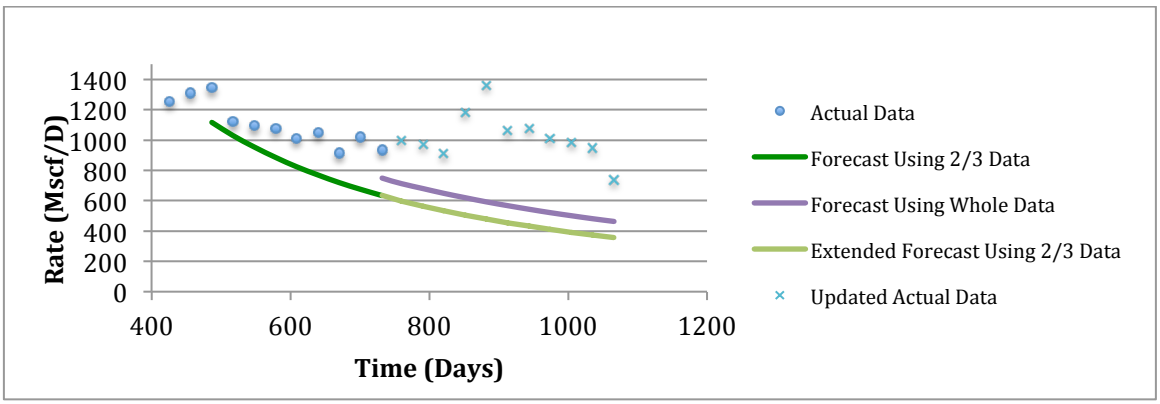

Figure II - 142: History Matching of Well#29, No.257628 Generated by LGA Model

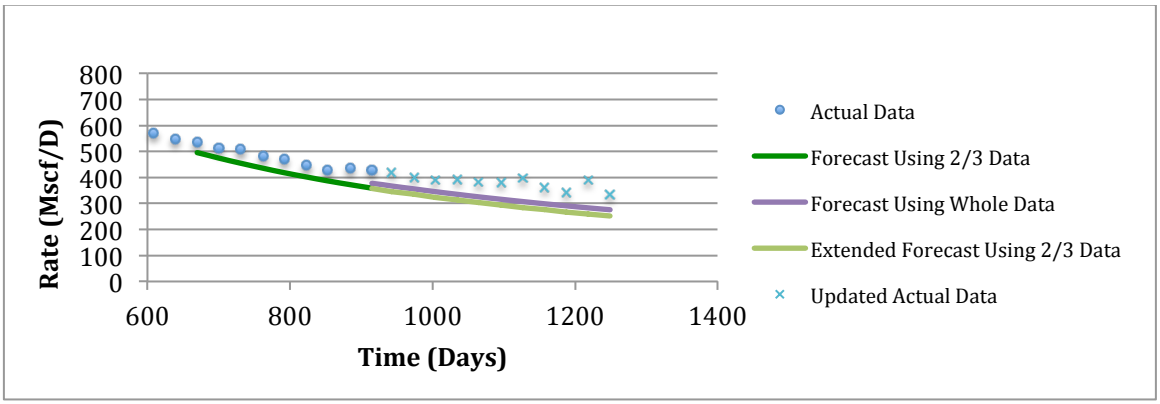

Figure II - 143: History Matching of Well#30, No.257685 Generated by LGA Model

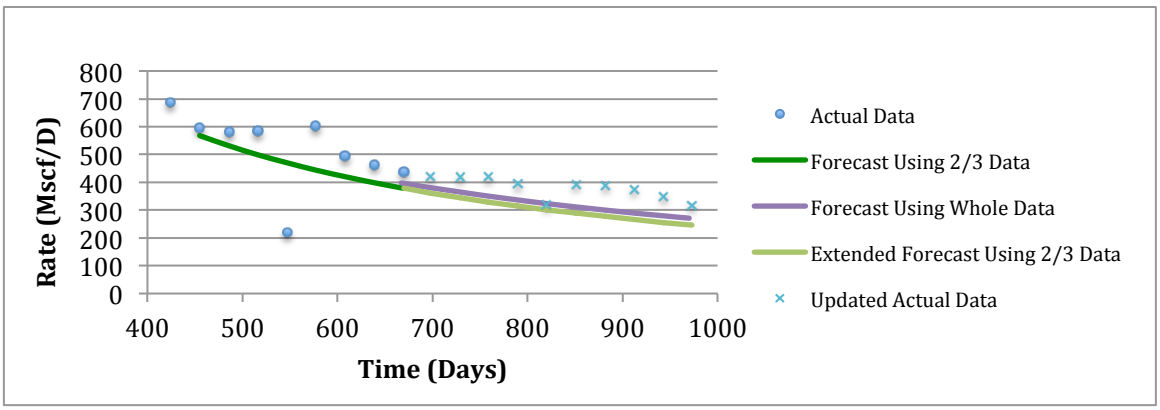

Figure II - 144: History Matching of Well#31, No.260046 Generated by LGA Model

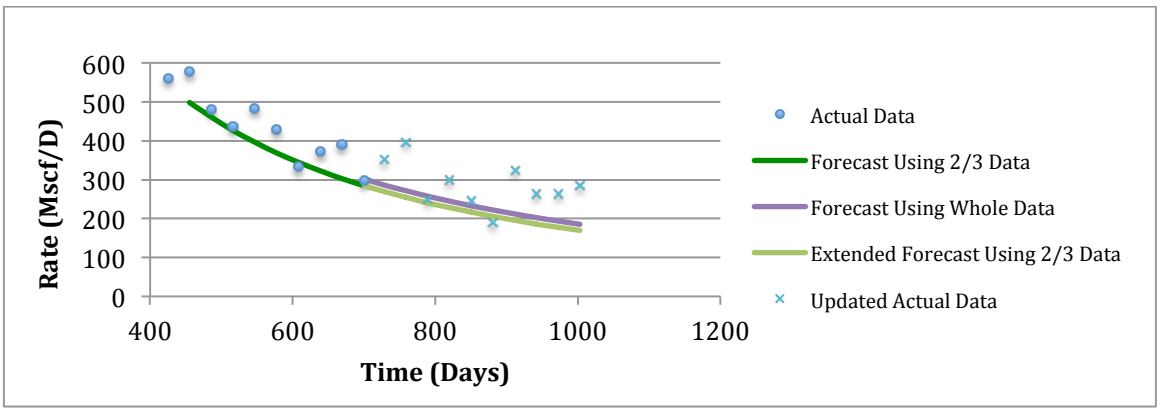

Figure II - 145: History Matching of Well#32, No.260047 Generated by LGA Model

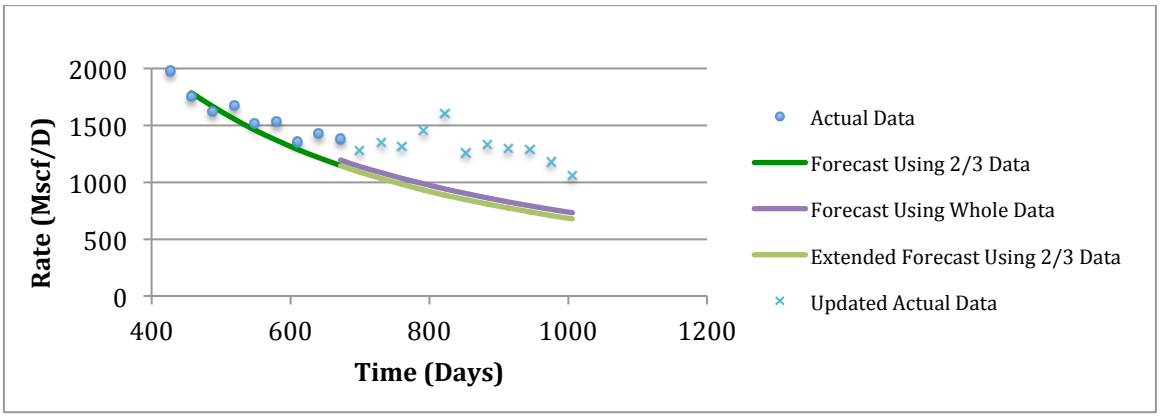

Figure II - 146: History Matching of Well#33, No.260071 Generated by LGA Model

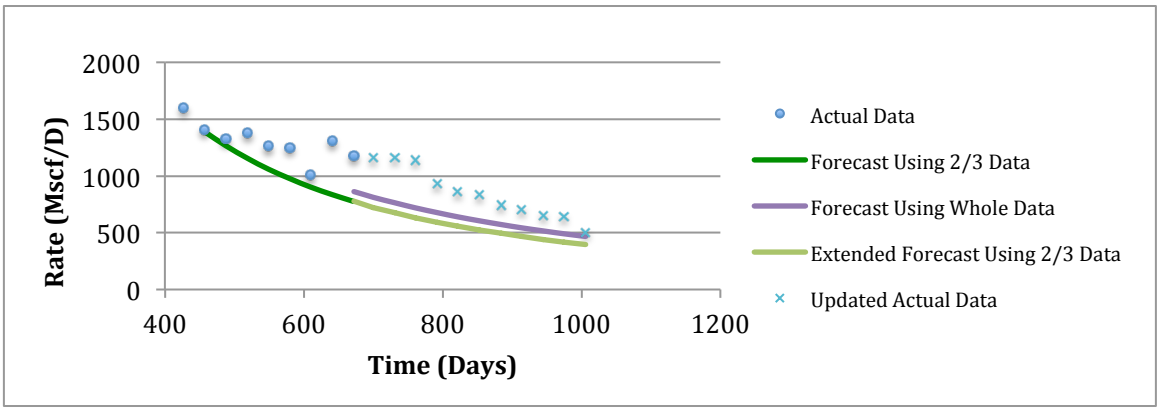

Figure II - 147: History Matching of Well#34, No.260182 Generated by LGA Model

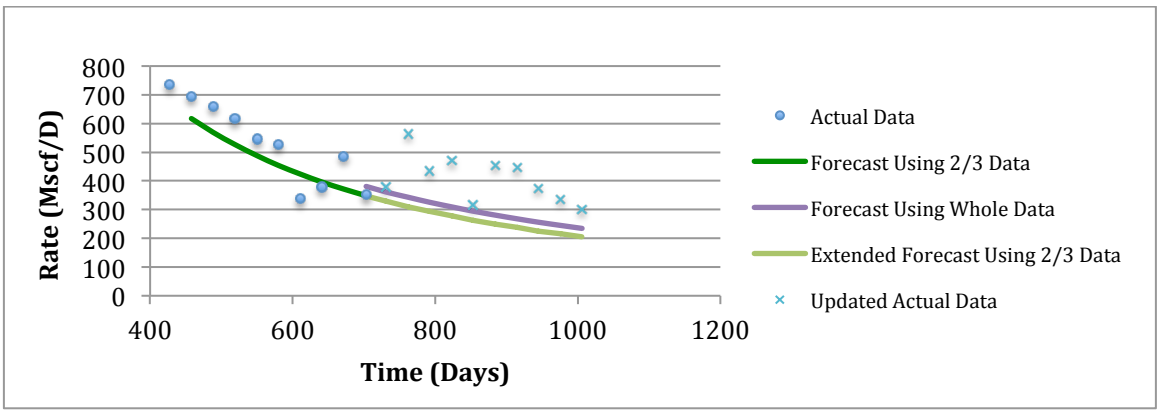

Figure II - 148: History Matching of Well#35, No.261381 Generated by LGA Model

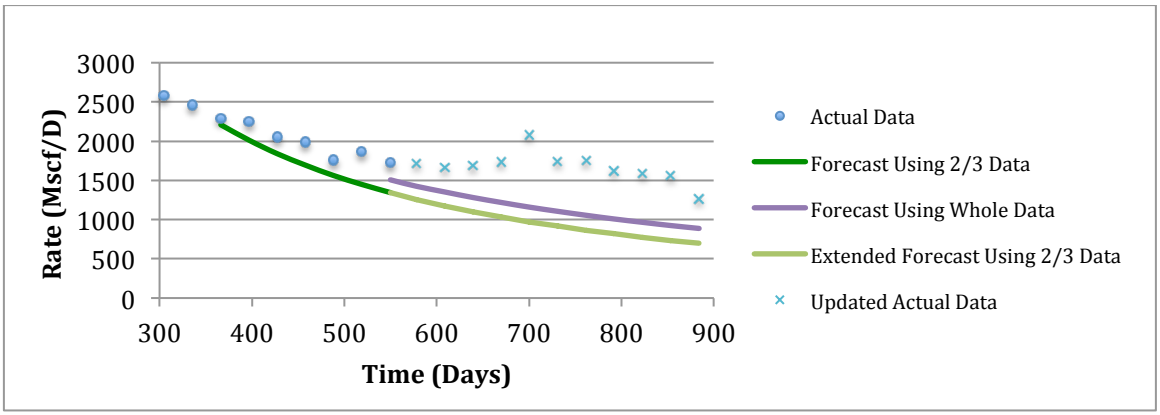

Figure II - 149: History Matching of Well#36, No.260379 Generated by LGA Model

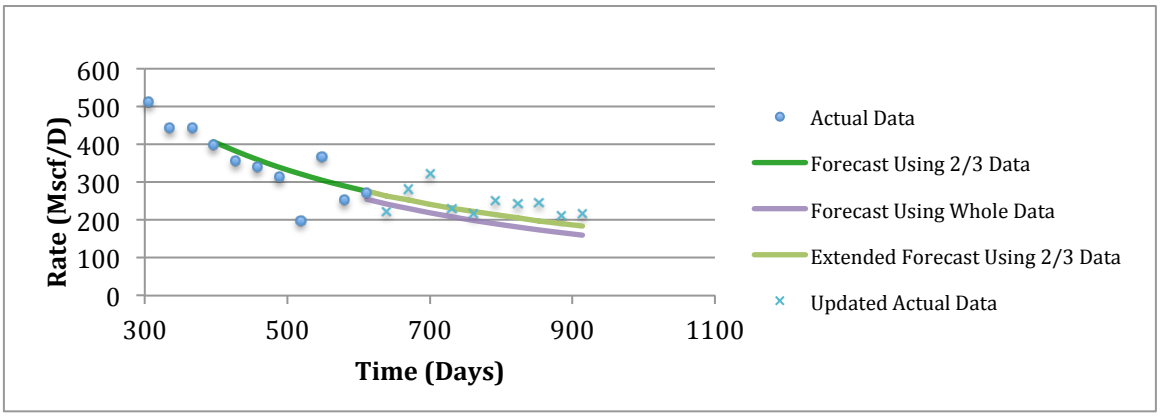

Figure II - 150: History Matching of Well#37, No.261320 Generated by LGA Model

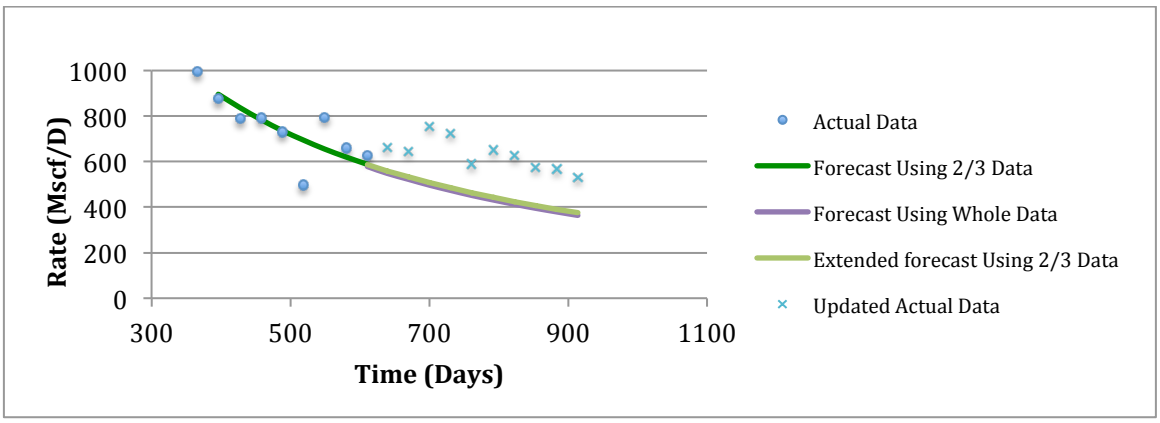

Figure II - 151: History Matching of Well#38, No.261632 Generated by LGA Model

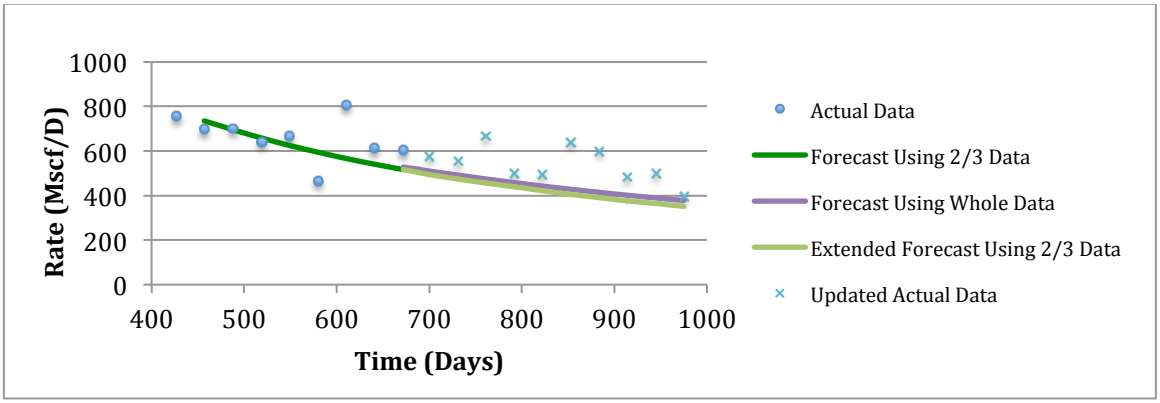

Figure II - 152: History Matching of Well#39, No.261443 Generated by LGA Model

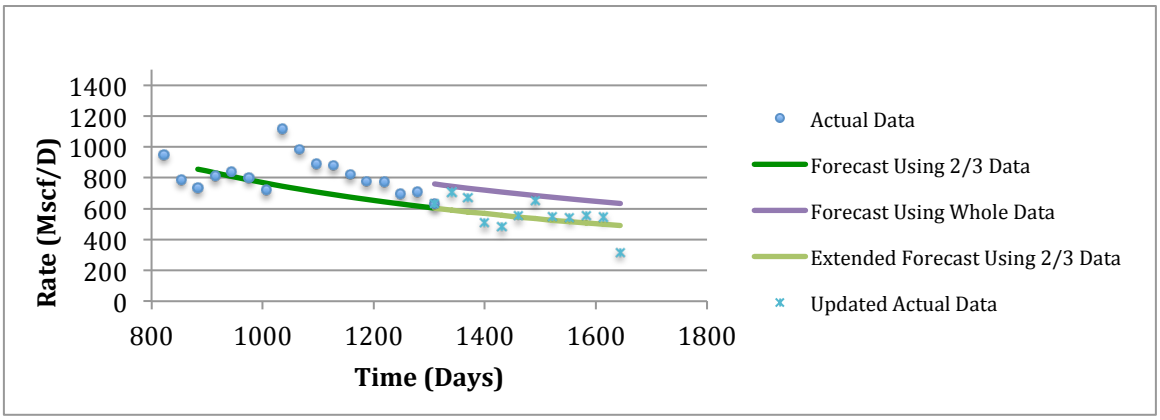

Figure II - 153: History Matching of Well#1, No.251105 Generated by Duong's Model

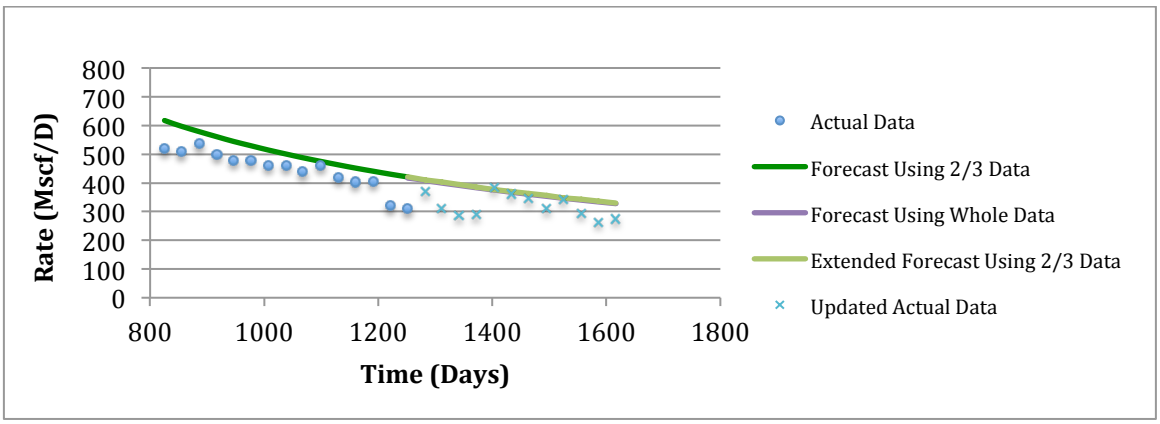

Figure II - 154: History Matching of Well#2, No.252769 Generated by Duong's Model

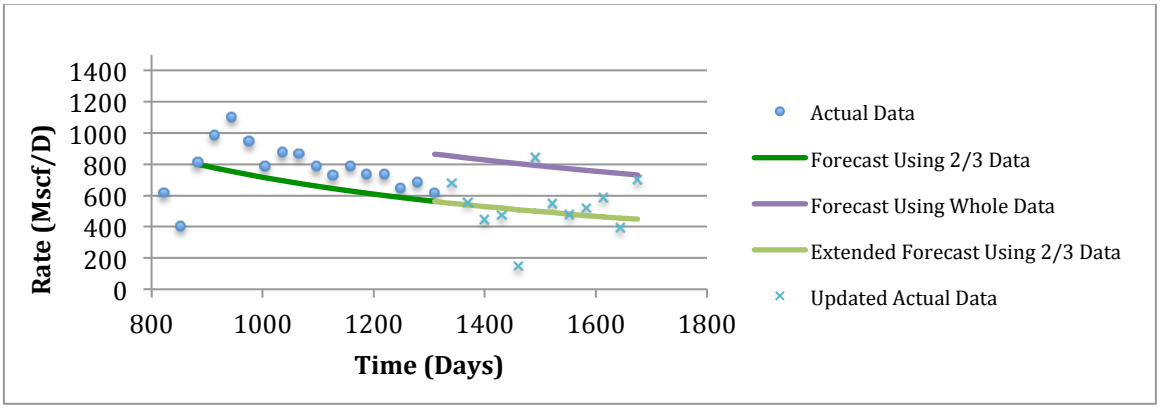

Figure II - 155: History Matching of Well#3, No.251816 Generated by Duong's Model

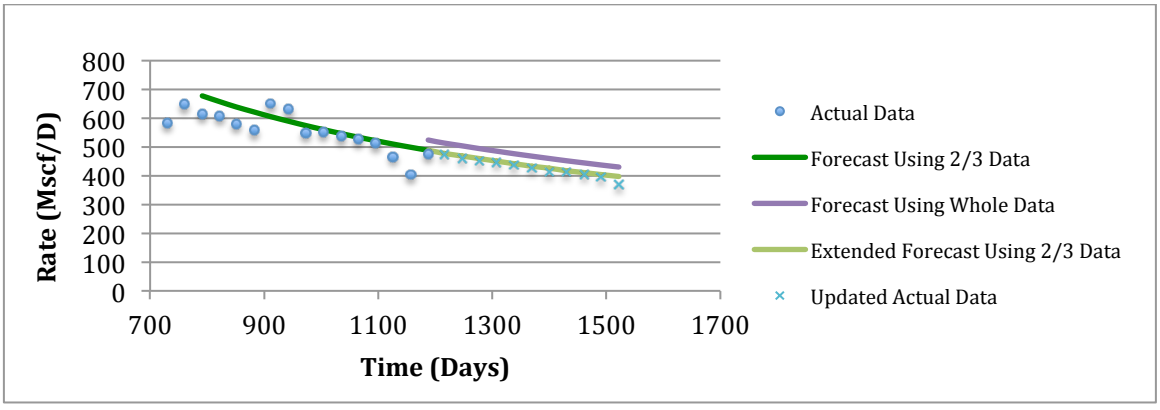

Figure II - 156: History Matching of Well#4, No.251773 Generated by Duong's Model

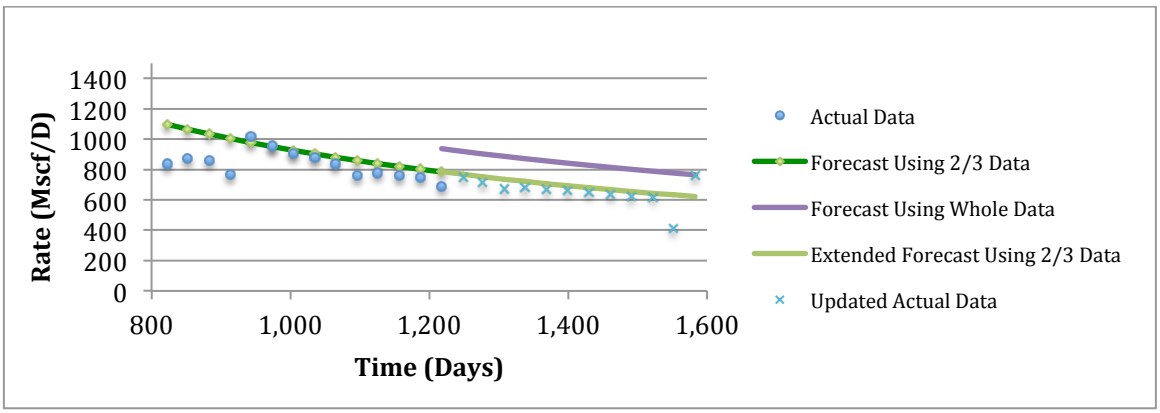

Figure II - 157: History Matching of Well#5, No.251817 Generated by Duong's Model

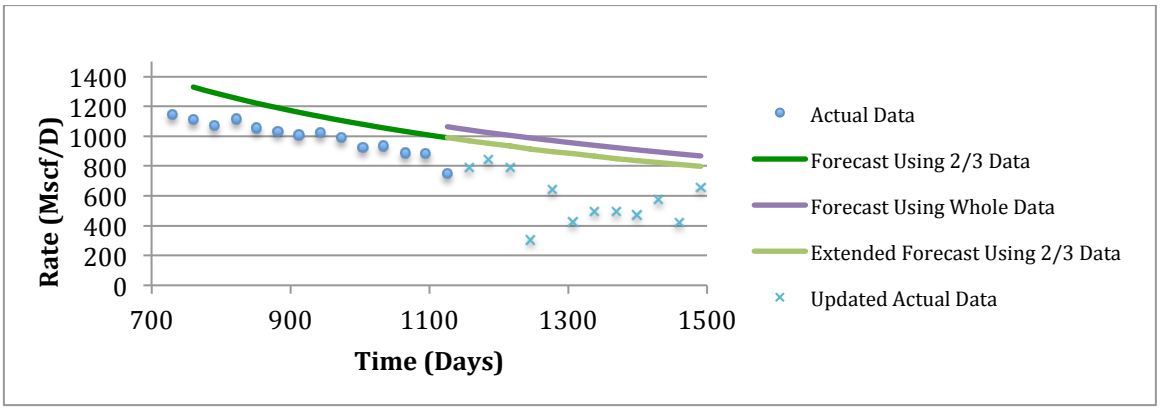

Figure II - 158: History Matching of Well#6, No.255994 Generated by Duong's Model

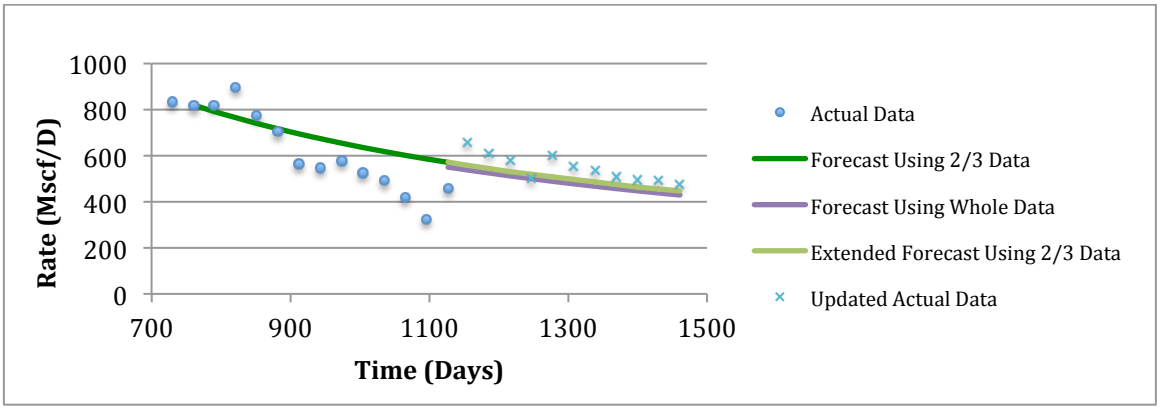

Figure II - 159: History Matching of Well#7, No.255435 Generated by Duong's Model

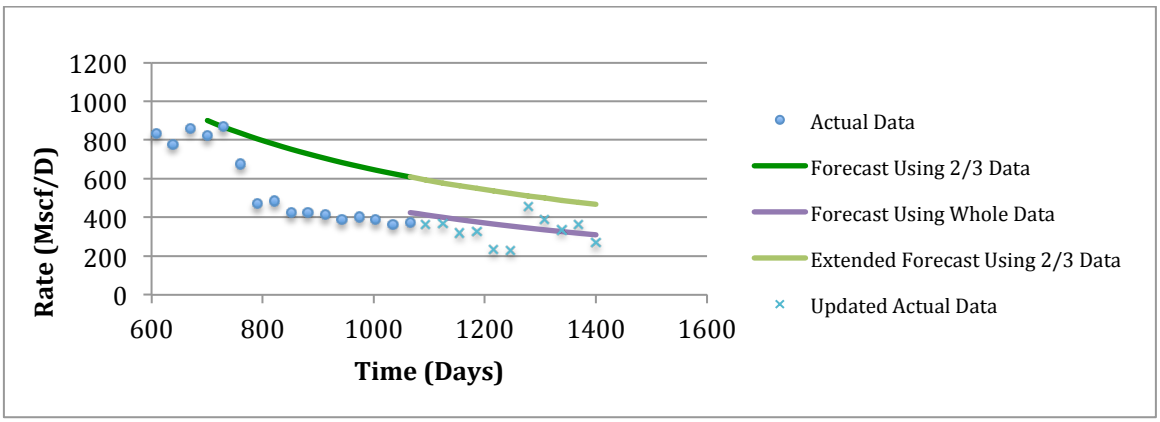

Figure II - 160: History Matching of Well#8, No.255730 Generated by Duong's Model

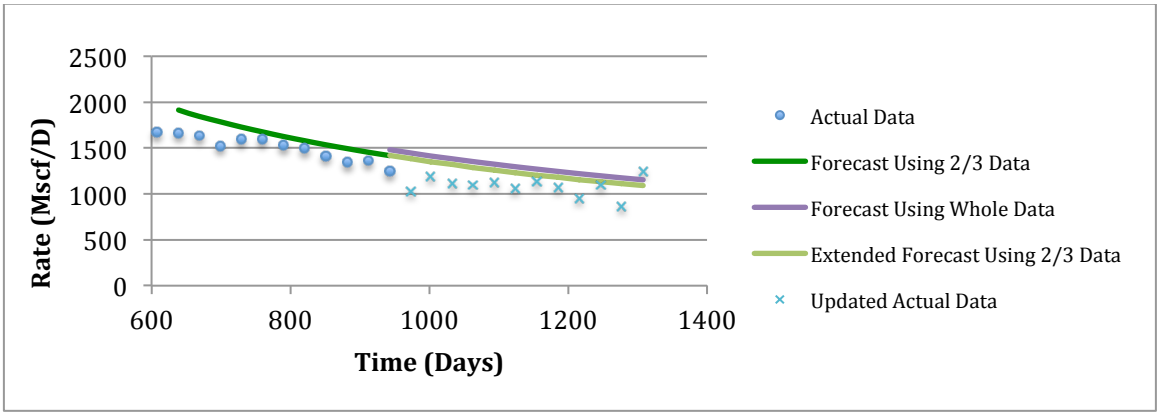

Figure II - 161: History Matching of Well#9, No.254447 Generated by Duong's Model

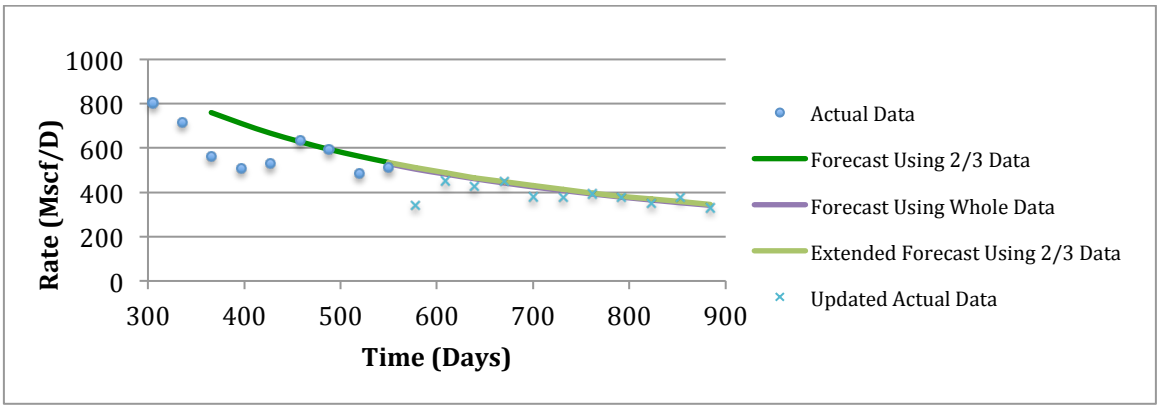

Figure II - 162: History Matching of Well#10, No.263658 Generated by Duong's Model

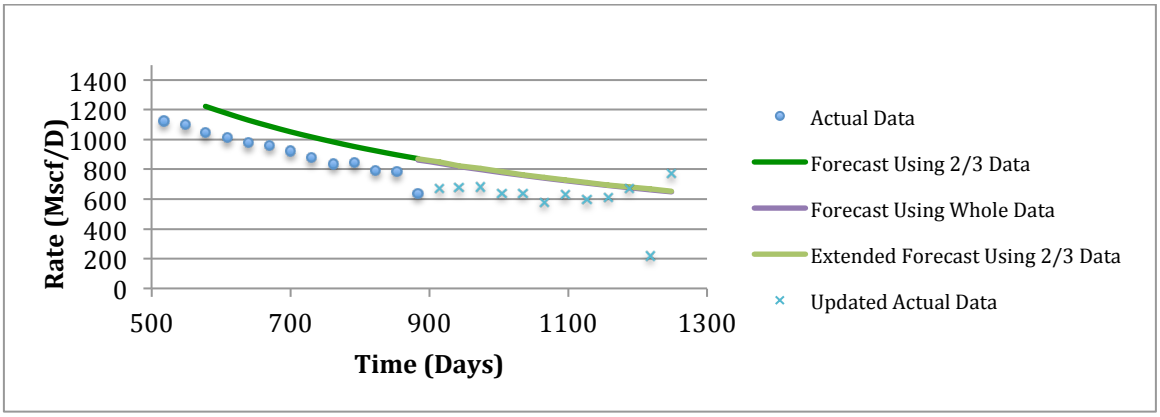

Figure II - 163: History Matching of Well#11, No.258106 Generated by Duong's Model

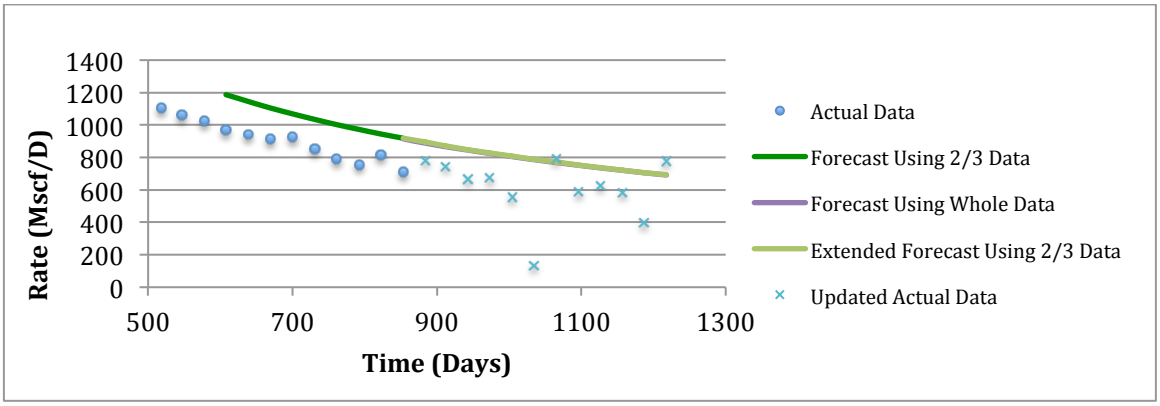

Figure II - 164: History Matching of Well#12, No.258900 Generated by Duong's Model

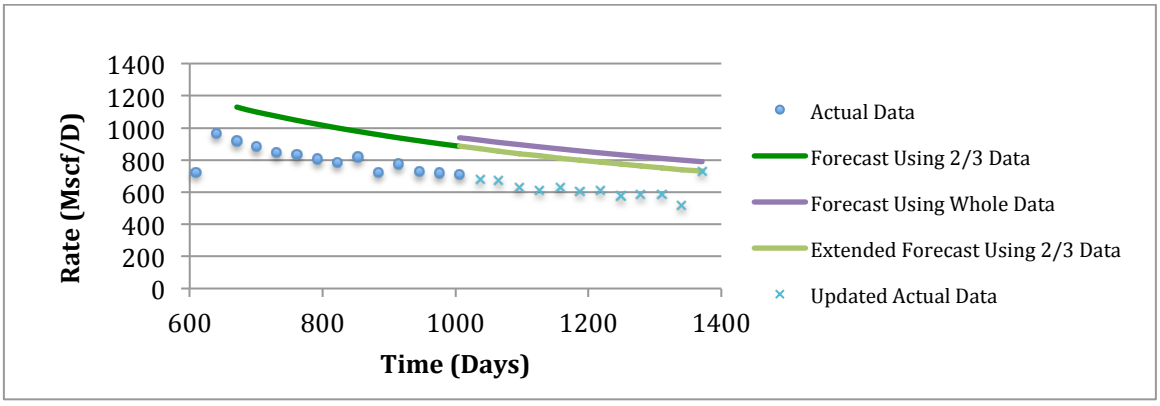

Figure II - 165: History Matching of Well#13, No.257263 Generated by Duong's Model

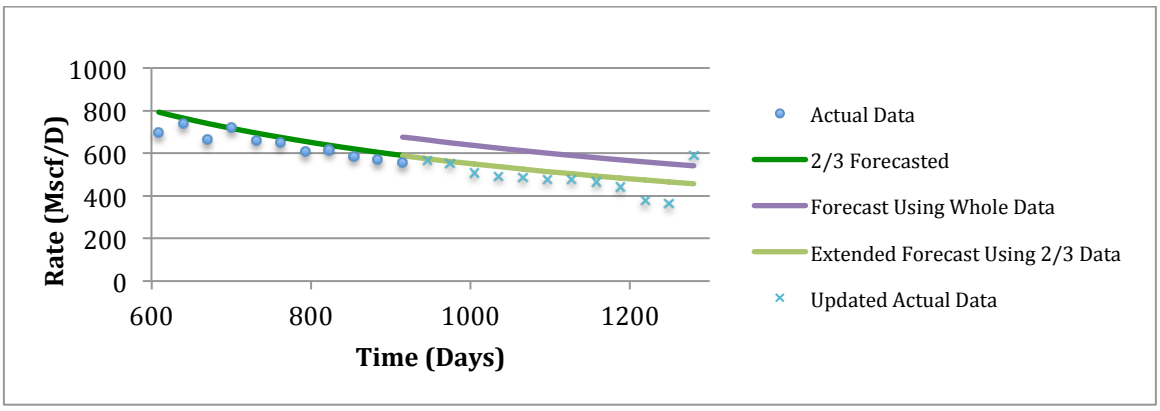

Figure II - 166: History Matching of Well#14, No.257862 Generated by Duong's Model

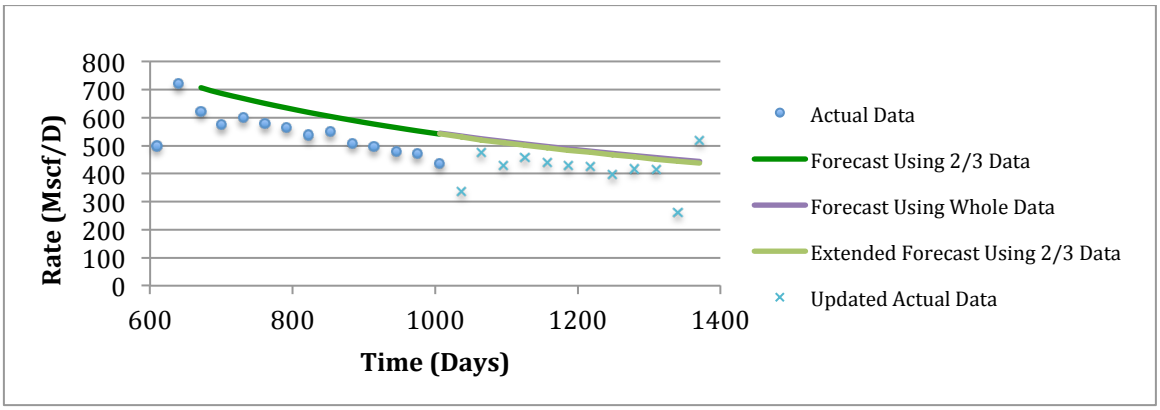

Figure II - 167: History Matching of Well#15, No.254843 Generated by Duong's Model

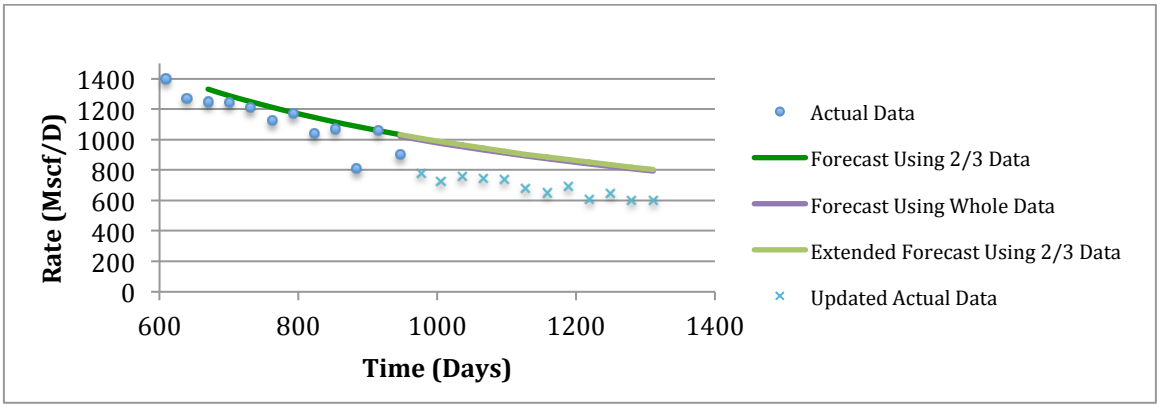

Figure II - 168: History Matching of Well#16, No.258036 Generated by Duong's Model

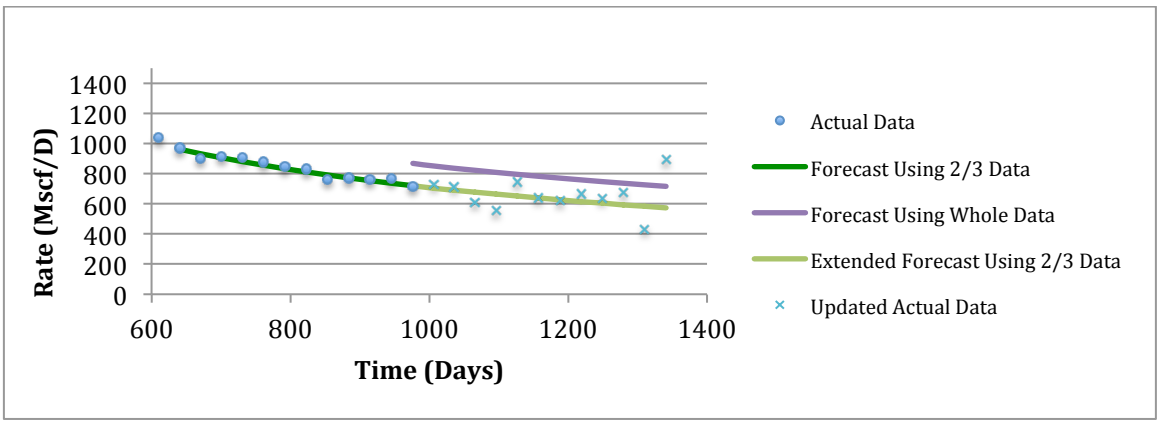

Figure II - 169: History Matching of Well#17, No.257955 Generated by Duong's Model

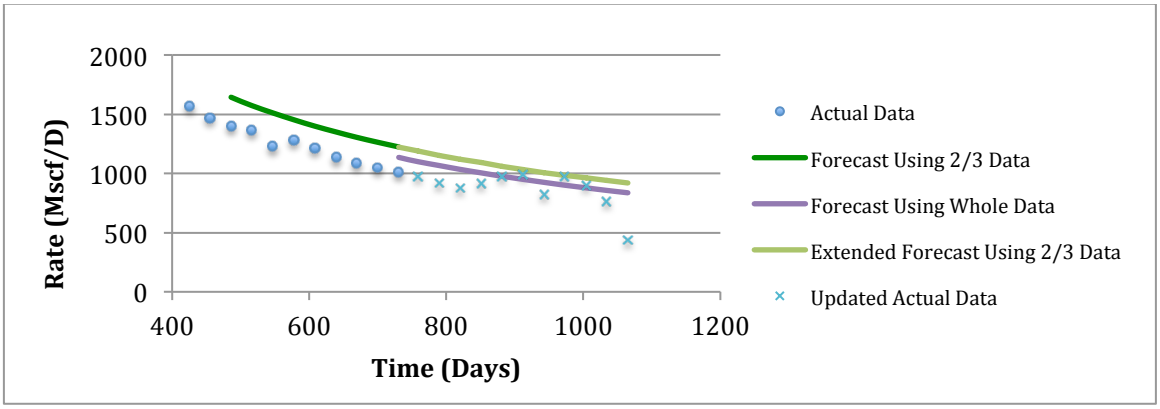

Figure II - 170: History Matching of Well#18, No.259883 Generated by Duong's Model

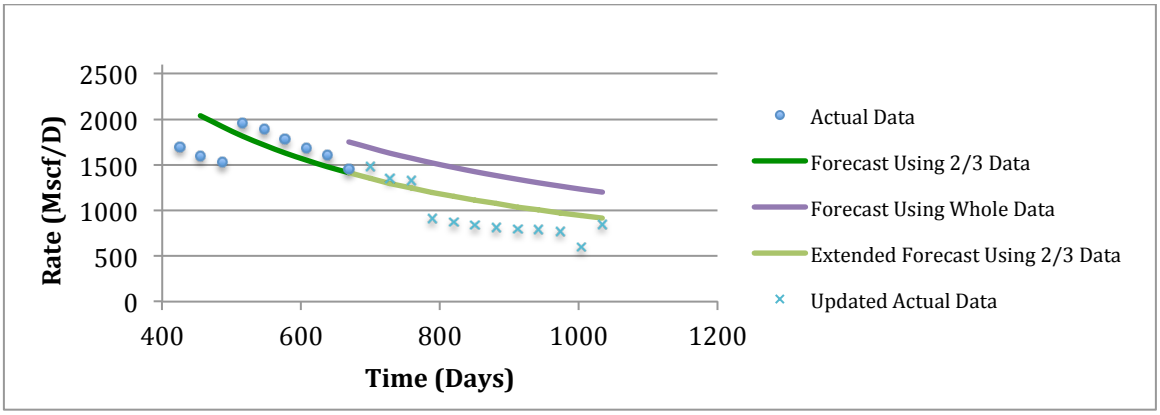

Figure II - 171: History Matching of Well#19, No.259429 Generated by Duong's Model

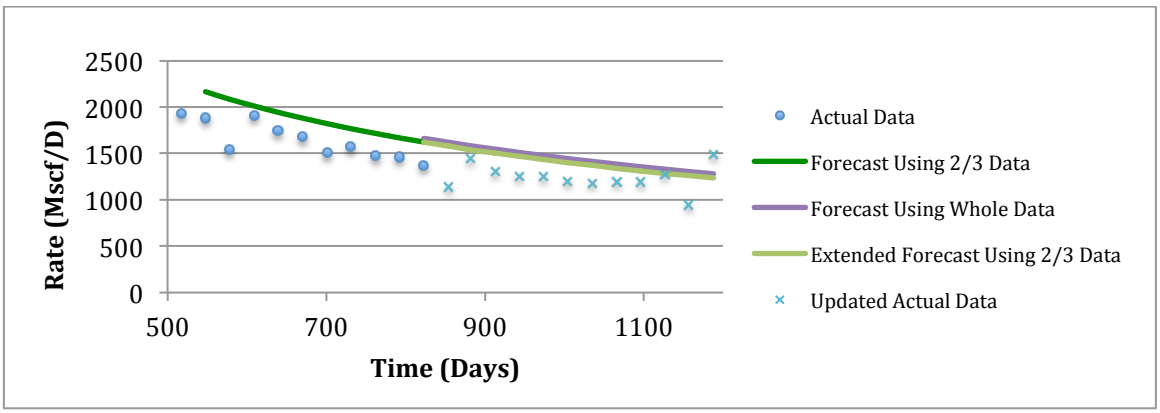

Figure II - 172: History Matching of Well#20, No.258903 Generated by Duong's Model

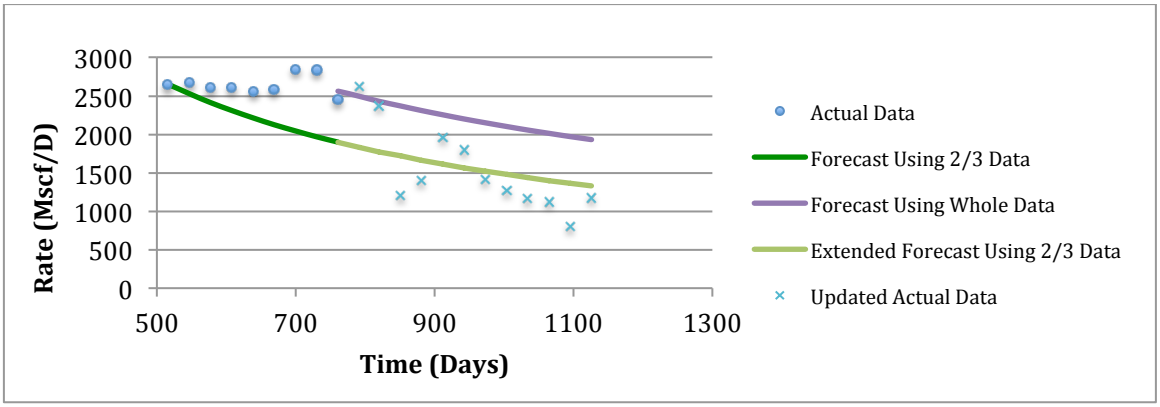

Figure II - 173: History Matching of Well#21, No.260129 Generated by Duong's Model

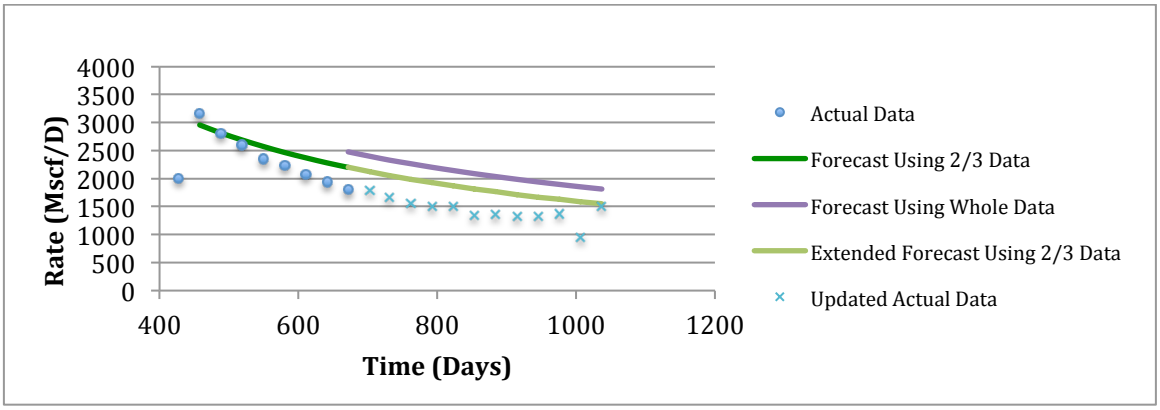

Figure II - 174: History Matching of Well#22, No.260720 Generated by Duong's Model

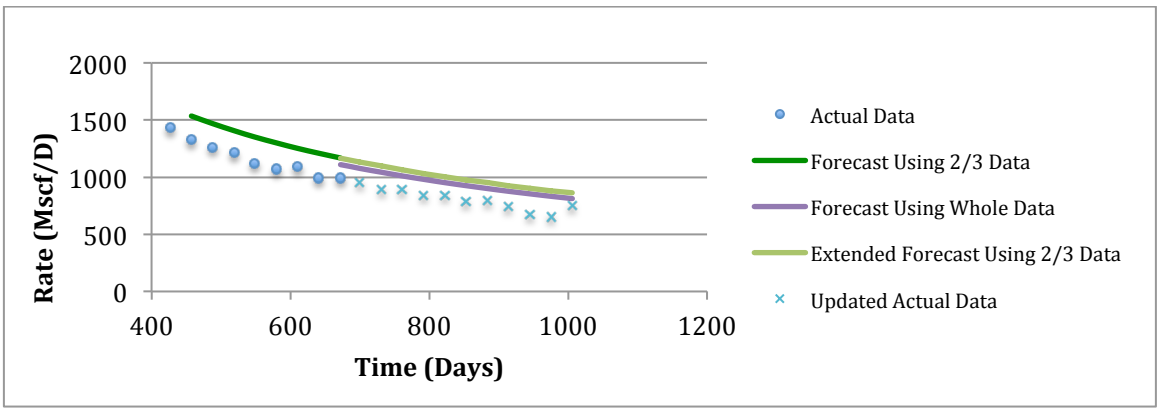

Figure II - 175: History Matching of Well#23, No.261439 Generated by Duong's Model

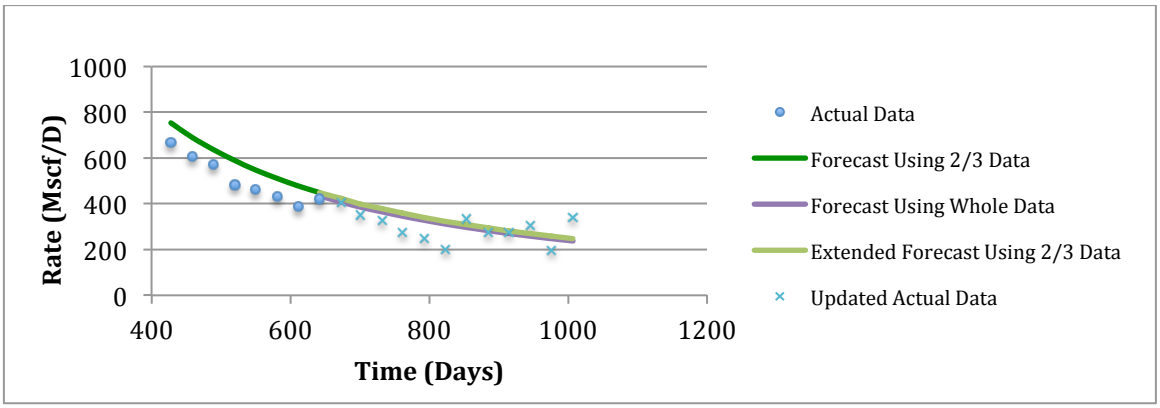

Figure II - 176: History Matching of Well#24, No.260211 Generated by Duong's Model

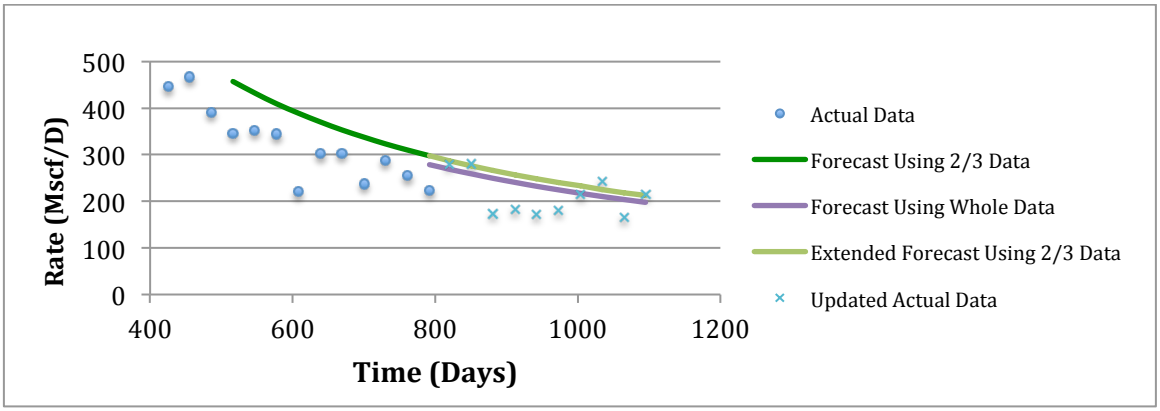

Figure II - 177: History Matching of Well#26, No.258131 Generated by Duong's Model

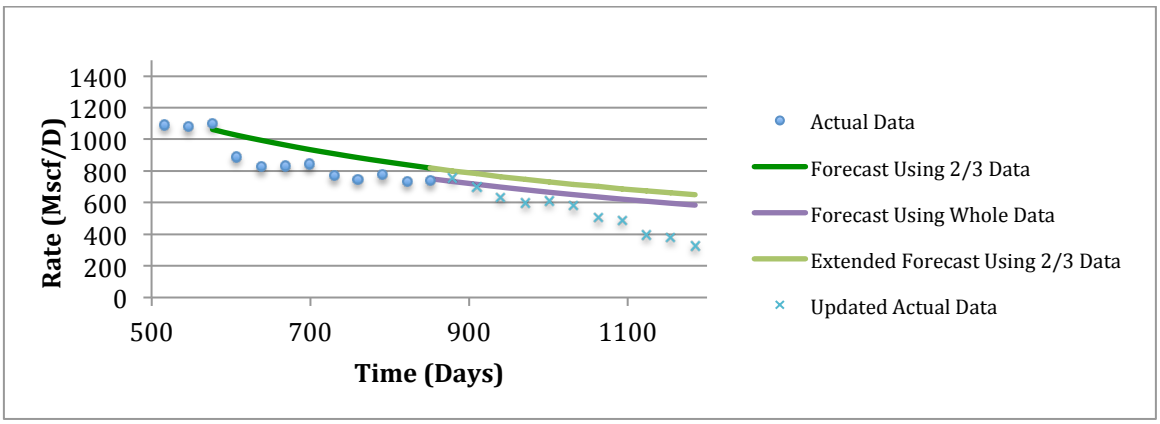

Figure II - 178: History Matching of Well#27, No.257683 Generated by Duong's Model

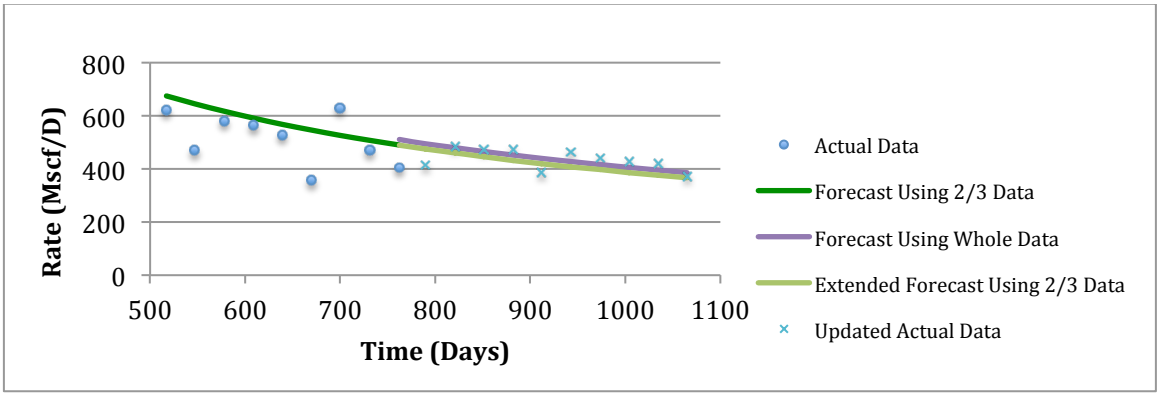

Figure II - 179: History Matching of Well#28, No.257687 Generated by Duong's Model

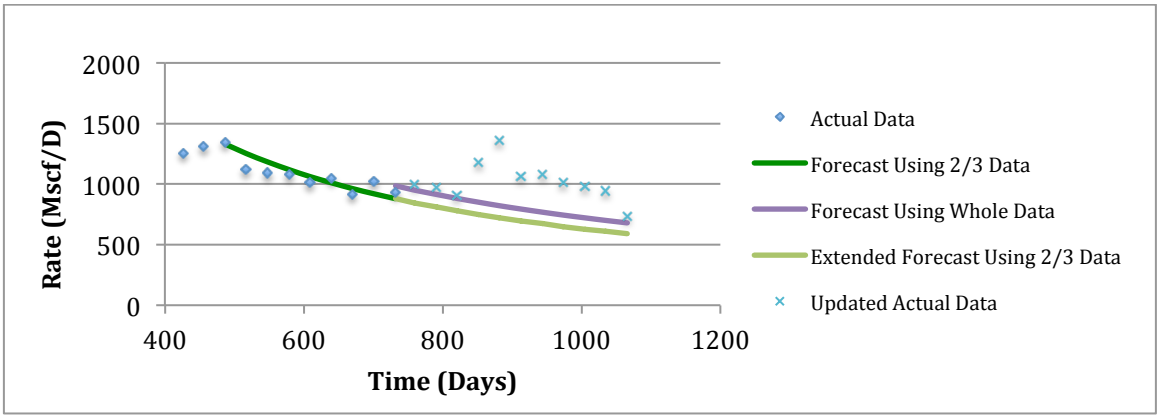

Figure II - 180: History Matching of Well#29, No.257628 Generated by Duong's Model

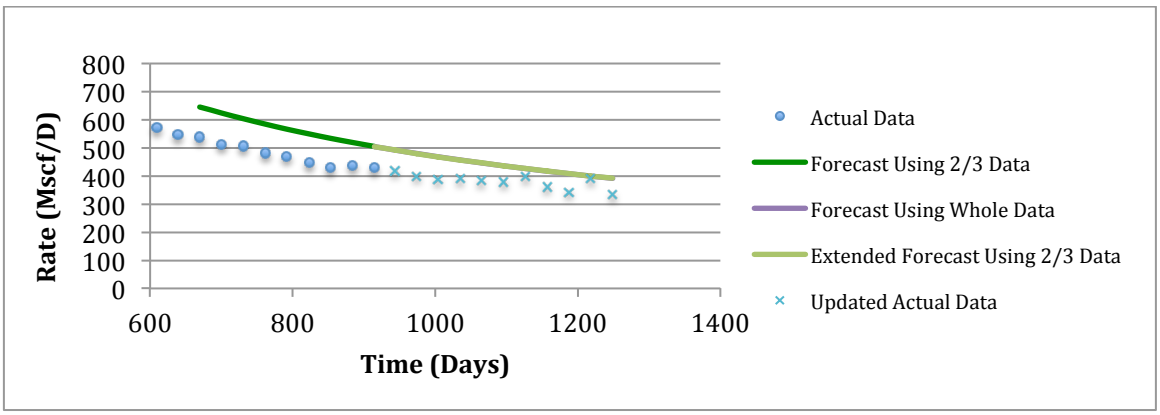

Figure II - 181: History Matching of Well#30, No.257685 Generated by Duong's Model

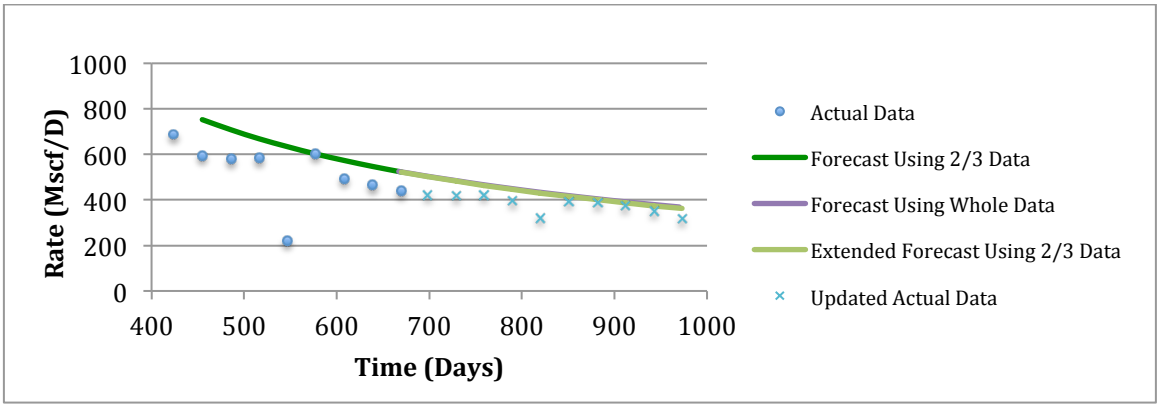

Figure II - 182: History Matching of Well#31, No.260046 Generated by Duong's Model

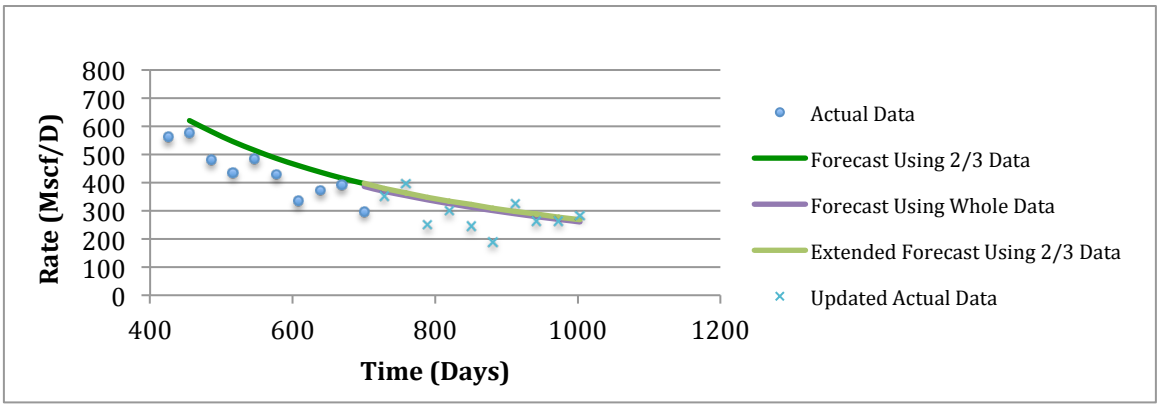

Figure II - 183: History Matching of Well#32, No.260047 Generated by Duong's Model

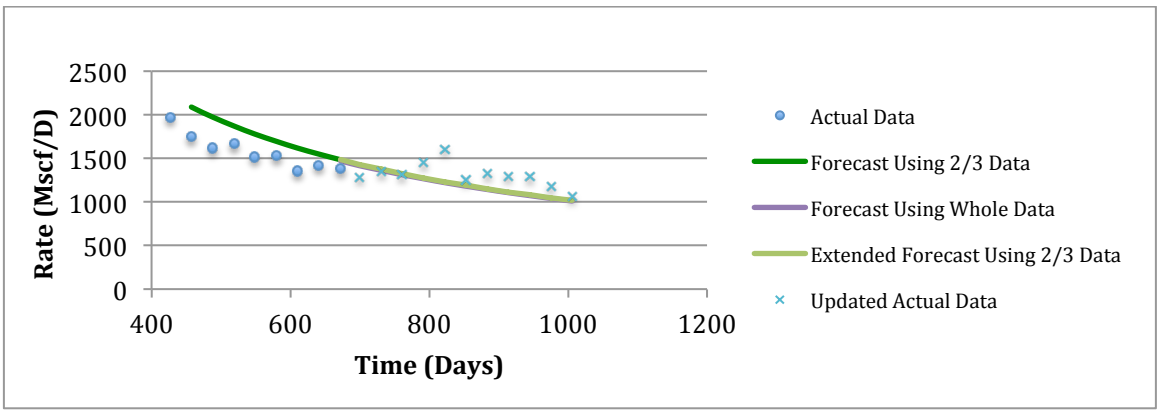

Figure II - 184: History Matching of Well#33, No.260071 Generated by Duong's Model

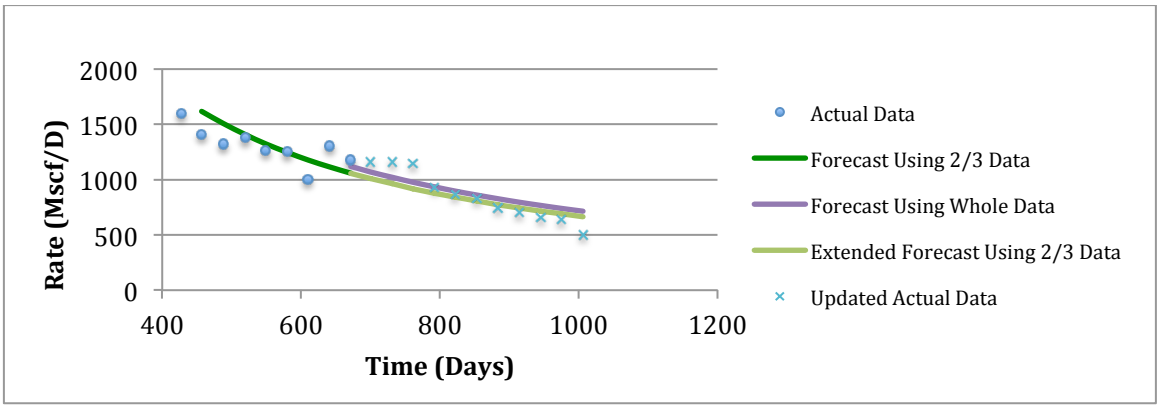

Figure II - 185: History Matching of Well#34, No.260182 Generated by Duong's Model

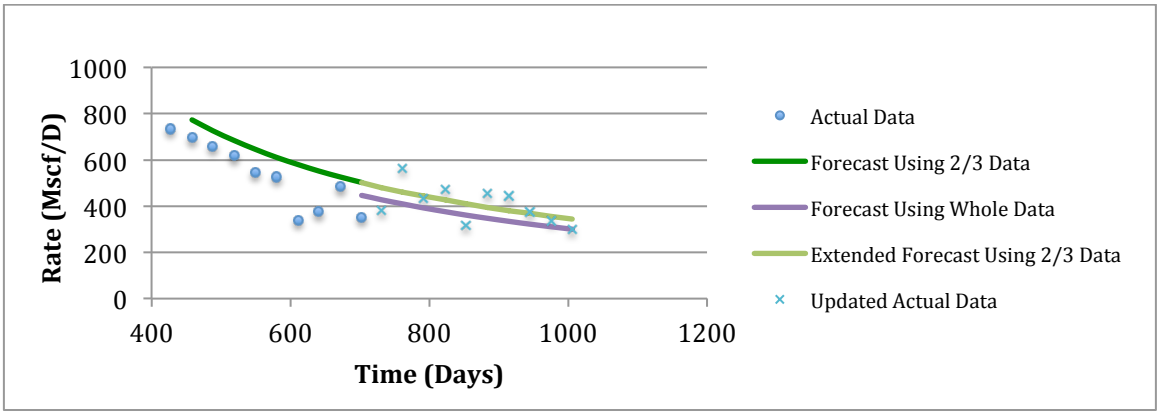

Figure II - 186: History Matching of Well#35, No.261381 Generated by Duong's Model

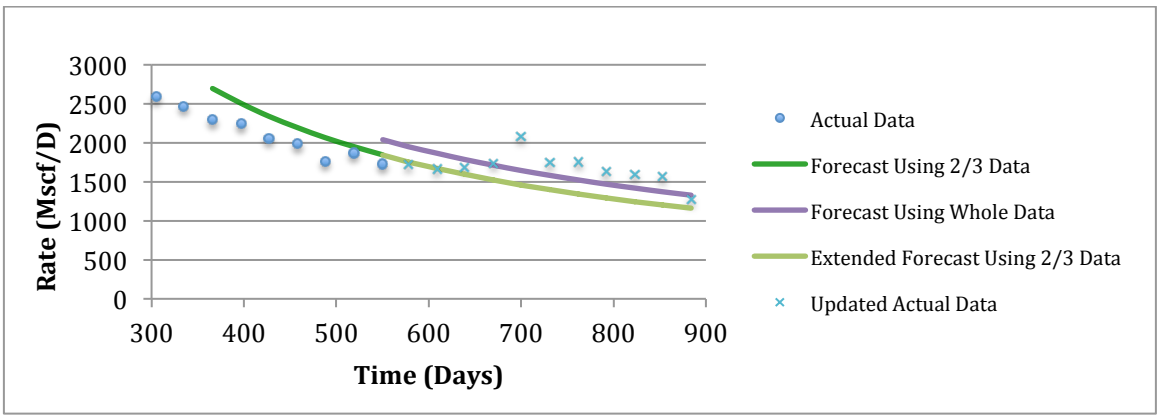

Figure II - 187: History Matching of Well#36, No.260379 Generated by Duong's Model

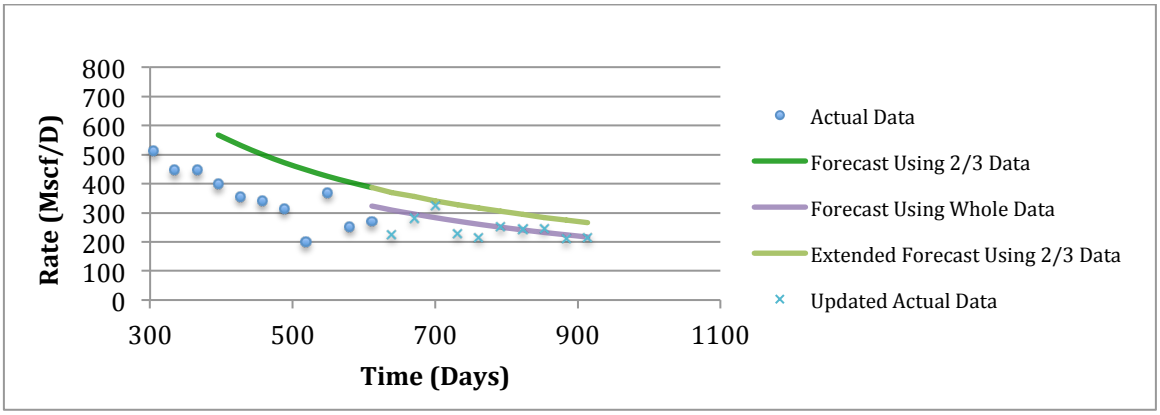

Figure II - 188: History Matching of Well#37, No.261320 Generated by Duong's Model

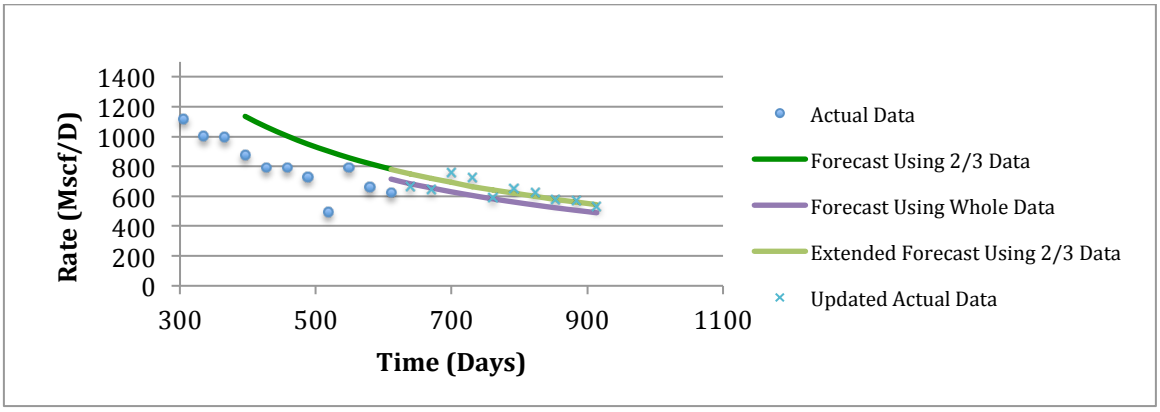

Figure II - 189: History Matching of Well#38, No.261632 Generated by Duong's Model

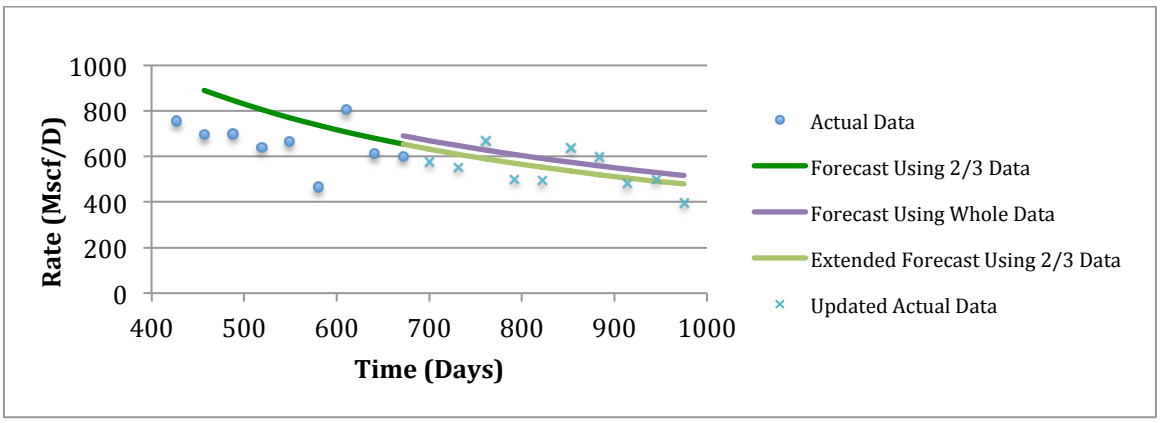

Figure II - 190: History Matching of Well#39, No.261443 Generated by Duong's Model

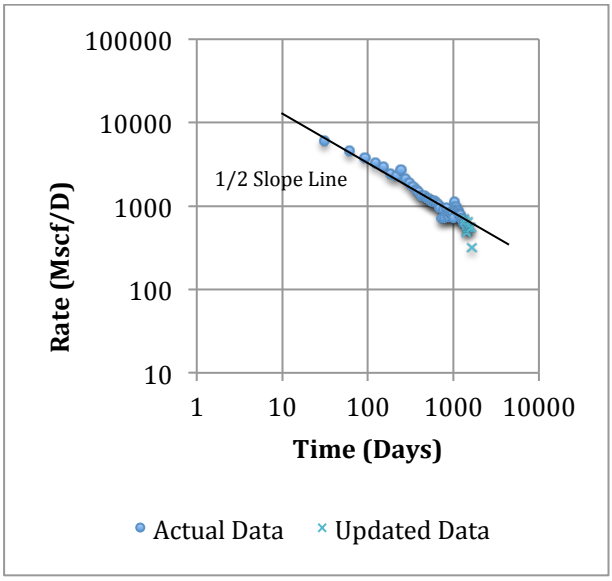

(a)

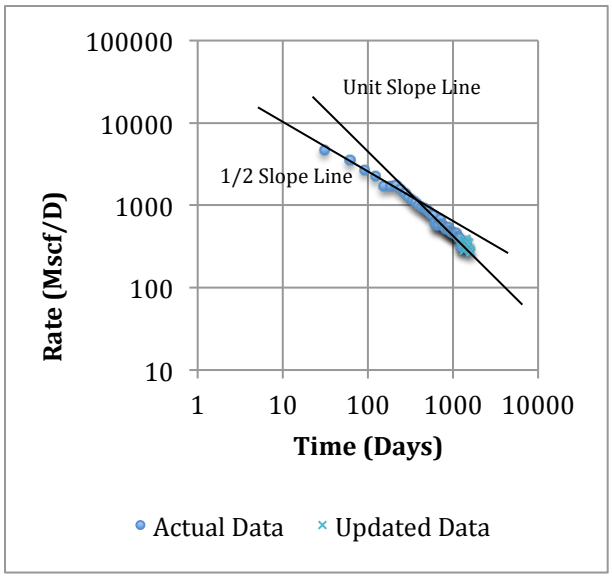

(b)

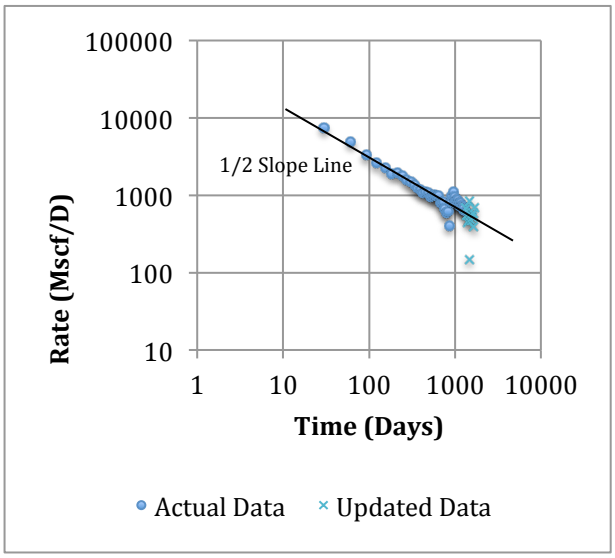

(c)

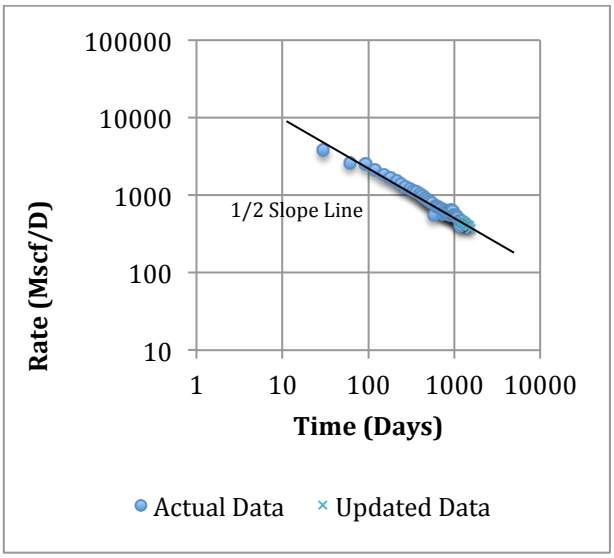

(d)

Figure III - 1 (a-d): Flow Regime Diagnosis Plots of Well#1, #2, #3 and #4

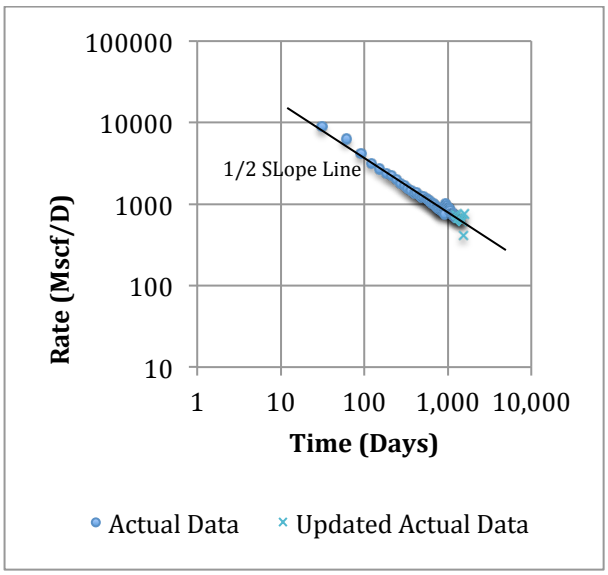

(a)

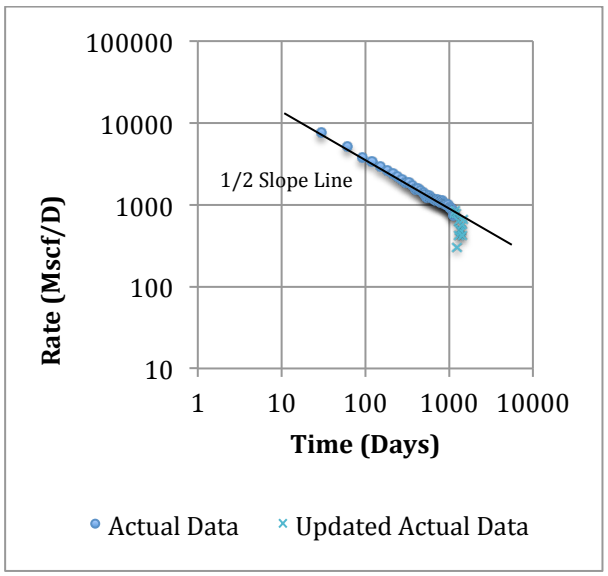

(b)

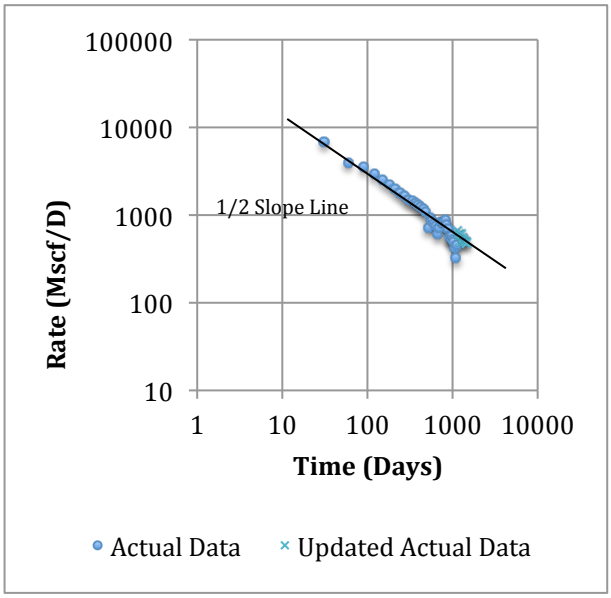

(c)

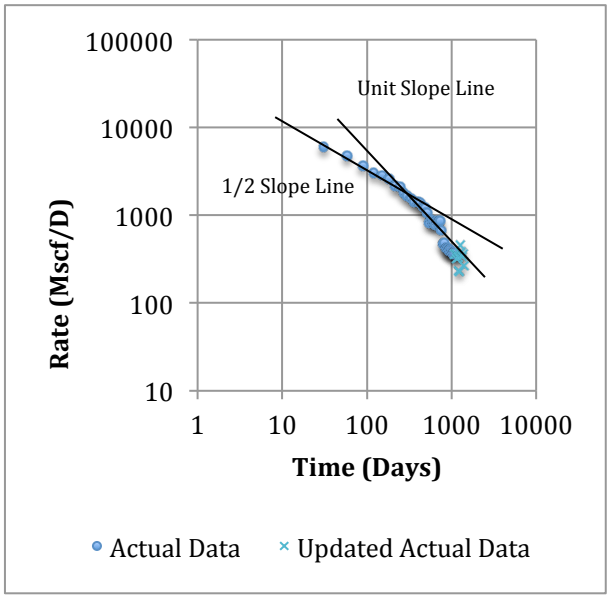

(d)

Figure III - 2 (a-d): Flow Regime Diagnosis Plots of Well#5, #6, #7 and #8

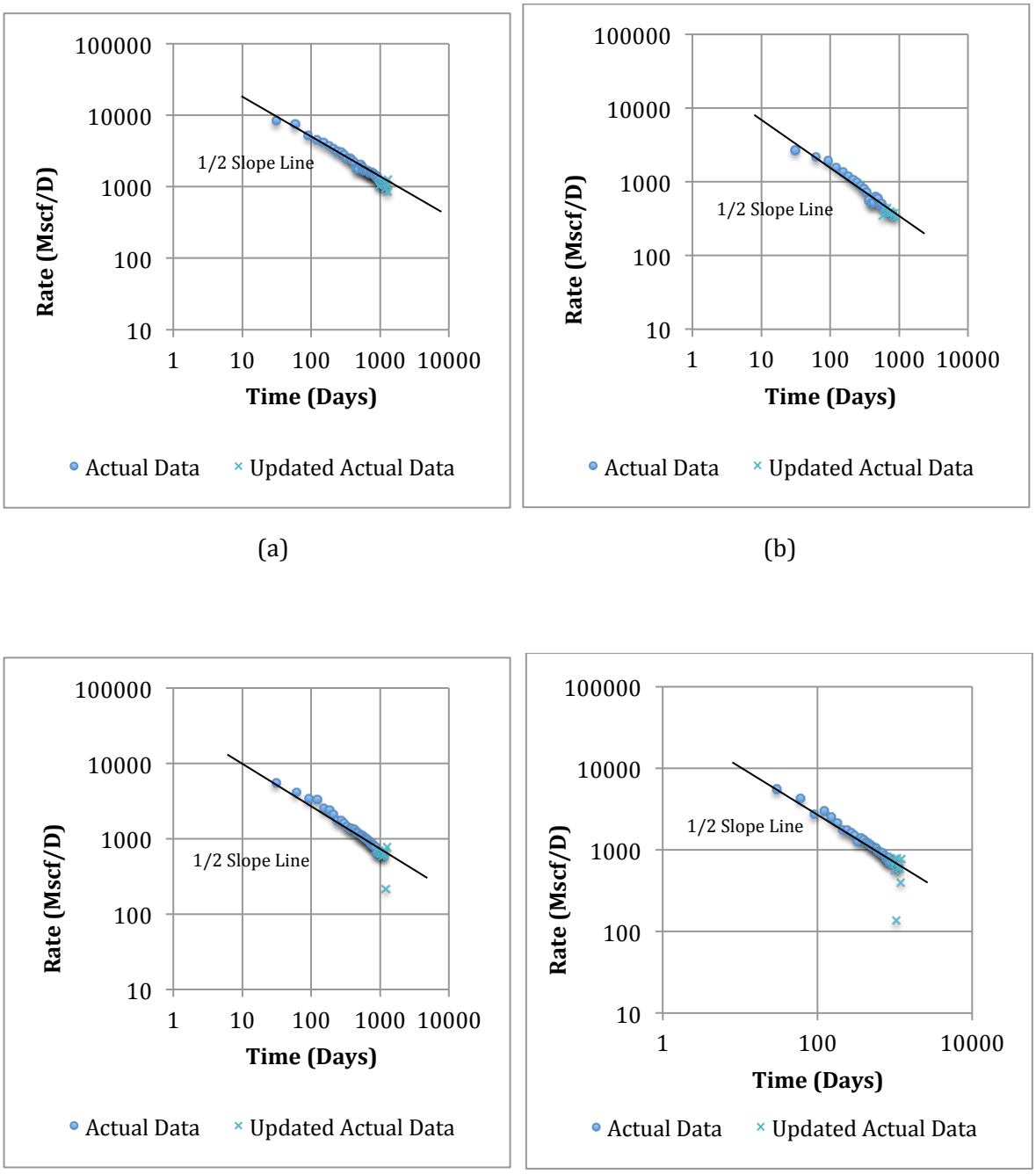

Figure III - 3 (a-d): Flow Regime Diagnosis Plots of Well#9, #10, #11 and #12

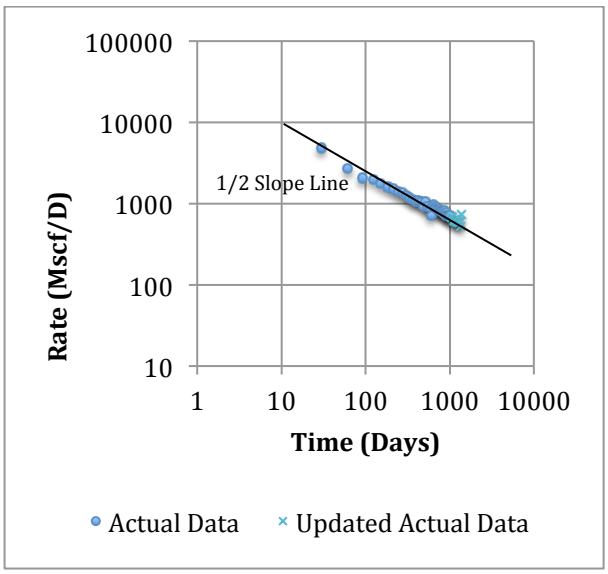

(a)

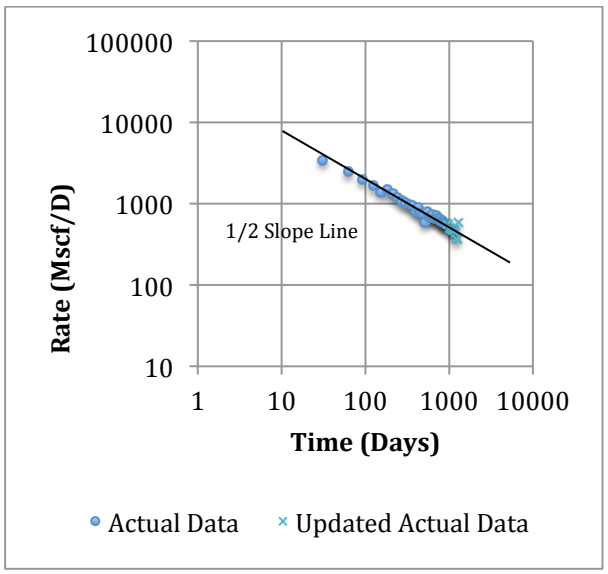

(b)

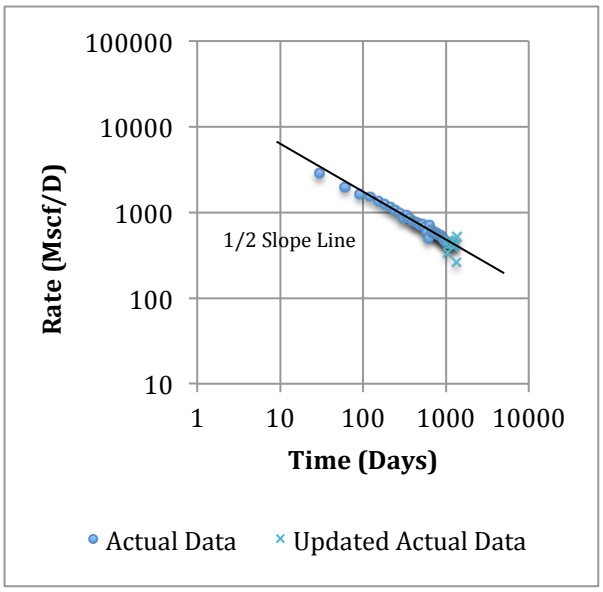

(c)

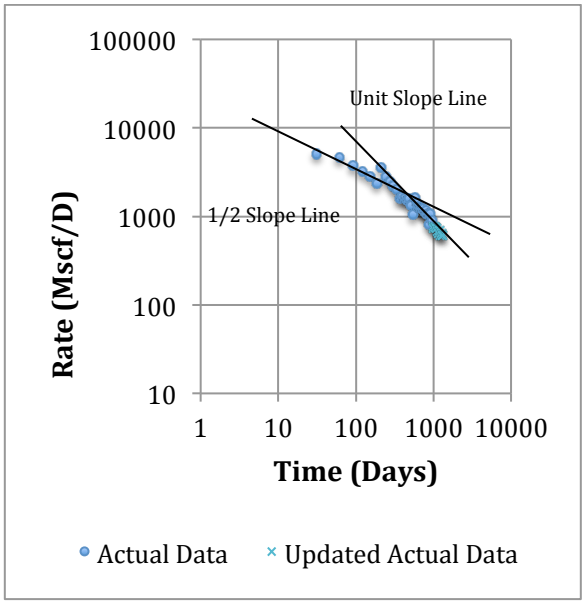

(d)

Figure III - 4 (a-d): Flow Regime Diagnosis Plots of Well#13, #14, #15 and #16

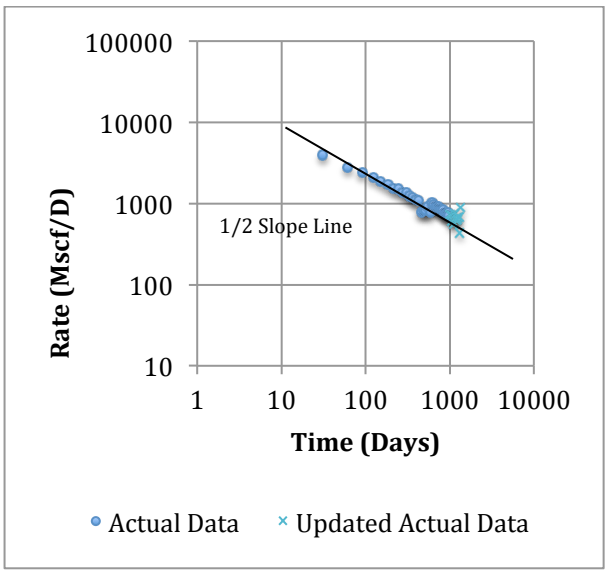

(a)

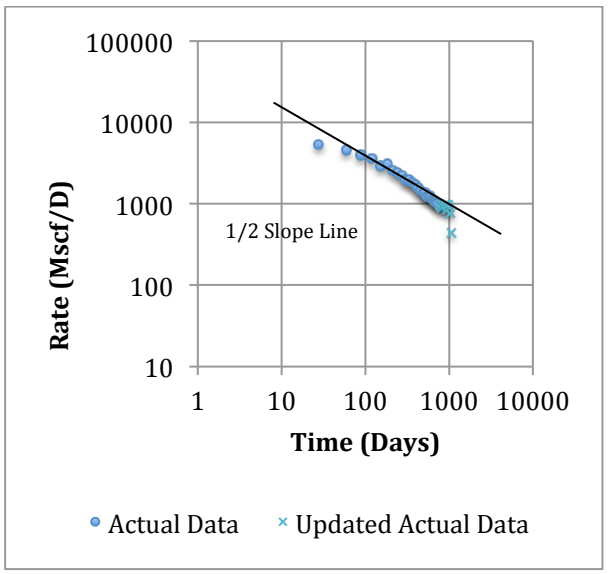

(b)

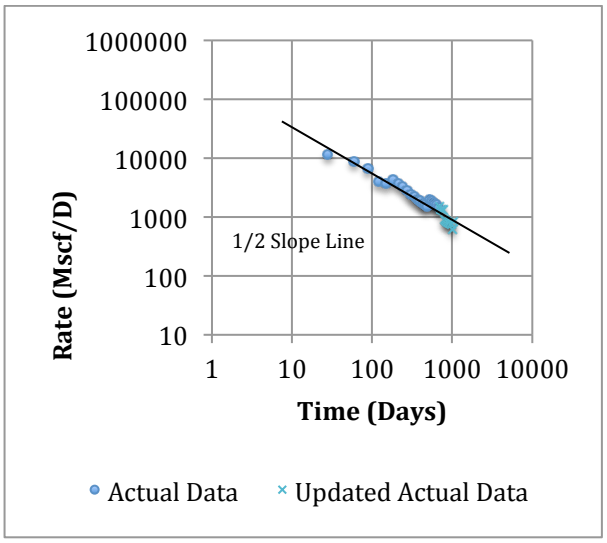

(c)

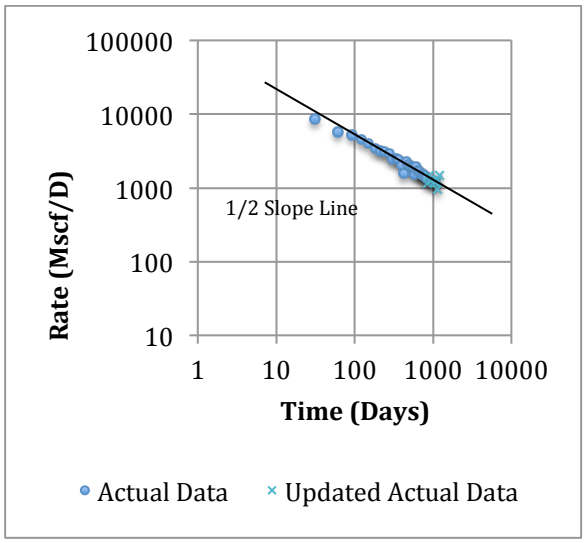

(d)

Figure III - 5 (a-d): Flow Regime Diagnosis Plots of Well#17, #18, #19 and #20

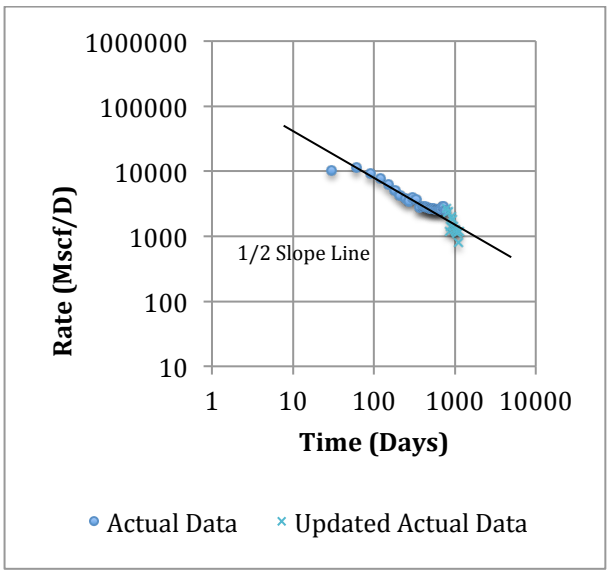

(a)

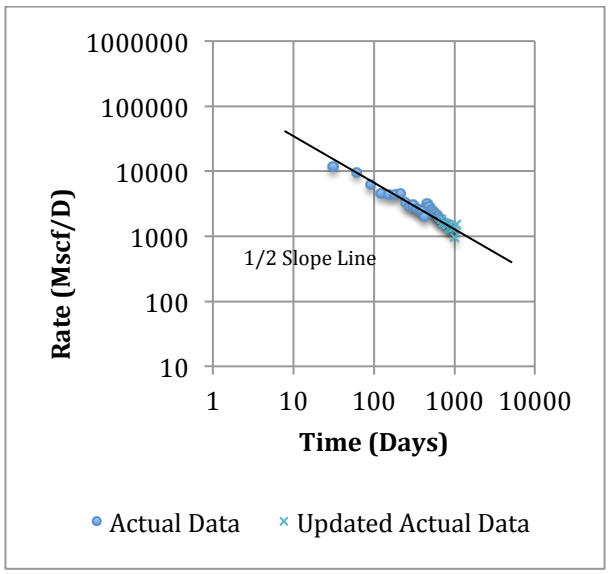

(b)

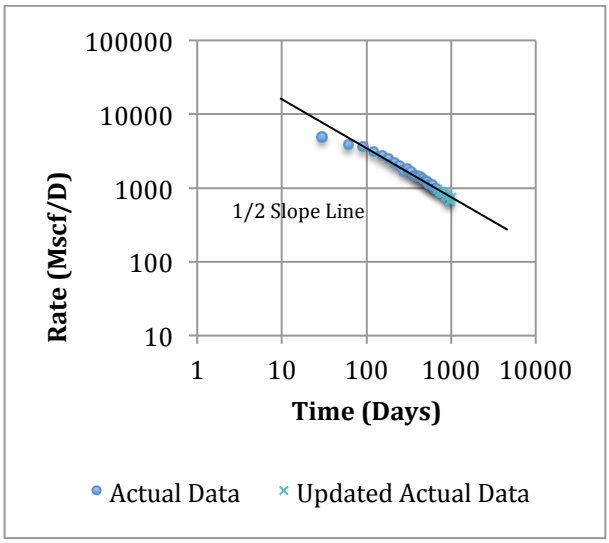

(c)

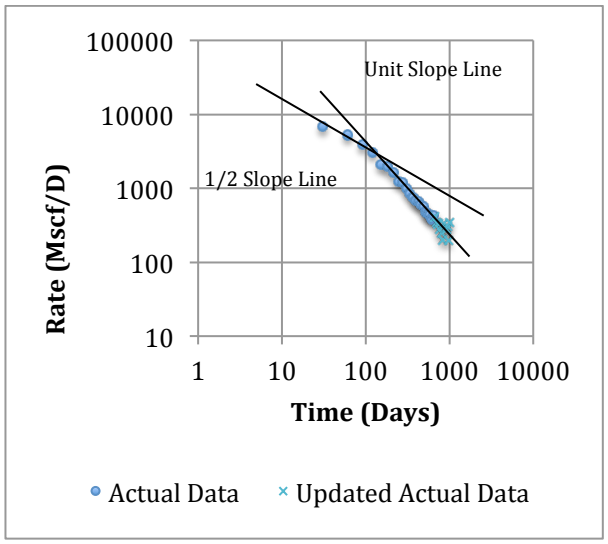

(d)

Figure III - 6 (a-d): Flow Regime Diagnosis Plots of Well#21, #22, #23 and #24

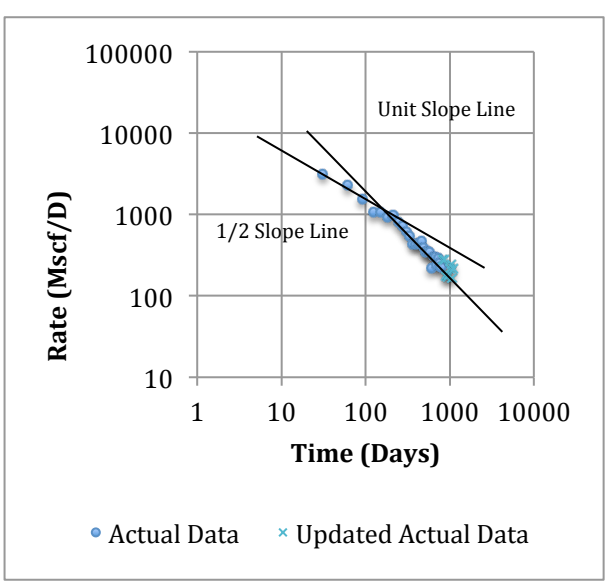

(a)

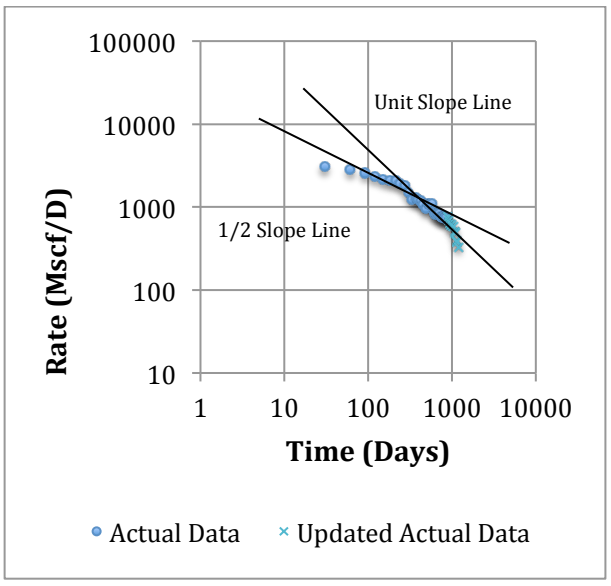

(b)

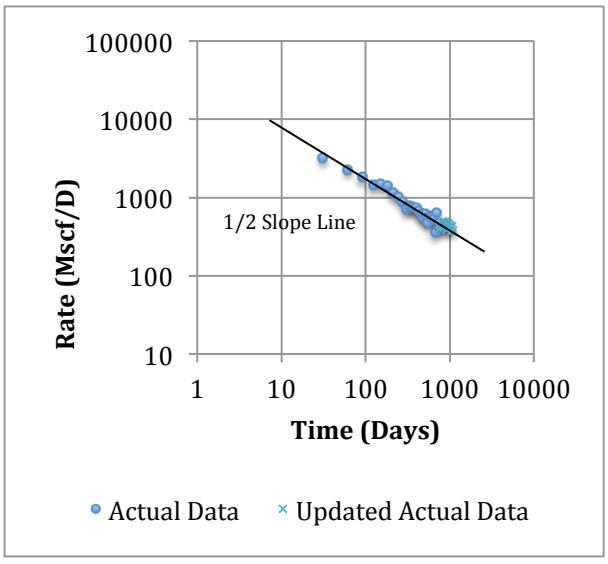

(c)

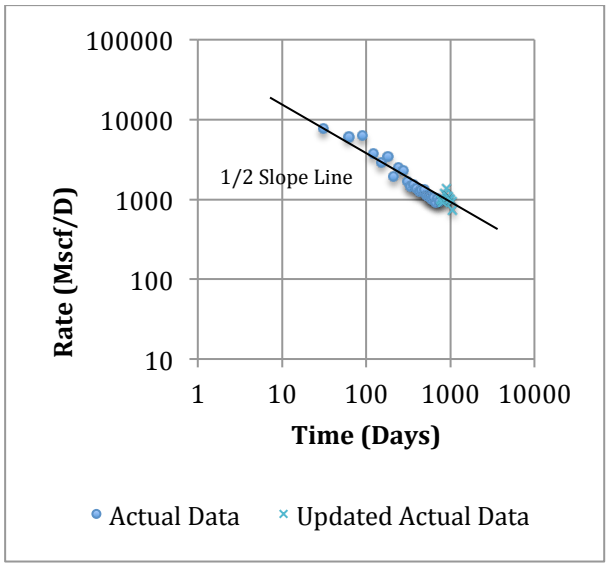

(d)

Figure III - 7 (a-d): Flow Regime Diagnosis Plots of Well#26, #27, #28 and #29

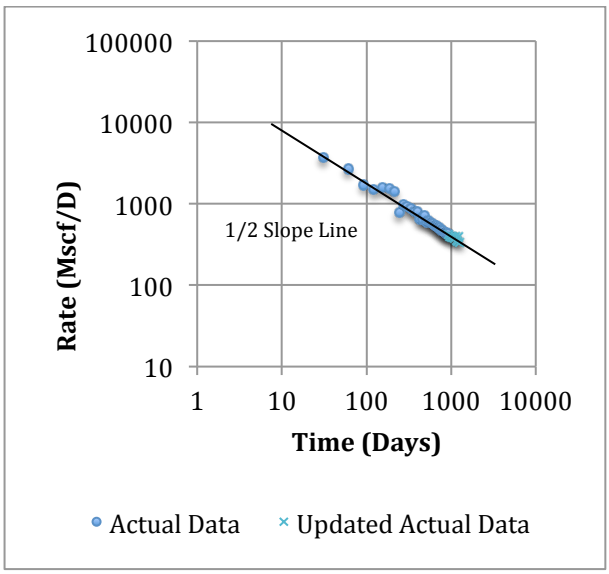

(a)

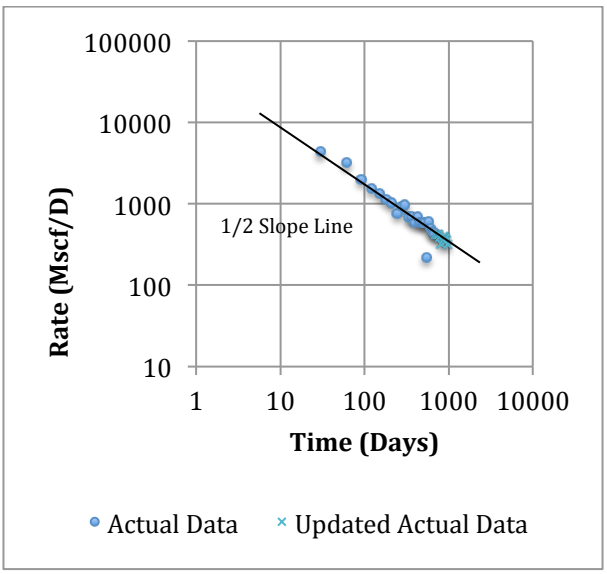

(b)

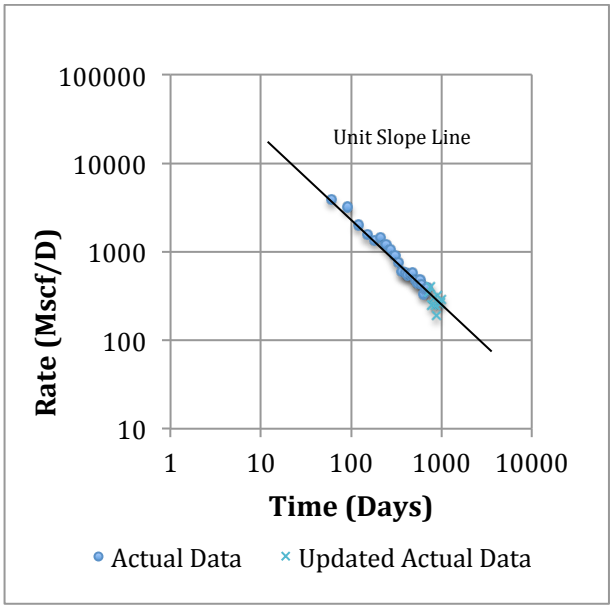

(c)

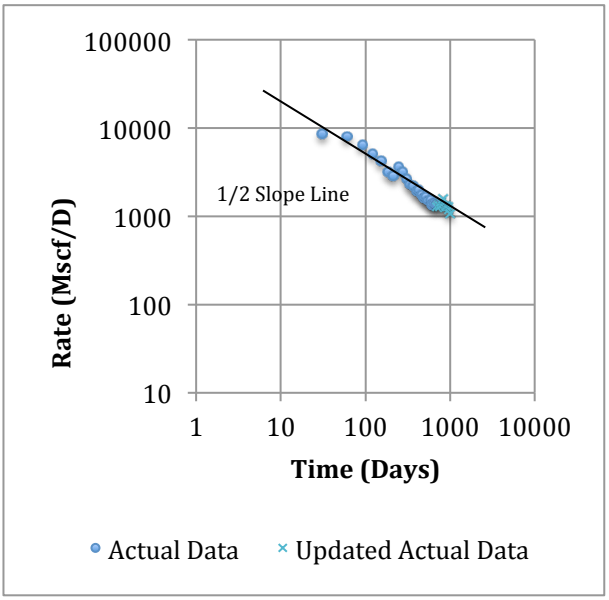

(d)

Figure III - 8 (a-d): Flow Regime Diagnosis Plots of Well#30, #31, #32 and #33

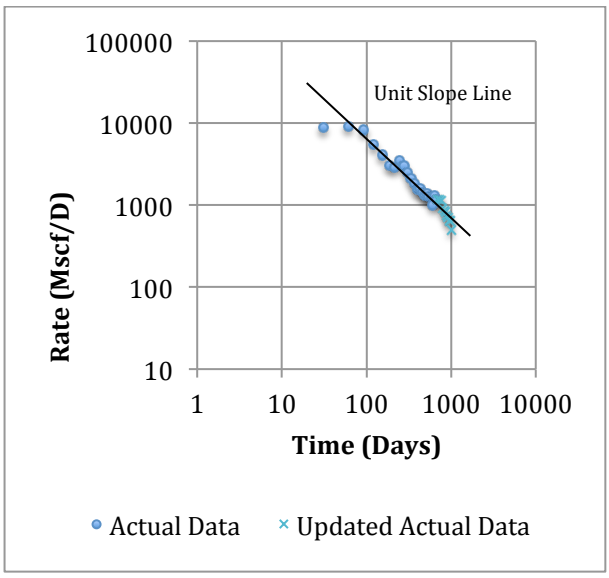

(a)

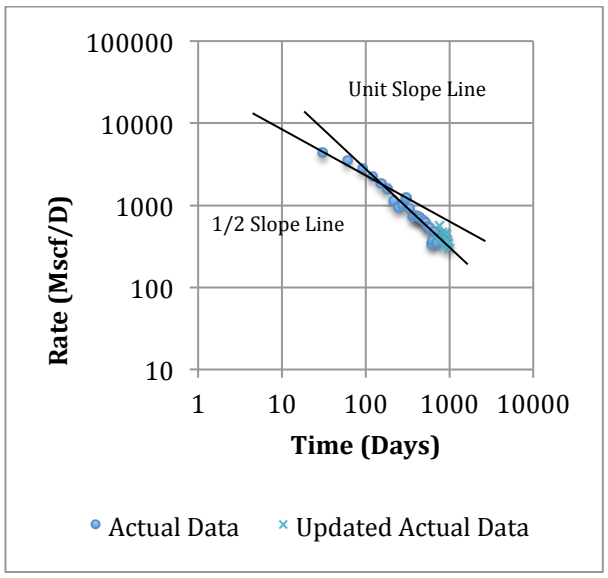

(b)

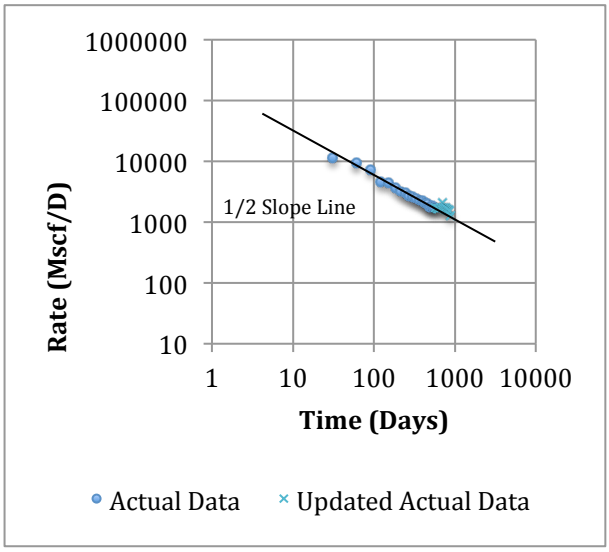

(c)

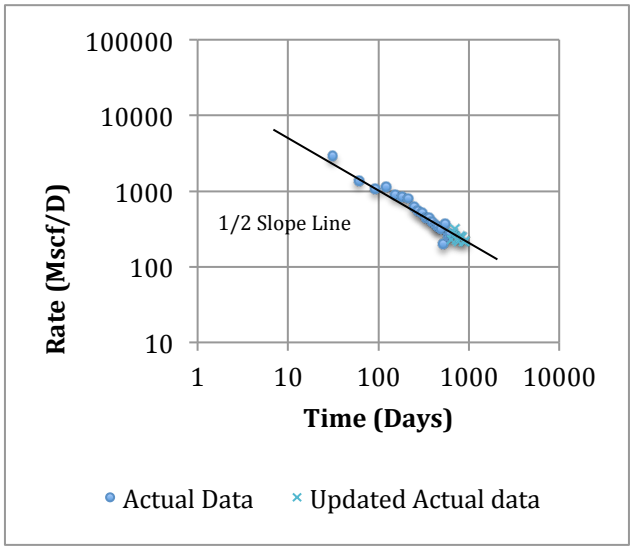

(d)

Figure III - 9 (a-d): Flow Regime Diagnosis Plots of Well#34, #35, #36 and #37

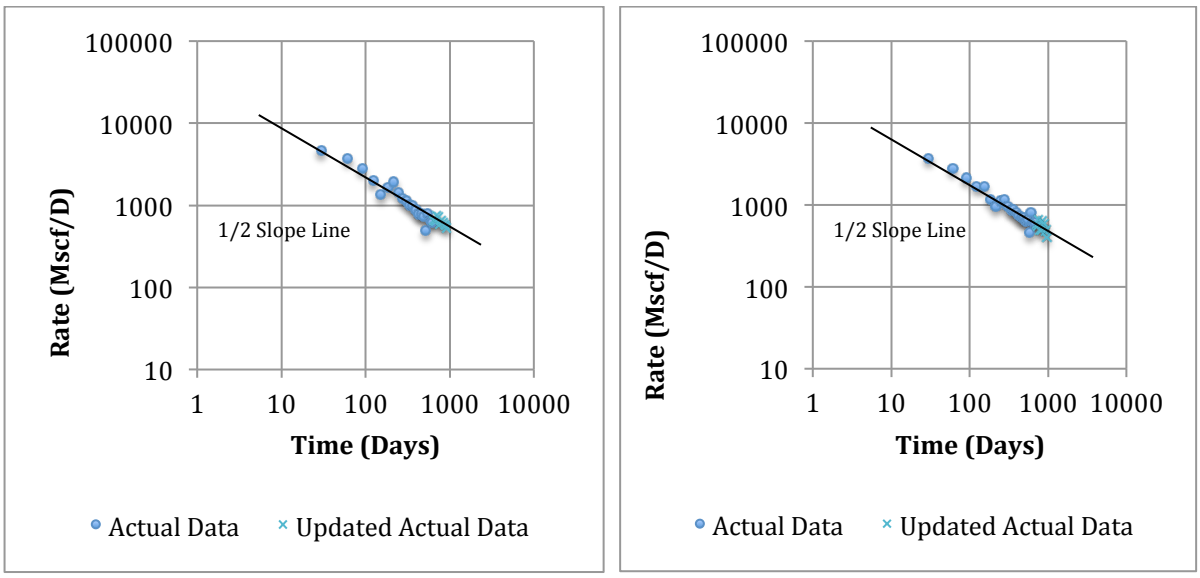

(a) (b)

Figure III - 10 (a-b): Flow Regime Diagnosis Plots of Well#38 and #39